PROGRESS IN RESEARCH

April 1, 2008 - March 31, 2009

CYCLOTRON INSTITUTE

Texas A&M University

College Station, Texas

PROGRESS IN RESEARCH

APRIL 1, 2008- MARCH 31, 2009

Prepared By

The Cyclotron Institute Staff

Texas A&M University

College Station, TX 77843-3366

Phone: (979) 845-1411
Fax: (979) 845-1899

Web: http://cyclotron.tamu.edu

August 2009

TABLE OF CONTENTS

SECTION II: HEAVY ION REACTIONS

SECTION III: NUCLEAR THEORY

SECTION IV: ATOMIC, MOLECULAR AND MATERIALS SCIENCE

SECTION V: SUPERCONDUCTING CYCLOTRON, INSTRUMENTATION AND RIB UPGRADE

Introduction
April 1, 2008 – March 31, 2009

Progress in research and operations at the Texas A&M Cyclotron Institute is summarized in this report for the period April, 1, 2008 through March 31, 2009. The format follows that of previous years. Sections I through IV contain reports from individual research projects. Operation and technical developments are given in Section V. Section VI lists the publications with Cyclotron Institute authors and the Appendix gives additional information including talks presented by members of the Institute during the past year. Once again, the full volume of this year's Progress in Research is available only on our web site (http://cyclotron.tamu.edu). *Since most of the contributions presented here are truly reports on progress in research, results and conclusions should not be quoted from the report without the consent of the authors.*

We have now completed 4 1/2 years of the Upgrade Project which ultimately will give us accelerated radioactive beams at intermediate energies. The progress on the project continues to be good—we remain reasonably close to schedule. The K150 cyclotron is operational but routine operation awaits the full radiation monitoring system, which is being installed now. Beam line magnets and vacuum systems for the refurbished machine are in place and operational. A change in scope for the project was approved at the last Technical review. We now plan to run H^- and D^- beams with a foil stripper rather than H^+ and D^+ through the deflector. This should substantially reduce the buildup of radioactivity at the exit of the machine.

Institute programs continue to thrive. Dr. Cody Folden joined the Institute us as a new Assistant Professor of Nuclear Chemistry. He is developing a program in heavy-element research. During the past year, Dr. Saskia Mioduszewski won the APS Goeppert-Mayer Award and Dr. Rainer Fries received an NSF Career Award.

Some highlights of work over the past year are given below.

Research highlights:

(1) Prompted by a flood of new measurements on superallowed beta decay since the 2005 survey, a new critical survey of world data has been published, which also includes improved isospin symmetry-breaking corrections, an updated analysis of the possible contribution of systematic uncertainties to these corrections, and the inclusion of atomic effects in the calculated statistical rate functions *f*. The resultant corrected $\mathcal{Ft}$ values are self consistent and yield a more precise value of the CKM matrix element V_{ud} than has been obtained before. When this result is combined with the best current value for V_{us}, the CKM unitarity sum becomes 0.99995(61), a stunning confirmation of the standard model expectation.

(2) A new technique has been developed to determine spectroscopic factors for neutron transfer reactions. The new technique uses the asymptotic normalization coefficient to fix the geometry of the neutron bound in the residual nucleus and the peripheral contribution to the cross section.

(3) Experimental evidence for a quantum phase transition in nuclei, driven by the neutron/proton asymmetry has been found. Free energies derived using the Landau approach are consistent with a line of first-order phase transitions terminating at a point where the system undergoes a second-order transition.

(4) Work at TAMU previously demonstrated that the beta-minus decay of ^{198}Au in gold was in fact independent of temperature (<0.04% difference between 19K and room temperature) and we have now obtained a similar result for the electron-capture decay of ^{97}Ru.

(5) As part of the UCNA collaboration, the β asymmetry parameter in neutron decay has been measured for the first time using ultra-cold neutrons. Improvements to the system and the greater statistics accumulated this year are expected to result in a 0.3% measurement, which would be competitive with existing cold neutron beam experiments.

(6) The heavy element group has begun preparations for their initial experiments, including target preparation, constructing a data acquisition system, and simulations of MARS for the transmission of complete-fusion evaporation products. In summer 2009, alpha particles slowed by degraders will be used to calibrate the MARS velocity filter for slow ions (~0.02c).

(7) We have observed isoscaling for elements with Z=1-17 over a broad range of isotopes from the reactions of ^{86}Kr and ^{78}Kr projectiles with ^{64}Ni and ^{58}Ni targets. The N/Z of the source was calculated from the isotopically identified fragments and experimentally measured neutrons emitted from reconstructed quasi-projectiles. The isoscaling parameter alpha is seen to increase with increasing difference in the neutron composition of the sources and decrease with increasing excitation energy.

(8) The in-medium ρ-meson spectral function developed at TAMU, which has been widely used to interpret dilepton spectra in heavy-ion collisions, has been applied to dilepton photo-production off nuclear targets. Without tunable parameters, a good description of the dilepton invariant-mass spectra, as measured by CLAS at JLAB, emerges, providing a link between heavy-ion and JLAB physics.

(9) The spectral functions of pions in asymmetric nuclear matter become dependent on their charges. Using those determined from the couplings of pions to the delta-resonance--nucleon-hole excitations in nuclear matter, we have studied in a thermal model their effects on the ratio of negatively charged to positively charged pions. In the neutron-rich matter formed in heavy ion collisions, this ratio is enhanced by the isospin-dependent pion in-medium effect, and the effect is comparable to that due to

the uncertainties in the theoretically predicted stiffness of the nuclear symmetry energy at high densities.

(10) A new surface-integral based scattering and reaction theory for charged particles has been developed which bypasses existing difficulties focusing on integrated properties.

(11) Our resonance recombination model, which improves quark coalescence models for hadronization at RHIC, has been implemented into relativistic Langevin simulations for strange and charm quarks in an expanding fireball for semi-central 200 AGeV Au-Au collisions. The elliptic flow of the resulting meson spectra can reproduce the empirically observed constituent quark-number scaling in kinetic energy from 0 to 3 GeV.

(12) The relaxation time and thereby the shear viscosity of nuclear matter were determined within a semi-classical kinetic approach, using the experimental data on the centroid energies and widths of the isoscalar giant monopole and dipole resonances.

As in the past, Institute scientists remain active in a number of collaborative research efforts around the world. Major programs include: a measurement of Michel parameters in normal μ^+ decay at TRIUMF in Vancouver, B.C.; mass measurements using the Penning Traps at Argonne National Laboratory and the University of Jyvaskyla; continued work with STAR collaboration at RHIC; and the measurement of neutron beta decay with the UCNA collaboration.

Once again, I am indebted to Dr. Y.-W. Lui for assembling this report.

R.E. Tribble
August 10, 2009

SECTION I

NUCLEAR STRUCTURE, FUNDAMENTAL INTERACTIONS, AND ASTROPHYSICS

Giant monopole resonance in Mo and Zr isotopes

D. H. Youngblood, Y. -W. Lui, Krishichayan, J. Button, and R. Polis

While the Giant Monopole Resonance (GMR) is a nearly symmetric Gaussian like peak in Sn isotopes and heavier nuclei, the GMR in Zr is an almost symmetric peak with a pronounced high energy tail that significantly affects the energy of the GMR and hence the nuclear compressibility extracted from its position[1]. Hartree-Fock-RPA calculations of ^{90}Zr [2] predicted the shape and relative strength of this tail reasonably accurately, though the energy of the GMR was too high in the calculation. We have studied giant resonances in ^{90,92} Zr, ^{92,96,100}Mo with inelastic scattering of 240 MeV α particles using the MDM spectrometer at small angles including 0^o to see if this feature persists in other nuclei having N,Z ~ 50,40. The horizontal acceptance of the spectrometer was $4^o$and ray tracing was used to reconstruct the scattering angle. The vertical acceptance was set at 2^o. The focal plane detector measured position and angle in the scattering plane and covered from E_x ~ 8 MeV to E_x > 55 MeV, depending on scattering angle. The out-of-plane scattering angle was not measured. Position resolution of approximately 0.9 mm and scattering angle resolution of about 0.09^o were obtained. Sample spectra are shown in Fig. 1. The multipole components of the giant resonance peak were obtained[1] by dividing the peak into multiple

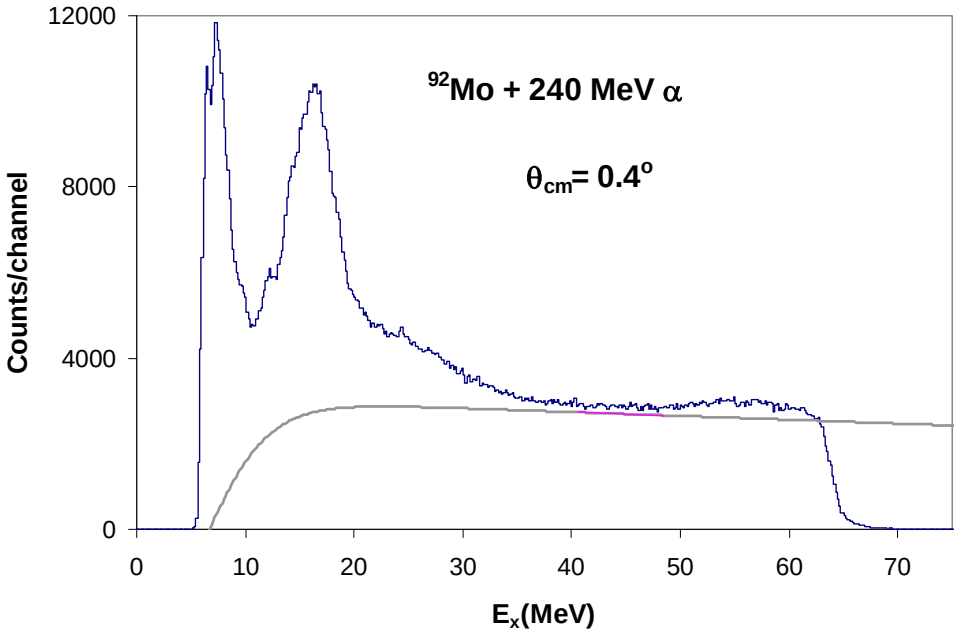

FIG. 1. Inelastic α spectrum obtained at center of mass angle 0.4^o for 240 MeV α particles bombarding ^{92}Mo.

regions (bins) by excitation energy and then comparing the angular distributions obtained for each of these bins to distorted wave Born approximation (DWBA) calculations. The uncertainty from the multipole fits was determined for each multipole by incrementing (or decrementing) that strength, then adjusting the strengths of the other multipoles to minimize total χ^2. This continued until the new χ^2 was 1

unit larger than the total χ^2 obtained for the best fit. Approximately 100% of the E0 EWSR strength was located in each of the nuclei, and the distributions obtained are shown in Fig. 2. In ^{92}Zr and especially ^{92}Mo the high energy component of the GMR is very broad, while in the other nuclei it is much narrower. Moreover in ^{92}Mo, the high energy component contains ~65% of the total E0 strength, so that the centroid energy in ^{92}Mo is more than 2 MeV higher than in ^{90}Zr. The source of this high energy component is not apparent. In deformed nuclei, the GMR splits into two components, one almost coincident with the quadrupole and a second at the normal monopole position[3]. This splitting is very different as the lower and narrower component in ^{92}Mo is approximately where the GMR would be expected, and the other component is substantially higher in energy.

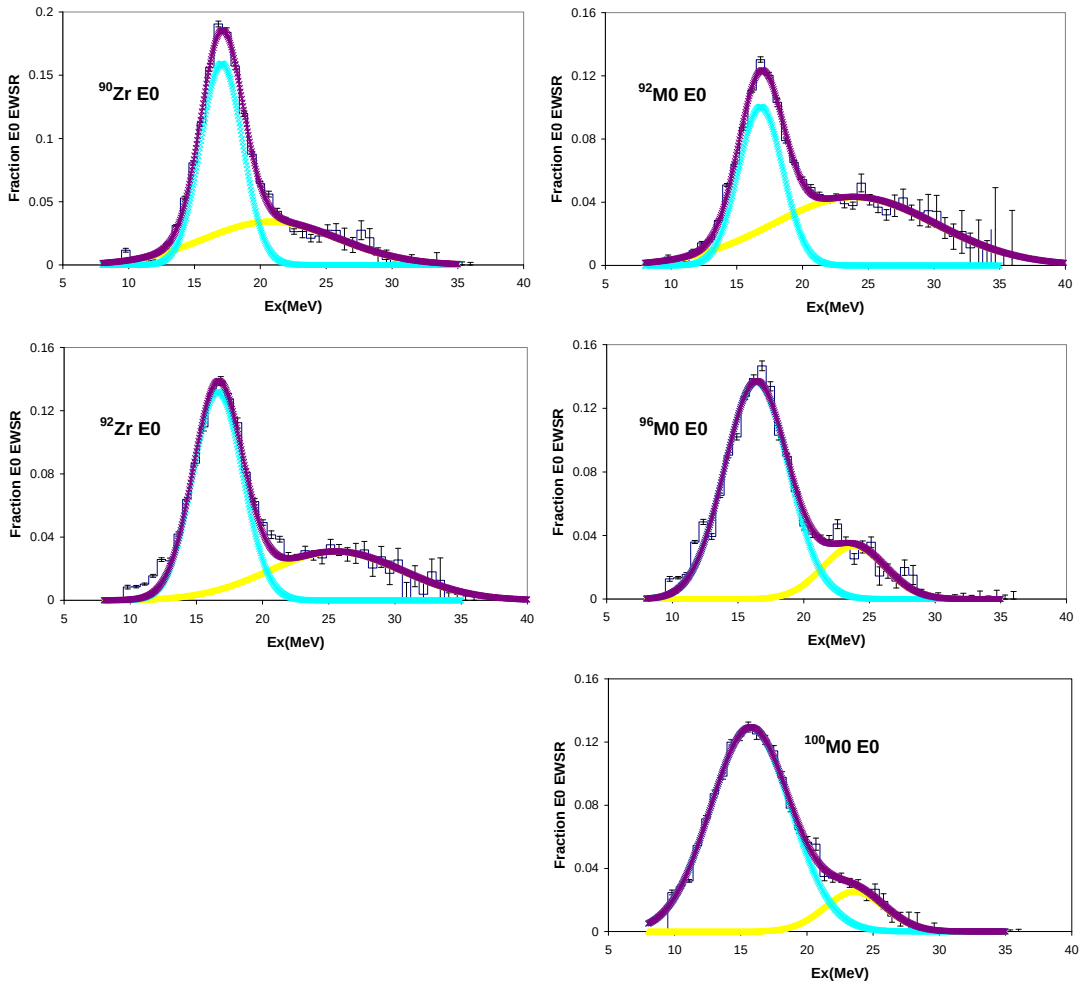

FIG. 2. E0 strength distributions obtained from fits. Two peak Gaussian fits are shown.

[1] D.H. Youngblood *et al.*, Phys. Rev. C **69**, 054312 (2004).

[2] I. Hamamoto, H. Sagawa, and X. Z. Zhang, Phys. Rev. C **56**, 3121 (1997).

[3] U. Garg *et al.*, Phys. Rev. Lett. **45**, 1670 (1980).

Double folding optical parameters for studying giant resonances using a 240 MeV ^{6}Li beam

Krishichayan, X. Chen, Y. -W. Lui, Y. Tokimoto, J. Button, and D. H. Youngblood

Alpha inelastic scattering has been a valuable tool for studying isoscalar giant monopole resonances (ISGMR) for many years [1-3]. A comparison of the results of systematic studies of the isoscalar giant monopole resonance (ISGMR) in stable nuclei with calculations using the Gogny interaction resulted in a value K_{nm} = 231±5 MeV [1]. Calculations with other interactions and relativistic models have shown that the location of the GMR is also sensitive to the symmetry energy and studies of stable Sn isotopes have led to some constraints on K_{sym} [4]. To better determine the contribution from symmetry energy ISGMR measurements can be extended to unstable nuclei using inverse reactions. Chen et al. [5,6] have explored the possibility of using ^{6}Li as a target in studies of giant resonances in unstable nuclei.

We have studied elastic scattering of 240 MeV ^{6}Li ions on ^{24}Mg, ^{28}Si, ^{40}Ca, ^{48}Ca, ^{58}Ni, ^{90}Zr, and ^{116}Sn and inelastic scattering to low-lying states of these targets to develop a systematic optical potential that can be used in Giant Resonances studies of unstable nuclei.

A beam of 240 MeV ^{6}Li ions from Texas A&M K500 superconducting cyclotron, after passing through the beam analysis system, bombarded self-supporting target foils in the target chamber of the multipole-dipole-multipole (MDM) spectrometer. Data for elastic and inelastic scattering were taken at spectrometer angle from 5^{o} to 38^{o}.

Elastic scattering data were fit with optical model calculations using the program, ECIS with WS phenomenological potentials and density dependent folding (DDF) calculations were carried out with the folding code DFPD4. These potentials were then used to calculate differential cross sections using ECIS.

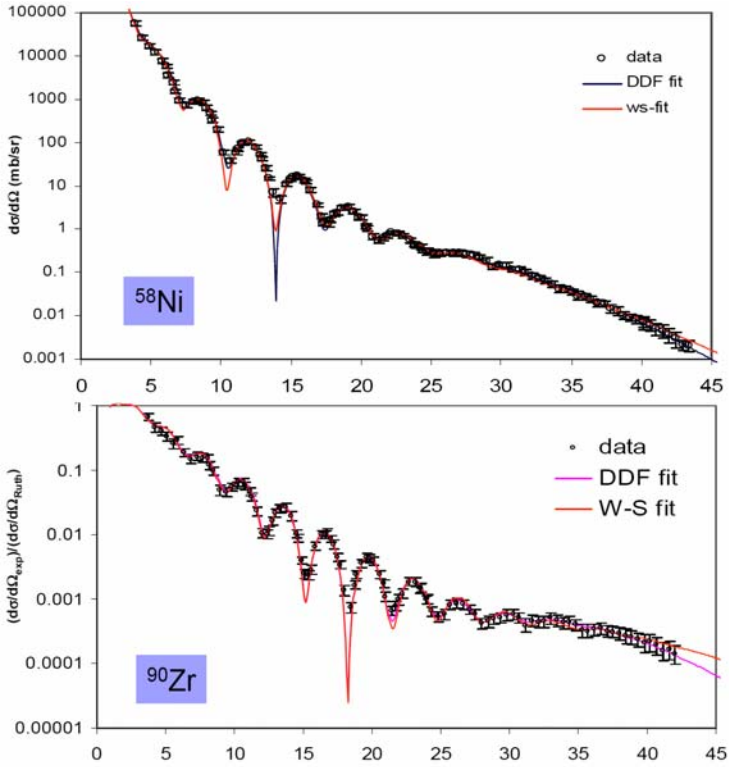

FIG. 1. Angular distribution of the cross sections of the elastic data and fits using WS and double folding potentials.

The optical potential parameters obtained from the folding model fit for ^{24}Mg, ^{28}Si, ^{58}Ni, ^{90}Zr, and ^{116}Sn are listed in Table I and the calculated angulated angular distribution of the cross-section for ^{58}Ni and ^{90}Zr are shown in

TABLE I. Optical parameters sets obtained from the analysis of 240 MeV ^{6}Li scattering with DDF (density dependent double folded potential) fit.

Target	N_r	scaling	**W (MeV)**	r_{i0} (fm)	a_i (fm)	J_v (MeV fm^3)	J_w (MeV fm^3)	χ^2	σ_r (mb)
^{24}Mg	0.823	1.062	**58.67**	0.731	1.204	242	154	1.04	1799
^{28}Si	0.887	1.0624	**41.33**	0.905	1.048	256	136	1.46	1757
^{58}Ni	0.8746	1.0594	**35.331**	1.027	1.048	244.6	112	0.93	2397
^{90}Zr	0.8778	1.0661	**33.343**	1.09	1.0063	239.5	101.43	1.1	2792
^{116}Sn	0.659	1.0	**28.77**	1.151	0.905	202.1	89.9	0.98	2956

Fig. 1. Folding model DWBA calculations for low-lying 2^+ and 3^- states of target nuclei were carried out with ECIS. B(EL) values for 2^+ and 3^- state were extracted by fitting the inelastic scattering cross sections and are in agreement with the adopted values.

^{48}Ca: test nucleus

In order to establish unique optical potentials for ^{6}Li scattering for nuclei where elastic scattering has not been measured using the available experimental data, we have fit the volume integrals of the imaginary part of the nuclear potentials (see Table I) for target nuclei with respect to the mass number and a value for J_w corresponding to ^{48}Ca was extracted from the fit. Keeping this J_w = 117 MeV fm^3 constant, several sets of W_i, r_{i0}, and a_i were calculated using the expression for J_w given as:

$$J_W = \frac{1}{A_T A_p}\int W(r)d\tau$$
$$= \frac{4\pi}{A_T A_p}\sum_{r=1}^{r=20}\frac{W}{e^{(r-R_{i0})/a_i}}r^2 dr$$

where W(r) is the imaginary part of the optical potential and A_T and A_P are the mass numbers of the target and projectile. These different sets of parameters were used to calculate the cross sections for elastic scattering and inelastic scattering to low-lying states of ^{48}Ca. Meanwhile, optical parameters were also extracted by fitting the experimental data. Both sets of parameters were used for DWBA calculations (using double folding model) of the cross sections for low-lying states (2^+ and 3^- states) for ^{48}Ca. The angular distributions of the cross sections for these states are shown in Fig.2.

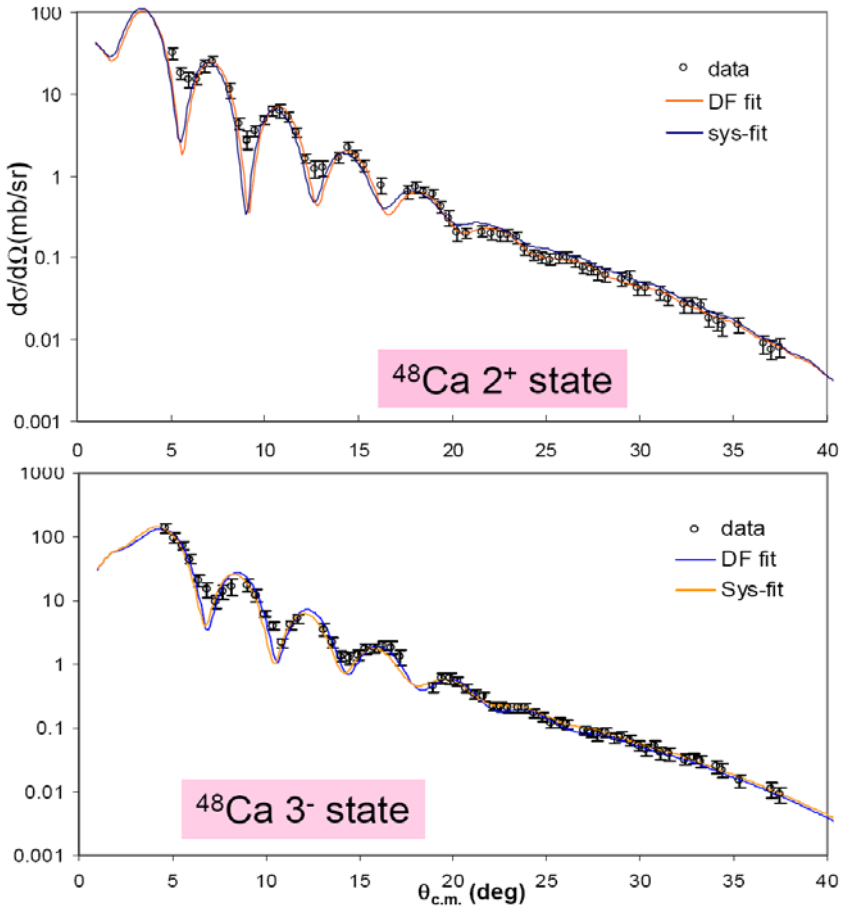

FIG. 2. The differential cross sections calculated with folding model using two sets of parameters for inelastic scattering to 2^+ and 3^- states of ^{48}Ca.

[1] D. H. Youngblood, H. L. Clark, and Y. -W. Lui, Phys. Rev. Lett. **82**, 691 (1999).

[2] D. H. Youngblood, Y. -W. Lui, H. L. Clark, B. John, Y. Tokimoto, and X. Chen, Phys. Rev. C **69**, 034315 (2004).

[3] T. Li *et al.*, Phys. Rev. Lett. **99**,162503 (2007).

[4] S. Shlomo, V. Kolomietz, and G. Colo, Eur. Phys. J. A **30**, 23 (2006).

[5] X. Chen, Y. -W. Lui, H. L. Clark, Y. Tokimoto, and D. H. Youngblood, Phys. Rev. C **79**, 024320 (2009).

[6] X. Chen, Ph.D. Thesis, Texas A&M University, 2008.

β and β-delayed proton decay of ^{31}Cl

L. Trache, A. Banu, J. C. Hardy, V. E. Iacob, M. McCleskey, B. T. Roeder, E. Simmons,
A. Spiridon, R. E. Tribble, A. Saastamoinen,[1] J. Aysto,[1] T. Davinson,[2]
G. Lotay,[2] and P. J. Woods[2]
[1]*University of Jyvaskyla, Jyvaskyla, Finland,*
[2]*University of Edinburgh, Edinburgh, United Kingdom*

In heavier nuclei close to the proton drip line, in the sd-shell region for example, the rates of radiative proton capture reactions on $_{Z}$A nuclei are dominated by resonances. These resonances are excited states above the proton threshold in $_{Z+1}$A+1 nuclei. We aim at populating them by the beta-decay of their $_{Z+2}$A+1 isobars and study their further decay by proton or gamma emission. Such is the case with ^{23}Al and ^{31}Cl which we started to study in 2007 [1, 2]. We have extended the study of the decay of proton-rich ^{31}Cl with an experiment in November 2008 in which we aimed at:

a) decreasing the minimum of proton energies reached below 300 keV
b) increasing the statistics in the gamma-ray spectra.

We have produced and separated ^{31}Cl using MARS using the same (p,2n) reaction in inverse kinematics starting with a beam of ^{32}S @ 40 MeV from K500. We had similar rates and purity of the secondary beam

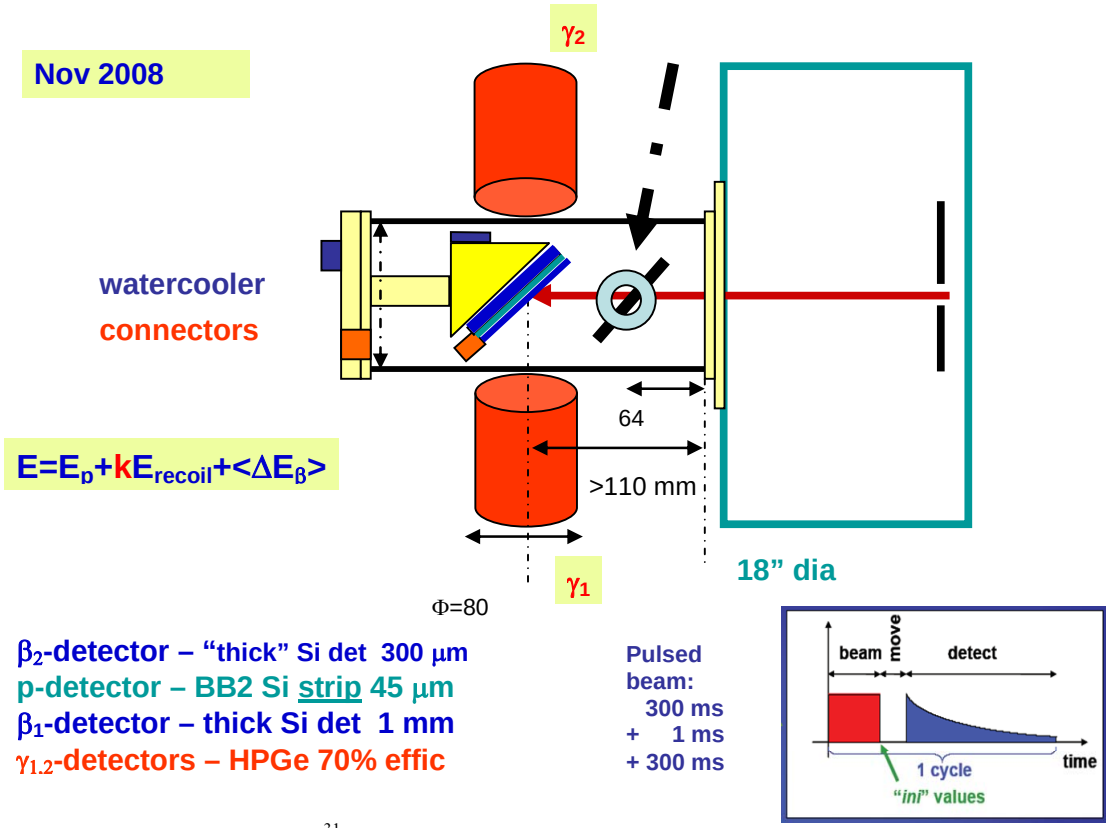

FIG. 1. The setup used for the ^{31}Cl run in Nov. 2008.

as the year before [2]: 3-4000 pps and 85% purity at the target detector. We used a setup as the one used before, except that we added now a second, identical, Ge detector.

The secondary beam was slowed down from about 34 MeV/u using the rotating Al degrader and was implanted in a thin detector (the "proton detector") in the middle of the Si telescope shown in Fig. 1. Two "beta detectors" were placed before and after it to detect the positrons emitted. We pulsed the beam from the cyclotron in cycles of 300 ms irradiation, 1 ms pause ("move") and 300 ms "detect" times. The measurements were only done off-beam in the last part of the cycle. To realize goal a) we replaced the W1-65 detector used previously with an even thinner detector and with narrower strips: a BB2-45 made by Micron Semiconductors Ltd., UK. To control the depth of the implantation distribution, and limit the rate impinging on the live detectors to <500 pps, we had to limit the momentum spread of the secondary beam to ± 0.27%. As expected, the background at low energies in the proton detector, due to the much more probable beta decay events not followed by the emission of a proton, was reduced very much. If in the previous detector we could see a large background below about 400 keV, in this case this background was pushed below 300 keV, or lower. In fact, at this point, the noise of the electronics was becoming the limiting factor. A proton spectrum is shown in the next report [3].

For the b) part of the experiment, we have removed the β_1 and the proton detector and replaced the latter with a 125 μm Al foil. The secondary beam was implanted in this thicker foil and we would open the momentum slits to obtain a larger rate. In each of the 70% HpGe detectors situated at 90° outside the chamber we obtained a statistics double from the one we had in Nov 2007. More recently, in spring of 2009, the lifetime of ^{31}Cl was measured with an accuracy <0.5% [4].

At this time, all data are still being analyzed.

[1] L. Trache *et al.*, *Progress in Research*, Cyclotron Institute, Texas A&M University (2006-2007), p. I-29; http://cyclotron.tamu.edu/2007%20Progress%20Report/index.html; L. Trache et al., *Progress in Research*, Cyclotron Institute, Texas A&M University (2007-2008), p. I-9; http://cyclotron.tamu.edu/2008%20Progress%20Report/index.html

[2] L. Trache *et al.*, Proceedings of the 10th Symposium on Nuclei in the Cosmos Mackinac Island, Michigan, July 2008; http://pos.sissa.it//archive/conferences/053/163/NIC%20X_163.pdf and arXiv/0901.0330.

[3] E. Simmons *et al.*, *Progress in Research*, Cyclotron Institute, Texas A&M University (2008-2009), p. I-8.

[4] V. E. Iacob *et al.*, (to be submitted).

Measurements of very low energy protons from β-delayed p-decays

E. Simmons, L. Trache, A. Banu, M. McCleskey, B. Roeder, A. Spiridon, R. E. Tribble
A. Saastamoinen,[1] J. Aysto,[1] T. Davinson,[2] P. J. Woods,[2] G. J. Lotay[2]
[1]*Department of Physics, University of Jyvaskyla, Jyvaskyla, Finland,*
[2]*School of Physics, University of Edinburgh, Edinburgh, United Kingdom.*

In the last two years, we have taken a strong interest in investigating beta-delayed proton decays of proton-rich nuclei, primarily motivated by unanswered questions in nuclear astrophysics. In particular we are looking at reactions important in H-burning in novae [1]. Through a series of experiments, we have developed a new experimental technique that has produced favorable results. The general set-up includes a thin Si strip detector (proton detector) in front of a thicker Si detector (beta detector), although in the more recent experiments for ^{23}Al and ^{31}Cl a thin Si detector was also placed in front of the proton detector to act as a second beta detector. The two (or three) detectors are then mounted onto an Al frame and cooled with water running through a pipe on the back of the frame in order to help reduce the noise. This telescope is placed at 45° with respect to the beam axis so that Ge detectors (one or two, depending on the experiment) may be placed close to the chamber and at 90° with respect to the beam axis in order to detect the gamma rays. The resonances of interest require that we measure low energy protons. To do this we chose to implant the exotic nuclei in the center of the proton detector. We produce and separate these nuclei with MARS, in-flight, in inverse kinematics. For implantation we slow them from 30-40 MeV/u by using a rotatable Al degrader, which is controlled such that the source nuclei of interest are stopped in the center of the proton detector. The beam from the cyclotron was then pulsed on and off, with cycles depending on their lifetime. We have applied this technique for ^{23}Al [2] and ^{31}Cl [3]. Here we want to report on efforts made to lower the minimum proton energy that we can measure.

In both cases studied, the proton branchings are very small, at the percent level. Each decaying event produces a small signal in the proton detector due to the energy loss of the positron. This is a continuum spectrum, with shape and maxima given by the size and thickness of the detector. In the rarer case when a proton is emitted after beta decay, the proton is fully stopped in a few microns of Si and all energy of the proton (hundreds of keV or more) adds to the energy loss of the positron. This results in proton peaks with a tail on their high-energy side. This tail depends on how thick and large the detector is, and affects the resolution, of course. More importantly, the thickness and size of the detector determine the shape of the beta-only background continuum at low energy (about 200 keV to 500 keV), limiting the minimum proton energies which can be measured. In this region, the continuous beta contribution becomes a dominant feature. When it is combined with the noise that arises from the beam line and electronics, the peaks can not be clearly identified. A goal of our recent beta-delayed proton decay experiments was to minimize this beta contribution as much as possible. One way to do this is to change the dimensions of the proton detector. Two different proton detectors have been used up to this point in time, the W1 and the BB2, both created by Micron Semiconductor Ltd.

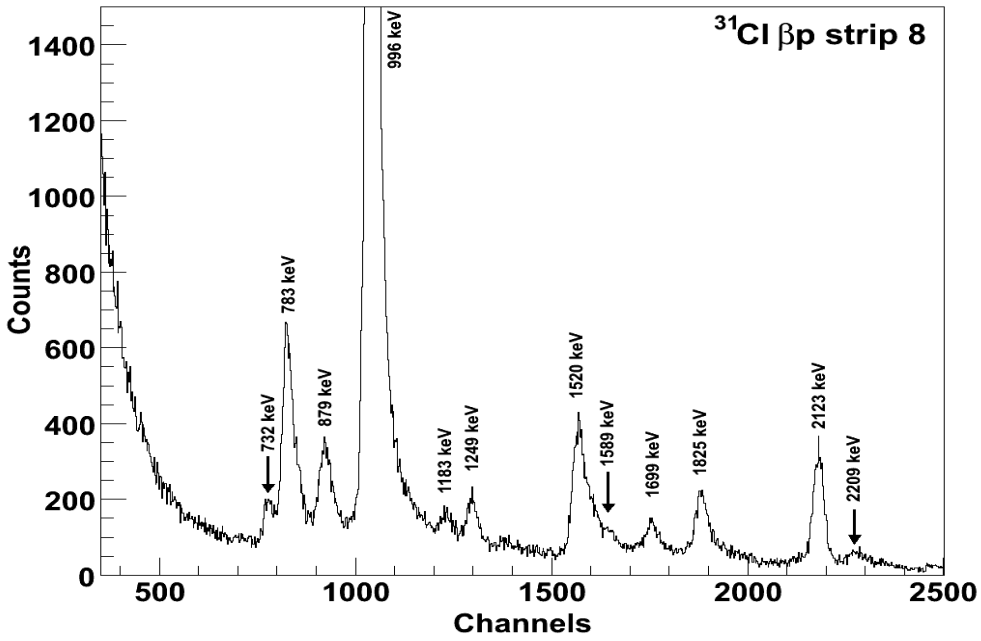

FIG. 1. A proton spectrum from the ^{31}Cl experiment done in 2007 with the W1-65 proton detector.

The ^{23}Al and ^{31}Cl experiments that were preformed in 2007 both used a W1-65 as proton detector. This Si detector has 16 strips on the front and 16 strips on the back, it is 65 μm thick and the width of the strips is about 3.1 mm. A reasonable 40 keV (fwhm) resolution was obtained for the proton peaks and the spectra are virtually background free down to about 400 keV (Fig. 1). Below these energies, a beta continuum is clearly visible and becomes a problem for the identification of low energy proton peaks. In order to minimize the background we put a multiplicity $M_x=M_y=1$ condition on x- and y- strips, and that the energies measured on each side are equal. In more recent ^{23}Al and ^{31}Cl experiments we have used a BB2-45 Si strip detector for protons. The BB2 detector has 24 strips on the front and 24 on the back. It is

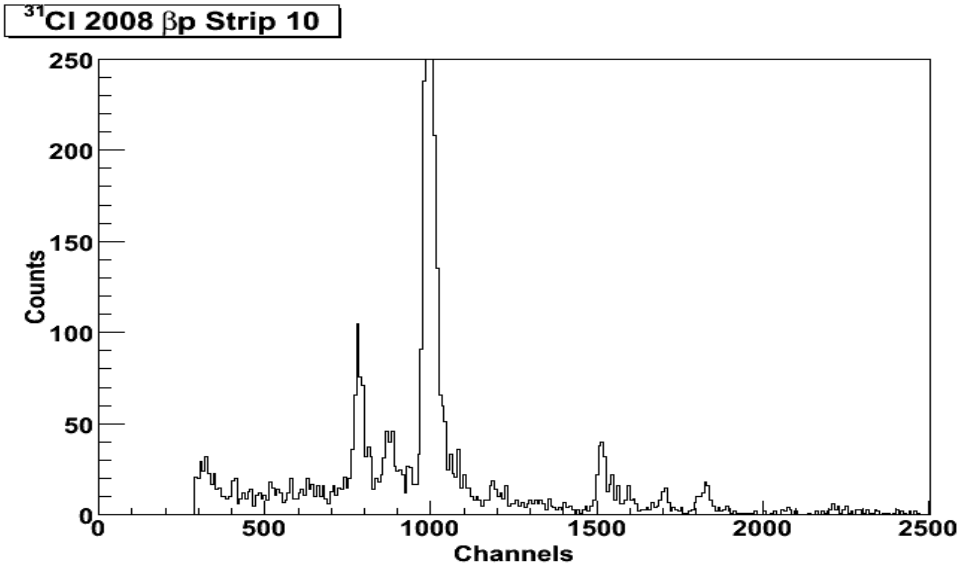

FIG. 2. A spectrum from the ^{31}Cl experiment done in 2008 with the BB2-45 proton detector. Only part of statistics is shown, but resolution is visibly better and the minimum energy threshold goes below 300 keV.

45 μm thick and its strips are about 1mm in width. Comparing the results of these experiments we found that decreasing the width of the strips and making the proton detector thinner noticeably reduced the beta continuum in the low-energy range and allowed the peaks to become more visible. Same multiplicity and energy conditions were used. At this point, the beta continuum became lower than the electronic noise in our setup, and the noise was the limiting factor (Fig. 2). The spectra are clean down to 280 keV or lower.

[1] A. Coc, *Proceedings of the 10th International Symposium on Origin of Matter and Evolution of Galaxies (OMEGA07)*; http://nucl.sci.hokudai.ac.jp/~omeg07/.

[2] L. Trache *et al.*, *Progress in Research*, Cyclotron Institute, Texas A&M University (2006-2007), p. I-29; http://cyclotron.tamu.edu/2007%20Progress%20Report/index.html

[3] L. Trache et al., *Progress in Research*, Cyclotron Institute, Texas A&M University (2006-2007), p. I-9; http://cyclotron.tamu.edu/2008%20Progress%20Report/index.html

Production of new radioactive beams ^{46}V, ^{6}He, ^{20}Mg and ^{13}O with MARS

L. Trache, A. Banu, M. McCleskey, B. Roeder, E. Simmons, A. Spiridon, R. E. Tribble, V. Goldberg, H. I. Park, P. J. Woods,[1] G. Lotay,[1] and D. Shetty[2]

[1]*School of Physics, University of Edinburgh, Edinburgh, United Kingdom,*

[2]*Western Michigan University, Kalamazoo, Michigan*

This year we continued to produce and separate radioactive beams needed for our physics program using the Momentum Achromat Recoil Spectrometer MARS. For years this has become a well-known process and it is typical that MARS tuning takes less than a shift, even for new cases. A few of the beams this year were new and special in one way or another: ^{6}He, ^{13}O, ^{20}Mg, ^{46}V. A few of the parameters and the performances obtained are presented here.

In August 2008, we studied the production and separation of ^{46}V. We used a primary beam of ^{47}Ti accelerated to 30 MeV/u. The target was H_2 gas cooled at LN_2 temperature. The gas cell windows were made of thinnest havar foils we have (0.16- mils=4 μm each) and the pressure inside was 2 atm. The secondary beam of ^{46}V was produced in the fusion-evaporation reaction p(^{47}Ti, ^{46}V)2n. The secondary beam was identified and tuned with a 989μm position sensitive detector in the focal plane of MARS (the "target detector"). Fig. 1 shows the energy loss versus Y position in the target detector, with the final slits SL4 open vertically to ±1.6 cm, before the final separation of ^{46}V. The N=Z+2, N=Z+1 and N=Z lines of isotopes are clearly visible. In the end we have centered the N=Z species in the center of the detector and closed the vertical slits to ±0.40 cm to select the desired species. The final production rate obtained for

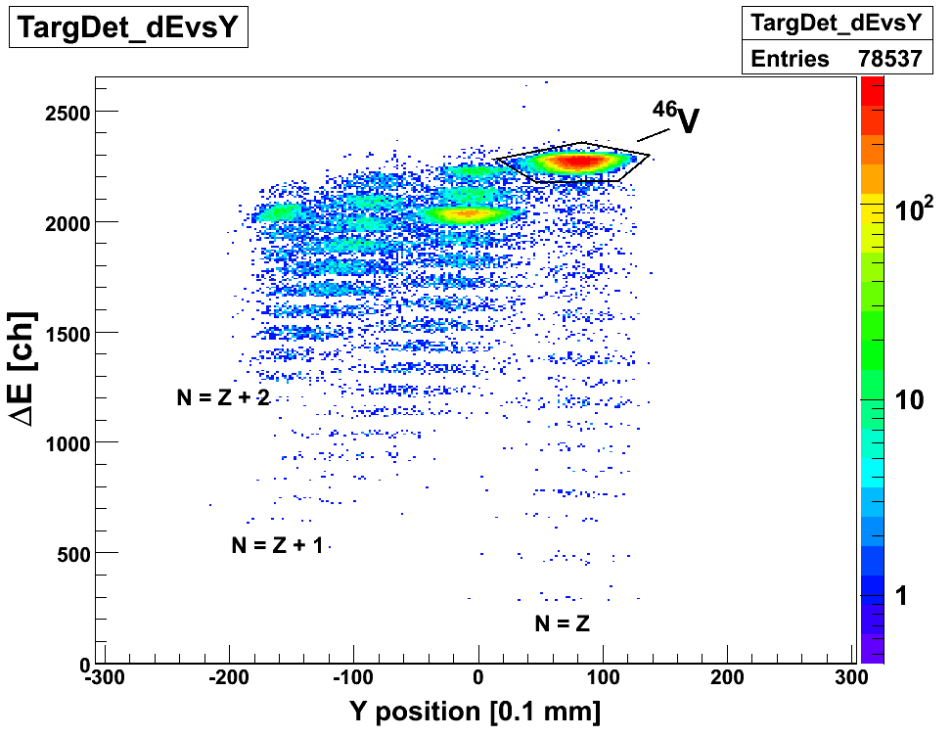

FIG. 1. Production of ^{46}V. Energy loss versus position on Y axis.

^{46}V was 1300 events/nC (incident beam measured in coffin) with 3% impurities. The impurities are due mostly to reactions of the beam with the gas cell windows. Later in the year we have used isotopically enriched ^{47}Ti in the ECR source and increased the energy of the incident beam to 32 MeV/u. We have delivered about 20 kHz of ^{46}V for the group of Prof. J.C. Hardy. They made precision lifetime measurements, part of the on-going program to study superallowed β-decays.

A few months later, we produced and separated ^{6}He. We investigated different production mechanisms with two primary beams: $^{7}Li^{+2}$ at 20 MeV/u and $^{7}Li^{+1}$ at 8 MeV/u. The target was deuterium gas cooled at LN_2 temperature. The gas cell windows were again 0.16 mils thick each and the pressure inside was 1.5 atm. We started with $^{7}Li^{+2}$ as primary beam and we investigated three mechanisms: fragmentation, transfer and fusion-evaporation. The fragmentation reaction ($v_{6He} = v_{7Li}$ at 20 MeV/u) was the only one to yield a significant production rate, 280 ev/nC. With $^{7}Li^{+1}$ as primary beam we investigated the transfer reaction d(^{7}Li, $^{6}He_{g.s.}$)$^{3}He_{g.s.}$ and observed a production rate for ^{6}He of 233 ev/nC. This beam is intended for experiments proposed by a group from Western Michigan University.

In February 2009, we prepared for another experiment in the series of measurements of β-delayed proton decay of proton-rich nuclei [1]. The aim of this experiment, planned with the group from the University of Edinburgh, is to measure the β-p emission from ^{20}Mg and use these measurements to study the 448 keV resonance, of crucial importance for the ^{19}Ne(p,γ)^{20}Na reaction in stars. For now, the purpose of the run was to study the production and separation of ^{20}Mg, before starting the decay measurements. The ^{20}Mg beam was obtained from a beam of ^{24}Mg at 48 MeV/u through fragmentation on a 306μm Be target. Fragmentation is not the typical production mechanism used in MARS, so far. The major problems were, as expected, a low production rate for ^{20}Mg and a very large contamination with ^{10}C, of same q/m, which cannot be avoided in the present MARS configuration. After separation with MARS, we have also tried to use Al degraders placed after the target to attempt reducing an observed background scattering (off the degrader ladder?!) and the ^{10}C contamination. We tried two thicknesses for the degrader, 15 mil and 25 mil. The latter gave better ^{20}Mg to ^{10}C ratio, 0.06, and ^{20}Mg production rate, 1.5 ev/pnC. We estimate that even this very low rate obtained will suffice for the proposed experiment and the large contamination with ^{10}C will not affect the off-beam measurement because these ions pass through the thin proton detector, but we intend to try other reactions to find better production rate and purity.

Another challenging secondary beam obtained this year was ^{13}O. We have developed it for the study of the unbound ^{14}F nucleus using the resonant elastic proton scattering in inverse kinematics and the thick target method. We started from a ^{14}N primary beam at 38 MeV/u incident on the H_2 gas-cell at p=3 atm. We have obtained a production rate of 13.2 part/nC and a total rate of about 4000 pps. The purity of the beam was 75% with ^{10}C the main impurity. The intended experiment was performed in two runs in March and April and is described separately [2].

[1] L. Trache *et al.*, *Progress in Research*, Cyclotron Institute, Texas A&M University (2007-2008), p.I-11; http://cyclotron.tamu.edu/publications.html

[2] V. Goldberg *et al.*, *Progress in Research*, Cyclotron Institute, Texas A&M University (2008-2009), p.I-21.

The structure of ^{23}Al studied with breakup at intermediate energies

A. Banu, L. Trache, B. Roeder, E. Simmons, R. E. Tribble, F. Carstoiu,[1]F. Negoita,[1]
F. Rotaru,[1] N. Orr,[2] L.Achouri,[2] B. Laurent,[2] M. Chartier,[3] B. Fernandez-Dominguez,[3]
S.Paschalis,[3] B. Pietras,[3] P. Roussel-Chomaz,[4] L. Gaudefroy,[4] R. Lemmon,[5] M. Labische,[5]
W. Catford,[6] N. Patterson,[6] J. Thomas,[6] M. Freer,[7] M. Horoi,[8] and Bonaccorso[9]
[1]*IFIN-HH, Bucharest, Romania,*
[2]*LPC, Caen, France,*
[3]*University of Liverpool, Liverpool, United Kingdom,*
[4]*GANIL, Caen, France,*
[5]*CCLRC Daresbury Laboratory, Daresbury, United Kingdom,*
[6]*University of Surrey, Surrey, United Kingdom,*
[7]*University of Birmingham, Birmingham, United Kingdom,*
[8]*Central Michigan University, Mount Pleasant, Michigan,*
[9]*University of Pisa, Pisa, Italy*

We report on the use of one proton-removal reactions of loosely bound nuclei at intermediate energies as an indirect method in nuclear astrophysics, with particular reference to the results of an experiment carried out at GANIL that investigated a cocktail beam around ^{23}Al at 50 MeV/nucleon. Momentum distributions of the core fragments, inclusive and in coincidence with γ rays detected at the target position with 8 Germanium clovers of the powerful gamma spectrometer EXOGAM [1], were measured. The parallel and transverse momentum distributions of the core measured in one-nucleon removal (breakup) reactions are the spectroscopic tools available to determine the single particle structure of the loosely bound, exotic nuclei, due to their sensitivity to the angular momentum of the orbital involved. By measuring the core momentum distributions, from the shape one can determine the quantum numbers of the s.p. orbital, and from the integrated total and partial cross sections one is able to extract the corresponding asymptotic normalization coefficients (ANCs) of the wave function's components [2]. One can extract also the spectroscopic factors, but the values are parameter dependent. Our experiment was aimed to determine with an independent method the structure of the ground state of ^{23}Al by measuring the inclusive one-proton breakup cross section at intermediate energies, as well the configuration mixing from coincidences with gamma rays from the ^{22}Mg core left excited after the proton removal. The proton breakup reactions can provide information needed to determine astrophysical reaction rates for radiative proton captures (p,γ) that are outside the reach of other direct or indirect methods, or can give complementary information to the one obtained from transfer reactions (the ANC method [3]) which requires radioactive beams of much better purity and intensity. This new method was successfully applied in the past to the study of ^{8}B [2] and ^{9}C [4] breakup and the ANCs determined were used to determine the astrophysical S-factors for the proton radiative capture reactions ^{7}Be(p,γ)^{8}B and ^{8}B(p,γ)^{9}C, respectively.

The method has also the advantage that can be used for beams of low quality, such as cocktail beams, and intensities as low as a few pps. In the experiment E491 at GANIL, a primary ^{32}S beam at 95 MeV/u impinged on a C target and SISSI was used to separate 14 secondary beams at 1.95 Tm rigidity.

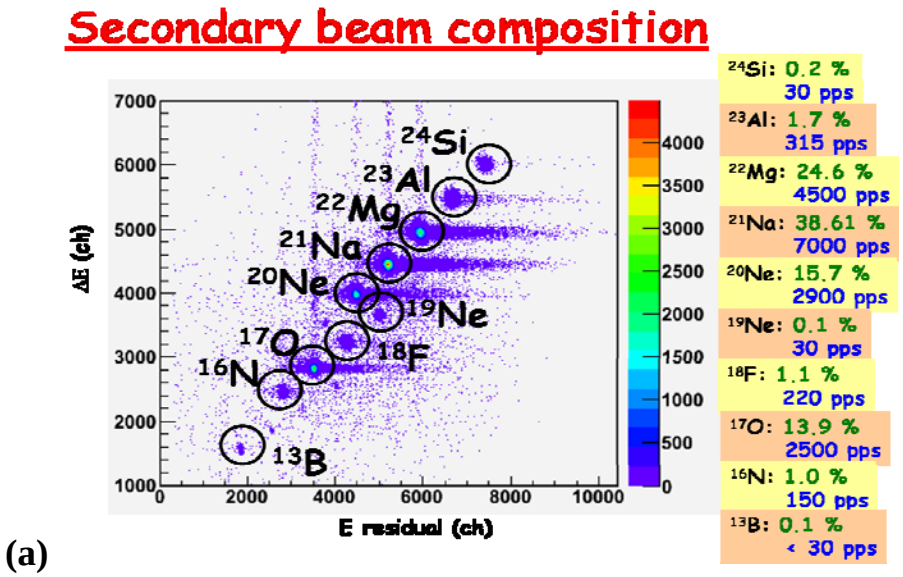

(a)

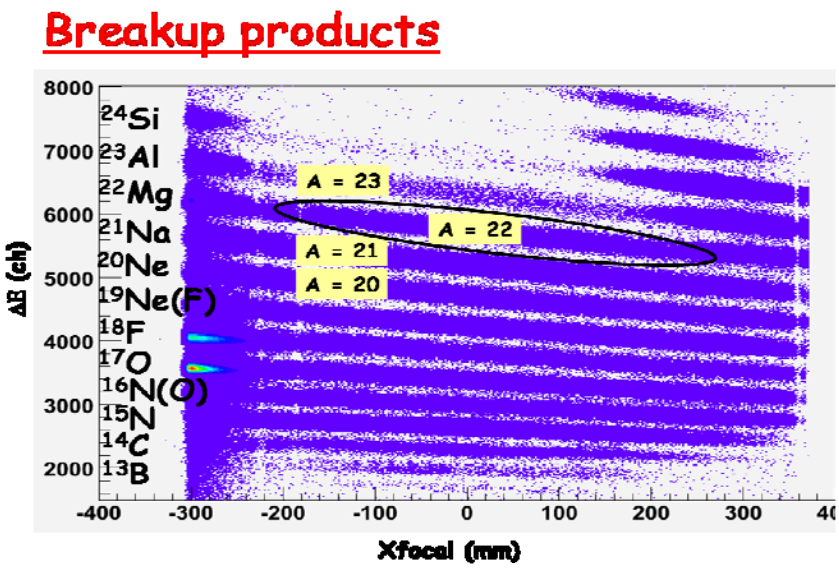

(b)

FIG. 1. (a) Composition of the secondary cocktail beam: 14 ion species were produced, their production rates is also illustrated in the figure. (b) Separation of the breakup products by their mass and position in the focal plane of the SPEG energy loss spectrometer at GANIL. The "gate" corresponding to mass A = 22 shows the distribution of the ^{22}Mg fragments resulted from ^{23}Al breakup.

They impinged on another C target at the entrance of the spectrometer SPEG that was tuned to measure the momentum of the cores after one-proton removal. EXOGAM was positioned around the target. Only preliminary results on the proton breakup of ^{23}Al are presented in the following. Fig. 1 (a) shows the composition of the secondary cocktail beam that was used in the experiment along with the production

rates for some of the 14 ion species. Fig. 1 (b) shows the selection of the breakup fragments by their mass and position in the focal plane of the SPEG energy loss spectrometer at GANIL. Fig. 2 (a) shows the gamma lines detected by EXOGAM in coincidence with the fragments resulting from the breakup of ^{23}Al.

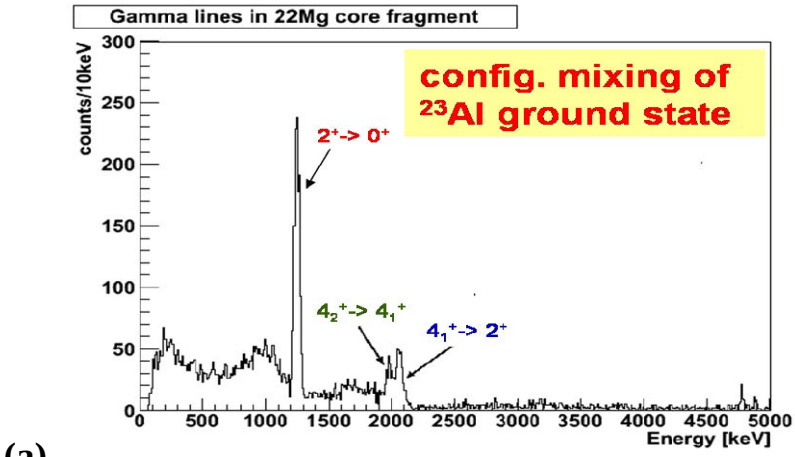

(a)

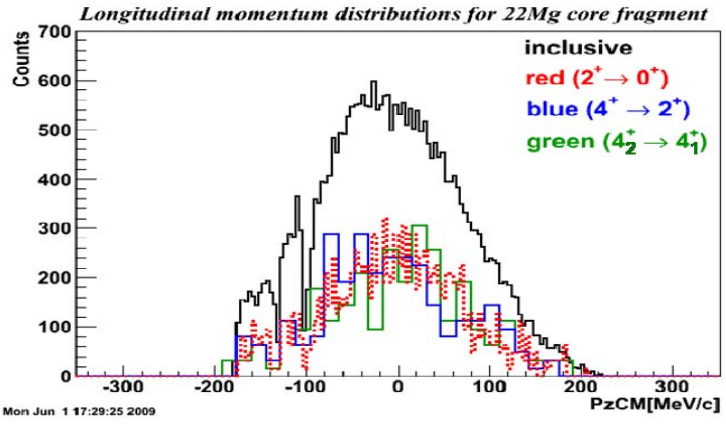

(b)

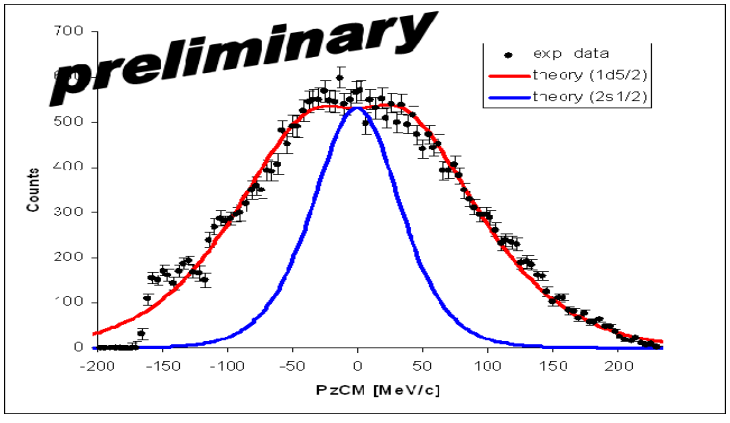

(c)

FIG. 2. (a) Measured gamma lines (Doppler corrected) depopulationg excited states in ^{22}Mg breakup fragments: 1246.98 keV, 1984.8 keV, and 2061.09 keV giving us information about the configuration mixing characterizing the ground state of ^{23}Al. (b) Corresponding longitudinal momentum distributions in the rest frame along with the inclusive longitudinal momentum distributions. Their widths are about 200 MeV/c (FWHM) and are reproduced by theoretical calculations for d5/2 wave states. Note that the drops around -100 and -140 MeV/c are of instrumental nature, reflecting some non-functioning pads in the SPEG focal plane detectors. (c) Direct comparison between experimental inclusive longitudinal momentum distribution and the theoretical calculations: in red colour with d5/2 wave states and in blue colour with s1/2 wave states. (See text for details)

An add-back procedure was implemented and used here to increase the gamma-ray detection efficiency, and the spectrum is corrected for Doppler shift. The lines observed correspond to transitions in ^{22}Mg, attesting that the ^{22}Mg core is left in various excited states after the removal of the least bound proton. That provides us with information about the configuration mixing that characterizes the ground state of ^{23}Al. We observe clearly three gamma lines: 1246.98 keV ($2_1^+ \rightarrow 0_{gs}^+$), 2061.09 keV ($4_1^+ \rightarrow 2_1^+$), and 1984.8 keV ($(3^+,4^+,5^+) \rightarrow 4_1^+$), attesting for a large and complex configuration mixing. Fig. 2 (b) shows the corresponding longitudinal momentum distributions in the rest frame of the projectile and the inclusive longitudinal momentum distribution. The widths of these momentum distributions are approximately 200 MeV/c (FWHM) and are reproduced by theoretical calculations carried out with an extended version [5] of the Glauber model incorporating second-order noneikonal corrections. Double folding semi-microscopic potentials proton-target and core-target were calculated using the JLM effective nucleon-nucleon interaction. The potentials were used to evaluate the scattering matrix elements needed to describe the nuclear breakup process. The measured momentum distributions for the ^{22}Mg core agree in shape (about 200 MeV/c width) with those calculated for the $1d_{5/2}$ orbital, not with those for $2s_{1/2}$ (about 60 MeV/c width), as illustrated in Fig. 2 (c). This confirms the ground state spin and parity for ^{23}Al to be $J^\pi = 5/2^+$, not $1/2^+$, a distinction very important for the rate of the astrophysical reaction, and in agreement with the results from beta decay [6]. A detailed discussion of these results will be given elsewhere [7].

[1] F. Azaiez and W. Korten, Nucl. Phys. News, **7**, Nr. 4, 21 (1997).

[2] L. Trache *et al*., Phys. Rev. Lett. **87**, 271102 (2001) ; L. Trache, F. Carstoiu, C. A. Gagliardi, R. E. Tribble, Phys. Rev. C **69**, 032802 (R) (2004).

[3] H. M. Xu, C. A. Gagliardi, R. E. Tribble, A. M. Mukhamedzhanov, and N. K. Timofeyuk, Phys. Rev. Lett. **73**, 2027 (1994); A. M. Mukhamedzhanov *et al*., Phys.Rev. C **56**, 1302 (1997); C. A. Gagliardi *et al*., Phys. Rev. C **59**, 1149 (1999).

[4] L. Trache, F. Carstoiu, A. M. Mukhamedzhanov, and R. E. Tribble, Phys. Rev. C **61**, 024612 (2000).

[5] F. Carstoiu, E. Sauvan, N. A. Orr, and A. Bonaccorso, Phys. Rev. C **70**, 054602 (2004).

[6] V. E. Iacob, Y. Zhai, T. Al-Abdullah, C. Fu, J. C. Hardy, N. Nica, H. I. Park, G. Tabacaru, L. Trache, and R. E. Tribble, Phys. Rev. C **74**, (2006) 045810; A. Ozawa *et al.*, Phys. Rev. C **74**, 021301 (R) (2006).

[7] A. Banu *et al*., (to be submitted).

Use of neutron transfer reactions to indirectly determine neutron capture cross sections on neutron-rich nuclei

M. McCleskey, A. M. Mukhamedzhanov, R. E. Tribble, L. Trache, E. Simmons, A. Spiridon, A. Banu, B. Roeder, V. Goldberg, X. F. Chen, and Y.-W. Lui

Cross sections for the capture of low-energy neutrons on unstable neutron-rich nuclei are important for nuclear science and their reliable knowledge is increasingly requested by nuclear astrophysics to test quantitatively the nucleosynthesis in the r-process, by nuclear engineering for the design of new reactors using novel fuel cycles, and by national security. It is difficult, and in many cases impossible, to make direct measurements for all the reactions for which good cross sections are needed. We must build systematics, make structure and reaction models, and use indirect approaches. One such approach is to combine several neutron transfer reactions at different laboratory energies to extract information that can be used to determine reliably neutron capture cross sections at low energies.

The radiative neutron capture reaction ^{14}C(n,γ)^{15}C is being used as a test case for such an indirect determination. Our approach intends to combine information from the peripheral reaction of 12 MeV/u ^{14}C on a thin ^{13}C target and the non-peripheral reaction of 60 MeV deuterons on a thin ^{14}C target, both populating the same states in neutron-rich nucleus ^{15}C. From the ^{13}C(^{14}C,^{15}C)^{12}C experiment we will determine the asymptotic normalization coefficient (ANC) and we will use the non-peripheral (d,p) reaction on ^{14}C to obtain the spectroscopic factor (SF) which will then be used to calculate the radiative capture at astrophysical energies.

Unlike proton capture at astrophysical energies, neutron capture is not an entirely peripheral process. As such, there will be a contribution from the interior of the nucleus when computing the transition matrix element:

$$\sigma_{(n,\gamma)} = SF\left|\langle \Phi_{B=(An)} \left| O_{elm} \right| \Phi_A \chi_n^{(+)} \rangle\right|^2$$
$$= SF\left|M_< + M_>\right|^2 = \left|(SF)^{1/2} M_< + C_{nlj}\left(M_> / b_{nlj}\right)\right|^2 \qquad (1)$$

The overlap integral $\langle \Phi_B | \Phi_A \rangle$ in the exterior region behaves as $b_{nlj} h_l(ikr)$ where h_l is a Hankel function and the normalization factor b_{nlj} is the single particle ANC. Therefore,

$$M_> \approx b_{nlj} \langle h_l(i\kappa r) \left| O_{elm} \right| \chi_n^{(+)} \rangle$$

and for the correct evaluation of the second term in Eq. (1), the knowledge of the ANC (C_{nlj}) extracted from peripheral reactions is sufficient, but for the evaluation of the first one an unambiguous determination of the SF and of the overlap integral in the interior of the nucleus are also needed. For a peripheral reaction like (p,γ), the ANC would be all that is needed, however we will also have to consider the contribution from the interior for a (n,γ) reaction. Information to assess it can be extracted from a combination of neutron transfer reactions.

Progress in the analysis of the $^{13}C(^{14}C,^{15}C)^{12}C$ experiment

In September of 2007 we measured neutron transfer and elastic scattering of a 12MeV/u ^{14}C beam on a thin ^{13}C target using the MDM spectrometer and the MDM detector. At 12 MeV/u the transfer of a neutron from the ^{13}C target to the ^{14}C beam is a peripheral process. The goal of that experiment was to determine the ANC for ^{15}C. Elastic scattering was measured to determine the optical model potential (OMP) needed for DWBA calculations.

Position calibration of the detector was achieved through the elastic scattering of the beam off a 200μg/cm^2 Au target, which then passed through a five finger mask. Position at each of the four position sensitive avalanche counters was calculated for the five resulting rays using RAYTRACE code. The calculated positions were compared with those observed and a linear fit was made. RAYTRACE was also used to perform the raytrace reconstruction where the angle and position in the focal plane observed in the detector was related to the scattering angle in the target and the excitation energy. The angular distribution from 2 to 20 degrees in the lab frame was measured for elastic scattering of ^{14}C on ^{13}C and for the neutron transfer reaction $^{13}C(^{14}C,^{15}C)^{12}C$ from 2 to 8 degrees.

The elastic scattering cross section is compared in Fig. 1 with that calculated with an OMP obtained from a semi-microscopic double folding procedure using the JLM effective interaction. The optical model parameters (renormalizations and ranges) N_V=0.37, N_w=0.70, t_V=1.2 fm and t_W=1.75 fm were those from the general procedure established earlier from the study of elastic scattering of loosely

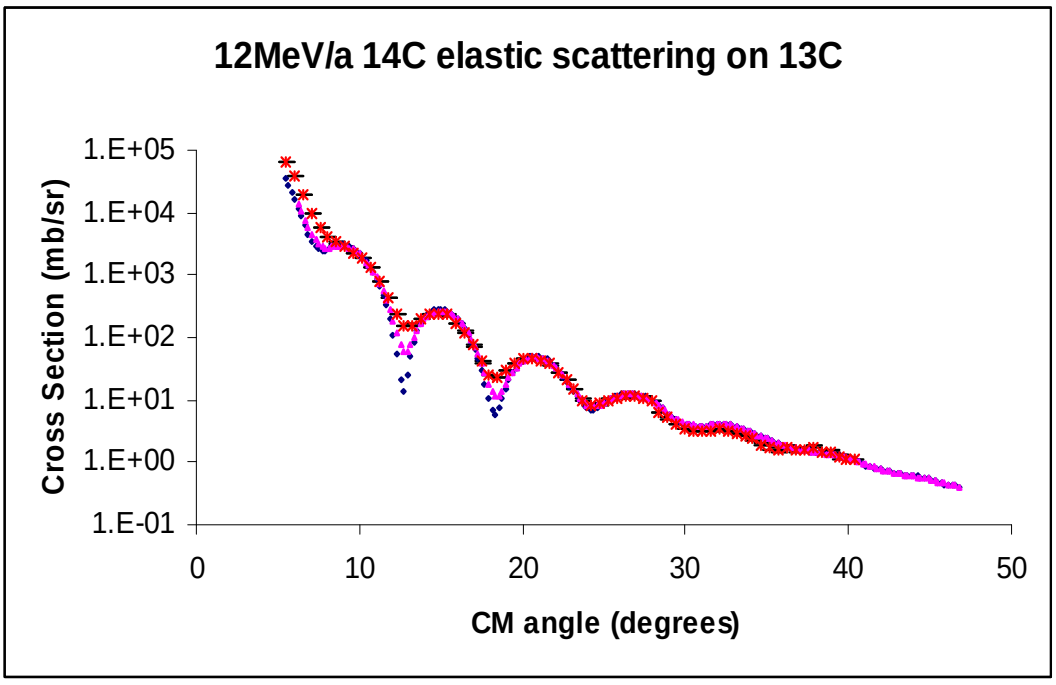

FIG. 1. Elastic scattering of 12MeV/a ^{14}C on ^{13}C. The red X's are the measured elastic scattering with statistical error bars shown; the blue squares are the calculation made using an optical model potential and a double folding procedure; the magenta triangles are the same calculation but smoothed using a Gaussian smearing function.

bound p-shell nuclei [1,2]. The overall agreement is good; in particular, the position of the minima and maxima, the oscillation period and the trend of the absorption are reproduced, therefore no further optimization was attempted at this stage. Then, the surface region of this potential was fitted with a Woods-Saxon potential, which was used to perform a DWBA calculation of the neutron transfer $1p_{1/2} \rightarrow 2s_{1/2}$ using the PTOLEMY code (Fig. 2). The normalization of the DWBA calculated cross section to the

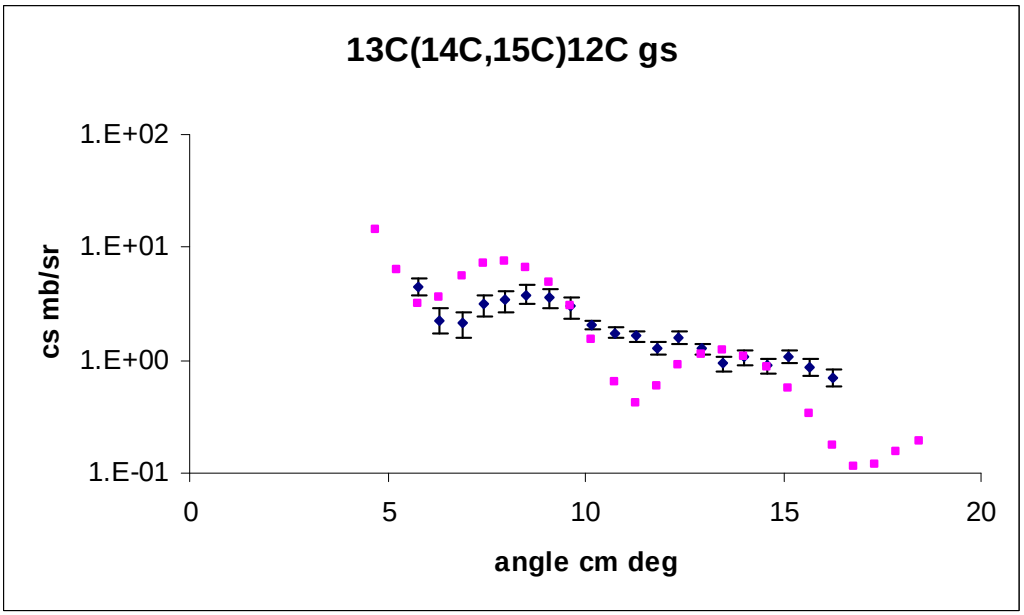

FIG. 2. Neutron transfer of 12MeV/a ^{14}C from ^{13}C forming ^{15}C in the ½$^{+}$ ($2s_{1/2}$) ground state. The blue diamonds are the experimental results, the magenta squares are the DWBA calculation using PTOLEMY.

experimental measurement gives the spectroscopic factor.

$$\frac{d\sigma}{d\Omega}_{\exp} = SF(^{13}C,1p_{1/2}) \cdot SF(^{15}C,2s_{1/2}) \frac{d\sigma}{d\Omega}_{DWBA}$$

The single particle ANC, b, is found by taking the ratio of the wave function calculated in the asymptotic region to the Hankel function over the radius. The ANC for ^{13}C(1p1/2) is known to be C^2=2.40 +/- 0.12 fm^{-1} [1]. Finally, this gives us the ANC for ^{15}C using:

$$C^2 = SF \cdot b^2$$

We found $C^2(2s_{1/2}) = 1.91 \pm 0.17$ fm^{-1} (this value is still preliminary).

There is a discrepancy of approximately a factor of two in the measured elastic scattering at small angles (less than 4 degrees lab) compared with the calculated value. Also, the low-lying, first excited J^{π}=5/2^{+} state 0.74 MeV in ^{15}C dominated the transfer measurements and the cross section for the ground state was very low. Therefore, in May of 2009, we performed a second experiment with the same beam and target as in 2007; however, we used the Oxford detector, which allowed for a better particle ID. Scattering off the gold target was measured at both +4 and -4 degrees (lab) and the comparison of the cross sections at these angles indicates that the angle measured on MDM was off by approximately 0.3

degrees. Elastics and neutron transfers on ^{13}C were re-measured from 2 to 17 degrees. Particle ID using the energy loss and residual energy signals from the Oxford detector is shown in Fig. 3. Analysis of this experiment is ongoing. The above preliminary results will likely change once the correction for spectrometer angle is made and the additional statistics for the transfer reaction is added.

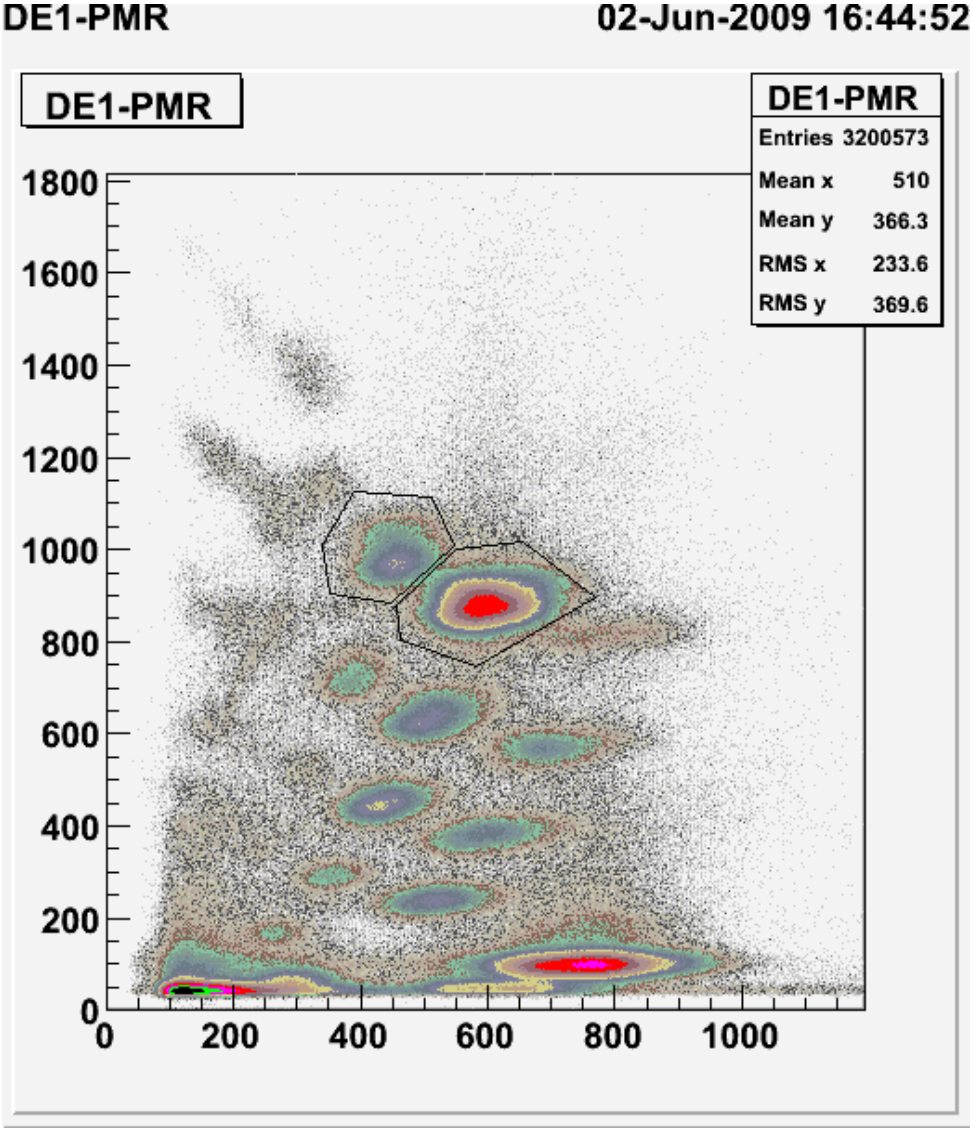

FIG. 3. Particle ID using ΔE-E_{res}

[1] L. Trache *et al.*, Phys. Rev. C **61**, 024612 (2000).

[2] F. Carstoiu *et al.*, Phys. Rev. C **70**, 054610 (2004).

[3]. T. Al-Abdullah, PhD thesis, Texas A&M University, 2007.

Search for ^{14}F via the reaction ^{13}O + p

V. Z. Goldberg, G. G. Chubarian, B. T. Roeder, A. Banu, M. McCleskey, E. Simmons, G. Tabacaru, L. Trache, R. E. Tribble, G. V. Rogachev,[1] E. Johnson,[1] M. A. Coronado,[1] J. Mitchell,[1] and C. Fu[2]

[1]*Department of Physics, Florida State University, Tallahassee, Florida 32306, USA*

[2]*National Institute of Standards and Technology (NIST), Gaithersburg, MD, USA*

Beams of exotic (radioactive) nuclei are mainly used to obtain new data on exotic nuclei in nuclear reactions. These beams are most easily produced at high energies (> 30 MeV/u) via projectile fragmentation or fusion-evaporation reactions in inverse kinematics due to the high negative Q-value for these reactions. Therefore, the beam ions produced in the reactions also have relatively high energy. However, various experimental and theoretical considerations often require lower energy beams (< 10 MeV/u). In these cases, the ISOL method of exotic beam production is preferable, where available. Unfortunately, as one approaches the limits of particle stability and the time delay between the beam production in the ISOL target and re-acceleration increases, the final yield for the most exotic nuclei is greatly reduced. Taking into account the low cross section for the initial production of the most exotic nuclei, slowing down the beam in a medium and then re-accelerating could result in a non-negligible loss in intensity.

In a recent experiment at the Texas A&M University (TAMU) Cyclotron Institute, a search for the resonance states in ^{14}F was conducted. There exist no experimental data on this exotic odd-odd nucleus. ^{14}F has three neutrons less than the lightest known particle-bound Fluorine isotope (^{17}F) and is also expected to be unstable to proton decay [1]. To study ^{14}F, the reaction ^{13}O+p resonant scattering employing the thick target inverse kinematics method (TTIK) [2] was used. The most effective reaction to produce ^{13}O ($T_{1/2}$=8.6ms) at TAMU was found to be ^{1}H(^{14}N, ^{13}O)2n (Q-value = =-29.1 MeV) with E(^{14}N) ≥ 31.2 MeV/u. However, the TTIK requires that the beam energy should be relatively low (~10 MeV/u) [3].

Since the ISOL method mentioned above is unavailable at TAMU and difficult or impossible to use at other facilities for ^{13}O, we used a different approach for the experiment. The ^{13}O secondary beam was produced with a ^{14}N primary beam at 38 MeV/u impinging on a hydrogen gas target, cooled by liquid nitrogen, with a pressure of 3 atm. The 31 MeV/u ^{13}O beam resulting from the fusion-evaporation reaction was then separated and delivered to the target chamber with the conventional MARS [4] approach. The intensity of the ^{13}O secondary beam was ≈5x10^{3} p/s for a ^{14}N beam intensity of ≈100 pnA. A thick polypropylene foil of (≈1.5 mm) was placed in the middle of the MARS scattering chamber to degrade the beam energy of the ^{13}O (see Fig. 1). This energy degrader was necessary in order to reduce the ^{13}O beam to the energies required for the TTIK method. Next, the beam passed through a 0.1 mm Bicron-400 plastic scintillator placed 100 mm downstream from the polypropylene foil. Two PMTs around the scintillator provided the start time signal and a measurement of the intensity of the beam. The sum of the PMT signals was also used to analyze the specific energy loss in the scintillator. The 10% energy resolution provided for complete separation of ^{13}O events from ^{10}C events (≈12% contamination in the beam) (Fig. 2). Following the scintillator (10mm distance), the beam enters the TTIK scattering

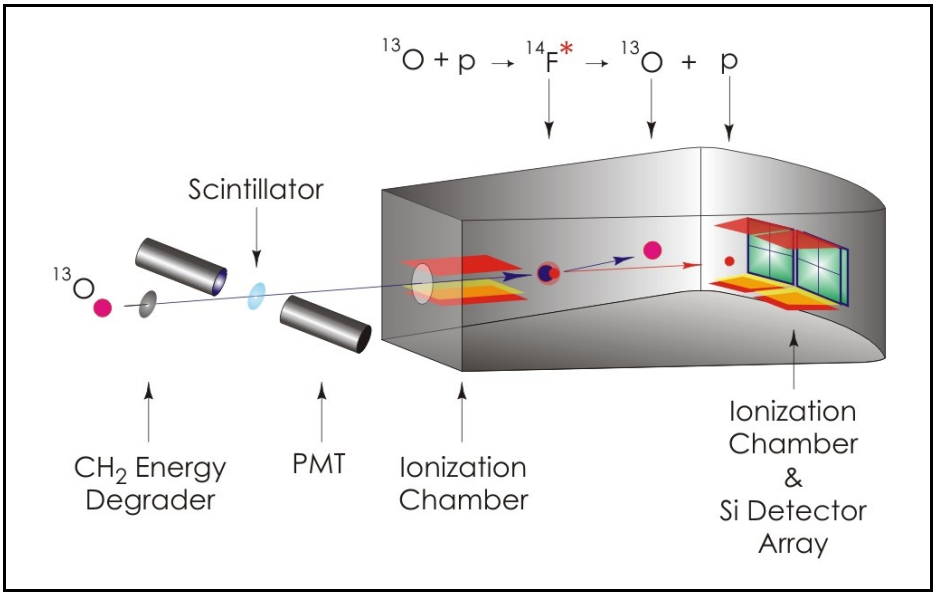

FIG. 1. Diagram showing the TTIK chamber and the detector setup

chamber [3] (see Fig. 1) through a thin Havar window (3μm). The TTIK chamber was filled with methane gas (CH_4) to provide the target to study the ^{13}O+p resonant interaction. At the entrance of the TTIK

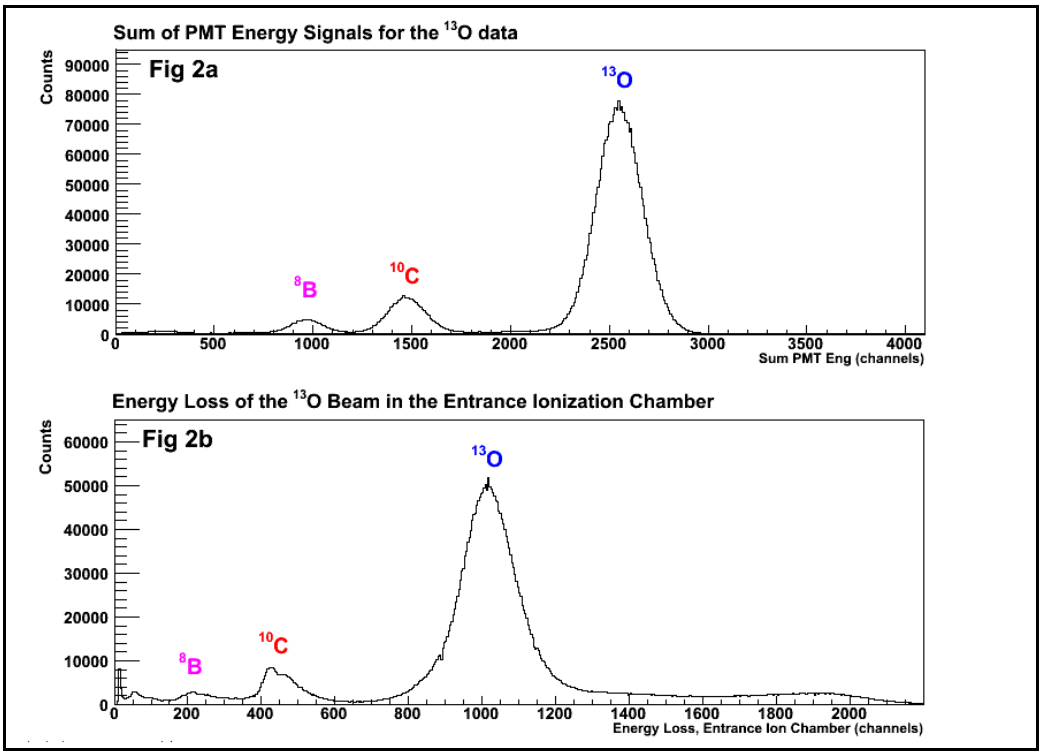

FIG. 2. Energy spectra obtained from the sum of the PMT signals (2a) and the energy loss in the Entrance Ionization Chamber (2b). The ^{13}O events are well separated from the contaminants in the beam in both cases.

chamber, there was a windowless ionization chamber working with the gas in the scattering chamber. At the entrance of the TTIK scattering chamber, the energy of ^{13}O was ≈11MeV/u, but due to energy straggling in foils and the scintillator, the beam energy spread was ≈16 MeV, and the angular divergence was about 2 degrees. However, the loss of intensity due to slowing down the energy was less than 10% according to events in the entrance ionization chamber. One of the advantages of the TTIK method is that, despite this poor beam quality, it is still possible to study resonance reactions with an expected final energy resolution better than 100 keV. The energy resolution of the entrance ionization chamber is better than the width of the beam and this can be used to further improve the final resolution during the offline data analysis.

The pressure of the gas in the chamber was adjusted to stop the ^{13}O ions before the Si detector telescopes placed near the wall of the scattering chamber. Before the detector telescopes, there were two small ionization chambers. This detection system provides for the clear identification of the protons from the reactions in the scattering chamber. The ^{13}O measurements were made with methane gas in the chamber and with a gas mixture of Ne+CO_2 (background measurements). In addition, measurements were made with the ^{14}O beam (instead of ^{13}O) to compare results with published data for previous measurements of resonances in ^{15}F [5]. The analysis of this data is ongoing and we expect to have some results within a few months.

[1] J. P. Vary, P. Maris, A. Shirokov, Int. J. Mod. Phys. E **17**, Suppl. 1, 109-121 (2008).
[2] K. P. Artemov *et al.*, Sov. J. Nucl. Phys. **52**, 408 (1990).
[3] C. Fu, V. Z. Goldberg, G. V. Rogachev *et al.*, Phys.Rev. C **77**, 064314 (2008).
[4] R. E. Tribble, R. H. Burch, and C. A. Gagliardi, Nucl. Instrum. Methods Phys. Res. **A285**, 441 (1989).
[5] V. Z. Goldberg, G. G. Chubarian, G. Tabacaru *et al.*, Phys. Rev. C **69**, 031302 (2004).

Superallowed beta decay

J. C. Hardy, I. S. Towner, V. E. Iacob, N. Nica, L. Chen, H. I. Park, J. Goodwin,
L. Trache, and R. E. Tribble

Superallowed $0^+ \rightarrow 0^+$ beta decay between T=1 analogue states has been a subject of continuous and often intense study for five decades. The *ft* values of such transitions are nearly independent of nuclear-structure ambiguities and depend uniquely on the vector part of the weak interaction. Their measurement gives us access to clean tests of some of the fundamental precepts of weak-interaction theory, and, over the years, this strong motivation has led to very high precision being achieved in both the experiments and the theory used to interpret them. We have a major program at the Cyclotron Institute to study superallowed beta decay.

To obtain the *ft* value for any transition, three quantities must be measured: the half life of the parent, the Q_{EC} value for the transition of interest and the branching ratio for that transition. This year we produced a complete new survey [1] of existing data on these superallowed decays to replace our previous one [2], which was already out of date. Although the latter was published as recently as 2005, there has been an avalanche of new measurements – some from our group and some from a variety of other groups worldwide – that have been published in the intervening time.

As in all our surveys, the new one provides a critical evaluation of all the experimental data for each superallowed transition and obtains final *ft* values from the averaged results. To these *ft* values are applied improved radiative and isospin-symmetry-breaking corrections [3] in order to derive a final set of "corrected ft values", denoted $\mathcal{Ft}$. Two new features were added this time: The calculated statistical rate function, *f*, now accounts for possible excitation in the daughter atom [4], a small effect but one which merits inclusion at the present level of experimental precision; and we have re-examined the systematic uncertainty associated with the isospin symmetry-breaking corrections by evaluating the radial-overlap correction using Hartree-Fock radial wave functions [5] and comparing the results with our earlier calculations, which used Saxon-Woods wave functions.

With the updated world data and improved corrections the $\mathcal{Ft}$ values are completely consistent with one another as shown in the right panel of Figure 1. Since these corrected $\mathcal{Ft}$ values are inversely proportional to the square of the vector coupling constant, G_V, the constancy of G_V is demonstrated to 1.3 parts in 10^4. Not only is this an important confirmation of the Conserved Vector Current (CVC) hypothesis but it sets the stage for using the average value of G_V to test a fundamental principle of the electroweak standard model: the unitarity of the Cabibbo-Kobayashi-Maskawa (CKM) matrix. The up-down quark mixing element of that matrix, V_{ud}, is given by $V_{ud} = G_V / G_F$, where G_F is the weak interaction constant for the purely leptonic muon decay. The value of V_{ud} is a key component of the most demanding test available for the unitarity of the CKM matrix, the sum of squares of its top-row elements [1]. Superallowed nuclear beta decays provide by far the most precise and reliable value for V_{ud} and, in fact, that element is also the most precisely known one in the CKM matrix – by an order of magnitude! Its value, as obtained from our new survey and analysis is 0.97425(22), a result that is consistent with, but a factor of two more precise than, our previous value [2].

For several decades, the top-row unitarity sum differed from unity by several standard deviations but, over the past several years, new results from kaon decay have demonstrated conclusively that the value of another element of the top row, V_{us}, was not correct. The now accepted value for V_{us}, when combined with the nuclear value for V_{ud}, yields a unitarity sum of 0.99995(61). This stunning confirmation of CKM unitarity is not only a significant verification of the standard model but the uncertainty quoted on the sum provides a tight limit on any possible new physics beyond the standard model.

In short, superallowed $0^+ \rightarrow 0^+$ beta decay provides a high-profile application of nuclear-physics measurements to the study of fundamental symmetries, a subject of vital interest to both nuclear and particle physicists. Although much has already been achieved in this field by nuclear physicists, improvements are still possible. Reducing the uncertainty on the unitarity sum – and, with it, the scope for new physics – remains the primary goal of our research program.

The left panel of Fig. 1 shows the experimental *ft* values while the right panel shows the corrected $\mathcal{F}t$ values. The principal difference between the two panels is the inclusion of the nuclear-structure-dependent corrections, δ_{NS} and δ_C, in the derivation of the $\mathcal{F}t$ values. Since these corrections were determined [3] completely independently of the superallowed decay data, the consistency of the $\mathcal{F}t$ values is also a powerful validation of these calculated corrections: obviously they act very well to remove the considerable "scatter" that is apparent in the left panel and is effectively absent in the right one.

The 2009 survey [1], which considered a body of world data comprised of more than 145

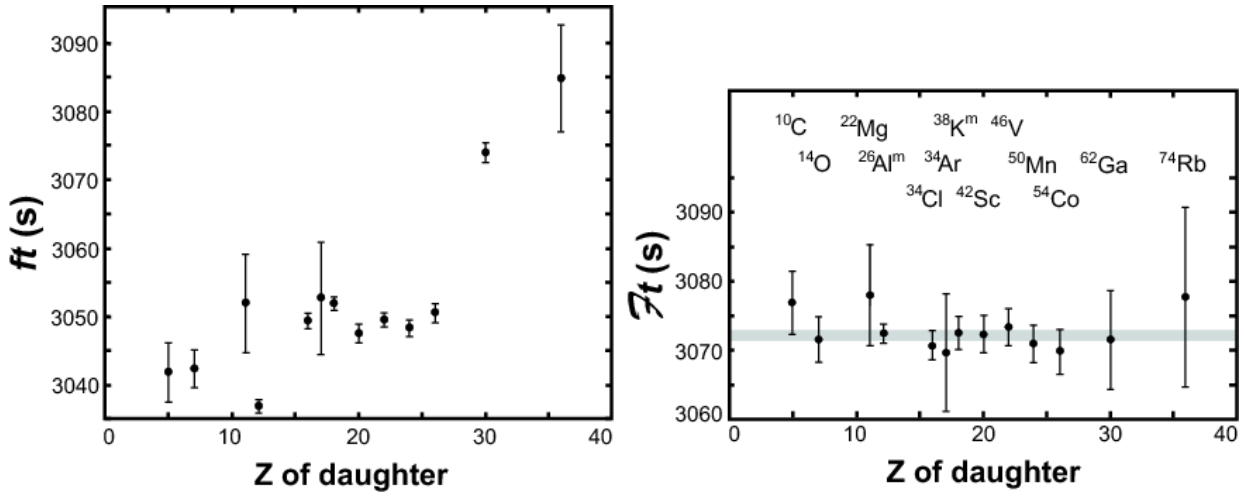

FIG. 1. Results from the 2009 survey [1]. The uncorrected *ft* values for the thirteen best known superallowed decays (left) are compared with the same results after corrections have been applied (right). The grey band in the right-hand panel is the average $\mathcal{F}t$ value, including its uncertainty.

individual measurements, presents a remarkably consistent picture for the nuclear results. Even so, it is still possible for well selected experiments to make real improvements. For example, the validation of the nuclear-structure-dependent correction terms can be improved by the addition of new transitions selected from amongst those with large calculated corrections. If the *ft* values measured for cases with large calculated corrections also turn into corrected $\mathcal{F}t$ values that are consistent with the others, then this must

verify the calculations' reliability for the existing cases, which have smaller corrections. At TAMU we are focusing on T_z = -1 parent nuclei, which consistently have higher predicted structure-dependent correction terms than the well known T_z = 0 cases. In that context, during this past year we have been working on half-life measurements for the decays of ^{26}Si [6] and ^{38}Ca [7].

There are also compelling reasons to confirm and improve the *ft* values for the T_z = 0 cases as well. After all, these are the transitions that principally determine the value of V_{ud}. Since ^{46}V was a key transition that led to important improvements in the structure-dependent corrections when its Q_{EC} value was found to have been incorrectly measured by reaction studies in the past, we have been re-measuring its half-life [8] to be sure that no errors are lurking there. In addition we have extended Penning-trap measurements of Q_{EC} values to ^{34}Cl and ^{38}K^{m} [9], both to improve the precision on these two values and to test more completely for systematic differences between reaction-based and Penning-trap-based Q_{EC} value measurements.

We also continue to focus on improving and securing our analysis procedures for precise branching-ratio measurements. We are working to improve the temperature-stability of our new laser-based system intended to determine the source-to-HPGe-detector distance for each sample delivered by our tape-transport system; and we have continued our source measurements and Monte Carlo calculations to thoroughly characterize our beta detector [10].

[1] J. C. Hardy and I. S. Towner, Phys. Rev. C **79**, 055502 (2009) and *Progress in Research*, Cyclotron Institute, Texas A&M University (2008-2009), p. I-27.

[2] J. C. Hardy and I. S. Towner, Phys. Rev. C **71**, 055501 (2005).

[3] I. S. Towner and J. C. Hardy, Phys. Rev. C **77**, 025501 (2008).

[4] I. S. Towner and J. C. Hardy, *Progress in Research*, Cyclotron Institute, Texas A&M University (2008-2009), p. III-21.

[5] I. S. Towner and J. C. Hardy, *Progress in Research*, Cyclotron Institute, Texas A&M University (2008-2009), p. III-24.

[6] V. E. Iacob, J. C. Hardy, V. V. Golovko, J. Goodwin, N. Nica, H. I. Park, L. Trache and R. E. Tribble, *Progress in Research*, Cyclotron Institute, Texas A&M University (2008-2009), p. I-30.

[7] H. I. Park, J. C. Hardy, V. E. Iacob, V. V. Golovko, J. Goodwin, N. Nica, M. McCleskey, E. Simmons, L. Trache, and R. E. Tribble, *Progress in Research*, Cyclotron Institute, Texas A&M Univeristy (2008-2009), p. I-33.

[8] H. I. Park, J. C. Hardy, V. E. Iacob, J. Goodwin, V Horvat, N. Nica, E. Simmons, L. Trache, and R. E. Tribble, *Progress in Research*, Cyclotron Institute, Texas A&M University (2008-2009), p. I-34.

[9] J. C. Hardy, *Progress in Research*, Cyclotron Institute, Texas A&M University (2008-2009), p. I-36.

[10] V. V. Golovko, V. E. Iacob, J. C. Hardy and D. Melconian, *Progress in Research*, Cyclotron Institute, Texas A&M University (2008-2009), p. V-36.

Superallowed $0^+ \rightarrow 0^+$ nuclear β decays: A new survey with precision tests of the conserved vector current hypothesis and the standard model

J. C. Hardy and I. S. Towner

Beta decay between nuclear analog states of spin-parity, $J^\pi = 0^+$, and isospin, T = 1, has been a subject of continuous and often intense study for five decades. The strengths, or *ft* values, of such transitions are nearly independent of nuclear-structure ambiguities and depend uniquely on the vector part of the weak interaction. Thus, their measurement has given nuclear physicists access to clean tests of some of the fundamental precepts of weak-interaction theory and, over the years, this strong motivation has led to very high precision being achieved in both the experiments and the theory required to interpret them.

As befits such an important issue, we have undertaken periodic surveys of the relevant world data (see, for example, refs [1-5]). Even though the last survey closed as recently as 2004, a large amount of significant new data has appeared in the four years since then, so that survey was already out of date. We have now published a thorough new overview [6] in which we critically survey all relevant measurements formally published before September 2008.

Compared with our last review, there are numerous improvements: First, we have added 27 recently published measurements and eliminated 9 references, either because they have been superseded by much more precise modern results or because there are now reasons to consider them fatally flawed; of particular importance, the new data include a number of high-precision Penning-trap measurements of decay energies. Second, we have used the recently improved isospin symmetry-breaking corrections [7], which were motivated by these new Penning-trap results. Third, our calculation of the statistical rate function *f* now accounts for possible excitation in the daughter atom, a small effect but one which merits inclusion at the present level of experimental precision. Finally, we have re-examined the systematic uncertainty associated with the isospin symmetry-breaking corrections by evaluating the radial-overlap correction using Hartree-Fock radial wave functions and comparing the results with our earlier calculations, which used Saxon-Woods wave functions; the provision for systematic uncertainty has been changed as a consequence.

The new corrected $\mathcal{Ft}$ values are impressively constant – see Fig. 1 – and their average, when combined with the muon lifetime, yields the up-down quark-mixing element of the Cabibbo-Kobayashi-Maskawa (CKM) matrix, $V_{ud} = 0.97425 \pm 0.00022$. The unitarity test on the top row of the matrix becomes $|V_{ud}|^2 + |V_{us}|^2 + |V_{ub}|^2 = 0.99995 \pm 0.00061$. Both V_{ud} and the unitarity sum have significantly reduced uncertainties compared with our previous survey, although the new value of V_{ud} is statistically consistent with the old one. From these data we also set limits on the possible existence of scalar interactions, right-hand currents and extra *Z* bosons. Finally, we discuss the priorities for future theoretical and experimental work with the goal of making the CKM unitarity test even more definitive.

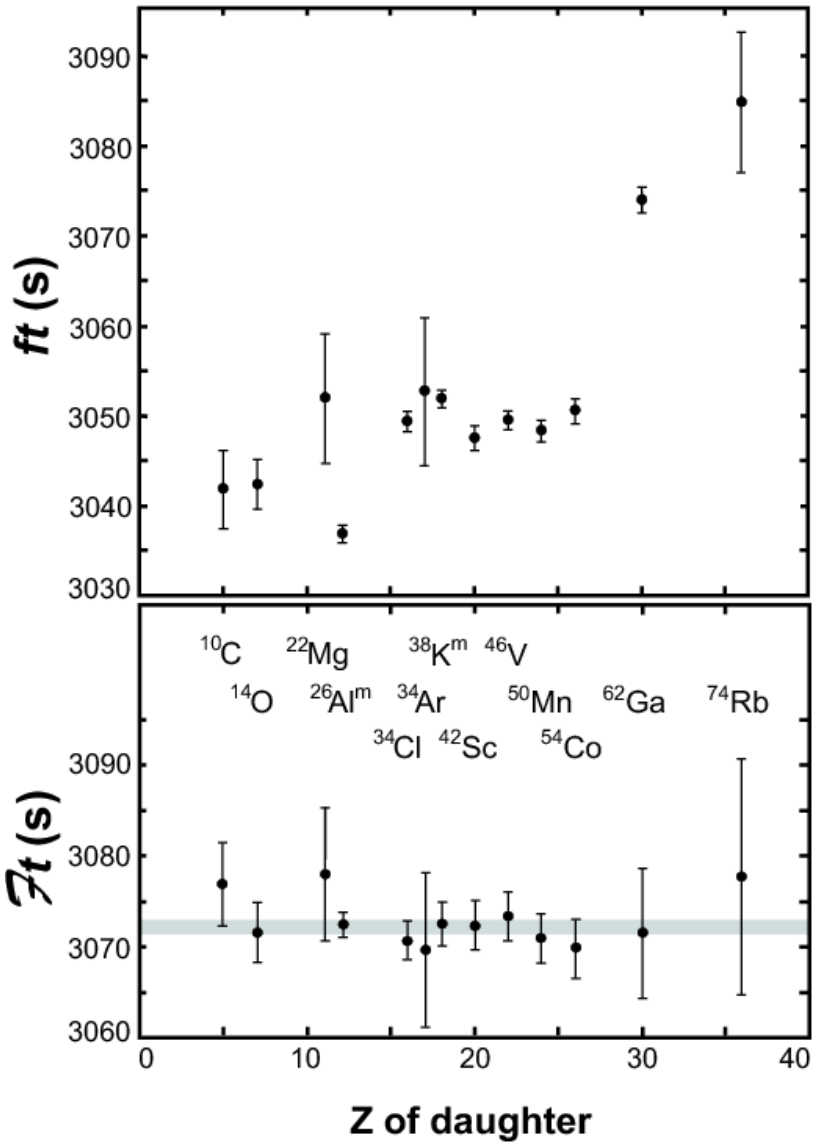

FIG. 1. In the top panel are plotted the experimental *ft* values. In the bottom panel, the corresponding $\mathcal{F}t$ values are given; they differ from the top panel principally by inclusion of the nuclear-structure-dependent corrections. The horizontal grey band in the bottom panel indicates the average $\mathcal{F}t$ value with its uncertainty.

[1] I. S. Towner and J. C. Hardy, Nucl. Phys. **A205**, 33 (1973).

[2] J. C. Hardy and I. S. Towner, Nucl. Phys. **A254**, 221 (1975).

[3] V. T. Koslowsky, E. Hagberg, J. C. Hardy, H. Schmeing, R. E. Azuma and I. S. Towner, *Proc. 7th Int. Conf. on Atomic Masses and Fundamental Constants*, ed. O. Klepper (T. H. Darmstadt, 1984) p. 572.

[4] J. C. Hardy, I. S. Towner, V. T. Koslowsky, E. Hagberg and H. Schmeing, Nucl. Phys. **A509**, 429 (1990).

[5] J. C. Hardy and I. S. Towner, Phys. Rev. C **71**, 055501 (2005).
[6] J. C. Hardy and I. S. Towner, Phys. Rev. C **79**, 055502 (2009).
[7] I. S. Towner and J. C. Hardy, Phys. Rev. C **77**, 025501 (2008).

^{26}Si half-life measurement

V. E. Iacob, J. C. Hardy, V. Golovko, J. Goodwin, N. Nica, H. I. Park, L. Trache and R. E. Tribble

If ^{26}Si is to yield an *ft*-value with sufficient precision to contribute meaningfully to the evaluation of V_{ud} from superallowed β decay, experimental precision must be improved from the world-average results given in the most recent, 2009 survey [1]. Since that survey closed, a significantly more precise Q_{EC}-value result has already been published [2], thus providing considerable incentive for improving both the half-life and branching-ratio values. This report describes progress on our measurement of the ^{26}Si half-life, which aims at a precision of better than 0.1%.

The experimental set-up was similar to the one described in [3] except that, for the first time, the time profile of the deposited activity was recorded contemporaneously with the decay data [4]. An ^{27}Al beam accelerated to 30 *A* MeV impinged on a hydrogen gas target kept at liquid-nitrogen temperature and at a pressure of at 2 atmospheres. The ejectiles recoiling from the target passed through the MARS spectrometer, from which a pure beam of ^{26}Si at 25 *A* MeV was obtained with an intensity of more than 40×10^3 particles/s. This beam was then extracted into air, passed through a 0.3-mm-thick plastic scintillator as well as Al degraders, and eventually was implanted in the 76-μm-thick mylar tape of our fast tape-transport system. The measurement consisted of repeated computer-controlled cycles, in which the activity was collected for a few seconds; then the beam was turned off and the collected activity was moved in 188 ms to the center of a 4π proportional gas counter, where the decays were detected and multiscaled for 45 s (about 20 half-lives of ^{26}Si). These collect-move-detect cycles were repeated until the desired statistics had been acquired. Typically an individual run would record 4×10^6 decay events at one choice of experimental parameters. These parameters would then be changed and another 4×10^6

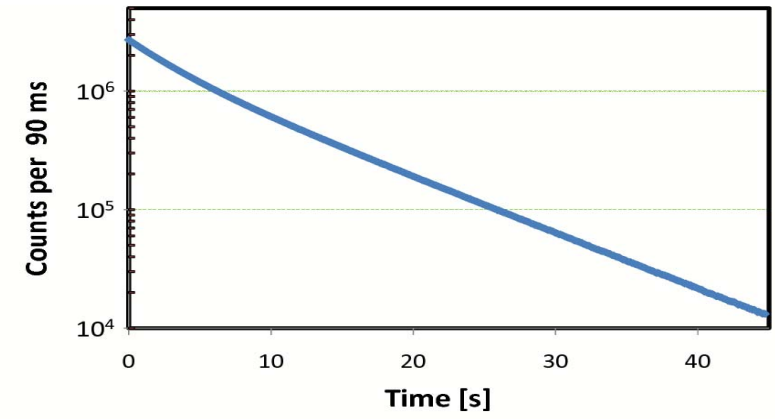

FIG. 1. Total decay spectrum of the combined β^+-decays of ^{26}Si and its daughter ^{26}Al.

decay events recorded, after which another change would be made and a new run begun … and so on. In total, more than 260×10^6 decay events were recorded for ^{26}Si and its daughter ^{26}Al. The total time-decay spectrum obtained is presented in Fig. 1.

Special care was given to checking the consistency of the results. Using the same techniques as described in [3], we split the experiment into separate runs and, from one to another, we changed the parameters that are critical in the electronic setup: dead-times (3, 4, 6 and 8 μs), discriminator thresholds (150, 200 and 250 mV) and detector bias (2550, 2650, 2750 and 2850 V). As the signal generated by the detector is split in two chains, each of which has a different pre-set dominant dead-time, in our analysis we first compared the two data-streams within each run. After correction for the different dead times, no difference was observed in the fitted half-life, as one would expect for events originating from the same data stream but differing only in dominant dead time. We than tested the stability of the fitted results from run to run, thus testing for any systematic dependence on the three critical parameters. As seen from the results displayed in Fig. 2, no systematic bias was observed.

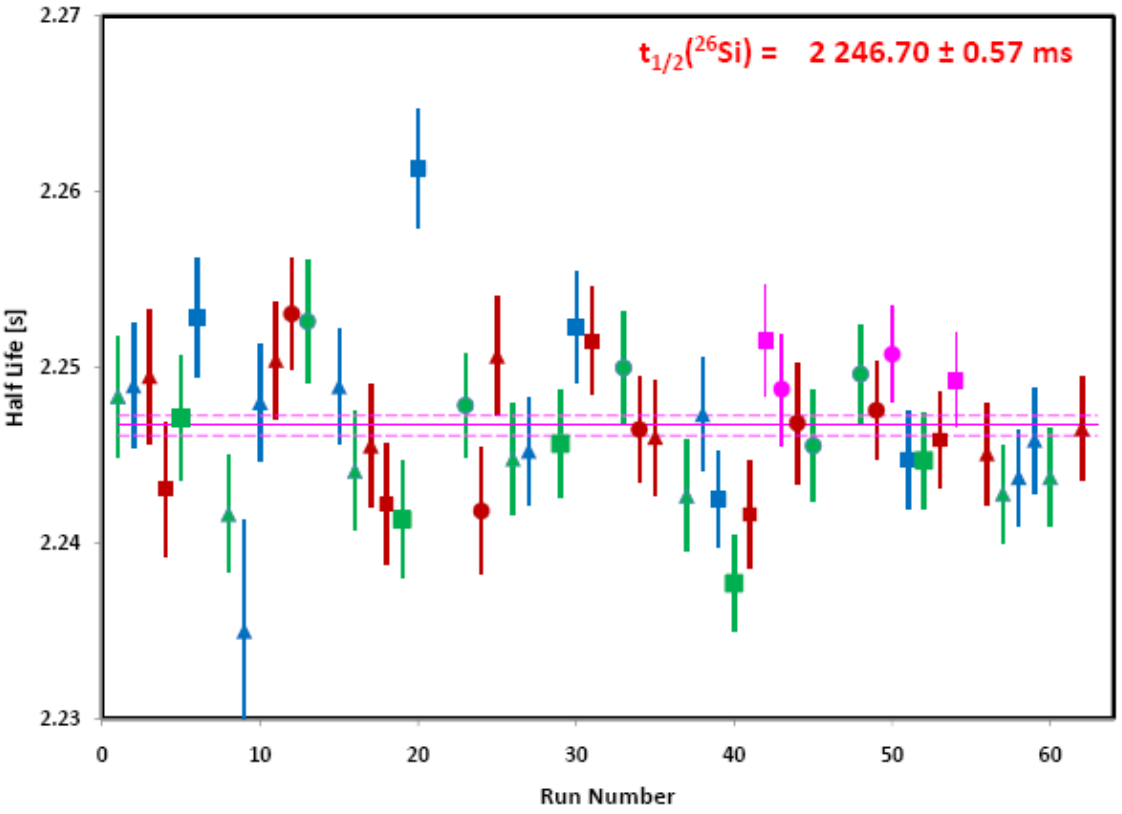

FIG. 2. Search for possible systematic errors in the half life of ^{26}Si. The data points are identified by color and symbol: triangles/squares/circles correspond in order to 150mV/200mV/250mV discriminator settings while blue/green/maroon/purple correspond to detector-bias settings of 2550V/2650V/2750V/2850V.

Our preliminary result for the ^{26}Si half-life, $t_{1/2} = 2246.70(57)$ ms (statistical uncertainty only), disagrees with the current world average [1], a number that is dominated by a recent measurement by

Matea *et al.* [5], $t_{1/2}$ = 2228.3(27) ms. We have carefully studied the experimental arrangement described by Matea *et al.* and conclude that the difference between their result and ours is a consequence of their neglecting the difference in detection efficiency between the parent and daughter nuclei, ^{26}Si and ^{26}Al, respectively. For the scintillation detector used in [5] the detection efficiency for β's originating from ^{26}Si is considerably higher than that for the β's originating from ^{26}Al, which has a lower end-point energy. While this is an important correction for the Matea *et al.* scintillator detector, it only has a minor contribution in our set-up with a high-efficiency proportional gas counter; nevertheless we do make the correction. Using the efficiencies as we obtain them from an approximate Monte Carlo simulation of the Matea *et al.* experimental set-up [5], we conclude that a proper correction to their measured data would bring their reported half-life into agreement with our new result.

[1] J. C. Hardy and I. S. Towner, Phys. Rev. C **79**, 055502 (2009).

[2] T. Eronen *et al.*, Phys. Rev. C **79**, 032802(R) (2009).

[3] V. E. Iacob, J. C. Hardy, J. F. Brinkley, C. A. Gagliardi, V. E. Mayes, N. Nica, M. Sanchez-Vega, G. Tabacaru, L. Trache, and R. E. Tribble, Phys. Rev C **74**, 055502 (2006).

[4] V. E. Iacob and J.C. Hardy, *Porogress in research,* Cyclotron Institute, Texas A&M University (2008-2009), p. V-43.

[5] I. Matea, J. Souin, J. Aysto, B. Blank, P. Delahaye, V. -V. Elomaa, T. Eronen, J. Giovinazzo, U. Hager, J. Hakala, J. Huikari, A. Jokinen, A. Kankainen, I. D. Moore, J. -L. Pedroza, S. Rahaman, J. Rissanen, J. Ronkainen, A. Saastamoinen, T. Sonoda, and C. Weber, Eur. Phys. J. A **37**, 151 (2008).

High precision half-life measurement of ^{38}Ca

H. I. Park, J. C. Hardy, V. E. Iacob, V. V. Golovko J. Goodwin, N. Nica, M. McCleskey,
E. Simmons, L. Trache, and R. E. Tribble

Progress on the half-life measurement of ^{38}Ca has been previously reported [1,2]. From approximately 19 million β events recorded under various detecting conditions (*i.e.*, different settings for dominant dead time, bias voltage of gas counter, and threshold of discriminator), the measured half-life is 0.4434(4) s, which is consistent with, but much more precise than, the average of all the previous measurements, 0.4400(78) s.

To further improve the precision of the measurement, we performed another ^{38}Ca half-life experiment with the same ^{1}H(^{39}K, 2*n*) reaction at a primary beam energy of 30*A* MeV. Our experimental arrangement was the same as described before [1, 2]. The overall statistics were substantially improved, but throughout the entire run the level of ^{35}Ar ($t_{1/2}$ = 1.77 s) impurity was observed to vary up to ~3% in the reaction products. Since we were depositing ^{38}Ca mid-way through the tape, some ^{35}Ar was simultaneously deposited near the back of the tape. We considered this contribution to the decay of ^{38}Ca and its daughter ^{38}K in extracting the half-life of ^{38}Ca. Although our preliminary result, $t_{1/2}$(^{38}Ca) = 0.4431(2) s, agrees with our previous measurement, we are planning to conduct the final half-life measurement of ^{38}Ca in the fall of 2009, during which we will reduce the ^{35}Ar contamination by depositing ^{38}Ca near the back of the tape, thus ensuring that the ^{35}Ar passes entirely through.

[1] H. I. Park *et al*., *Progress in Research*, Cyclotron Institute, Texas A&M University (2006- 2007), p. I-58.

[2] H. I. Park *et al*., *Progress in Research*, Cyclotron Institute, Texas A&M University (2007- 2008), p. I-30.

The half-life of ^{46}V

H. I. Park, J. C. Hardy, V. E. Iacob, J. Goodwin, V. Horvat, N. Nica, E. Simmons,
L. Trache, and R. E. Tribble

A recent Penning-trap Q_{EC} measurement of the superallowed β decay of ^{46}V [1, 2] raised the $\mathcal{F}$t value by nearly three standard deviations from the average of all other well-known superallowed transitions. This anomaly stimulated questions about the possible presence of systematic effects for all reaction-based Q-value measurements [3] and led to a theoretical reexamination of the isospin-symmetry-breaking corrections for the ^{46}V transition, as well as for a number of other cases [4]. These new corrections resulted in the restoration of CVC consistency and brought the CKM matrix into better agreement with unitarity. Throughout these changes, it was always assumed that the half-life of ^{46}V was completely correct although the accepted Q_{EC} value had been found to be flawed. Therefore, we are measuring a new precise half-life of ^{46}V to see if this assumption is correct.

Essential to this experiment was the development of a ^{47}Ti beam to produce ^{46}V. For our first attempt in the summer of 2007, the ^{1}H(^{47}Ti, 2n) ^{46}V reaction was used at a primary beam energy of 30A MeV. Although some ^{47}Ti beam was accelerated with natural titanium source material, we were not able to collect any data because of the extremely low beam intensity. However, the observed production rate of ^{46}V indicated that the experiment would be possible with a beam current of as little as 25 nA from the cyclotron. More recently, with enriched ^{47}Ti and the same ^{1}H (^{47}Ti, 2n) ^{46}V reaction at primary beam energy of 30A MeV, enough beam was produced to allow us to conduct a test run on the half-life of ^{46}V. The main purpose of this test was to optimize MARS settings and to verify the presence of ^{46}V with our detection system. These results indicated that we could improve the experimental conditions by increasing the primary beam energy to 32A MeV because the maximum cross section for ^{46}V was predicted at this energy.

We tried the experiment again on October 2008. It turned out that the production of a ^{47}Ti beam at 32A MeV was a real challenge for the accelerator. For most of the time, the beam current was less than 10 nA, which barely met the minimum β-particle counting rate required from a statistics point of view. Furthermorer, we were able to obtain data for only one third of the seven-day requested beam time. Our experimental arrangement was the same as for the half-life measurement of ^{38}Ca [5]. With repeated cycles of 1 s/0.192 s/10 s collect/move/count times, over 30 million β events were recorded for one set of dominant dead times. Unfortunately, the useful beam time was not sufficient for us to check for systematic errors. However, our result for the half-life, 0.4226(1) s, agrees with the average of all previous measurements, 0.4225(1) s.

Another five-day run followed in December 2008 to improve the overall statistics of the data and to check for any possible systematic errors. Unfortunately, our analysis revealed a small systematic effect on half-life in this measurement. The main cause has now been identified and eliminated. The final experiment is scheduled in June 2009 to complete the precise half-life measurement of ^{46}V.

[1] G. Savard, F. Buchinger, J. A. Clark, J. E. Crawford, S. Gulick, J. C. Hardy, A. A. Hecht, J. K. P. Lee, A. F. Levand, N. D. Scielzo, H. Sharma, K. S. Sharma, I. Tanihata, A. C. C. Villari, and Y. Wang, Phys. Rev. Lett. **95**, 102501 (2005).

[2] T. Eronen, V. Elomaa, U. Hager, J. Hakala, A. Jokinen, A. Kankainen, I. Moore, H. Penttilä, S. Rahaman, A. Saastamoinen, T. Sonoda, J. Äystő, J. C. Hardy and V. Kolhinen, Phys. Rev. Lett. **97**, 232501 (2006).

[3] J. C. Hardy, I. S. Towner, and G. Savard, Int. J. Mass Spectrom. **251**, 95 (2006).

[4] I. S. Towner and J. C. Hardy, Phys. Rev. C **77**, 025501 (2008).

[5] H. I. Park *et al*., *Progress in Research*, Cyclotron Institute, Texas A&M University (2007- 2008), p. I-30.

JYFLTRAP : Q_{EC}-values of the superallowed decays of ^{34}Cl and $^{38}K^{m}$

J. C. Hardy

We have already completed and published two successful measurements of the Q_{EC} values for superallowed $0^+ \rightarrow 0^+$ transitions from $T_z = 0$ nuclei using the JYFLTRAP Penning-trap mass spectrometer at the University of Jyvaskyla cyclotron facility in Finland. The first comprised the results for $^{26}Al^{m}$, ^{42}Sc and ^{46}V [1] and the second, ^{50}Mn and ^{54}Co [2]. Our collaboration has now performed a third experiment, to measure the Q_{EC} values for the superallowed decays of ^{34}Cl and $^{38}K^{m}$. The Q_{EC} values for these two transitions have previously been determined to a claimed high precision with (p,n) threshold measurements, and combined (p,γ) and (n,γ) Q-value measurements, the methods used in the past before Penning traps became available for on-line measurements. They have never been measured with a Penning trap. These two cases thus provide an excellent means to test carefully for any systematic discrepancies between reaction-based and trap-based measurements, a subject of some concern [3] when one combines both types of measurement in the determination of a world average.

As we did in our previous experiments, we produced ^{34}Cl and $^{38}K^{m}$ via (p,n) reactions. A powerful advantage of this approach is that, not only were the superallowed emitters of interest produced in the primary reactions but ions from the target material itself – the beta-decay daughters of these emitters – were also released by elastic scattering of the cyclotron beam. As explained in Ref. [1], with the JYFLTRAP system we can isolate a specific nuclide from the reaction products and measure the cyclotron frequency of its ions in the Penning trap. For each determination of a Q_{EC} value, the cyclotron frequency measurements were interleaved: first we recorded a frequency scan for the daughter, then for the mother, then for the daughter and so on. This way, most potential systematic effects could be reduced to a minimum or eliminated. For each measurement, data were collected in several sets, each comprising ~10 pairs of parent-daughter frequency scans taken under the same conditions.

The experimental data are still being analyzed.

[1] T. Eronen, V. Elomaa, U. Hager, J. Hakala, A. Jokinen, A. Kankainen, I. Moore, H. Penttilä, S. Rahaman, A. Saastamoinen, T. Sonoda, J. Äystő, J. C. Hardy, and V. Kolhinen, Phys. Rev. Lett. **97**, 232501 (2006).

[2] T. Eronen, V. -V. Elomaa, U. Hager, J. Hakala, J. C. Hardy, A. Jokinen, A. Kankainen, I. D. Moore, H. Penttila, S. Rahaman, S. Rinta-Antila, J. Rissanen, A. Saastamoinen, T. Sonoda, C. Weber, and J Aysto, Phys. Rev. Lett. **100**, 132502 (2008).

[3] J. C. Hardy, I. S. Towner, and G. Savard, Int. J. Mass Spectrometry **251**, 95 (2006).

Half-life of the electron-capture decay of ^{97}Ru: Precision measurement shows no temperature dependence

J. R. Goodwin, V. V. Golovko, V. E. Iacob, and J. C. Hardy

This experiment was undertaken to investigate whether the half life of the electron-capture decay of ^{97}Ru atoms located in a metallic environment shows any temperature dependence, as has been claimed for the electron-capture decay of ^{7}Be in a recent publication [1].

Previous publications claiming to observe a temperature dependence of β^-, β^+ and electron-capture-decay half-lives [1-3] have used the so-called "Debye effect" to explain the phenomenon. The authors claim that the conduction electrons, present in a metal, comprise a sort of plasma, which they refer to as a Debye plasma. They argue that this plasma changes the phase space available for the decay and thus increases (for β^- or electron-capture decay) or decreases (for β^+-decay) the nuclide's half life. The change in phase space would be enhanced, they argue, if the source is cooled to very low temperatures. Although the half-life changes, which were reported at low temperature (~12K), were less than their proposed theory indicated, they were in the same direction.

We set out by repeating one of the reported experiments: the measurement of the half-life of ^{198}Au in gold at room temperature and at 19K [4]. Spillane *et al*. [3] had claimed a 3.6(10)% effect but we found no effect and set an upper limit of 0.04%, two orders of magnitude lower than their claims. Having shown no effect to exist for the β^--decay of ^{198}Au, we have now turned to a case of electron-capture: the decay of ^{97}Ru.

We used a natural ruthenium sample obtained from Goodfellow Corporation. This was in the form of a single crystal, 8 mm in diameter, 1 mm thick, and with a purity of 99.999%. The crystal was activated twice – once for the low-temperature measurement, and then again later for the measurement at room temperature – in a flux of ~10^{10} neutrons/cm^2·s for 10 s at the Texas A&M Triga reactor.

We used the same experimental set-up as we used for the ^{198}Au experiment [4]; as in that experiment, the set-up was unchanged for both the cold (19K) and room-temperature measurements. The activated sample, containing ^{97}Ru among other activities, was placed upon the cold head of a CryoTorr 7 cryopump. A 70% HPGe detector was placed directly opposite the sample, and just outside the plate covering the cryopump. A cavity had been bored in the cover-plate such that only 3.5 mm of stainless steel remained between the sample and the face of the detector. The distance between the detector and cryopump remained constant throughout the measurement.

Six-hour γ-ray spectra were acquired and saved consecutively over a period of 29 days for each measurement. All these spectra were collected for an identical, pre-set live time. Throughout the experiment, we synchronized the time, prior to each day's collection, using the signal broadcast from radio station WWVB. The system dead time was always below 4%; so, since the TRUMP^{TM} card used in our data collection corrects for dead-time losses, our results were nearly independent of dead-time losses. However, to bring our precision down to about 0.1%, we performed an additional procedure to allow us to determine the presence of any residual, rate-dependent effects. This procedure involved measuring the 662 keV γ-ray peak from a ^{137}Cs source, then repeatedly re-measuring this peak in the

presence of a ^{133}Ba source, which was moved nearer and nearer the detector. Moving the barium source closer to the detector increased both the dead time and the number of chance coincidences. By plotting peak areas versus dead time, we found the residual loss to be 5.5(25) x 10^{-4} per 1% increase in dead time. This correction was then applied to all spectra.

We used the least-square peak-fitting program gf3 in the RADware series [5], to analyze the spectra. Use of this program allowed us to make very accurate determinations of spectral backgrounds and areas. Each peak was analyzed and then corrected for residual, rate-dependent effects, as mentioned above. The decay curves resulting from this analysis were plotted as a function of time and fitted by a single exponential with a code based on ROOT [6]. This code uses the maximum likelihood method and has been tested previously by us to a precision of 0.01%, with Monte Carlo generated data.

From our analysis of the 216-keV delayed γ-ray in ^{97}Tc, the daughter of ^{97}Ru, we obtained a half-life of 2.8382 ± 0.0013 d for the cold-temperature measurement, and of 2.8370 ± 0.0013 d for the room temperature measurement. These results demonstrate that the half-life of ^{97}Ru is the same within 0.1% at room temperature and at 19K.

Since their delayed γ-rays were present in the spectra as well, we have also obtained data at both temperatures for two other isotopes, ^{103}Ru and ^{105}Rh, which both decay by β^- emission. We were able to show that neither of these isotopes undergoes a change in half-life, as would be predicted by the "Debye theory":

- For ^{103}Ru, our measurements yield a half-life of 39.210 ± 0.016 d at room temperature and 39.219 ± 0.025 d at 19K. These results are also the same within 0.1%.
- For ^{105}Rh, our measurements obtain a half-life of 35.347 ± 0.036 h at room temperature, and a half-life of 35.314 ± 0.023 h at 19K. These results are the same within 0.2%

In conclusion, so far our measurements neither confirm the claimed observation of the temperature dependence of half-lives nor corroborate the so-called Debye theory, which was devised to explain the effect. Our measurements so far have included ^{198}Au, ^{97}Ru, ^{103}Ru, and ^{105}Rh, cases which include both β^--decay (^{198}Au, ^{103}Ru, and ^{105}Rh) and electron-capture-decay (^{97}Ru) processes.

[1] B. Wang *et al.*, Eur. Phys. J. A **28**, 375 (2006).

[2] B. Limata *et al.*, Eur. Phys. J. A **28**, 251 (2006).

[3] T. Spillane *et al.*, Eur. Phys. J. A **31**, 203 (2007).

[4] J. R. Goodwin, V. V, Golovko, V. E. Iacob and J. C. Hardy, Eur. Phys. J. A **34**, 271 (2007).

[5] D. Radford, **http://radware.phy.ornl.gov/main.html** (private communication).

[6] R. Brun and F. Rademakers, Nucl. Instrum. Methods Phys. Res. **A389**, 81 (1997).

Tests of internal-conversion theory and efficiency calibration with precise γ- and x-ray spectroscopy: the $^{197}Pt^{m}$ case

N. Nica, C. Balonek, J. C. Hardy, M. Hernberg, V. E. Iacob, J. Goodwin, J. Nolan and M. B. Trzhaskovskaya[1]

[1]*Petersburg Nuclear Physics Institute, Gatchina RU-188300, Russia*

As the next case in a series of precision internal-conversion-coefficient (ICC) measurements [1, 2] designed to test internal-conversion theory, we have studied the 346.5-keV, *M4* transition from the decay of $^{197}Pt^{m}$. The previously measured α_K for this transition, 4.02(8) [3], which is shown as the grey points in Fig. 1 at the marked $^{197}Pt^{m}$ location, disagrees with modern Dirac-Fock calculations whether or not the atomic vacancy caused by the electron-capture process is incorporated in the theory.

The technique we use is to measure the intensity ratio of the K x-ray peaks relative to the γ-ray peak for the transition of interest. Our precision depends on there being no other significant contributors to the x-ray peaks (or to the γ-ray peak). One can easily see that a measurement on the 346.5-keV γ transition presents a number of challenges. We produce $^{197}Pt^{m}$ by neutron activation of enriched ^{196}Pt, and one of the main difficulties is that the cross section for producing the ^{197}Pt ground state (σ_{th} = 0.72 b) is 16-times larger than that for producing the isomer of interest (σ_{th} = 0.044 b). The ^{197}Pt ground state β^- decays with a 19.9-hr half-life to states in ^{197}Au, whose subsequent γ-decays involve internal conversion and give rise to gold K x rays. These x rays are very close in energy to the platinum x rays, whose intensity we need to determine. However, since the half-life of $^{197}Pt^{m}$ is 95.4 min we are able to use a time analysis of the decay spectra to help with the separation.

Another difficulty comes from the strong 77.4-keV γ ray which is produced by the ^{197}Pt ground state β^- decay and effectively obliterates the platinum K_β peaks (75-78 keV). Moreover, this γ ray creates a scattering "shelf" to lower energies in the γ-ray spectrum, which complicates the background in the region of the platinum K_α x rays. Once again, we must make use of the different half-lives to separate the peaks of interest from the background. These complications have served to limit our precision compared with our previous results.

We prepared two samples, S1 and S2, at the Cyclotron Institute from 97.4%-enriched ^{196}Pt as a thin powder held between thin mylar foils. These ensembles were separately activated in the Triga reactor at the Nuclear Science Center of Texas A&M University. Source S1 contained 0.7 mg of the powder and was activated for 4 h; while S2 contained 1.5 mg and was activated for 1 h.

We measured γ-ray spectra from each activated source for about two weeks using our very precisely efficiency-calibrated HPGe detector [4]. Next we carefully scanned the spectra from both sources and identified all γ-ray peaks, using intensity ratios and decay curves. Based on this γ-ray-intensity information, we then calculated the contribution, if any, to the platinum K x-ray region from each impurity activity detected.

Because of the long activation time for sample S1, the initial counting rate in our detector was very high, leading to dead-times of up to 40%. This restricted the accuracy of our half-life analysis.

Furthermore, this source also included a much higher contribution from impurities. As a result, we did no further analysis of the S1 spectra and concentrated on source S2.

With this source we successfully separated the K x-rays associated with the $^{197}Pt^{m}$ *M4* transition from the 77.4-keV γ ray and gold K x-rays caused by the decay of the ^{197}Pt ground state. The resulting decay curve for the platinum K x-rays and the measured decay curve for the 346.4-keV γ ray were then fitted with a common half-life and their ratio obtained. Our result, $\alpha(K)_{exp}=4.25(5)$, can be compared with the theoretical calculations of 4.275 (with the vacancy included in the "frozen orbital" approximation) and 4.19 (no vacancy). Our result is statistically consistent with both calculations (see Fig. 1) and removes the discrepancy that the previous measurement had indicated.

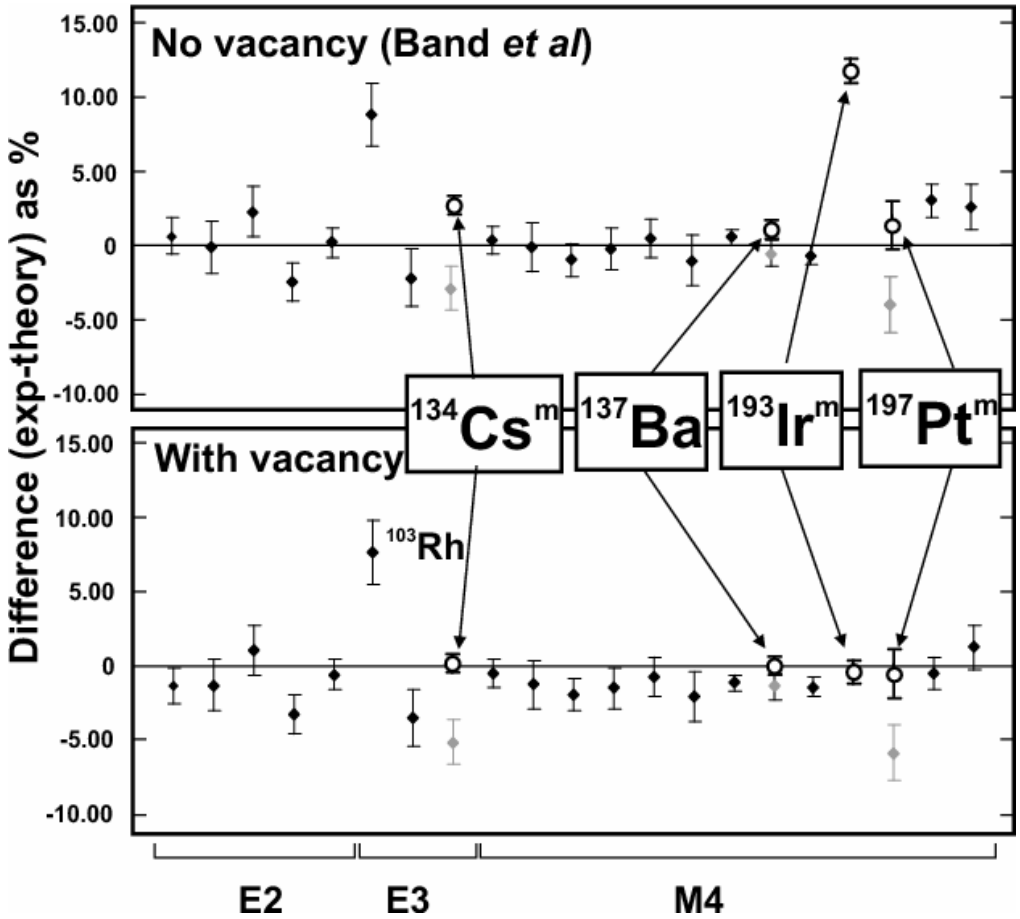

FIG. 1. Percentage differences between the measured and calculated ICCs for two Dirac-Fock calculations: one (top) is without the atomic vacancy and the other is with it included in the "frozen orbital" approximation. The points shown as solid diamonds in both plots correspond to the twenty cases that have better that 2% precision [5]; as indicated at the bottom, five are for E2 tranditions, three for E3, and the remainder are for M4 transitions. The points shown as open circles correspond to our recently measured α_K values. The grey points with error bars at the same horizontal positions are the previous α_K results, which our measurements replace.

[1] N. Nica *et al.*, Phys. Rev. C **70**, 054305 (2004); Phys. Rev. C **71**, 054320 (2005); Phys. Rev. C **75**, 024308 (2007); Phys. Rev. C **77**, 034306 (2008).
[2] J. C. Hardy *et al.*, Appl. Radiat. Isot. **64**, 1392 (2006); Appl. Radiat. Isot. **66**, 701 (2008).
[3] I. N.Vishnevsky *et al.*, Bull. Acad. Sci. USSR, Phys. Ser. **51**, No.5, 23 (1987).
[4] R. G. Helmer *et al.*, Nucl. Instrum. Methods Phys. Res. **A511**, 360 (2003).
[5] S. Raman *et al.*, Phys. Rev. C **66**, 044312 (2002).

United States nuclear data program evaluated nuclear structure data file (ENSDF) at Texas A&M

N. Nica[1] and J. C. Hardy
[1]*Under contract with Brookhaven National Laboratory*

As Since 2005, when we started our data evaluation effort at the Cyclotron Institute, Texas A&M University has become an important participant in the nationwide United States Nuclear Data Program (USNDP), to which we contribute about 10% of the total effort. Our work continued in 2008-09 with the *A*=97 mass-chain evaluation [1]: this encompassed all publications since 1993, when this mass chain was last fully evaluated [2].

The A=97 mass chain is a large one, composed of 14 different elements (Br, Kr, Rb, Sr, Y, Zr, Nb, Mo, Tc, Ru, Rh, Pd, Ag and Cd); it contained 71 datasets* in 1993 [2], and the new evaluation, when published, will contain 90 [1]. As well, the number of lines in the database files† will be 15,000, a 50% increase over what it was before. Fig. 1 shows a detailed comparison for each nucleus, where one can see significant increases in data particularly for Sr, Tc and Ru (numbers 4, 9 and 10 respectively). There is also a significant increase in the number of publications, about 328 now compared to 236 before. From Fig. 2 one can see that, with 15,000 lines, the *A*=97 mass chain will rank among the largest ones.

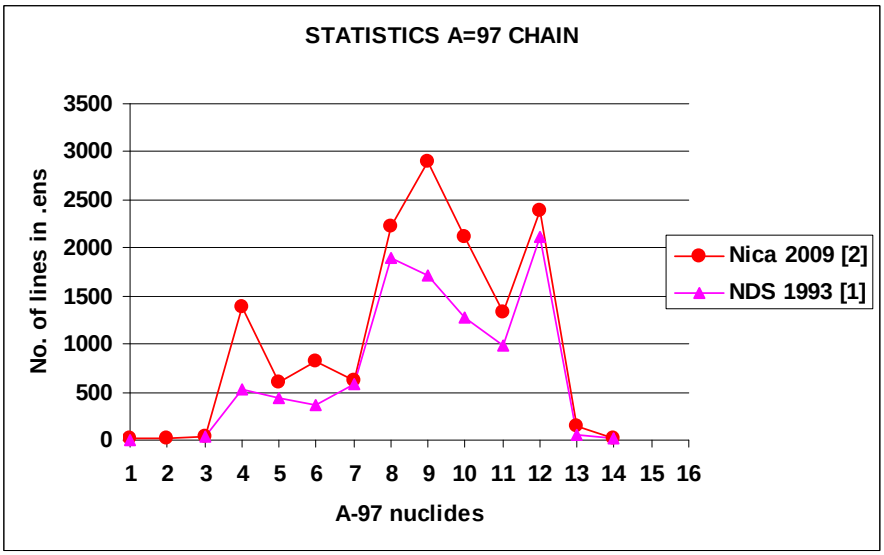

FIG. 1 Comparison of the new evaluation [1] with the previous one [2], showing the number of database lines for each of the 14 nuclei of A=97 mass chain. They appear from lightest to heaviest (left to right).

* A dataset collects the data for one nucleus as measured in a particular decay or reaction, frequently by several independent experiments. The "Adopted Levels, Gammas" dataset, one for each nucleus, is built from the decay and reaction datasets for that nucleus. It gives the best and most extensive data for each nucleus.

† The database file (.ens file), one for each dataset, is written in the special ENSDF data format where one line (sometimes extended) contains typical data for a nuclear level, a particular nuclear transition, or other types of data, as well as comment lines.

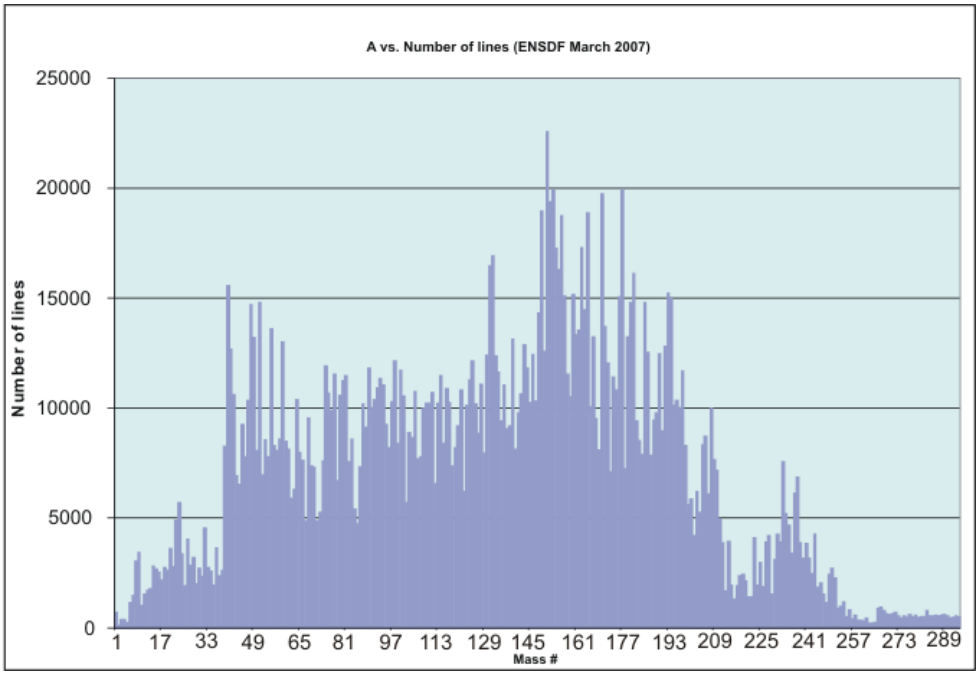

FIG. 2. The number of lines in the data-base files for each mass chain in ENSDF as of March 2007. With 15,000, lines the new evaluation for *A*=97 will be among the largest chains.

With two-thirds of an FTE dedicated to evaluation, the Cyclotron Institute is making an important contribution to the U.S. national nuclear data program, and its official establishment as an evaluation center would be desirable. While evaluation now is located predominantly in national laboratories, we are proof that this activity can be done successfully in a university environment at lower costs. Furthermore, at a university some evaluation work can be done with the help of students. Thus, in addition to its intrinsic value for the community, evaluation could also become a tool for teaching nuclear physics.

[1] N. Nica, Nucl. Data Sheets (to be published).
[2] A. Artna-Cohen, Nucl. Data Sheets **70**, 85 (1993).

Branching ratio of electron capture in the decay of ^{100}Tc

I. Ahmad,[1] A. Algora,[2] J. Äystö,[3] T. Eronen,[3] A. Garcia,[4] S. A. Hoedl,[4] A. Jokinen,[3] D. Melconian, I. D. Moore,[3] H. Penttilä,[3] S. K. L. Sjue,[4] H. E. Swanson,[4] and S. Triambak[4]

[1]*Argonne National Laboratory, Argonne, Illinois*

[2]*Instituto de Fisica Corpuscular, University of Valencia, Valencia, Spain*

[3]*University of Jyväskylä, Jyväskylä, Finland*

[4]*CENPA, University of Washington, Seattle, Washington*

We have completed analysis of the experiment to measure the electron capture branch for ^{100}Tc. The spectrum of x-rays observed in anti-coincidence with a scintillator (which has near 4π coverage to veto the dominant β^- branch) is shown in Fig. 1. The branching ratio for electron capture was found to be $B(\mathrm{EC}) = (2.6\pm0.4)\times10^{-5}$, and this was published in Physical Review C [1]. This branching ratio can be used as a benchmark calculation for models of two-neutrino and neutrinoless double-β decay.

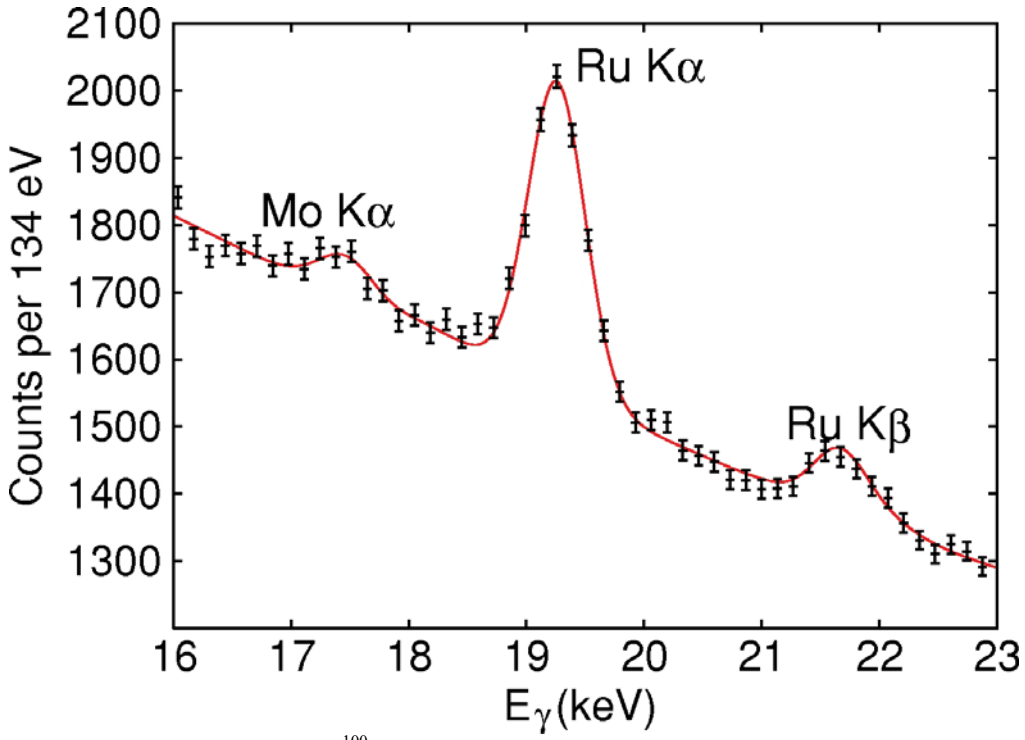

FIG. 1. X-ray spectrum from ^{100}Tc. The Mo x-rays are produced in EC decays while the dominant Ru x-rays are produced following β^- decays.

In the fall of 2009, we are going to perform a similar experiment to measure the EC branch of ^{116}In, again at the JYFL facility in Jyväskylä. The structure of nuclei in the region of A=116 are known to have small deformations which affect theory calculations; the EC branch of ^{116}In, like ^{110}Tc, can also serve as a benchmark calculation for interpreting the results of double-β decay experiments.

[1] S. K. L. Sjue *et al.*, Phys. Rev. C **78**, 064317 (2008).

The UCN-A experiment : measuring the β asymmetry using ultra-cold neutrons

D. Melconian and the UCNA collaboration[†]

Ultra-cold neutrons (UCN) offer the opportunity to measure properties of the neutron and its β-decay with unprecedented precision. The interest in using UCN over traditionally used cold neutrons are the fact that UCN are easily polarized and that they can be guided and bottled far away from production sources. At Los Alamos National Laboratory's LANSCE facility, a source of UCN has been developed where neutrons are produced via proton spallation from a Tungsten target and then converted into UCN by phonon downscattering in a solid deuterium "superthermal" moderator. These UCN are then guided through 12 m of shielding to the experimental area where the neutrons are polarized and observed in a very clean environment.

The UCNA collaboration recently published the result of the first measurement of the β asymmetry parameter, A_0, from UCN decay data collected in 2006 and 2007 [1]. The result is $A_0 = -0.1138(46)(21)$ where the first uncertainty is statistical and the second is systematic. This is in agreement with the currently accepted (Particle Data Group's) value of $A_0 = -0.1173(13)$ which is an average of cold neutron measurements (see Fig. 1).

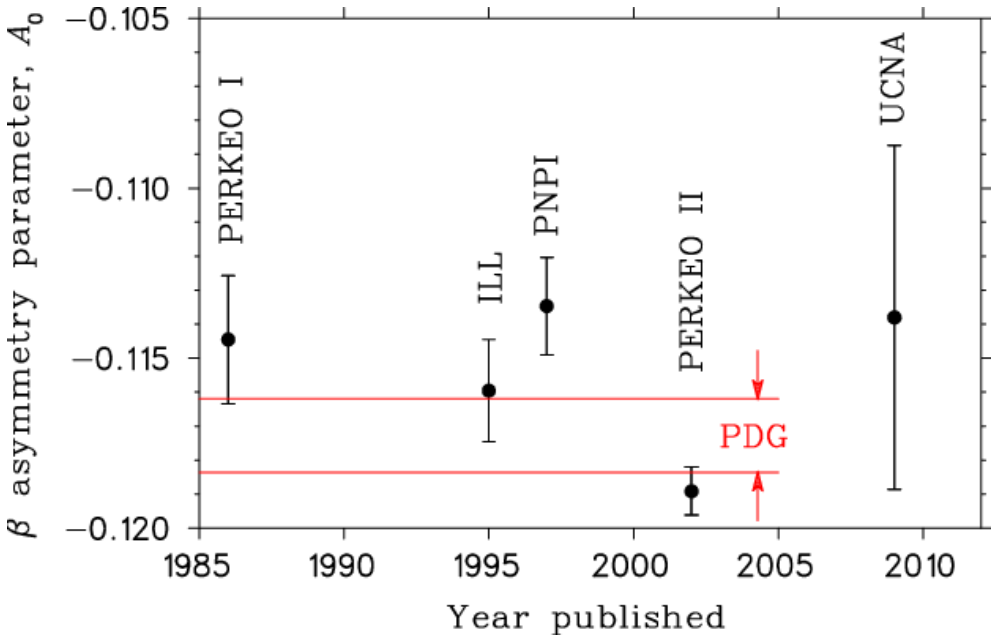

FIG. 1. Measurements of the β asymmetry of the neutron.

In 2008, we collected more data by running longer, increasing our transport efficiency and taking advantage of increased proton current for UCN production. Overall, our statistical uncertainty will be ≈5× better at less than 0.8%. New calibration sources have improved our energy calibration such that this, our dominant systematic uncertainty, has also been improved by a factor of five to 0.3%. Detailed depolarization measurements have reduced the systematic uncertainty due to depolarized UCN from 1.3%

to what we expect will be less than 0.4%. Once the analysis of the 2008 data is completed, we expect to have a statistics-limited measurement of A_0 below the 1% level of uncertainty, with systematics at the 0.6% level. This will resolve the scatter of results in the cold neutron measurements and represent the best measurement of the beta asymmetry in the neutron to date. Our ultimate goal is to measure A_0 to better than 0.3%.

[†]A. Saunders and A. R. Young spokespersons; the collaboration is formed by approximately 30 scientists from California Institute of Technology, Duke University, Idaho State University, University of Kentucky, Los Alamos National Laboratory, North Carolina State University, Texas A&M University, Virginia Tech University, the University of Washington and the University of Winnipeg.

[1] R. W. Pattie Jr. *et al.*, Phys. Rev. Letts. **102**, 012301 (2009).

Upgrade of the ^{37}K asymmetry measurment experiment

D. Ashery,[1] S. Behling, J. A. Behr,[2] I. Cohen,[1] A. Gorelov,[2] G. Gwinner,[3] K. P. Jackson,[2]
T. Kong,[4] D. Melconian, and M. R. Pearson[2]
[1]*Tel Aviv University, Tel Aviv, Israel*
[2]*TRIUMF, Vancouver, Canada*
[3]*University of Manitoba, Saskatchewan, Manitoba, Canada*
[4]*University of British Columbia, Vancouver, British Columbia, Canada*

.

β decay experiments have played a significant role in the development of the Standard Model (SM), starting with the classic experiment of C.S Wu *et al*. [1] that first provided experimental confirmation of parity violation in weak force interactions.

Low-energy nuclear physics experiments continue to play a critical role in testing predictions of the SM. β decay experiments are sensitive to new physics via the angular distribution of the decay; for example, the asymmetry in the emission of β's along the polarization axis is given by [2]:$(N_+-N_-)/(N_++N_-) = PA_\beta v_e/c$ where P is the average nuclear polarization, v_e is the positron's velocity and N_+ (N_-) is the number of observed β's emitted along (opposite to) the initial nuclear spin. The value of the correlation parameter, A_β, is sensitive to the form of the weak interaction; it will differ from the SM prediction if, for example, right-handed currents do in fact exist and have only escaped observation so far because they are heavily suppressed relative to the dominant *(V-A)* form of the weak interaction.

Our planned experiment will observe the decay of ^{37}K initially cooled and confined in a magneto-optical trap, with its nuclear spin polarized by optical-pumping. The experiment will be carried out at the ISAC/TRIUMF facility in Vancouver BC. Three ΔE-E β detectors will be placed around the trap with two in a back-to-back geometry along the axis of polarization, and a third monitor detector at 90º. Fig. 1 shows this geometry as viewed by the monitor detector. The Figure also shows the additional two micro-channel plates (MCPs) used to collect the recoiling ions and the shake-off electrons. Using this geometry, we will first perform a precision measurement of A_β, followed by further measurements of other correlation parameters.

We are in the process of upgrading our experimental setup that will allow us to make a precision measurement of A_β which was not possible in our first attempt due to large systematics [3]. The dominant systematic was found to be atoms which were lost from the trap, implanted onto the mirrors in front of the β detectors and depolarized before decaying. The key feature of the re-design is the addition of the shake-off electron MCP which will give us an extra coincidence condition which will ensure we only count decays which originated from the trapping region. Additional improvements include increasing the solid angle coverage of the β detectors by ~2× from the current setup (improving statistics) and replacing our DC-MOT with a novel AC-MOT [4] which will greatly reduce eddy currents while turning off the anti-helmholtz coils (needed for trapping) before polarizing and counting. The upgraded system will hopefully be in place to take data shortly after the facility shutdown during the 2010 winter Olympics in Vancouver.

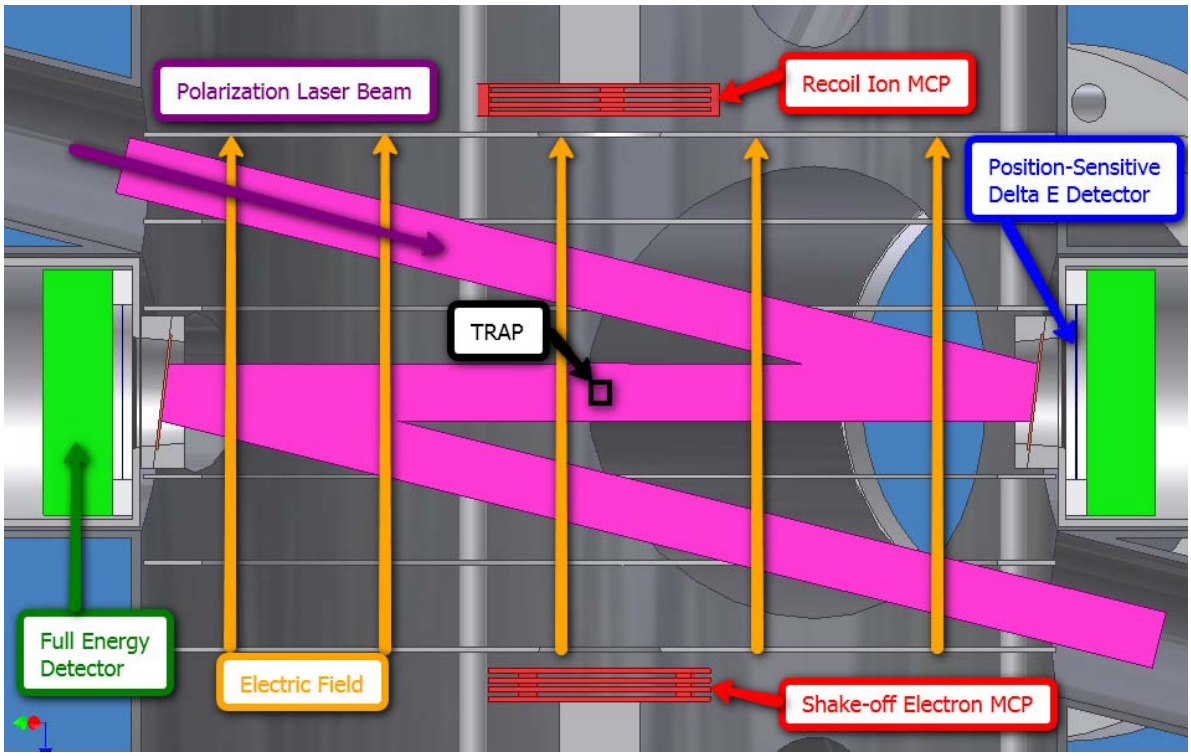

FIG. 1. A cut away view of the inside of the chamber from the point of view the 90° detector. The electrostatic hoops shown along the back wall produce the electric field shown in orange. The purpose of this field is to sweep the recoiling daughter (positive) ions towards one MCP, and the (negative) shake-off electrons into the opposite MCP. By requiring a signal in the shake-off electron MCP, we will ensure the β's observed in the ΔE-E detectors were polarized and decayed from the trapping region. The asymmetry in the observed rates of the two β detectors is proportional to the correlation parameter A_β.

[1] C. S. Wu *et al.*, Phys. Rev. **105**, 1413 (1957).

[2] J. D. Jackson, S. B. Treiman, and H. W. Wyld, Phys. Rev. **106,** 517 (1957).

[3] D. Melconian *et al.*, Phys. Lett. B **649**, 370 (2007).

[4] M. Harvey and A. J. Murray., Phys. Rev. Lett. **101**, 173201 (2008).

Spin physics with STAR at RHIC

P. Djawotho, J. L. Drachenberg, C. A. Gagliardi, L. Huo, M. Sarsour, R. E. Tribble,
and the STAR Collaboration

During the past year, our group efforts in STAR have focused on issues related to the trigger system for the electromagnetic calorimeters and analysis of forward rapidity data that were recorded with the Forward Pion Detector (FPD) and Forward Meson Spectrometer (FMS) during Run 8.

The primary STAR trigger for mid-rapidity jet physics is the "jet patch" (JP) trigger. The JP trigger accepts events where the sum of the transverse energy observed by the STAR Barrel or Endcap Electromagnetic Calorimeters (BEMC/EEMC) over a $\Delta\eta$ x $\Delta\varphi$ ~ 1x1 region surpasses a threshold. Through Run 8, there were 12 non-overlapping JPs in the BEMC, with 6 covering the region $-1 < \eta < 0$ and 6 more covering the region $0 < \eta < 1$. An additional 6 non-overlapping JPs covered the EEMC, $1.09 < \eta < 2$. This led to significant trigger inefficiency when the jet thrust axis fell near a boundary between two JPs. Even more important, this increased the bias in the JP trigger in two ways. Quark jets tend to have their energy more concentrated than gluon jets, which makes them more likely to deposit enough transverse energy within one of the JPs to satisfy the threshold. In a di-jet event, the pseudorapidities of the final-state jets are related to the momentum fractions, x_1 and x_2, of the partons that initiated the collision. Thus, the inefficiency near $\eta = 0$ directly correlates to reduced sensitivity for certain partonic kinematics.

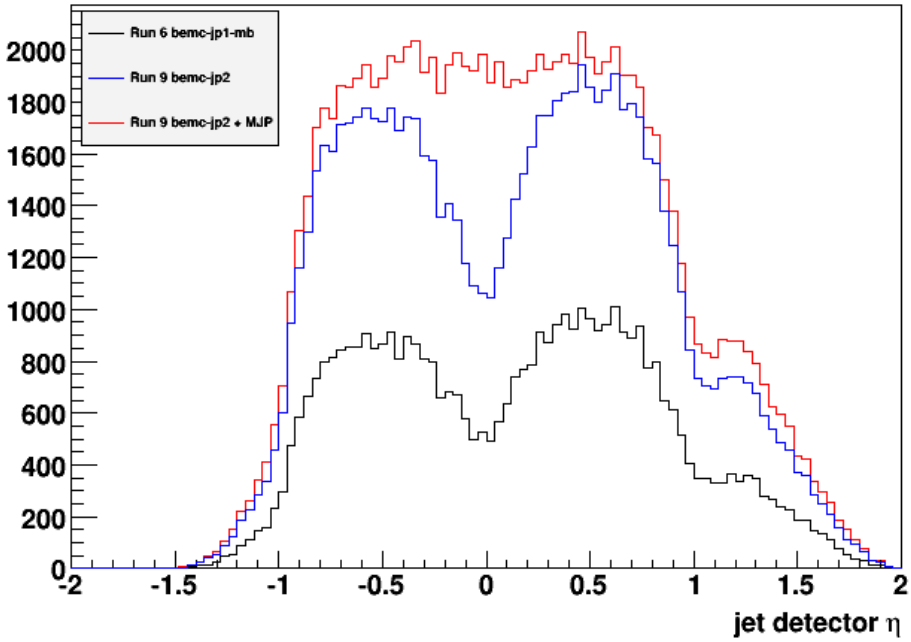

FIG. 1. Impact of the new overlapping jet patch near η=0. The red (blue) curve shows the jet yield for GEANT simulations of 200 GeV p+p PYTHIA events with partonic p_T in the range 11-15 GeV with (without) the new JP.

In April, 2008, we proposed a scheme to rewire and reprogram the BEMC and EEMC trigger electronics in order to provide additional JPs covering the pseudorapidity regions $-0.6 < \eta < +0.4$ and $0.4 < \eta < 1.4$. The changes were implemented last Fall, and have been in routine operation during Run 9. These new JPs reduce the inefficiencies at $\eta = 0$ and +1 significantly, as illustrated by the simulation study for the $\eta = 0$ gap in Fig. 1. It was not possible to eliminate the hard boundaries at $\varphi = 0$, $\pm\pi/3$, $\pm 2\pi/3$, and π at the same time. However, we have implemented a variation of the "Adjacent Jet Patch" (AJP) trigger that was tested during Run 5. In the new implementation, the AJP trigger requires a pair of JPs, which are next to each other in phi, to exceed a threshold that is set at half of the standard JP threshold. This significantly reduces, but does not eliminate, the inefficiency when jets fall close to the phi boundary between JPs. Trigger studies early in Run 9 indicate that the AJP trigger increased the jet trigger efficiency in 500 GeV p+p collisions by an additional 20-30%.

The simulations illustrated in Fig. 1 required us to enhance some features of the standard STAR trigger simulator code. Since then, we have converted the trigger simulator into a code that can be used to validate the electromagnetic calorimeter trigger performance on-line, in addition to its use to simulate the trigger performance off-line. The first demonstration of the power of this validation process came by running it over p+p data that had been recorded during Run 8. During the run, it had appeared that two JPs were less efficient than the others. Many tests, both by members of the Trigger group and by members of the Spin Physics Working Group, were unable to isolate any problem. Thus, no corrective action was taken during Run 8. In contrast, the new validation program pin-pointed the problem with <20 minute's worth of Run 8 data. It turned out that the problem involved a previously unknown failure mode of certain trigger modules that was not tested by the routine diagnostics. Following this proof of principle, the new validation program was set up to run automatically on the trigger data from every run. Typically, three minutes after the run ends, the validation results are saved to a pdf file that can be browsed over the web. This has given us the ability to isolate and fix problems with the trigger system, including several cases of the Run 8 failure mode, quickly during Run 9.

Members of our group are working toward the goal of reconstructing jets at forward rapidity using the Run 8 transverse spin data from the FMS together with the west Forward Time Projection Chamber. As a first step along this path, the transverse single-spin asymmetry, A_N, has been measured for π^0 production at large x_F and small p_T, using data that were recorded with the east FPD during Run 8. Previous STAR results from Runs 3, 5, and 6 appeared to show a non-monotonic behavior for A_N in the region $1.2 < p_T < 2.5$ GeV/c [1]. It has been suggested [2] that this behavior might indicate that the single-spin asymmetry arises from a combination of the Sivers and Collins effects, with the two processes dominating in different p_T regions. FPD data were recorded during the last few days of Run 8 to explore this possibility. Fig. 2 shows some of the results [3]. The Run 8 data are mostly consistent with results from previous runs. However, in the high-x_F, low-p_T region where the previous data were dominated by low-statistics RHIC Run 3 measurements, the Run 8 data show that A_N is smooth and monotonic. The same conclusion is found when looking at the p_T dependence of the Run 8 data for narrow bins in x_F [3]. These results were presented by J. Drachenberg for the STAR Collaboration at SPIN 2008.

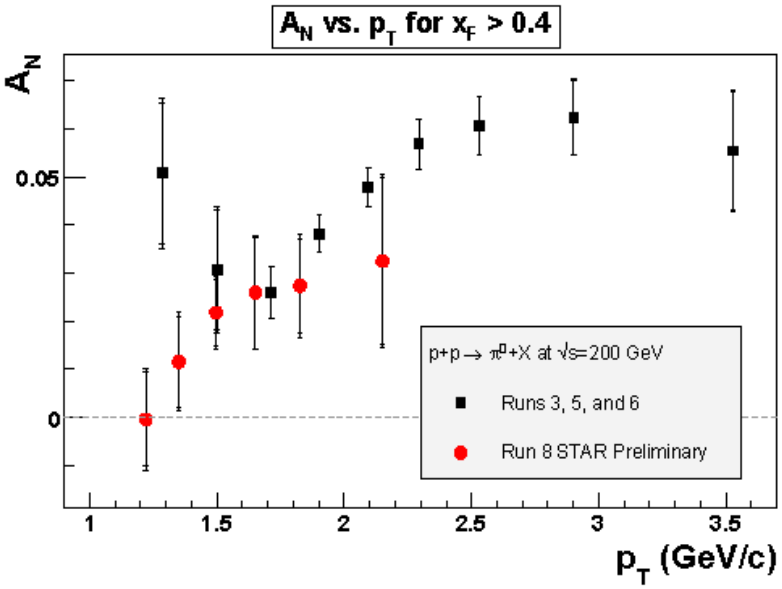

FIG. 2. A_N vs. p_T for inclusive π^0 production at $x_F > 0.4$. The inner error bars are statistical. The outer error bars add statistical and systematic uncertainties in quadrature. This figure is from [3].

Our group continues to handle a variety of administrative responsibilities in STAR. Last June, Dr. Gagliardi was elected to a two-year term as an at-large member of the Advisory Board. This past Fall, the new STAR Spokesperson appointed Dr. Gagliardi chair of the Trigger Board for Run 9. The Trigger Board is charged to ensure that STAR records the data necessary to achieve the Collaboration's stated physics goals. Drs. Gagliardi and Tribble have also participated on several STAR god-parent committees, including chairing three of them.

[1] B. I. Abelev *et al*. (STAR Collaboration), Phys. Rev. Lett. **101**, 222001 (2008).
[2] F. Yuan, Phys. Lett. **B666**, 44 (2008).
[3] J. L. Drachenberg, (for the STAR Collaboration), arXiv:0901.2763 [hep-ex].

TWIST: Measuring the space-time structure of muon decay

C.A. Gagliardi, R.E. Tribble, and the TWIST Collaboration

This past year, TWIST published improved measurements of the Michel parameters ρ and δ in normal muon decay [1] based on the final analysis of the data that were recorded during 2004. We found $\rho = 0.75014 \pm 0.00017(\text{stat.}) \pm 0.00044(\text{syst.}) \pm 0.00011(\eta)$ and $\delta = 0.75067 \pm 0.00030(\text{stat.}) \pm 0.00067(\text{syst.})$. These results were included in a new global analysis of muon decay measurements. The correlation between the uncertainties in ρ and δ was also included in the global analysis for the first time. We find the total contribution from right-handed muon couplings to be $Q^{\mu}_{R} < 0.0024$ with 90% confidence. This is a 20% reduction in the limit for Q^{μ}_{R} compared to the previous global analysis [2].

The focus of TWIST has now turned to the analysis of the final data sets, which were taken in 2006 and 2007. The leading systematics for ρ and δ in the 2004 analysis involved wire chamber response, energy scale calibration, and positron interactions. New procedures were developed very late in the 2004 data analysis to extract precise drift chamber distance vs. time relationships from the measured data. The new distance vs. time relationships came too late to be used in the primary 2004 data analysis. They were only used to estimate the chamber response systematic. They have now been adopted for the standard analysis of the ’06 and ’07 data, which reduces the corresponding systematic uncertainty dramatically. Work is underway to minimize the effects of the other two leading systematics. Overall, we expect that the final precisions for ρ and δ will be approximately ±0.0003. The final precision for $P_{\mu}\xi$ should be ±0.001 or better. Our group is playing a much smaller role in this final analysis round than we did for the 2002 and 2004 data analyses.

[1] R. P. MacDonald *et al*. (TWIST Collaboration), Phys. Rev. D **78**, 032010 (2008).
[2] C. A. Gagliardi, R. E. Tribble, and N. J. Williams, Phys. Rev. D **72**, 073002 (2005).

Toward understanding relativistic heavy-ion collisions with the STAR detector at RHIC

M. Cervantes, R. Clarke, M. Codrington, A. Hamed, S. Mioduszewski, and the STAR Collaboration

I. Calibrations

A. Barrel Pre-Shower Detector

We have been fine-tuning the calibrations of the BPS channels for the Run-7 (Au+Au collisions) data. We first recalculated the calibration factors by fitting the slopes of the ADC spectra. Fig. 1 shows the slopes before and after calibration. Then we applied these constants and required a 1 GeV charged track to pointing to a channel to check whether the resulting Minimum Ionizing Peaks (MIP's) were aligned for all channels as a result of these calibration factors.

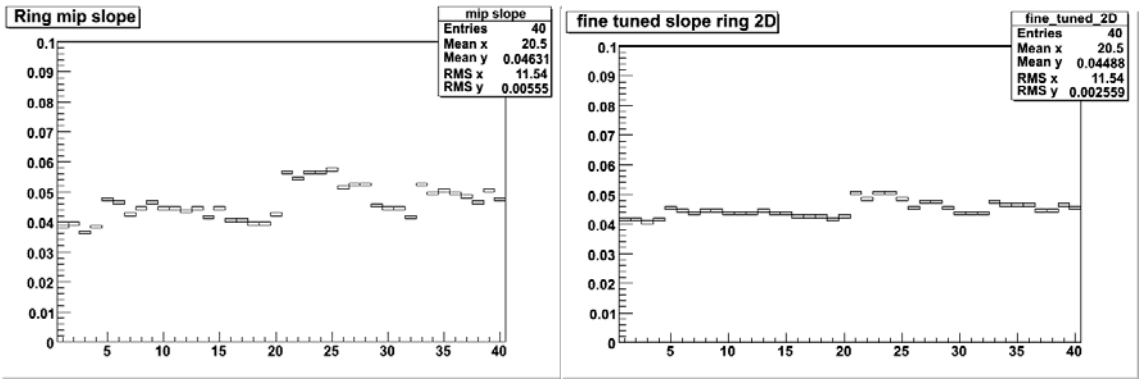

FIG. 1. Average slope per ring before calibration (left) and after calibration (right).

B. Barrel Shower Maximum Detector

We have also been working on the strip-by-strip (18000 strips total) calibration of the Barrel Shower-Max detector (BSMD). Since we are using the BSMD in the γ-jet analysis to discriminate between γ and π^0, fluctuations in the gain can smear out the differences in shower-shape observed for photons and π^0. A strip-by-strip calibration can hopefully sharpen the differences, making the shower-shape cut to identify direct photons more efficient. We plan to apply the calibrations and re-analyze the data, with the goal of reducing the systematic errors. Fig. 2 shows the ADC distribution of a single strip in the BSMD. The feature to note is that the spectrum is not a pure exponential in ADC.

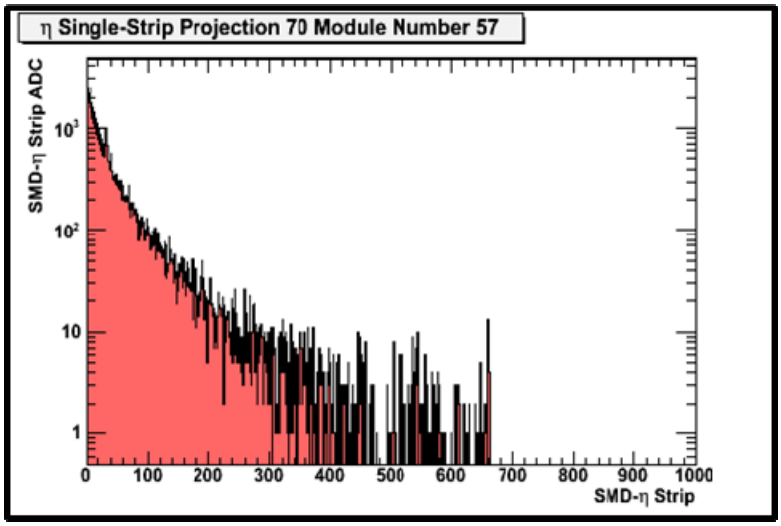

FIG. 2. ADC distribution of one BSMD strip.

Thus, fitting with a constant slope value depends strongly on the ADC range used in the fit. Therefore, we fit the ADC spectra with the following function,

$$e^{[P_0+P_1(x+\alpha x^2)]}$$

where α is a constant value for all strips and P_1 is the fit-extracted gain (per strip). Fig. 3 shows a profile histogram of the gains as a function of pseudorapidity. The left is before the calibration, and the right is after. The pseudorapidity dependence was kept the same through the calibration procedure. The gains per pseudorapidity bin were adjusted to match the average value. The spreads on the right have been reduced from the left, showing that the calibration has tightened up the distribution of relative gains per pseudorapidity bin.

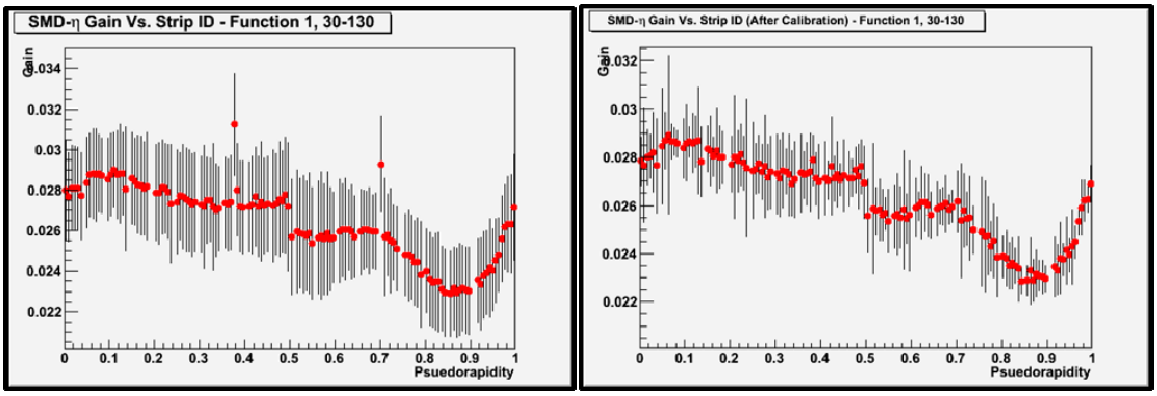

FIG. 3. Average gain as a function of pseudorapidity before calibration (left) and after calibration (right).

II. Physics Analyses

We are studying relativistic heavy-ion collisions with two different probes: bottomonium and γ-jet. The bottomonium measurement is important to disentangle competing effects, screening in the deconfined plasma vs. $q\bar{q}$ recombination, both possibly playing a role in the production of charmonium in heavy-ion collisions. Photon-hadron correlations (γ-jet) measure the medium-induced parton energy loss as a function of the parton's original energy.

A. Upsilon Analysis

We have performed the Upsilon analysis on the Run-8 d+Au data set, where the background is smaller. Fig. 4 shows the reconstructed mass from e^+e^- pairs (black) and like-sign pairs (red). There is very little background observed even without background subtraction, and a cut on the BPRS is not necessary with such a large signal-to-background ratio. This analysis now awaits results from embedding Upsilon particles into real events in order to evaluate the efficiency corrections.

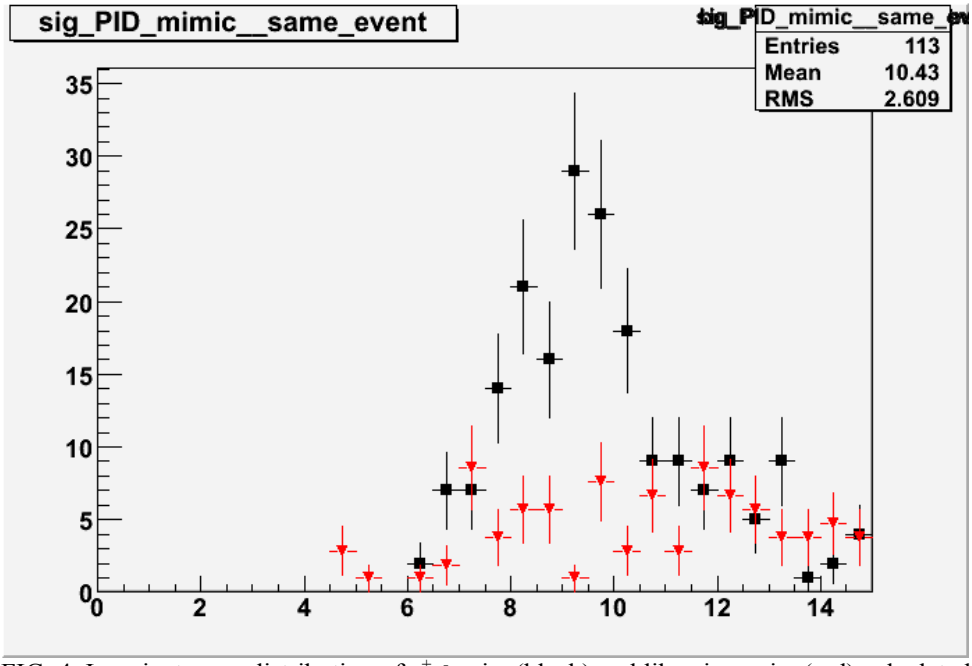

FIG. 4. Invariant mass distribution of e^+e^- pairs (black) and like-sign pairs (red) calculated in d+Au events.

B. Photon-Jet Analysis:

We have taken the initial analysis of γ-jet correlations in Run-7 Au+Au collisions, and recalculated the yields in bins of z_T, which is the fractional transverse momentum of the associated hadron to that of the trigger photon ($z_T = p_{T,associated}/p_{T,trigger}$), shown in Fig. 5. This gives us a more direct

measure of the modification of the fragmentation function due to the medium. The results have been presented at several national and international meetings (e.g. [1]-[3]). They also appeared in a theory paper in which our results were compared with a calculation of energy loss in the medium [4]. Recently, we have concentrated on finalizing a detailed study of the systematic errors for the publication of our results. We currently have a paper draft (to be submitted to Physical Review Letters) circulated within the STAR Collaboration. We plan to follow this letter with a longer, more detailed publication, which will include also the details of the π^0-triggered correlated hadron yields.

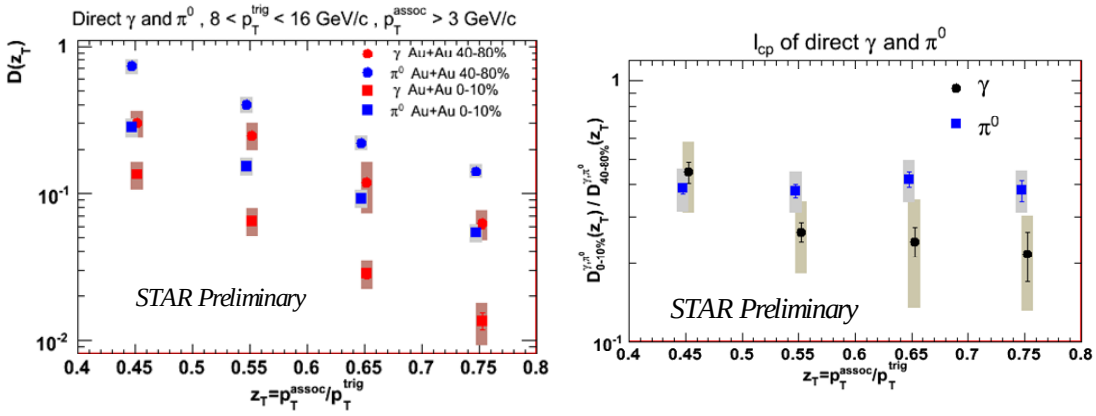

FIG. 5. (Left) Associated yields of hadrons correlated with a high-p_T direct γ (red) or π^0 (blue) trigger, as a function of z_T ($=p_T^{assoc}/p_T^{trig}$) for 0-10% centrality and 40-80% centrality. (Right) Ratio of central to peripheral yields for direct photon triggers (black) and π^0 triggers (blue).

[1] A. M. Hamed (for the STAR Collaboration), *Proceedings of the 34th International Conference on High Energy Physics (ICHEP 2008) (submitted);* arXiv:0810.3743.

[2] A. M. Hamed (for the STAR Collaboration), *Proceedings of the 3rd International Conference on Hard and Electromagnetic Probes of High-Energy Nuclear Collisions (HP2008) (submitted)*, arXiv:0809.1462.

[3] A. M. Hamed for the STAR Collaboration, J. Phys. G **35**, 104120 (2008).

[4] H. Zhang, J. F. Owens, E. Wang, and X. -N. Wang, arXiv:0902.4000.

SECTION II

HEAVY ION REACTIONS

The search for super heavy elements using alternative mechanisms

J. B. Natowitz, R. Wada, K. Hagel, T. Materna, Z. Chen, L. Qin, P. K. Sahu, G. Souliotis, G. Chubaryan, M. Barbui, S. Moretto,[1] D. Fabris,[1] M. Lunardon,[1] M. Morando,[1] G. Nebbia,[1] S. Pesente,[1] V. Rizzi,[1] G. Viesti,[1] V. Bocci,[2,3] A. Andrighetto,[3] M. Cinausero,[3] G. Prete,[3] Z. Majka,[4] A. Wieloch,[4] S. Kowalski,[5] F. D. Bechetti,[6] T. W. O'Donnell,[6] and H. Griffin[6]

[1]*Dipartamento di Fisica dell'Universita di Padova and INFN Sezione di Padova, Italy*

[2]*Dipartimento di Fisica dell'Universita di Brescia and INFN, Italy*

[3]*INFN Laboratori Nazionali di Legnaro, Italy*

[4]*Smoluchowski Institute of Physics, Jagiellonian University, Krakow, Poland*

[5]*Institute of Physics, Silesia University, Katowice, Poland*

[6]*University of Michigan, Ann Arbor, Michigan*

We reported in [1] the motivation and calibration for a search for super heavy elements using alternative reaction mechanisms. With the calibration complete, we have substantially refined the analysis reported in [1] to minimize the probability of identifying accidental events as super heavy element candidates.

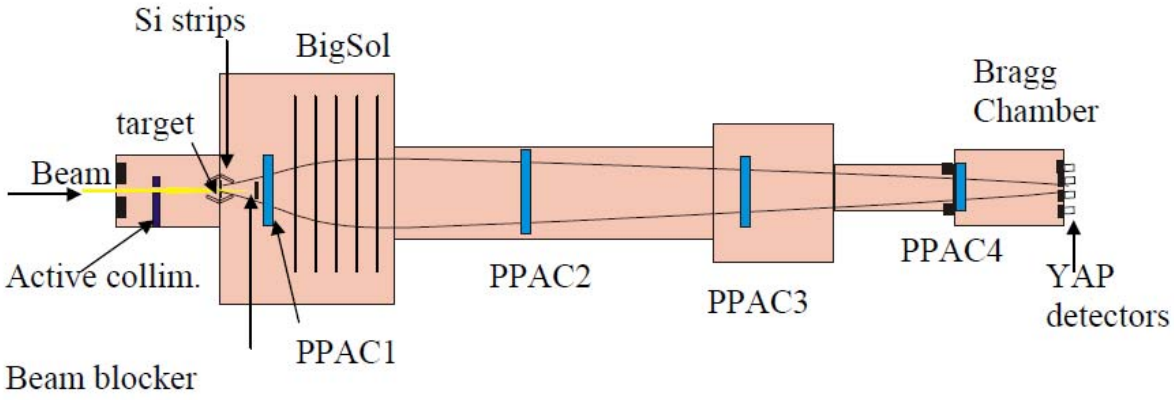

FIG. 1. Experimental setup.

Fig 1. shows the experimental setup. 7.5 MeV/u Au ions were incident on a Th target depicted on the left side of the figure. A 16 segment annular Parallel Plate Counter (labeled PPAC1) with a 2.5 cm hole in the center was positioned 25 cm downstream from the target. Three parallel plate counters were positioned at 3.3m (labeled PPAC2), 5.1m (labeled PPAC3) and 6.15m (labeled PPAC4) from the target. A 40cm gas ionization chamber(IC) was placed just past PPAC4. During the data taking part of the experiment a beam blocker depicted just in front of PPAC1 was inserted in order to block the beam and allow for reaction products emitted at angles larger than 6 deg to be detected in the IC downstream after passing through the BigSol magnet.

The experimental setup provided a number of redundant time measurements. These time measurements consisted of independent measurements of the time difference between PPAC3 and PPAC4, between PPAC2 and PPAC3, between PPAC2 and PPAC4 and between PPAC1 and PPAC4. All time measurements were required to be consistent in order for an event to be considered. We also implemented a pileup rejection scheme in which the time between two events in PPAC4 was measured and if the time between two event in PPAC4 was less than 8μs, the event was rejected.

The IC provided a measurement of the energy loss through eight 4.65 cm anodes. The energy loss in each anode of the IC was measured both in the traditional method of using a peak sensing ADC after signal shaping as well as measuring the trace of the raw signal using a flash ADC. The inclusion of the flash ADC for the purpose of analyzing the signal shape proved invaluable in rejecting spurious events.

After the calibration was completed, events were first filtered by requiring that the above mentioned time measurements were consistent, and that the pileup measurement indicated no pileup. Then products that were heavier than the beamlike particles were selected using the energy vs time measurement as shown in [1]. This narrowed the selection down to a few hundred events. The traces of the signals of each anode measured by the flash ADC from these events were then visually inspected and events were selected that showed no double peaks or any other abnormalities.

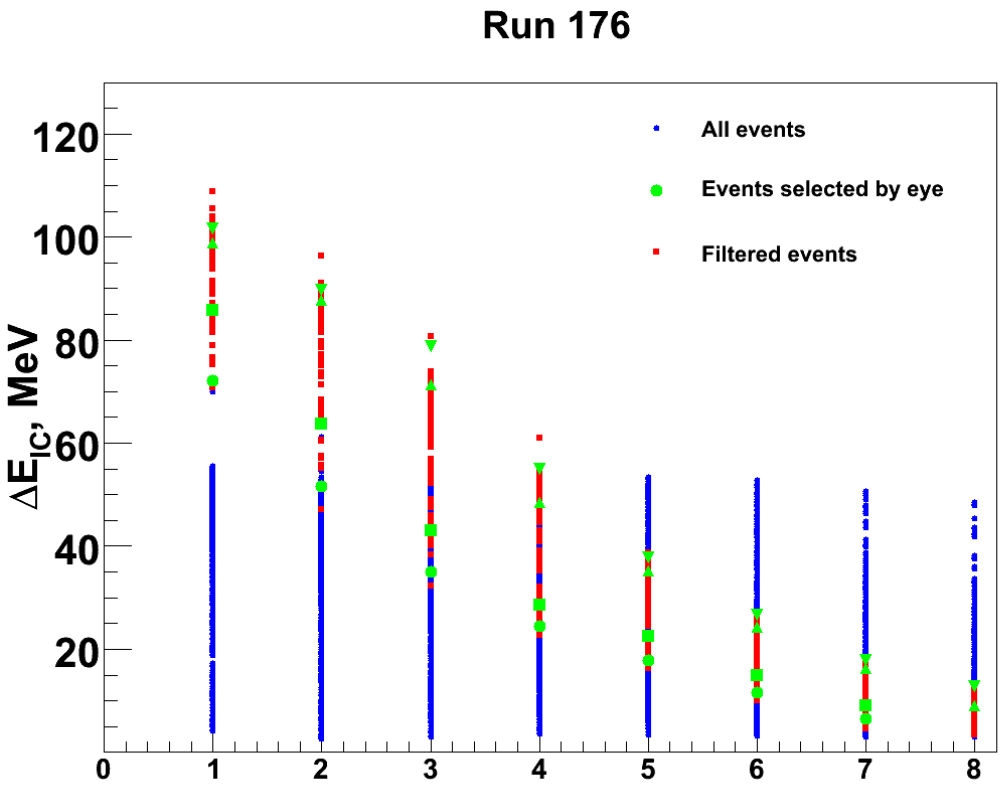

FIG. 2. IC Track profile for different classes of events.

The green symbols in Fig. 2 show the trace of these selected events as they traverse the anodes of the IC. The blue symbols in the top panel of Fig. 2 show the traces of the rest of the event sample. We note that the selected events show a different energy loss profile through the IC. They start out with a significantly higher than normal energy deposit in the first anode (75-100 MeV as opposed to about 40 MeV for normal events) and they lose energy at a much larger rate. This behavior could be consistent with heavy products.

Inspired by the significant difference of these selected events from normal events, we decided to investigate whether an interesting set of events could be obtained by simply filtering on the energy loss profile of heavy fragment candidates. We therefore selected events of a similar profile in delta E as that of the events that were found by eye in the first pass. In the first pass, no other requirements were placed on those vents. The red symbols in Fig. 2 show the events selected using this filtering technique. We note that the events selected follow the same trend as the visually selected events. After these events were selected, we examined the events to see how consistent they were with the different redundant measurements performed in this experiment.

The top panel of Fig. 3 shows the pileup rejection TAC for the complete sample of events for one run. The events at the far right in channel 2000 are events in which a second product did not fire PPAC4 for at least 8 μs after the event of interest. It is seen that this comprises the vast majority of the events when considering the entire event sample. In contrast, we observe in the lower panel that when gating on our selected IC profile filtered events that only two events in that run are left over in channel 2000 (events that show no pileup).

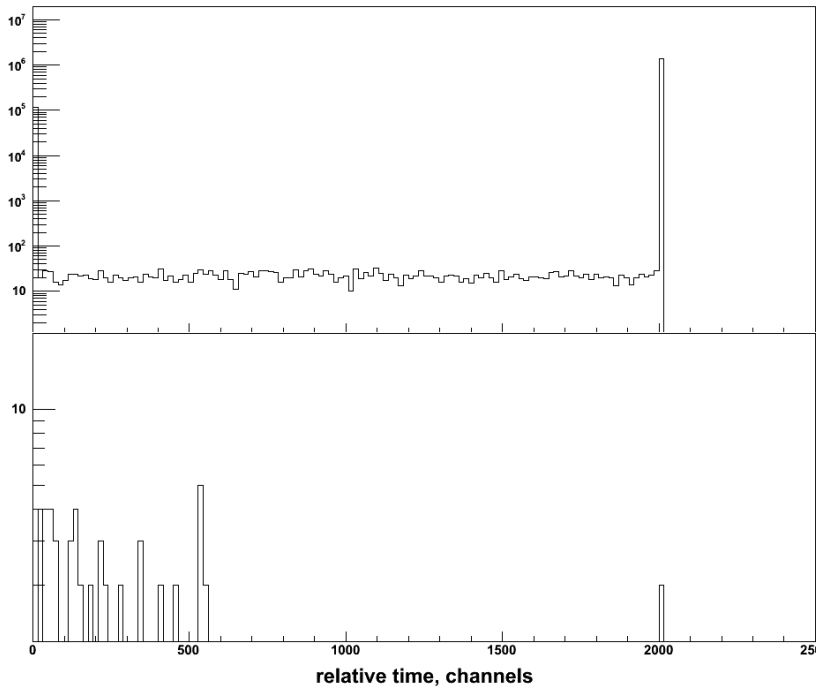

FIG. 3. Top panel: pileup rejection TAC for all events. Bottom panel: pileup rejection TAC for filtered events. An entry in channel 2000 means that there was not another event for 8us after the event of interest.

Fig. 4 shows the E vs t plot for all events (black), for events selected with the IC profile filter (blue) and filtered events requiring no pileup in the pileup rejection TAC (red) for the runs that were analyzed. We note that the filtered events (blue) indicate at face value products heavier than Au. However the majority of those events have entries in the pileup rejection TAC between 0 and 500 indicating that these events result from pileup. The events which indicate no pileup according to the pileup TAC rejection measurement are shown in red and also indicate heavy fragments.

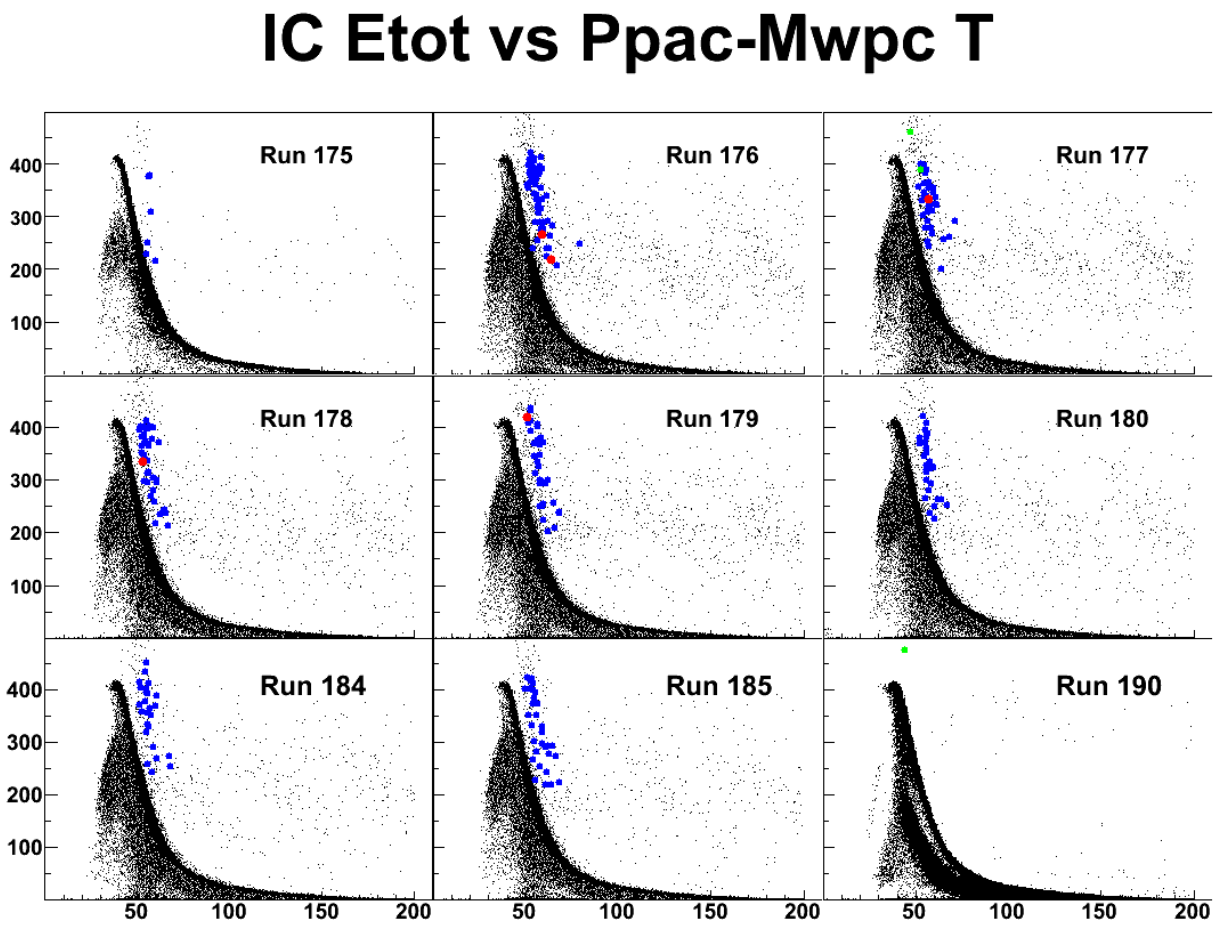

FIG. 4. E vs t for all events (black), IC ΔE profile filtered events (blue) and IC ΔE profile filtered events with no pileup (red).

We have also checked the various redundant timing measurements for the filtered events and found that most events have all time measurements consistent. In particular, those with tagged as pileup free had consistent time measurements.

We now exploit the flash ADC information to check further for consistency of the interesting "pileup free" events (red symbols in Fig. 4). We show in Fig. 5 a plot of the energy loss in the IC as measured from the peak sensing ADC vs the energy loss as measured from an analysis of the flash ADC. The black symbols show all events in the sample. The diagonal line shows where both measurements are equal and is drawn to guide the eye. We note that the majority of events yield the same energy

measurement when obtained from the peak sensing ADC or from the flash ADC. There are, however, events away from the diagonal indicating an inconsistency in one or both energy measurements. The blue symbols show the IC ΔE profile filtered events. These events are for seen for the most part to be away from the diagonal line indicating an inconsistency in the measurement of those events. The red symbols show the IC ΔE profile filtered events with the pileup rejection condition added. It is seen that only one of those events shows consistency between the two measurements.

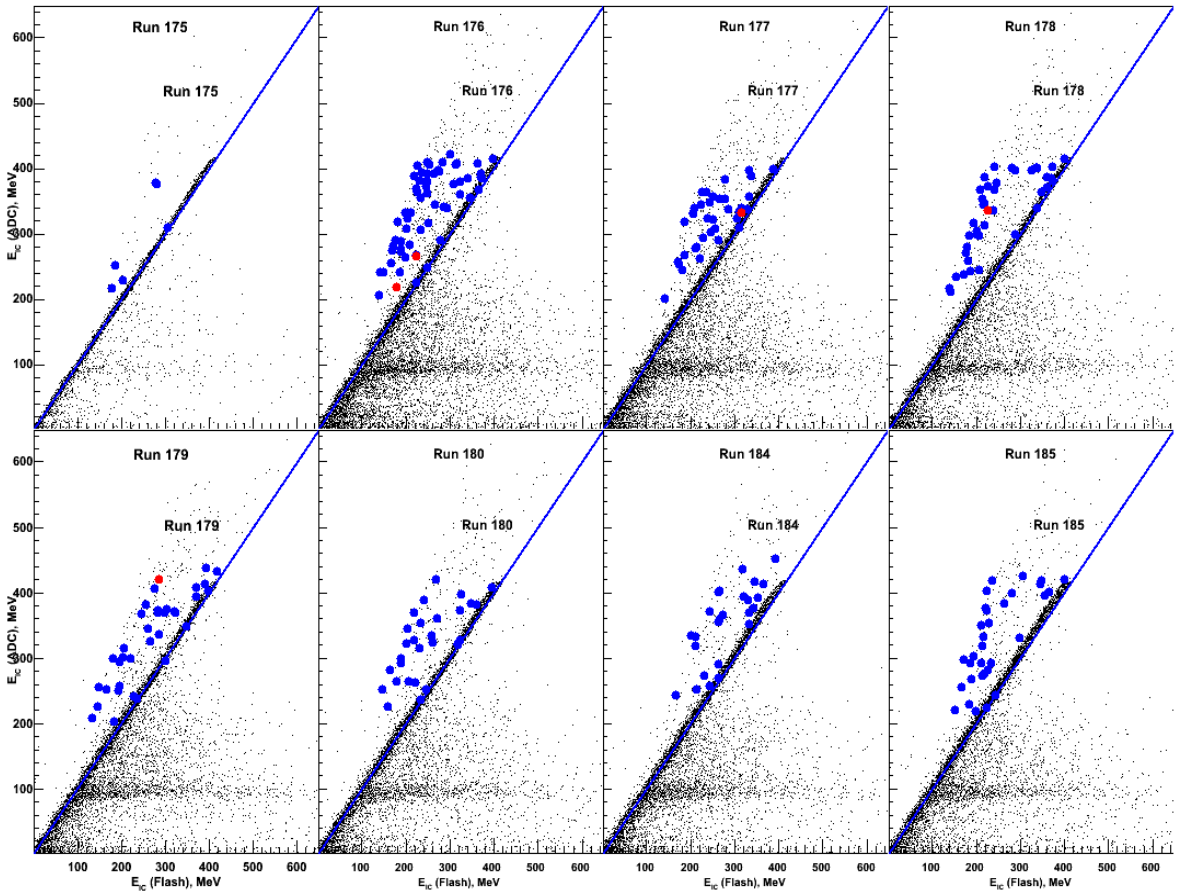

FIG. 5. E derived from Flash ADC plotted against E derived from Peak sensing ADC.

We have investigated the reason for a mismatch in measurements between a peak sensing ADC and the flash ADC. It is possible with a very low probability there could be an event which occurred near the end of an acquisition gate that was integrated by the shaper and was followed by a real event occurring at a very short time after the end of the acquisition of the previous event. This new event could have ended up as a signal added to that accidental event in the shaper and therefore passed to the peak sensing ADC. The events in the flash ADC are not shaped and therefore the previous accidental event would not have been observed in the flash ADC.

More work needs to be done to establish whether the one event that survives all cuts is real. Nevertheless, we used PPAC1 as a monitor and calibrated it using direct beam to obtain an estimate of an

upper limit of the cross section of such events. Using that information, we have established that for the amount of data analyzed to date that one event would indicate a cross section between 55-60 nb.

We are planning an experiment designed to increase the statistics to lower the upper limit of our measured cross section. We are also exploring ways to upgrade our pileup rejection techniques. In particular, pulsing the beam such that there would be no beam on target during the readout of an event would eliminate accidental events of the type that we speculate are causing the discrepancy between the peak sensing and flash ADC. We are also considering segmenting the anodes across the IC in an attempt to more easily recognize pileup events.

[1] P. Sahu *et al.*, *Progress in Research*, Cyclotron Institute, Texas A&M University (2007-2008), p. II-1.

Calibration of the ^{40}Ca + ^{40}Ca data taken on NIMROD-ISiS array

C. Bottosso, J. B. Natowitz, K. Hagel, R. Wada, M. Huang, A. Bonasera, G. Liu,[1]
G. Viesti,[2] M. Barbui,[2] S. Moretto,[2] G. Prete,[3] S. Pesente,[2] D. Fabris,[2]
Y. El Masri,[4] T. Keutgen,[4] S. Kowalski,[5] and A. Kumar[6]
[1]*Shanghai Institute of Applied Physics, Shanghai, China*
[2]*Dipartamento di Fisica dell'Universita di Padova and INFN Sezione di Padova, Italy*
[3]*INFN Laboratori Nazionali di Legnaro, Italy*
[4]*Universit´e Catholique de Louvain, Louvain-la-Neuve, Belgium,*
[5]*Institute of Physics, Silesia University, Katowice, Poland*
[6]*Nuclear Physics Laboratory, Department of Physics, Banaras Hindu University, Varanasi, India*

At low densities nuclear matter has the tendency to clusterize into α particles. Typically a Bose gas of α particles has the property of a condensate because the de Broglie wavelength of relative motion is much larger than the distance between two alpha particles. This indicates that α clusters could be a good candidate to observe the Bose Einstein Condensation (BEC). There are several suggestions [1] that one possible signature of this phenomenon is a strong fluctuation in the number of particles. Of course we have to assume that α particles exist inside particular nuclear states, but the Interactive Boson Model (IBM) and many experiments have proved that this assumption seems to be reasonable.

In order to investigate the properties of α clusters, an experiment was performed in August 2008 using the upgraded NIMROD-ISiS charged particle array [2], taking advantage of both its excellent isotopic resolution and the total angular coverage guaranteed by the 4π detectors. We chose to observe the α particles emitted by a ^{40}Ca projectile interacting with a ^{40}Ca target so as increase the probability of creating multiple α clusters. The system was studied at the three different energies of 35 MeV/u, 25 MeV/u and 10 MeV/u in order to understand changes in the characteristics of the α clustering as a function of excitation energy.

We have begun the calibration of the data set, starting with the particle identification (PID). We analyzed the spectra showing the CsI fast versus slow components, the Si versus CsI signals and, in the case of a Si – Si – CsI telescope, the ΔE -E plots of Si versus Si signals. For completeness, we also acquired signals collected from the back of the silicon detector wafers. PID is accomplished by setting gates around the linearized line of a particular element. Examples of the CsI fast vs. slow components and Si-CsI plots for the energy of 35 MeV/u are shown in Fig. 1 and Fig. 2.

We note that CsI detectors can resolve isotopes of elements with Z = 1 and Z = 2 and, for some crystals in the most forward rings, it is possible to see also lithium isotopes. On the other hand, the resolution of telescope arrays in many cases allows identification of isotopes of elements up to Z = 10.

Using the ΔE vs. E or fast vs. slow spectra a smooth line was drawn for each element along one isotope (usually the one with the highest intensity). Once the distance between the data points and the chosen line was computed, the data were displayed as function of the mass of each element. At this point, windows were placed around the centroid of each identified isotope.

The linearizations were examined run-by-run and all necessary adjustments were applied to compensate for small drift in gains.

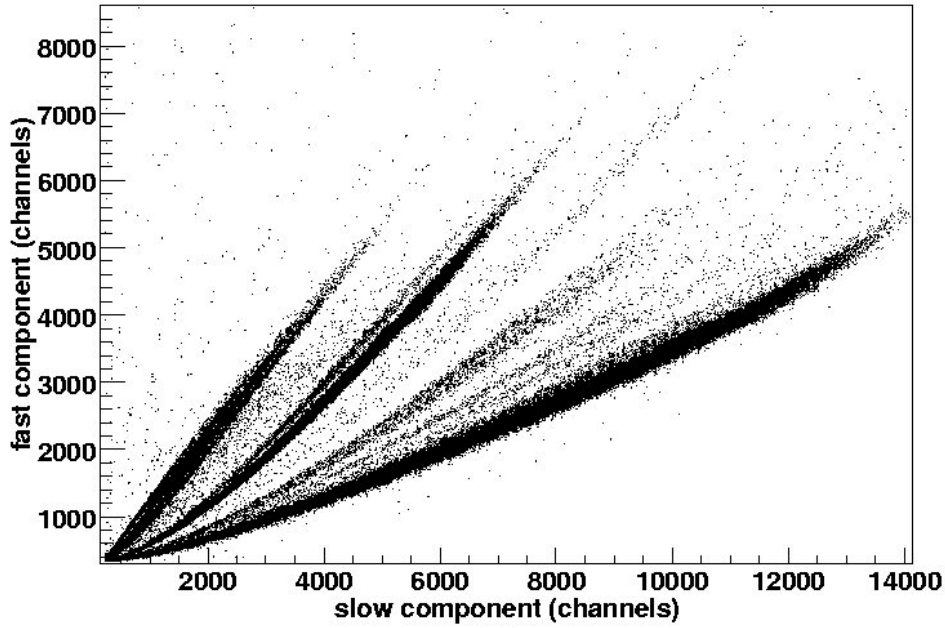

FIG. 1. Fast and slow components of CsI #4 are plotted. Hydrogen, Helium and Lithium isotopes are visible.

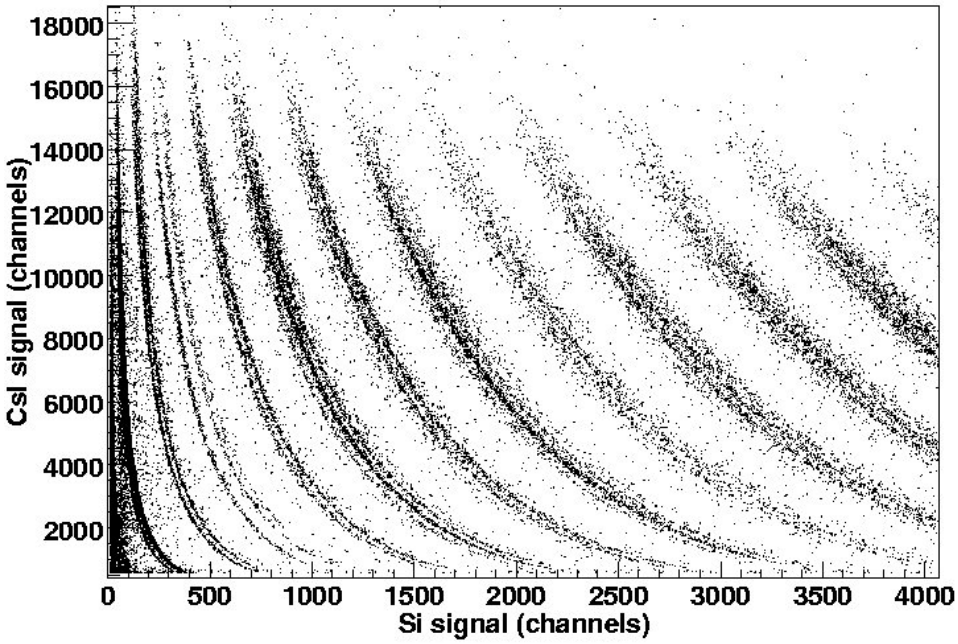

FIG. 2. Raw spectrum of a Si-CsI telescope in Ring 4.

The isotopic distribution obtained as a result of the linearization process is plotted in Figs. 3 to 5. In the CsI spectra elements with charge Z = 1, Z = 2 and Z =3 are shown. Elements with atomic number from 1 to 8 can be clearly resolved by the Si – CsI telescopes, whereas if we want to analyze heavier elements (up to Z = 14) we can look at the result of the linearization for Si – Si plots. Of course, both Si – CsI telescopes and Si – Si telescopes can also resolve lighter elements.

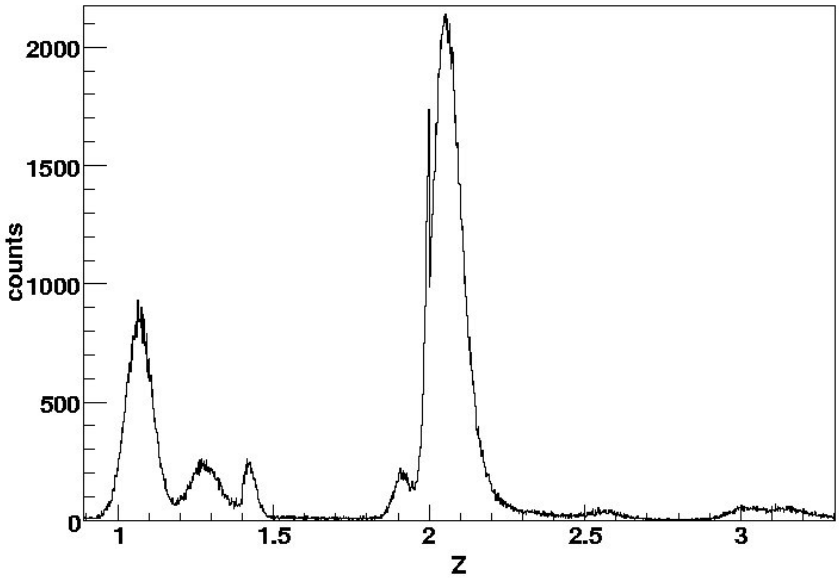

FIG. 3. Isotope distribution for a CsI detector in Ring 3.

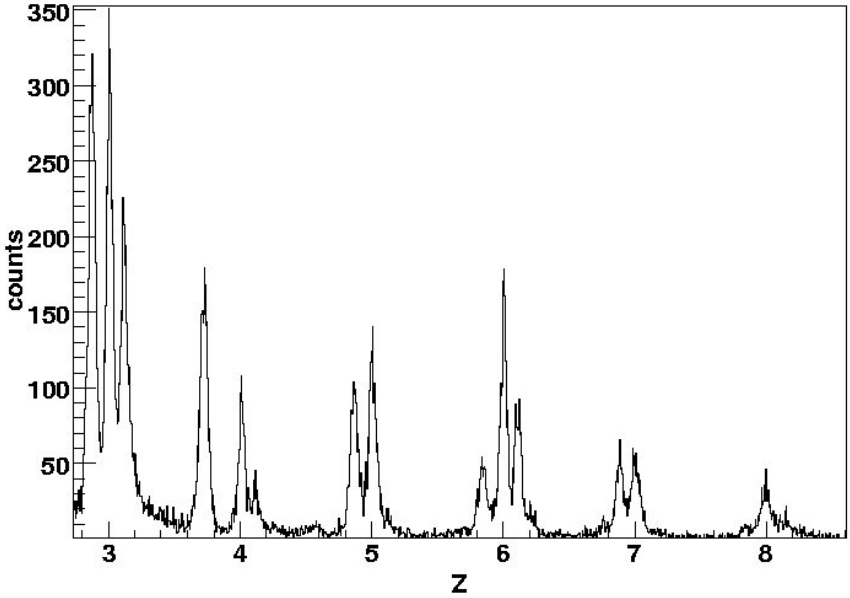

FIG. 4. Result of the linearization process for one Si -CsI telescope in Ring 2. Isotope identification of elements with charge up to Z = 8 is possible.

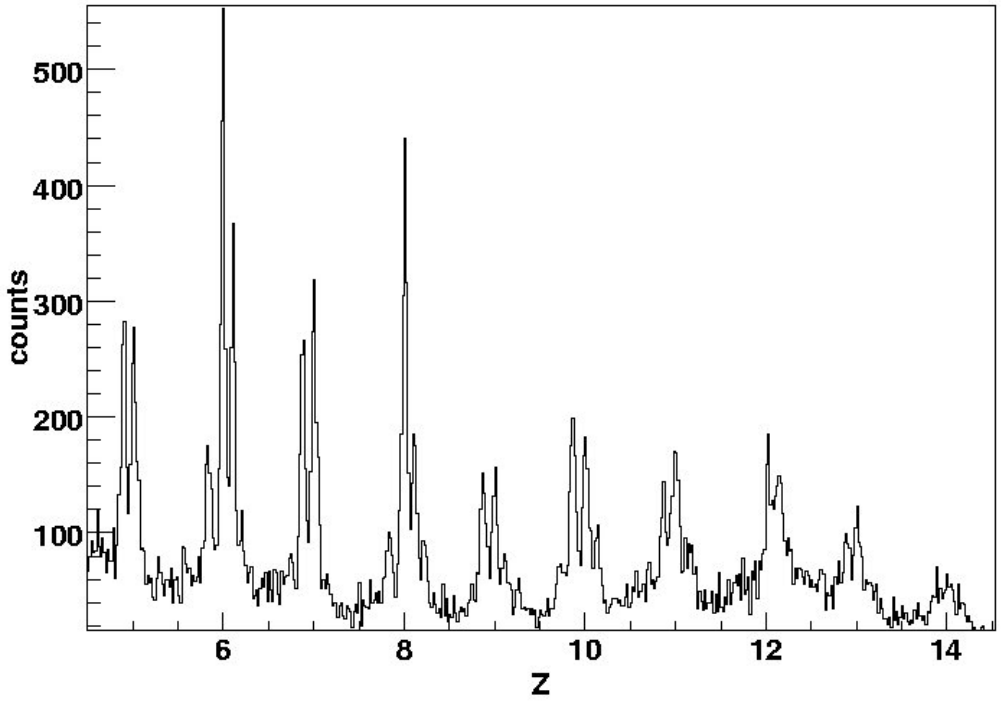

FIG.5. Result of the linearization process for a Si – Si – CsI telescope in Ring 4.

The linearization process is now complete. It was important to be able to identify isotopes of elements heavier than Helium because we could find, even though with low probability, 3-α systems collapsing to ^{12}C or 4-α systems collapsing to ^{16}O.

At the moment our next step will be the calibration in energy of the spectra that have been linearized. We foresee that in the next few weeks we will be able to proceed with the data analysis.

[1] S. Wuenschel *et al.*, Nucl. Instrum. Methods Phys. Res.. **A604**, 578 (2009)
[2] V. V. Begun and M. I. Gorenstein, Phys. Lett. B **653**, 190 (2007).

Energy loss of energetic ^{40}Ar, ^{84}Kr, ^{197}Au and ^{238}U ions in mylar, aluminum and isobutane

M. Barbui, S. Pesente,[1] D. Fabris,[1] M. Lunardon, [1] S. Moretto, [1] G. Nebbia, [1] G. Viesti, [1] M. Cinausero, [2]
G. Prete, [2] Z. Chen, K. Hagel, S. Kowalski,[3] J. B. Natowitz, L. Qin, and R. Wada
[1]*Dipartamento di Fisica dell'Universita di Padova and INFN Sezione di Padova, Italy*
[2]*INFN Laboratori Nazionali di Legnaro, Italy*
[3]*Institute of Physics, Silesia University, Katowice, Poland*

The BigSol Superconducting Solenoid Beam Line at the Texas A&M Superconducting Cyclotron was used to measure the stopping power of ^{40}Ar, ^{84}Kr, ^{197}Au and ^{238}U in mylar, aluminum and isobutane in the energy range from below 1 AMeV up to 15 AMeV.

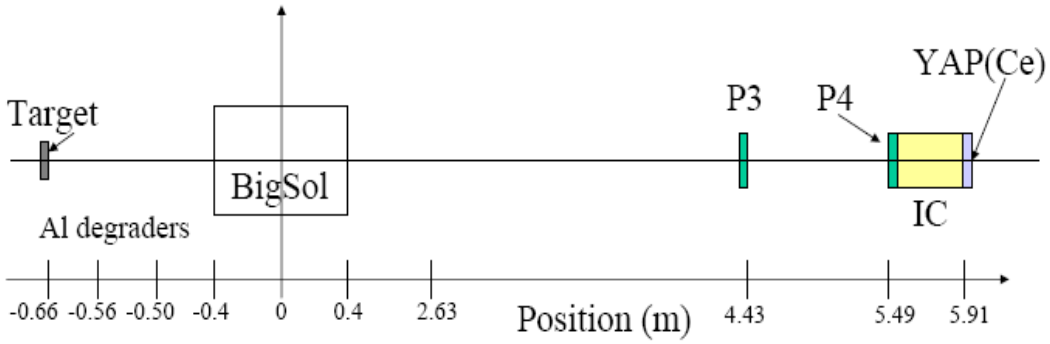

FIG. 1. Schematic lay-out of the BigSol beam line as used for this work.

A schematic lay-out of the experimental set-up is shown in Fig. 1 for more details see Ref.1. Two position sensitive PPAC detectors (P3 and P4) are used to measure the time of flight and to reconstruct the trajectory of the particles. A multi-anode Ionization Chamber (IC) is used either as a stopping detector or as a transmission detector for fragments that are stopped in an array of YAP(Ce) scintillators. The IC has an active area of 6.5x6.5 cm^2 and is equipped with 8 parallel anodes, each having a width of 4.65 cm along the beam direction. The IC is filled with isobutane gas at the pressure of 30 mbar. Consequently, the time-of-flight (tof) between P3 and P4, the entrance position in P4, the energy loss in P4 and energy loss in each of the IC segments are measured. For some calibration runs P3 was also removed.

The calibration of the energy loss in the IC was performed using the direct 14.85 AMeV ^{40}Ar and ^{84}Kr beams data (without the Al degrader) and the SRIM predictions for those beams [2]. Ppac P3 was removed from the beam line in order to reduce the material budget before the IC. Consequently, the absolute values of the energy loss presented in this work are normalized to the SRIM predictions for the 14.85 AMeV ^{40}Ar and ^{84}Kr.

The P3-P4 time of flight calibration was performed by using known delays to obtain the slope of the time to channel relationship. The time zero was determined for each ion using the time of flight measured for the direct beam without an Al degrader.

The calibration of the P4 energy signal was performed in two steps. For the particles stopped in the IC the energy loss in P4 was determined from the difference between the energy before P4 (calculated from the measured time of flight) and the measured energy in the IC. For the particles not stopped inside the IC, the direct beam data for runs in which P3 was removed from the line were used. For these the SRIM code was used to calculate the energy loss of the different beam particles in P4.

Al degraders having thicknesses in the range of 5-150 μm were placed at the target position to lower the incident energies. The thickness of the aluminum foils was measured in a separate run using a 6.27 AMeV $^{4}He^{2}H$ molecular beam, assuming that the SRIM stopping power for alpha particles in aluminum is correct. The statistical error on the aluminum degrader thicknesses is about 0.05% for all the layers. An average systematic error of about 4% was found comparing the thicknesses obtained using both the alpha particles and the deuterons resulting from the breakup of the molecular beam.

The experimental stopping power data for ^{40}Ar, ^{84}Kr, ^{197}Au and ^{238}U in mylar, aluminum and isobutane are shown in Figs 2-4 respectively and compared with the stopping power values predicted by the SRIM code.

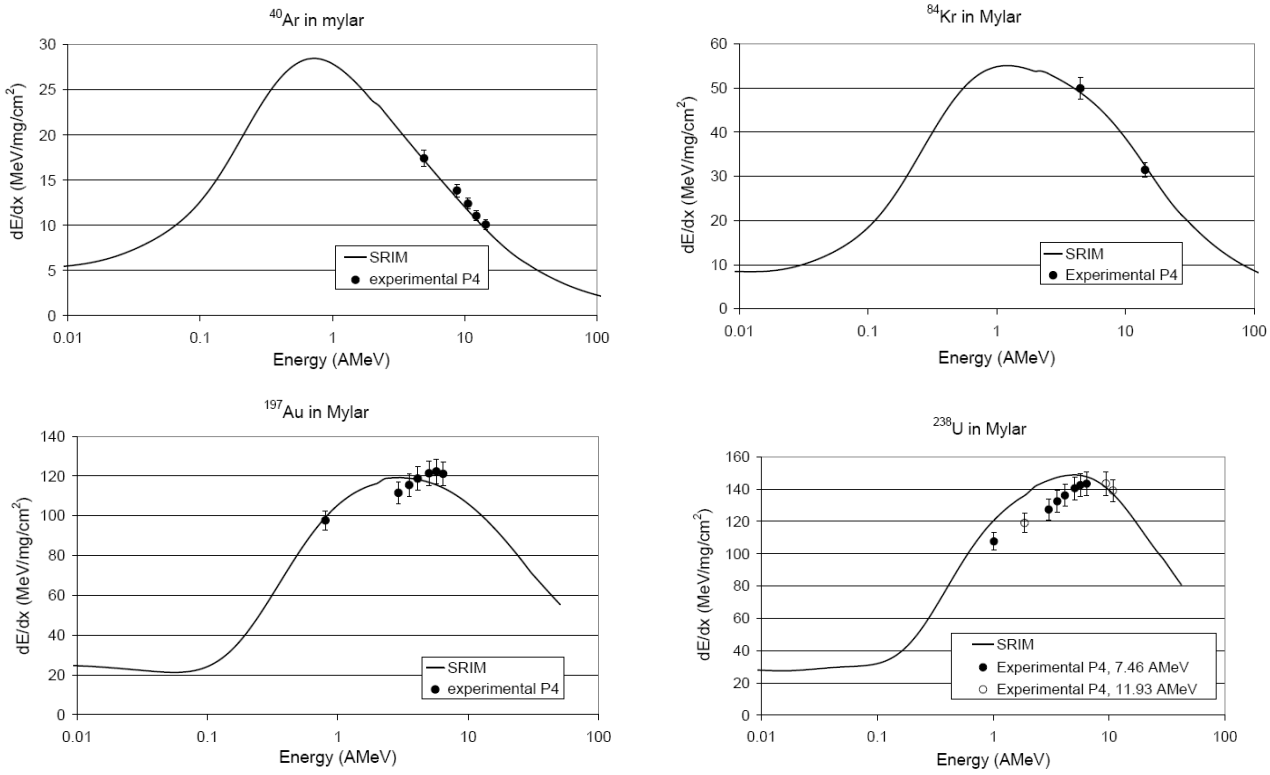

FIG. 2. Stopping powers of ^{40}Ar, ^{84}Kr, ^{197}Au and ^{238}U measured in mylar as a function of the ion energy. The black line shows the SRIM prediction for the stopping power. For the ^{238}U beams, the full and the open circles indicate the 7.46 AMeV and 11.93 AMeV beams, respectively. For details see the text.

The stopping powers ΔE/Δx for ions in mylar were obtained dividing the calibrated energy signal from the ppac P4 by its equivalent mylar thickness.

The results reported in Fig. 2 for ^{40}Ar, ^{84}Kr and ^{197}Au ions in mylar agree with the SRIM prediction to within 4%. The stopping power for the ^{238}U beam in the energy range from 7 to 0.8 AMeV seems to be overestimated by SRIM by about 9%, whereas for energies larger than 10 AMeV the agreement is good to within 1%.

The stopping power (ΔE/Δx) in aluminum was determined from the experimental range-energy curves. The results are reported in Fig. 3 as a function of the ion energies. The experimental stopping power for ^{40}Ar and ^{84}Kr particles in aluminum in the energy range from 14 to 10 AMeV is in very good agreement with the SRIM stopping power, being the average difference between the measured values and the SRIM prediction about 0.3%.

The measured stopping power points for ^{197}Au and ^{238}U particles in aluminum lie at the top of the Bragg peak region where no other experimental points are so far available [3-4]. The measured stopping power for ^{197}Au particles in aluminum indicates that SRIM underestimate the Bragg peak height by 10%, whereas the measured stopping power for ^{238}U in aluminum is on average a 4% higher than the SRIM prediction.

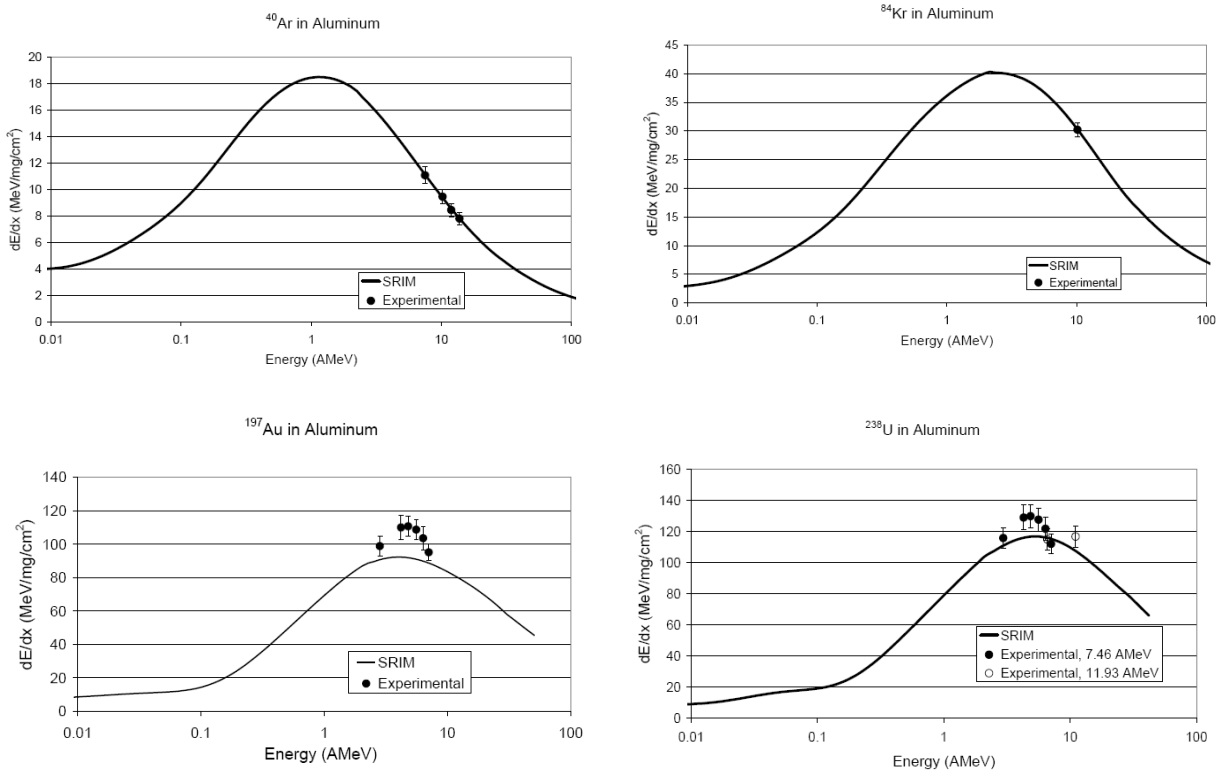

FIG. 3. Stopping powers of ^{40}Ar, ^{84}Kr, ^{197}Au and ^{238}U measured in aluminum as a function of the ion energy. The black line shows the SRIM prediction for the stopping power. For the ^{238}U beams, the full and the open circles indicate the 7.46 AMeV and 11.93 AMeV beams, respectively. For details see the text.

The energy loss for ions in isobutane was determined using the pulse height data for each anode on the IC For each anode the stopping power $\Delta E/\Delta x$ was obtained simply by dividing the measured energy in the i^{th} anode (MeV) by the anode thickness (mg/cm^2). Fig. 4 reports results the experimental stopping powers in isobutane gas as a function of the ion energies. The energy of an ion in the i^{th} anode (i=1 to 8) was obtained by subtraction of half of the measured energy loss in the i^{th} anode from the energy incident on that anode. These were divided by the mass A to obtain the energy per mass unit. For ions which are not stopped in the IC, the energy of the ion is obtained from the incident energy, determined from the tof, corrected by the energy loss in P4 and the total energy loss in the preceding anodes. In the case of ions stopping in the IC, the total energy measured in the IC is directly used instead of the energy derived from the tof measure. In Fig.4 the measured values are compared with the electronic stopping powers predicted by SRIM. For this comparison we have assumed that the part of the energy lost by nuclear stopping does not produce a signal in the counting gas. Thus the experimental data are compared with the electronic part of the stopping power.

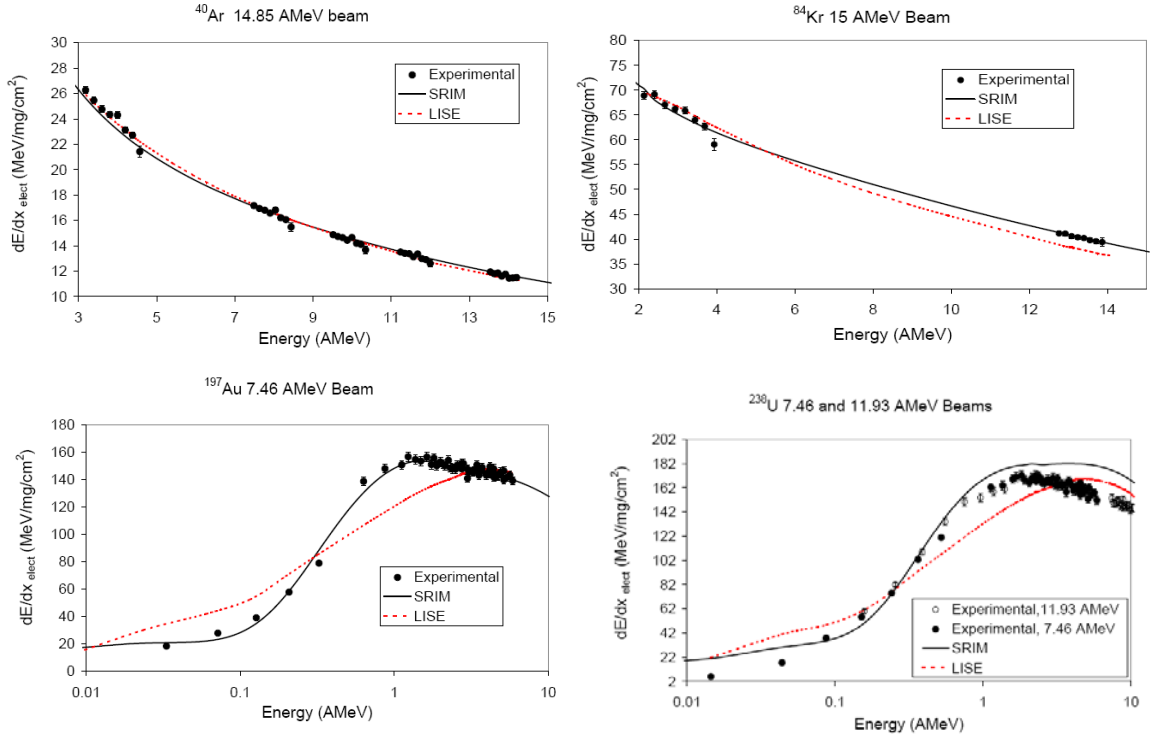

FIG. 4. Stopping powers of ^{40}Ar, ^{84}Kr, ^{197}Au and ^{238}U measured in the IC anodes. The black line shows the SRIM prediction for the electronic stopping power. The red dotted line shows the LISE prediction. For the ^{238}U beams, the open and full dots indicate the 11.93 AMeV and 7.46 AMeV beams, respectively. For details see the text.

Recalling that the absolute energy scale has been calibrated using the SRIM predictions for 14.85 AMeV Ar and Kr beams, the results for ^{40}Ar, ^{84}Kr and ^{197}Au show a very good agreement over the whole

energy range studied. Deviations between the experimental data and predicted values are, on average, within 3%. Larger deviations, on average about 10%, are evident in the case of ^{238}U projectiles.

For ^{40}Ar and ^{84}Kr the LISE [5] calculations are in a reasonable agreement with the data. Large deviations are seen in the case of the ^{197}Au and ^{238}U ions.

[1] M. Barbui *et al.*, Nucl. Instrum. Methods. Phys. Res. **B265**, 605 (2007).

[2] J. F. Ziegler, SRIM-2003, Nucl. Instrum. Methods Phys. Res. B219, 1027 (2004).

[3] H. Paul, Nucl. Instrum. Methods Phys. Res. **B261**, 1176 (2007); and references therein

[4] the collection of experimental data are available at the H. Paul web page (http://www.exphys.uni-linz.ac.at/stopping/) or at the SRIM site (http://www.srim.org/).

[5] O. Tarasov, D. Bazin, M. Lewitowicz and O. Sorlin Nucl. Phys. **A701**, 661 (2002).

Isotope distributions in Fermi energy heavy ion reactions

M. Huang, Z. Chen, R. Wada, A. Bonasera, T. Keutgen, K. Hagel, J. Wang, L. Qin, J. B. Natowitz, T. Materna, S. Kowalski, Y. Ma, G. Liu, M. Barbui, and C. Bottosso

Isotope distributions from the multifragmentation process are studied for heavy ion reactions near the Fermi energy domain. The ions, ^{64}Zn, ^{70}Zn and ^{64}Ni, were bombarded on targets of ^{58}Ni, ^{64}Ni, ^{112}Sn, ^{124}Sn, ^{197}Au and ^{232}Th at 40A MeV. Isotopes were measured inclusively at $\theta = 20^{o}$ using quad-Si detector telescopes. Isotopes are clearly identified up to Z<= 18. The measured energy spectrum of each isotope is integrated using a moving source fit to evaluate the multiplicity. The obtained isotope multiplicity is studied using a Modified Fisher Model [1]. The observed isotope multiplicities of all reaction systems are rather well reproduced in height and shape of the distributions for 3<=Z<= 18.

According to the Modified Fisher Model, the isotope yields can be given by the following expression:

$$Y(N_f, Z_f) = y_0 A_f^{-\tau} \exp\{[w(N_f, Z_f) + \mu_n N_f + \mu_p Z_f]/T\}, \quad (1)$$

Where y_0 is a normalization constant, τ is the exponent of the mass distribution, $W(N_f,Z_f)$ is Gibbs free energy. For the ground state nucleus $W(N_f,Z_f)$ can be expressed using the Weizecker-Beth Mass formula:

$$w(N_f, Z_f) = a'_v A_f - a'_s A_f^{2/3} - a'_c Z_f^2 / A_f^{1/3} - a_a A_f I_f^2 - \delta, \quad (2)$$

$$I_f = (N_f - Z_f)/A_f, \quad (3)$$

$$\delta = \begin{cases} = a_p / A_f^{0.5} & \text{for odd-odd nuclei,} \\ = 0 & \text{for odd-even nuclei,} \\ = -a_p / A_f^{0.5} & \text{for even-even nuclei} \end{cases} \quad (4)$$

The coefficients in Eq. (2) represent the volume, surface, Coulomb, asymmetry and possible pairing contributions to the free energy. When $\tau \neq 0$ is taken, the coefficients are not necessarily the same as those in the mass formula. The μ_n, μ_p and T denote neutron and proton chemical potentials, and temperature, respectively.

As the first step of this analysis, τ=0 is taken and all coefficients in Eq. (2) are fixed to Rohlf's parameters [2], which are a_V=15.75, a_S=17.8, a_C=0.71, a_a=23.7 and optimized a_p, T, μ_n and μ_p to reproduce the experimental multiplicity distributions. The optimization is made for the light isotopes with Z≤9 and the heavier isotopes, separately. In Fig.1, typical results are shown for the multiplicity distribution obtained from the ^{64}Ni+^{112}Sn reaction.

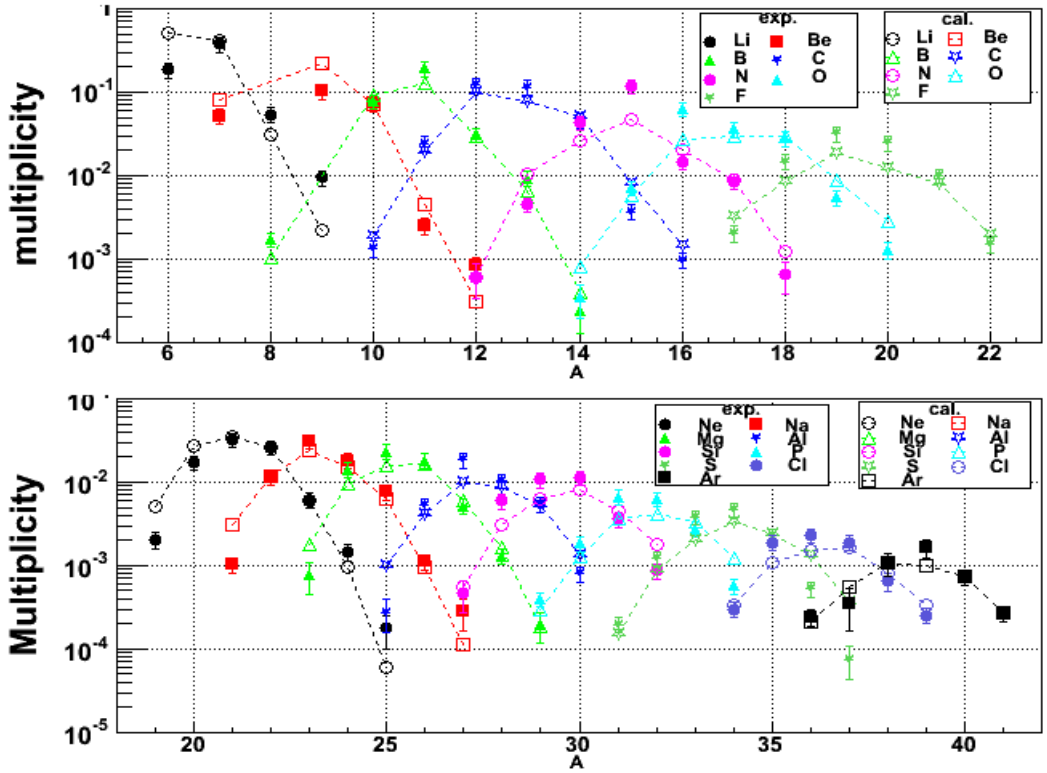

FIG. 1. Isotope multiplicity distributions for 3≤Z≤9 (upper panel) and 10≤Z≤18(lower panel) for ^{64}Ni+^{112}Sn. The solid symbols are experimental data and the open ones are calculated values.

In Fig. 2 the extracted neutron and proton chemical potentials, μ_n and μ_p, are plotted as a function of Z/A of the reaction systems. One can see clear linear correlations between the extracted chemical potentials and Z/A of the system, which indicates that the emitting source of the observed isotopes has higher (lower) neutron density for the neutron rich (poor) system and vice versa. The difference between μ_n and μ_p for the light fragments is larger than that for the heavier ones in all cases. Clear distinction is observed in the chemical potentials between lighter isotopes and heavier ones for a given Z/A of the system. The μ_n and μ_p values of the heavier isotopes for the neutron rich system become closer to those of the lighter isotopes for more symmetric systems. This suggests that the N/Z values of the emitting sources for lighter and heavier IMF are different. This may indicate the fact that the heavier IMF is emitted from the source after many neutrons are evaporated (neutron distillation). Extracted temperature are around 2.5 MeV for the lighter isotopes and about 3.5MeV for the heavier. The obtained pairing energy coefficient, a_p, are about a half in the value of the mass formula. Further studies with different parameter sets for the mass formula are now underway.

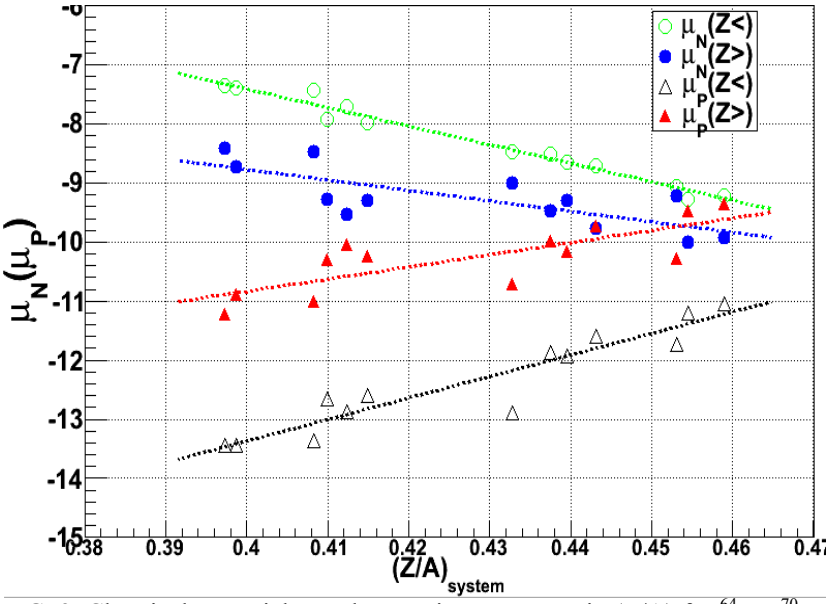

FIG. 2. Chemical potentials vs. the reaction system ratio (Z/A) for ^{64}Zn, ^{70}Zn and ^{64}Ni at 40 AMeV on targets of ^{58}Ni, ^{64}Ni, ^{112}Sn, ^{124}Sn, ^{197}Au and ^{232}Th. Green open circles are the neutron chemical potential for $3\leq Z\leq 9$ isotopes and blue solid circles are $9<Z\leq 18$ ones. Black open triangles are the proton chemical potential for $3\leq Z\leq 9$ isotopes and red solid triangles are $9<Z\leq 18$ ones.

[1] R. W. Minich *et al.*, Phys. Lett. B **118**, 458 (1982).

[2] James William Rohlf, *Modern Physics from a to Z0*, (Wiley, 1994).

Isotope asymmetry scaling

M. Huang, Z. Chen, R. Wada, A. Bonasera, T. Keutgen, K. Hagel, J. Wang, L. Qin, J. B. Natowitz, T. Materna, S. Kowalski, Y. Ma, G. Liu, M. Barbui, and C. Bottosso

Isotope yields can be given by the following expression along Modified Fisher Model [1],

$$Y(N_f, Z_f) = y_0 A_f^{-\tau} \exp\{[w(N_f, Z_f) + \mu_n N_f + \mu_p Z_f]/T\}, \quad (1)$$

Where y_0 is a normalization constant, τ is the exponent of the mass distribution, $W(N_f,Z_f)$ is Gibbs free energy. Then

$$w(N_f, Z_f)/T = \ln[Y(N_f, Z_f)A_f^{\tau}/y_0] - (\mu_n N_f + \mu_p Z_f)/T, \quad (2)$$

In Gibbs free energy the sum of the volume, surface and coulomb terms is about 8A MeV in the classical mass formula, and therefore one can write $w(N_f,Z_f)$ as

$$w(N_f, Z_f)/A \sim 8MeV - a_a I^2 - \delta, \quad (3)$$

in which $I=(N_f-Z_f)/A_f$ is isotopic asymmetry and δ is the pairing energy. Then from Eq. (2)

$$-\ln[Y(N_f, Z_f)A_f^{\tau}/y_0]/A \sim [-8MeV + a_a I^2 + \delta - (\mu_n N_f + \mu_p Z_f)/A]/T,$$

$$= [-8MeV + a_a I^2 + \delta - \mu_n I - (\mu_p + \mu_n)Z/A]/T, \quad (4)$$

Since Z/A ~ ½ in the last term, this indicates that the isotope yields can be scaled by I. When the isotope yield is normalized by the yield of the ^{12}C as given below,

$$R = Y(N_f, Z_f)A_f^{\tau}/[Y(^{12}C)12^{\tau}], \quad (5)$$

then

$$-\ln(R)/A = (-8MeV + a_a I^2 + \delta - \mu_n I)/T - (\mu_p + \mu_n)Z/A/T + \ln[Y(^{12}C)12^{\tau}]/12 \quad (6)$$

This also shows an isotopic asymmetry scaling similar to Eq. (4).

Following the above discussion, the experimental multiplicity of isotopes for ^{64}Zn+^{58}Ni, ^{64}Zn+^{92}Mo, ^{64}Zn+^{197}Au, at 26, 35, and 47 A MeV are examined with AMD-V calculations with Gogny interaction [2,3]. When $\tau = 0$ is used, the experimental isotope yields are well scaled by Eq. (4), but not by Eq. (6) as seen in Fig. 1, where the isotope multiplicity is plotted as a function of the isotopic asymmetry, I.

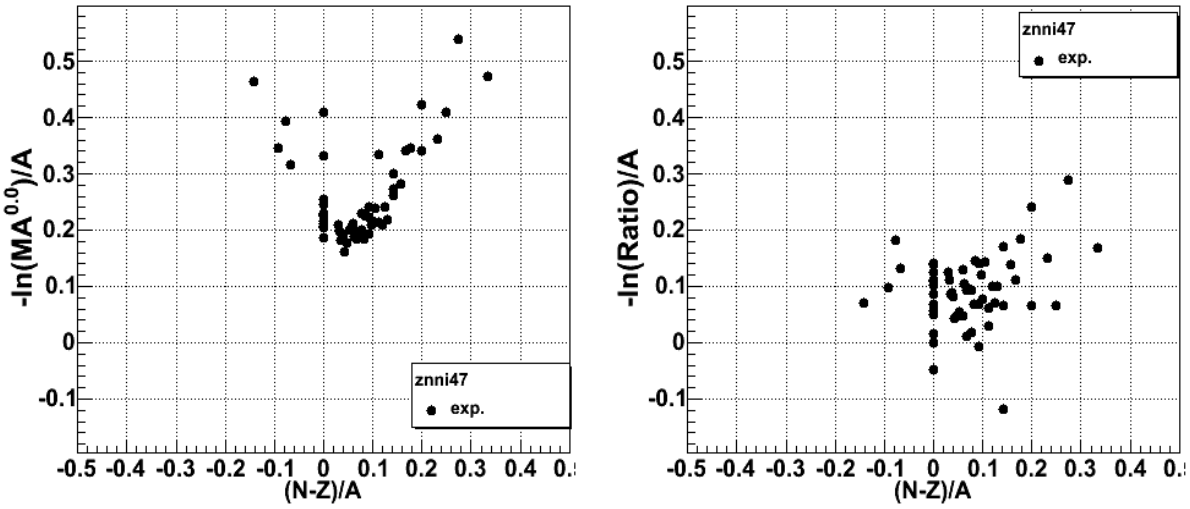

FIG. 1. Isotopic multiplicities are plotted using Eq. (4) (left panel) and Eq. (6) (right panel) with $\tau = 0$ for the violent collision of the case ^{64}Zn+^{58}Ni at 47 A MeV.

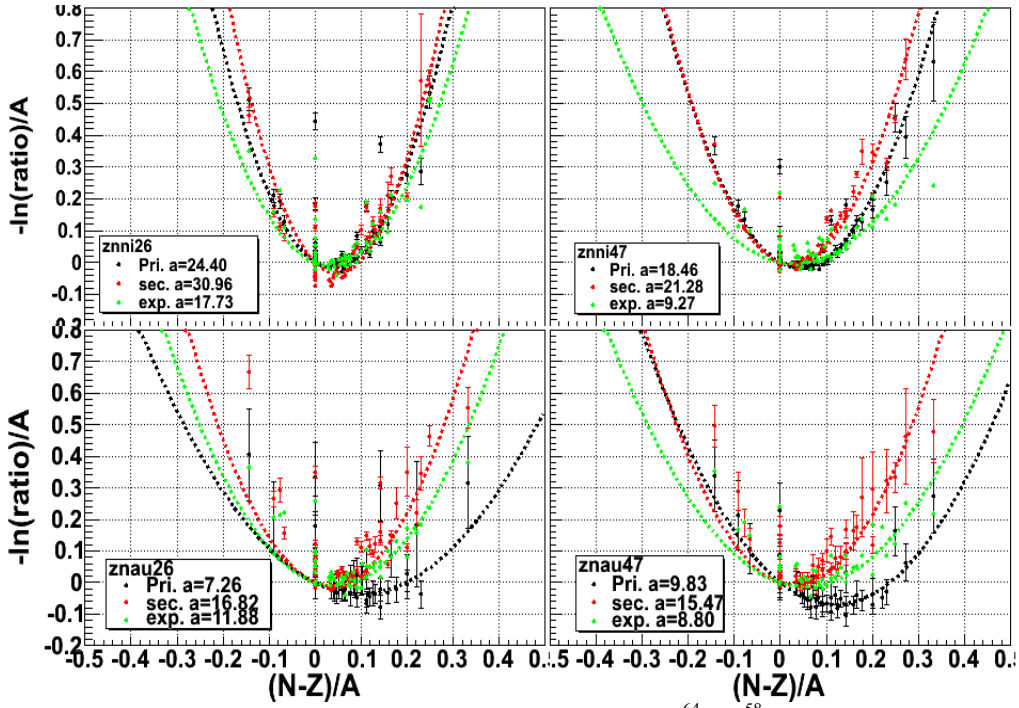

FIG. 2. Isotopic ratios are plotted for violent collisions of ^{64}Zn+^{58}Ni at 26A MeV and 47A MeV(upper panel), and ^{64}Zn+^{197}Au at 26A MeV and 47A MeV (lower panel) . The green circles represent experimental data, and the black symbols are for AMD-V primary and the red symbols for AMD-V+Gemini, respectively. The dashed lines correspond to the fits with Eq. (6).

On the other hand, if $\tau = 2.3$ is used, the isotopes are well scaled by Eq. (6), as seen in Fig. 2, in which the results of AMD-V simulations are also given. For AMD-V results, the primary and secondary isotope multiplicities are shown in each figure. The secondary yields are obtained by cooling the excited fragments of AMD-V at 300fm/c putting into Gemini[4]. As seen in the figures, the widths and the minima of the quadratic distributions depend significantly on the N/Z ratio of the reaction system and AMD-V simulations reproduce well these trends. On the other hand, the widths of the secondary products, which should be compared to the experimental results, show much narrower distributions. Further detailed studies are now underway.

[1] R. W. Minich *et al.*, Phys. Lett. B **118**, 458 (1982).
[2] R. Wada *et al.*, Phys. Rev. C **69**, 044610 (2004).
[3] A. Ono, Phys. Rev. C **59**, 853 (1999).
[4] R. J. Charity et al, Nucl. Phys. **A483**, 371 (1988).

Progress in BRAHMS

K. Hagel, R. Wada, J. B. Natowitz and the BRAHMS Collaboration

The final data with BRAHMS were taken in 2006. We have spent the last year in particular completing the analyses of the 200 GeV Cu + Cu data, the 200 GeV p + p data of run V and the 62.4 GeV p + p data of run VI. Several papers are in preparation.

Our analysis at the Cyclotron Institute and focused on completing the analysis of the 200 GeV p + p data of run V. We have analyzed the transverse momentum spectra extracted[1] to extract rapidity densities and information on stopping in p + p collisions and limiting fragmentation of both the rapidity densities and net proton distributions. Fig. 1 shows the rapidity densities of produced particles for both 62 GeV and 200 GeV plotted as a function of $y-y_{beam}$. We note that the forward rapidity data of particles at both energies join smoothly. This indicates a surprising phenomenon where the mechanism seems to be dictated by the difference from the beam rapidity regardless of the energy of the beam. This observation of the so called mechanism of limiting fragmentation has been observed and reported in a wide variety of RHIC data results.

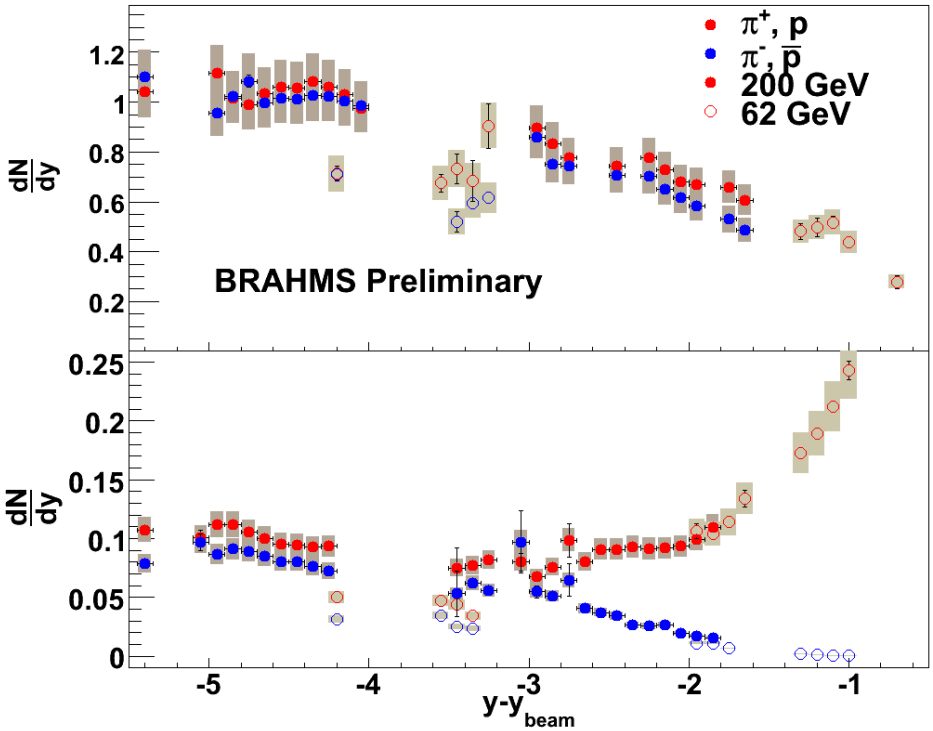

FIG. 1. Rapidity densities of produced particles in 200 and 62 GeV p + p collisions as a function of $y-y_{beam}$.

Fig. 2 shows the net proton dN/dy of both energies plotted as a function of the same variable. We have also included data from NA49 at 17.2 GeV. We observe remarkably consistent systematics that range from 17.2 GeV to 200 GeV. The solid curve in figure 2 shows the function $0.6\exp(y-y_{beam})$. This is the behavior expected in dN/dy when dN/dx is constant [2].

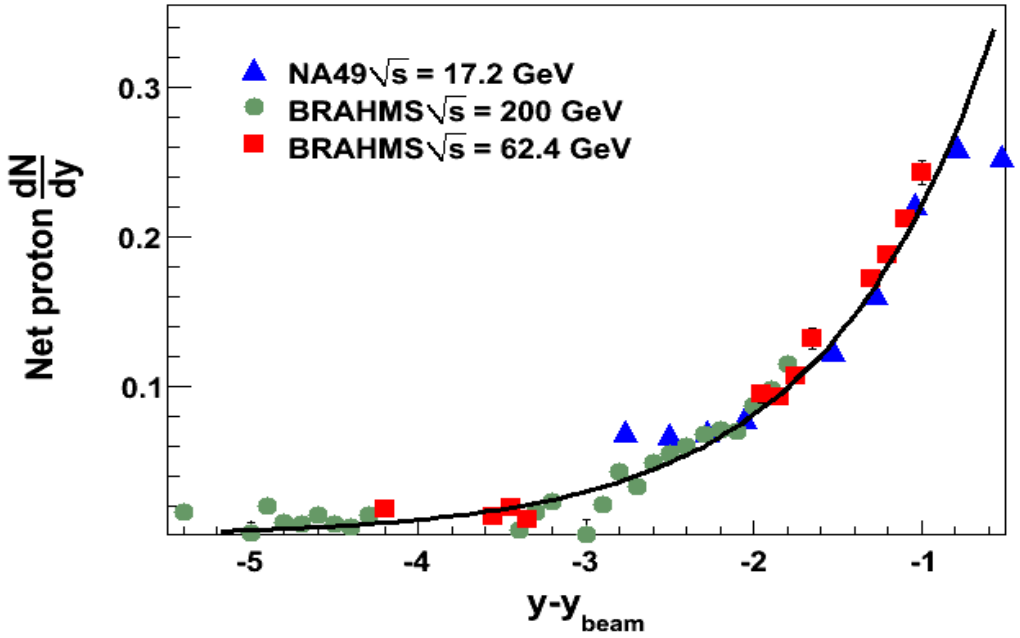

FIG. 2. Net proton dN/dy as a function of $y-y_{beam}$. The solid line represents the function $0.6\exp(y-y_{beam})$.

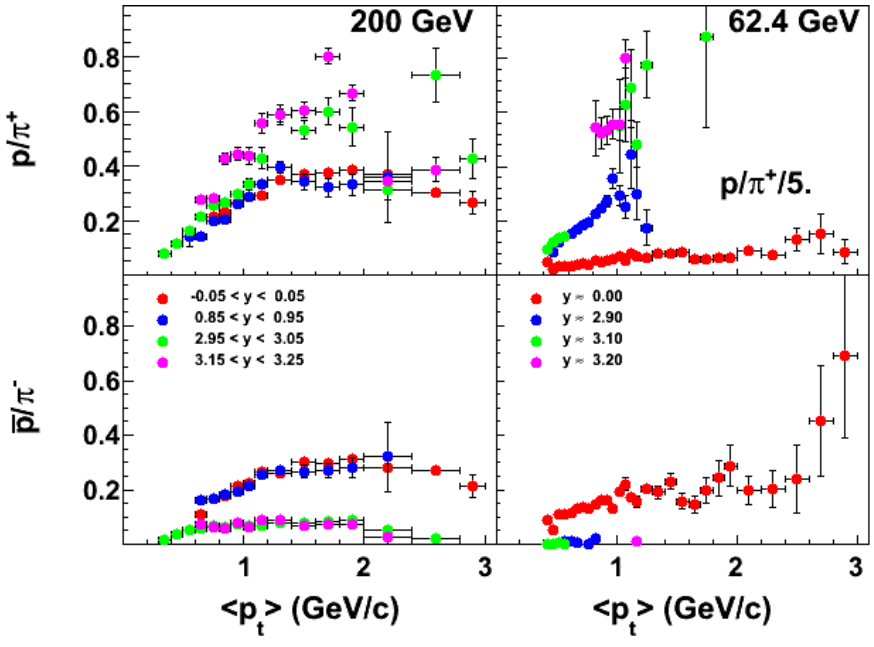

FIG. 3. p/pi for 200 and 62.4 GeV for various rapidities.

We also extracted p/π and K/π ratios for the different rapidities. Fig. 3 shows the p/π^+ and $pbar/\pi^-$ ratios for 200 and 62 GeV. We note an increase in p/π^+ and a decrease in $pbar/\pi^-$ with rapidity. We also note a stronger dependence of both p/π^+ and $pbar/\pi^-$ for the 62.4 GeV data. This probably results from the fact that the higher rapidity data at the lower energy is nearer to the beam rapidity of 4.2 than data at a similar rapidity at the higher energy. These data have been used to make conclusions regarding in medium effects by comparing them to the heavy ion data[3].

Fig. 4 shows the K^+/π^+ and K^-/π^- ratios for different rapidities at 200 and 62.4 GeV. A decrease in both K^+/π^+ and K^-/π^- with rapidity is observed. This data could provide information on strangeness enhancement (or the lack thereof) in p + p collisions.

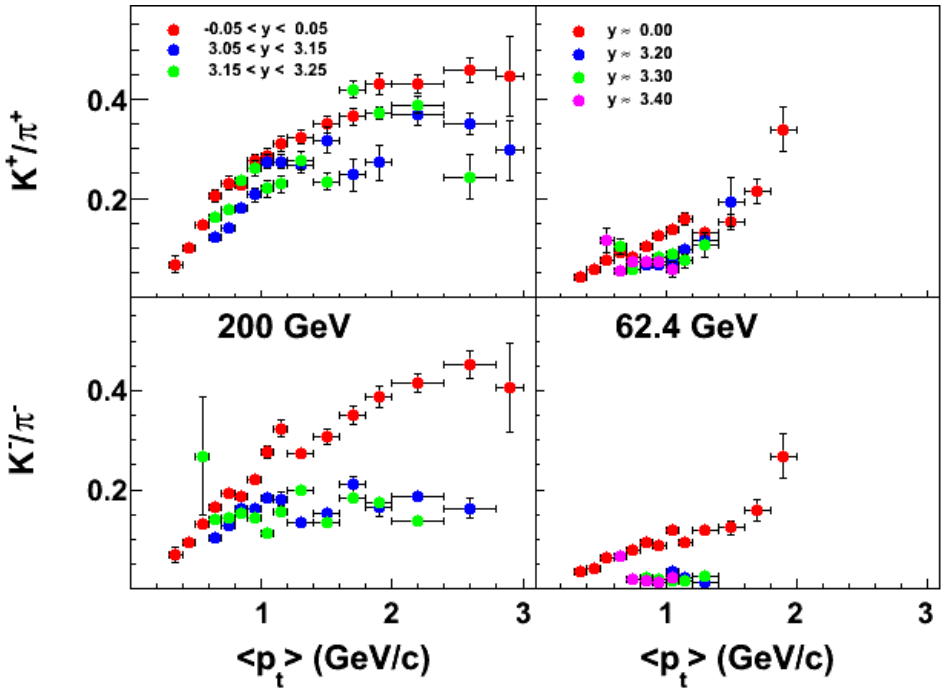

FIG. 4. K/pi for 200 and 62.4 GeV for various rapidities.

The results of the 200 and 62.4 GeV p + p data are summarized in a detailed paper that is in preparation by the BRAHMS collaboration.

[1] K. Hagel *et al.*, *Progress in Research*, Cyclotron Institute, Texas A&M University (2007-2008), p.II-9.

[2] Batisita and Covolan, Phys. Rev. D **59**, 054006 (1999).

[3] I. G. Arsene *et al.(* BRAHMS Collaboration), in preparation.

Measurements of production cross sections of neutron-rich nuclides from peripheral collisions of ^{40}Ar (15 MeV/nucleon) projectiles with ^{64}Ni, ^{58}Ni and ^{27}Al targets

G. A. Souliotis, M. Veselsky, S. Galanopoulos, M. Jandel, Z. Kolley, L. W. May, D. V. Shetty, S. N. Soisson, B. C. Stein, S. Wuenschel, and S. J. Yennello

A substantial part of our recent efforts has been directed in acquiring experience in the production and separation of RIBs in peripheral collisions in the energy range expected from the refurbished K150 cyclotron. The Institute's RIB upgrade plan comprises the implementation of a large-bore superconducting solenoid as a preseparator before a heavy-ion gas stopper [1]. Our recent measurements and simulations indicate that the application of the deep-inelastic transfer mechanism [2,3,4] appears to be a very effective way to obtain rare isotopes at the K150 energies.

Along these lines, aiming at obtaining systematics on production rates, we performed a series of measurements with a 15 MeV/nucleon $^{40}Ar^{9+}$ beam stricking targets of ^{64}Ni, ^{58}Ni and ^{27}Al. The projectile fragments were collected and identified using the MARS recoil separator applying the techniques developed and documented in [2,3]. The Ar beam was send on the primary target location of MARS with an inclination of 4^{o}. After interaction with the target, the fragments traversed a PPAC at the intermediate

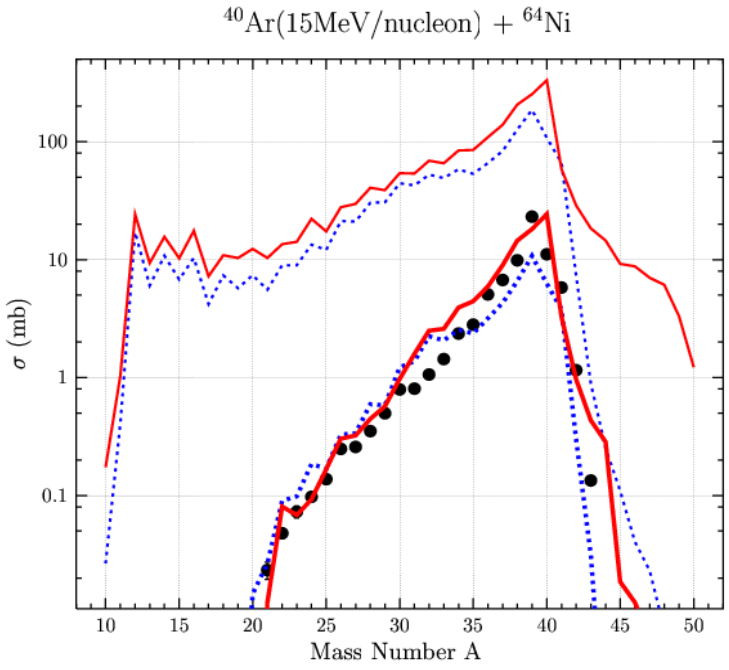

FIG. 1. Isobaric yield distributions from the reaction ^{40}Ar (15 MV/nucleon) +^{64}Ni. The data are given by the solid points. The upper set of lines shows the simulations obtained with the codes DIT [5] (dotted line) and CoMD [6] (full line) followed by the de-excitation code GEMINI [7]. The lower set of lines corresponds to the same calculations which have been filtered by the angular acceptance of the spectrometer.

image location (for position/Brho measurement and START time information) and then they were focused at the end of the device passing through a second PPAC (for image size monitoring and STOP time information). Finally the fragments were collected in a 5x5 cm^2 ΔE-E Si detector telescope (60 and 1000 μm thickness). Following standard techniques of Bρ-ΔE-E-TOF (magnetic rigidity, energy-loss, residual energy and time-of-flight, respectively), the atomic number Z, the mass number A, the velocity and the ionic charge of the fragments were obtained on an event-by-event basis (see, e.g. [3]).

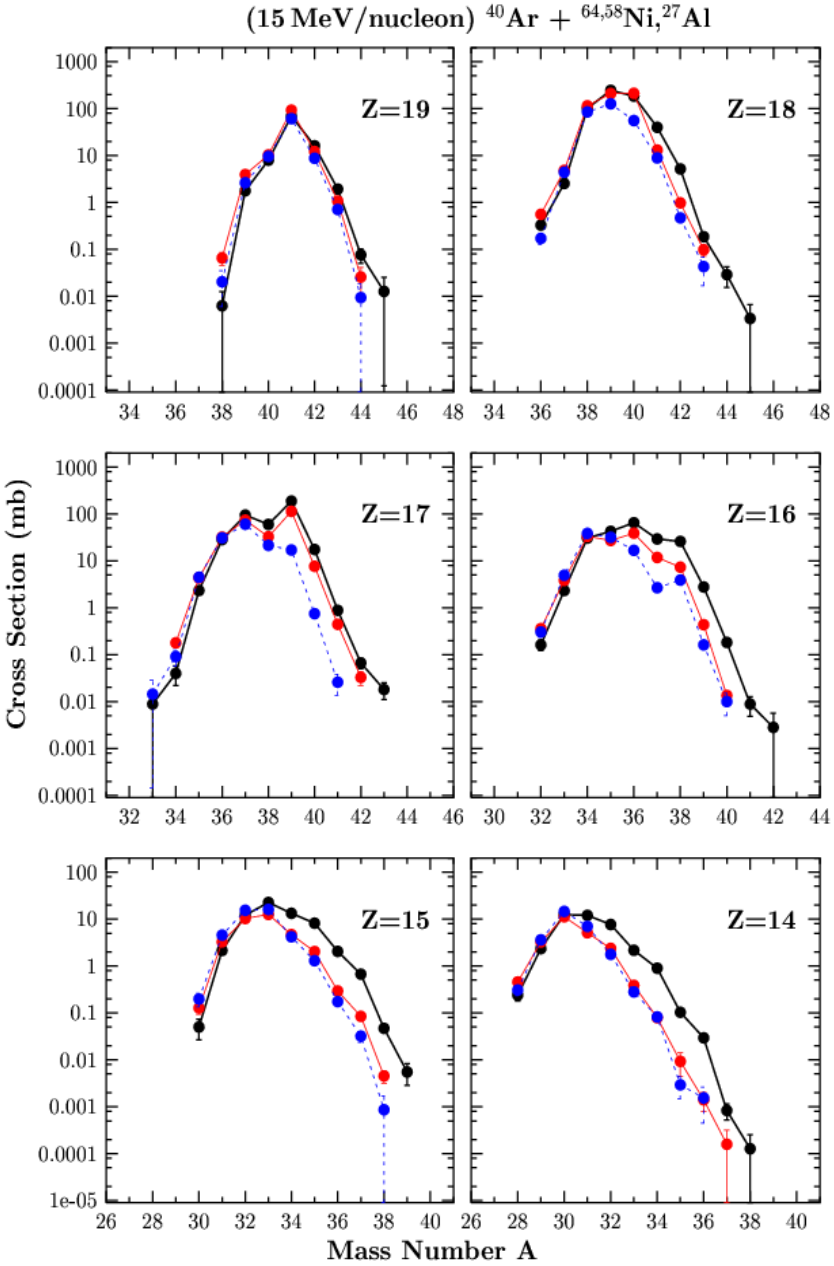

FIG. 2. Cross sections of the isotopes of elements Z=14-19 for the three reactions measured:^{40}Ar (15 MeV/nucleon) + ^{64}Ni,^{58}Ni, ^{27}Al represented with black, red and blue points respectively.

Data were obtained in a series of magnetic rigidity settings of the spectrometer to cover the energy and charge state distributions of the fragments. Fig. 1 shows the isobaric yield distributions obtained for the reaction ^{40}Ar+^{64}Ni. The data are given by the solid points. The upper set of lines shows the simulations obtained with the codes DIT [5] (dotted line) and CoMD [6] (full line) followed by the de-excitation code GEMINI [7]. The lower set of lines corresponds to the same calculations which have additionally been filtered by the angular acceptance of the spectrometer. The simulations seem to provide a reasonable description of the data. We used the ratio of the filtered to unfiltered DIT/GEMINI simulations to correct the measured data (obtained in the limited angular acceptance of the spectrometer) and extract total production cross sections for each isotope [2,3].

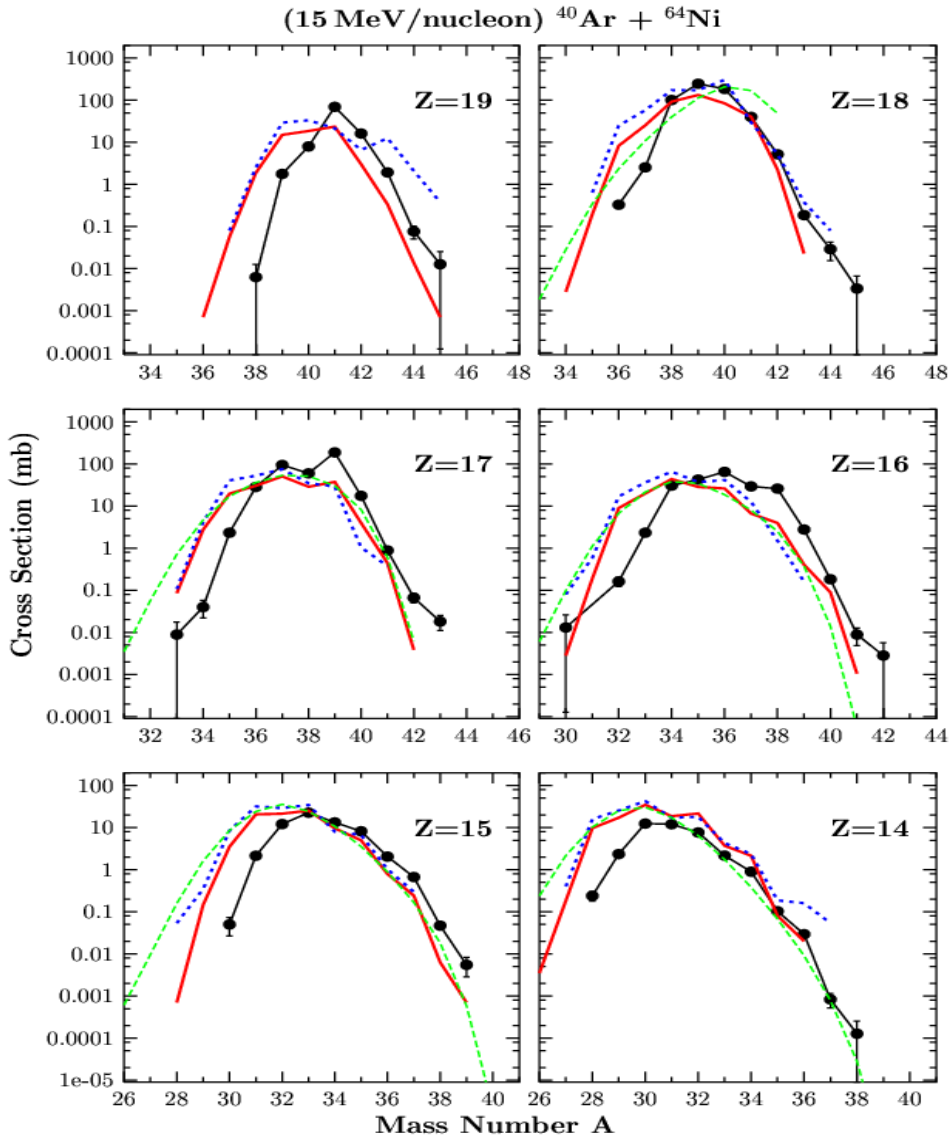

FIG. 3. Cross sections of the isotopes of elements Z=14-19 from the reaction ^{40}Ar (15 MeV/nucleon) + ^{64}Ni (black points). The red (full) line corresponds to the CoMD/GEMINI [6,7] calculation, whereas the blue (dotted) line corresponds to the DIT/GEMINI [5,7] calculation. The green (dashed) line shows the expectation of the EPAX parametrization [8].

Fig. 2 shows the cross sections of the isotopes of elements Z=14-19 for the three reactions measured: ^{40}Ar (15 MeV/nucleon) + ^{64}Ni,^{58}Ni, ^{27}Al, represented with black, red and blue points respectively. Fig. 3 shows the cross sections of the isotopes of elements Z=14-19 from the reaction ^{40}Ar (15 MeV/nucleon) + ^{64}Ni (black points). The red (full) line corresponds to the CoMD/GEMINI calculation, whereas the blue (dotted) line corresponds to the DIT/GEMINI calculation. Finally the green (dashed) line shows the expectation of the EPAX parametrization for high-energy fragmentation [8]. Figs. 2 and 3 show that along with proton-removal products, neutron-pickup products are produced in substantial yields, as expected from a deep-inelastic transfer mechanism at these energies [2,3,4]. From the present data we observe that very neutron-rich products are most abundantly produced, as expected, by the most neutron-rich ^{64}Ni target. Finally, both the standard DIT and the CoMD calculations seem to underestimate the most neutron-rich products.

We are currently working on detailed simulations of the cross sections using the improved version of the DIT model approach [4], as well as the CoMD code with careful description of the ground states of the nuclei involved in the reactions. On the experimental front, we are in the process of data analysis of a similar set of projectile-like fragments from a ^{86}Kr (15 MeV/nucleon) with heavy targets

[1] "A Proposed Facility Upgrade for the Texas A&M Univ. Cycloton Institute", accessible at: http://cyclotron.tamu.edu.

[2] G. A. Souliotis *et al.*, Phys. Rev. Lett. **91**, 022701 (2003).

[3] G. A. Souliotis *et al.*, Nucl. Instrum. Methods Phys. Res. **B204**, 166 (2003).

[4] M. Veselsky and G. A. Souliotis, Nucl.Phys. **A765**, 252 (2006).

[5] L. Tassan-Got, Nucl. Phys. **A524**, 121 (1991).

[6] M. Papa *et al.*, Phys. Rev. C **64**, 024612 (2001).

[7] R. Charity, Nucl. Phys. **A483**, 391 (1988).

[8] K. Suemmerer *et al.*, Phys. Rev. C **61**, 034607 (2000).

N/Z equilibration in the quasi-projectile of Ar, Ca+Sn reactions: experimental and simulation comparisons

L. W. May, A. Keksis, and S. J. Yennello

Experimental values of N/Z equilibration were calculated by the method developed by A. Keksis [1]. The isobaric yield ratios for the A=3,6,7,11,14,16 isobars were calculated from reactions of ^{40,48}Ca beams on ^{112,124}Sn targets. These isobar yield ratios were then plotted individually versus the N/Z of the quasi-projectile (QP) for the four systems. The $(N/Z)_{QP}$ was assumed to be a straight mixing between the initial target and projectile N/Z such that:

$$\frac{N}{Z}_{QP} = X * \frac{N}{Z}_{target} + Y * \frac{N}{Z}_{projectile}$$

The $(N/Z)_{QP}$ was varied and the value that gave the most linear fit through the four systems was assumed to be the N/Z value for the resulting QP. A "percent equilibrium" is defined as the change in the $(N/Z)_{QP}$ value between that of the initial projectile N/Z and the composite system N/Z. This method makes the assumption that N/Z equilibration has occurred when the entire system has reached the N/Z of the composite system and that each piece (quasi-projectile and quasi-target, QT) retains the N/Z of the equilibrated (composite) system.

Calculations performed with the iBUU (isospin-dependent Boltzmann-Uehling-Uhlenbeck) transport code [2] on the same systems were then analyzed to determine the $(N/Z)_{QP}$ from the code. The iBUU output gives test particle positions, momentum and identity (proton or neutron, originally target or projectile) at the moment the code ends. This information was used to locate the high-density center of the QP and a spherical geometry cut was applied in order to define a quasi-projectile. The test particles with the geometry cut were then used to calculate an N/Z value for the QP. The iBUU calculations were performed at impact parameters of b = 5,6,7,8,9 and 10 fm, and each was completed for two parameterizations of the equation-of-state (EOS), x=0 and x=-1. Since the experimental impact parameter distribution is not known, the $(N/Z)_{QP}$ values for the 6 impact parameters from iBUU were averaged together and used for comparison to the data.

Fig. 1 shows a comparison of the experimental and theoretical results. The y-axis is the N/Z value of the different results scaled by the N/Z of the composite system. Therefore, the composite system N/Z is set at 1 across the plot. The projectile and target N/Zs are shown for reference for each system. Experimental data is shown for two separate beam energies, 32 MeV/u and 45 MeV/u. Similarly, the iBUU results are shown for two beam energies as well as two parameterizations of the EOS. It can be seen that for the two systems with ^{40}Ca as the projectile, the theoretical results match rather closely with the experimental results and that a slight difference can be noted between the different beam energies and different EOS. However, the iBUU results for the ^{48}Ca systems vary noticeably from the experimental. The experimental and theoretical results are in some agreement but additional work is needed in order to understand the differences that are seen.

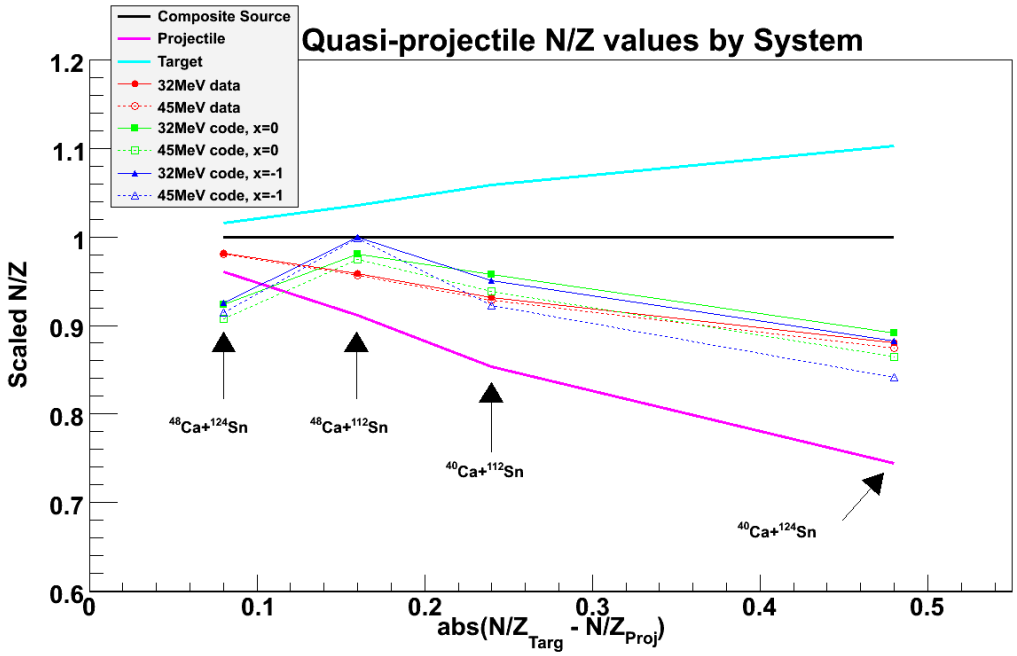

FIG. 1. Quasi-projectile N/Z scaled to the composite system N/Z (assumed to be equivalent to a fully N/Z equilibrated system) as a function of the absolute difference in N/Z between the initial projectile and

Further work would seek to include the Ar projectile systems as well as the inclusion of x=1 and x=-2 parameterizations of the EOS in iBUU calculations. Also, to better deal with the issue of unknown experimental impact parameter distribution, work could be done using the codes to correlate QP velocity to impact parameter. This result could then be used on the experimental data so that experimental QP velocities would determine a rough idea of the impact parameter distribution in the data.

[1] A. Keksis. Ph. D. Thesis, Texas A&M University, 2007.
[2] Li *et al.*, Phys. Rev. C **69**, 011603 (2004).

Point-to-Curve method of distance determination for use in linearization and particle identification

L. W. May, Z. Kohley, S. Wuenschel, K. Hagel, R. Wada, and S. J. Yennello

Particle identification in multi-detector arrays is done in various different ways. In the analysis of data taken on the NIMROD-ISiS array at the Cyclotron Institute at Texas A&M, a linearization technique is generally used in order to particle ID the various fragments picked up by the detector [1]. An important step in this linearization is determining the proximity of specific data points to lines in the data corresponding to specific elements. A new method of distance determination was developed in an attempt to improve upon this process of the linearization.

The new method, known as the Point-to-Curve method, was developed as a way to determine the exact and absolute distance between any given data point and a user-generated line defining an element on a ΔE-E plot. Previous methods had used a simple tracing in either the horizontal or vertical direction from the point until finding the nearest elemental line. Due to the known issue of the vertical and horizontal methods having trouble with data sets of very vertical or horizontal curvature, respectively, later iterations of the analysis code used a method that combined these ideas by searching along a 45° line. The Point-to-Curve method was created to provide the shortest distance calculation between a data point and any given curve representing an element.

The Point-to-Curve method uses the parameterization of the equation for the curve into a vector in terms of x and y values. For instance, a curve denoted by the equation $y = 3x^2-6x+10$ would become the vector $r = (x, 3x^2-6x+10)$. The value for the point in question, $p = (x_1, y_1)$, is then subtracted from the vector r giving $r-p = (x-x_1, 3x^2-6x+10-y_1)$. Since r – p is a measure of the deviation in x and y between the point and the curve, this value can be squared by taking the dot product $(r – p) \bullet (r – p)$. This equation is minimized yielding points on the curve, one of which will be the minimum for calculating the distance between the point and curve. The minimization is done by setting the derivative of the dot product equal to zero and solving for x. These values can be both real and imaginary, but as imaginary values give non-physical results, these values can be discarded. Since several possible real roots can be given as solutions, constraints can be placed on the output such that only the value within the desired range will be found. The one remaining solution is the x-intersection of the curve and the line drawn from the point to the curve with the smallest possible distance. This x-intersection value can then be used to find the y-intersection value from the equation of the curve and the distance formula applied to the intersection values and the value of the point to give the actual distance between the point and the curve.

The computationally intensive step in this method is in the factorization of the polynomial. Polynomial factorization has been demonstrated to be an NP-complete problem, meaning that the time it takes to factor the polynomial scales exponentially with the size of the polynomial. This is not a problem for polynomials of order 4 or less, since these can be solved analytically using known algorithms. A problem could arise if high order functions are used to model the line. However, for the types of plots common for ΔE-E and CsI fast-slow data this is not prohibitive as the use of spline fits allows the order of the resulting polynomial to be kept low enough (no greater than 5 or 6) that the time to factor the

polynomial is quite low. The factoring algorithm used in this case is that found in the GSL library packages linked in the ROOT analysis package.

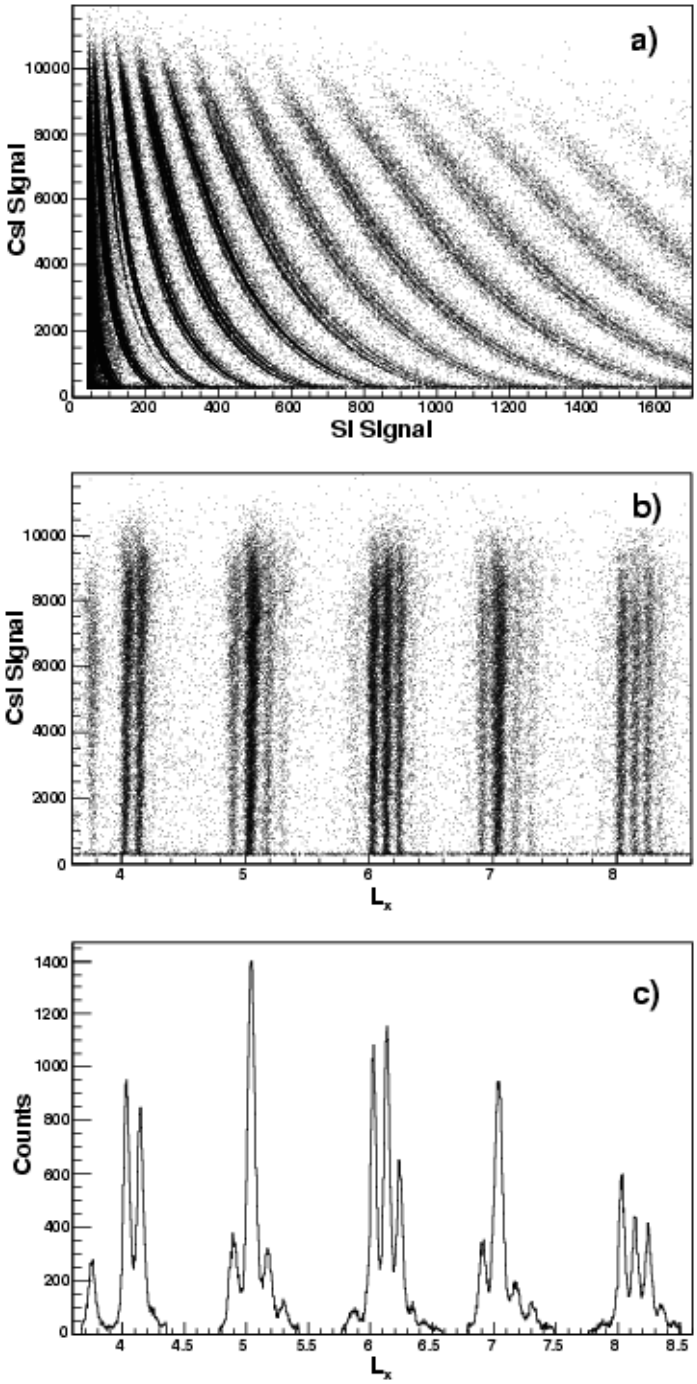

FIG. 1. An example step-through of the linearization process where a) A Si-CsI ΔE-E plot, b) a 2D plot of linearized x-axis versus the CsI signal and c) a 1D projection of the center plot with linearized x-axis versus counts calculated with the Point-to-Curve method. The linearized x-axis shows isotopes for Beryllium through Oxygen (Z=4-8).

While simulations of the Point-to-Curve method have shown that it indeed does return the shortest distance from a point to the line (compared to the horizontal, vertical and 45° line methods), current testing analysis on data of a 35MeV/A ^{70}Zn beam on a ^{70}Zn target taken using the NIMROD-ISiS array comparing the four methods gave interesting results [2]. A step-by-step breakdown of the linearization process can be seen in Fig. 1. The data showed no difference (within errors) between the horizontal, the 45° line or Point-to-Curve methods. The vertical method had great difficulty in analyzing the data due to the very vertical nature of the data set. While there is no difference in this particular data set (as seen from Table I), one can see that in deciding whether to use the horizontal or vertical methods, a decision must be made based on the curvature of the data. The Point-to-Curve method was developed for the purpose or performing equally well over all portions of the curvature of data so that one does not have to worry about the curvature of a data set ahead of time but rather can just use a single distance determination method for all data.

TABLE I. Peak sigmas with errors and percent contamination values with errors for the four distance calculation methods used on the ^{9}Be and ^{10Be} peaks.

	Peak	σ	σ error	% contamination	% contamination error
Vertical method	^{9}Be	0.01974	0.00039	41.861	1.173
	^{10}Be	0.06951	0.00054	16.225	0.798
Horizontal method	^{9}Be	0.01687	0.00028	3.908	0.408
	^{10}Be	0.02760	0.00044	4.067	0.399
45° line method	^{9}Be	0.02590	0.00028	3.835	0.407
	^{10}Be	0.02755	0.00045	4.015	0.399
Point-to-Curve method	^{9}Be	0.02568	0.00027	3.905	0.358
	^{10}Be	0.02764	0.00036	4.061	0.360

[1] S. Wuenschel *et al*, Nucl. Instrum. Method Phys. Res. **A604**, 578 (2009).
[2] Z. Kohley, private communication.

Reconstructed quasi-projectile source distributions as a probe of the nuclear equation of state

B. C. Stein, S. N. Soisson, G. A. Souliotis, D. V. Shetty, S. Wuenschel,
Z. Kohley, L. W. May, and S. J. Yennello

Products from the reaction of 45 MeV/A beams of ^{32,36}S on targets of ^{112,124}Sn were measured with the Forward Array Using Silicon Technology (FAUST) [1]. Charged particle identification and energy calibration of the array have been completed [2]. The design of the FAUST Array selects heavily against particles emitted from a target like source. For peripheral reactions, this allows for relatively straightforward definition of projectile like sources based on the total charge collected during a given event. For the investigation discussed here, projectile-like sources have been defined by selecting for events where the sum collected charge is equal to that of the incident sulfur beam (Z=16). Accepted events also must also be composed only of particles identified in both charge and mass. Given this event selection, quasi-projectile distributions are presented in terms of ΔN_{app} as defined below.

$$\Delta N_{app} = A_{beam} - \sum_{i}^{CP_{mult}} A_{frag,i} \text{ for events where } Z_{beam} = \sum_{i}^{CP_{mult}} Z_{frag,i}$$

Calculations have suggested that the nuclear equation of state provides a measurable driving force, increasing the rate of isospin equilibration between peripheral interacting nuclei of differing N/Z [3]. This implies that equation-of-state information may be gleaned from comparison of these reconstructed quasi-projectile distributions by varying the relative isospin asymmetry between the target

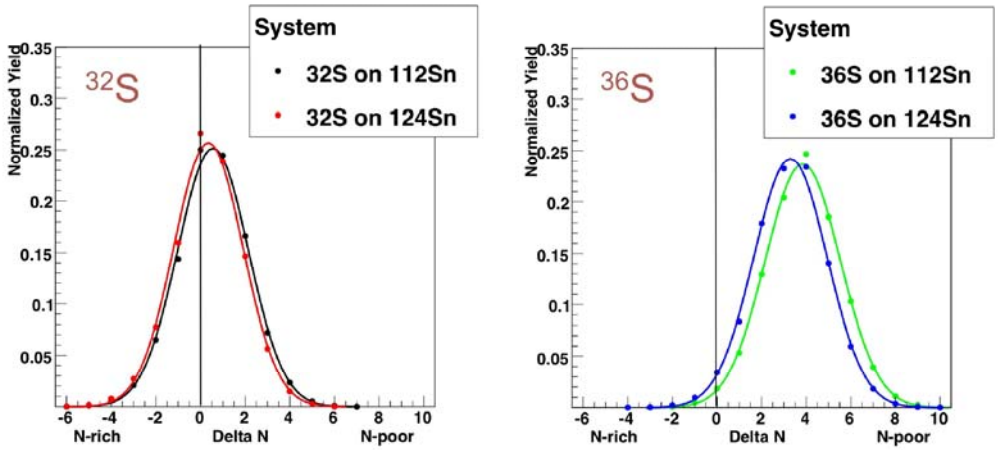

FIG. 1. ΔN distributions plotted to compare systems with a common beam. A Gaussian distribution has been fit to the data to increase readability. Notice that in both cases the distribution corresponding to the system with a larger isospin asymmetry between the target and projectile is more neutron rich. Statistical error bars are plotted.

and projectile. We would then expect the mean value of ΔN_{app} to decrease with increasing difference in

asymmetry between the target and projectile. This is observed in the data when comparing between systems with the same incident beam (but different targets) as shown in Fig. 1. Table I shows the same trend numerically. In both plots, the system with the ^{124}Sn target has a larger difference in N/Z between target and projectile, and in both cases the mean value of the quasi-projectile distribution is reduced (meaning the distribution is on average more neutron rich). Comparison between systems with a common target (but different beam particles) should also show this dependence. However, the production of unbound neutrons from the quasi-projectile sources would be expected to differ greatly between systems with a ^{36}S beam versus a ^{32}S beam. Since the reconstructed quasi-projectile distributions would be unequally affected by this difference in production, any difference observed between two systems sharing a common beam (but differing targets) may not accurately represent the actual difference in neutron richness of the two quasi-projectile distributions.

TABLE I. Statistics for the Gaussian fits to the ΔN distributions in Figure 1. The error quoted after each value corresponds to the error in the fit of the Gaussian distribution to the experimental points.

System	Mean	SD
^{32}S + ^{112}Sn	0.559 (4.7e-4)	1.580 (3.74e-3)
^{32}S + ^{124}Sn	0.351 (4.27e-3)	1.545 (3.31e-3)
^{36}S + ^{112}Sn	3.845 (3.78e-3)	1.680 (2.84e-3)
^{36}S + ^{124}Sn	3.293 (4.52e-3)	1.640 (3.40e-3)

Currently work is under way to compare the above results with the Constrained Molecular Dynamics Model (CoMD) [4]. Multiple instances of the model utilizing different equations of state, specifically different values of the symmetry energy, are being analyzed to show a trend in the relative progress towards isospin equilibration for the pairs of systems discussed above. Once this trend is demonstrated, the experimental results will be used to constrain the range of symmetry potentials to those which best reproduce the experimental observable.

[1] F. Gimeno-Nogues, et al., Nucl. Instr. and Meth. A 399 (1997) 94.
[2] B. C. Stein *et al.*, *Progress in Research*, Cyclotron Institute, Texas A&M University (2007 – 2008), p II-30.
[3] M. Colonna and M.B. Tsang, Eur. Phys. J. A **30**, 165 (2006).
[4] M. Papa *et al.*, Phys. Rev. C **64**, 024612 (2001).

The N/Z dependence of the nuclear caloric curve

S. Wuenschel, A. Bonasera, S. J. Yennello, G. A. Souliotis, D. V. Shetty,
S. N. Soisson, B. C. Stein, Z. Kohley, and L. W. May

Projectile fragmentation sources were identified from reactions of ^{86,78}Kr+^{64,58}Ni at 35 MeV/A collected with the upgraded NIMROD-ISiS array[1,2]. This data has been calibrated, particle identified, and analyzed to isolate the quasi-projectile source[3].

This source has been isolated using four data cuts. The first data cut was a minimum sum of charge detected in an event (sumZ) of 30 or greater. This cut was followed by a velocity cut [4] placed on the individual fragments to remove pre-equilibrium and target sources from the data. The third cut was a sumZ range of 30-34 to ensure that a consistent size of source is being studied. The final cut was based on the event shape and allowed only fairly spherical events to be retained. The source defined in this manner was then assigned an excitation energy from (1) where the sum is over the kinetic energy of the event fragments in the reconstructed frame of the event. The multiplicity of neutrons (M_n) was obtained from (2).

$$E^* = \sum_{i}^{Mcp} KE_i + M_n \langle KE_n \rangle - Q \qquad (1)$$

$$M_{QP} = \frac{M_{\exp} - M_{bkg}}{\left(Eff_{QP} + \frac{N_T}{N_P} Eff_{QT} \right)\left(\frac{.7}{.6} \right)} \qquad (2)$$

Using Eq. (2), the multiplicity of neutrons was corrected on an event-by-event basis for background (M_{exp} - M_{bkg}). The number of neutrons assigned to the quasi-projectile source was then calculated with source tagged neutrons from the HIPSE-SIMON [5] event generator coupled to a GEANT-3 [6] simulation of the Neutron Ball. The Neutron Ball efficiency for quasi-projectile neutrons (Eff_{QP}) and quasi-target neutrons (Eff_{QT}) was included as well as the target and projectile neutron numbers (N_T and N_P). A final correction factor was added because the neutron ball was calibrated to 70% efficiency while the simulation yields an overall 60% efficiency.

A new thermometer has been derived from the momentum quadrupole fluctuations of fragments in the source frame. For each fragment in an event the fluctuations can be defined as $Q_i = 2P_z^2 - P_y^2 - P_x^2$. The distribution of Qi across a class of events provides a variance that is linked to the temperature through (3).

$$\sigma^2 = 12 m_0^2 T^2 \sum_i (\zeta_i A_i) \qquad (3)$$

The beam (Z) axis was found to have residual collective behavior. This caused the derived fluctuation thermometer to provide temperature measurements dependent on the axis defined with the factor of 2. The thermometer was re-derived using only the transverse momentum to avoid this collective behavior. In this case $Q_i = P_x^2 - P_y^2$ is linked to the source temperature through (4).

$$\sigma^2 = 4m_0^2T^2\sum_i(\zeta_i A_i) \qquad (4)$$

The temperature obtained from this thermometer has been found to be fragment mass dependent. This dependence may be the result of Coulomb repulsion, fragment recoil during break up, or Fermi momentum of the nucleons in the fragments [7,8]. The Fermi momentum is only a viable concern for A≥2 fragments. This thermometer may be used for protons without contamination from Fermi momentum or concern about fragment recoil. In addition the effect of Coulomb will be relatively small compared to the more massive fragments.

Fig. 1 shows the caloric curve derived from the proton momentum fluctuations for the more

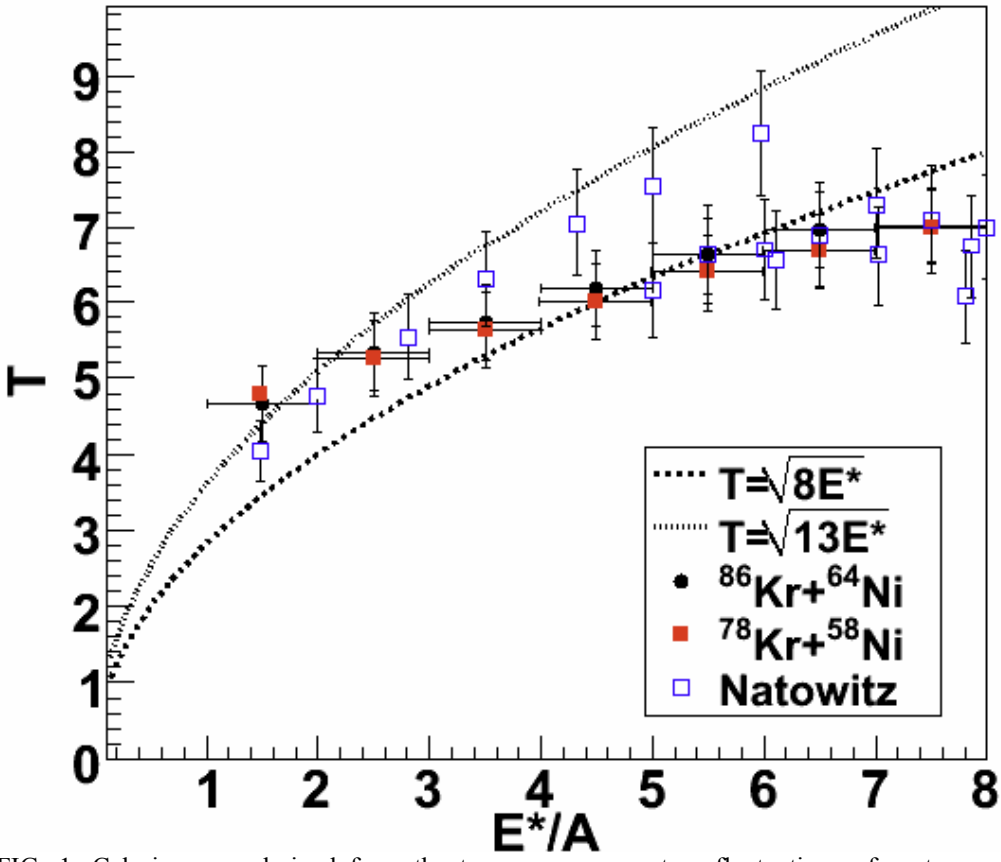

FIG. 1. Caloric curve derived from the transverse momentum fluctuations of protons with Natowitz compilation for reference [9].

neutron rich $^{86}Kr+^{64}Ni$ source and the less neutron rich $^{78}Kr+^{58}Ni$ source. These curves are plotted with two Fermi Gas curves for reference. An additional reference point is provided by the compilation of Natowitz *et al.* [9] from experimental measurements on similarly sized sources.

The momentum fluctuation thermometer agrees with the Fermi Gas ($T = \sqrt{(aE^*)}$, a=8,13) predictions at low excitation energy. In addition, at higher excitation energies, it flattens though it does not yield a completely flat plateau.

The two sources depicted in Fig. 1 yield temperatures that are nearly identical and are well within errors of each other. This thermometer does not exhibit a significant source N/Z dependence.

[1] S. Wuenschel *et al.*, *Progress in Research*, Cyclotron Institute, Texas A&M University (2006-2007), p II-34.

[2] S. Wuenschel *et al.*, Nucl. Instrum. Methods Phys. Rev. **A604**, 578 (2009).

[3] S. Wuenschel *et al.*, *Progress in Research,* Cyclotron Institute, Texas A&M University (2007-2008), p II-28.

[4] J. Steckmeyer et al., Nucl. Phys. **A686**, 537 (2001).

[5] D. Lacroix, A. V. Lauwe, and D. Durand, Phys. Rev. C **69**, 054604 (2004).

[6] GEANT http://wwwasd.web.cern.ch/wwasd/geant/.

[7] S. Wuenschel, Ph. D. Thesis, Texas A&M University (2009).

[8] W. Bauer, Phys. Rev. C **51**, 803 (1995).

[9] J. B. Natowitz *et al.*, Phys. Rev. C **65**, 034618 (2002).

Isotopic scaling of Z=1-17 fragments

S. Wuenschel, R. Dienhoffer, S. J. Yennello, G. A. Souliotis, D. V. Shetty,
S. N. Soisson, B. C. Stein, Z. Kohley, and L. W. May

Projectile fragmentation sources were identified from reactions of ^{86,78}Kr+^{64,58}Ni at 35 MeV/A collected with the upgraded NIMROD-ISiS array [1,2]. This data has been calibrated, particle identified, and analyzed to isolate the quasi-projectile source [3,4].

In heavy-ion collisions, fragment yield ratios $R_{21}(N,Z)$, obtained from two sources differing only in N/Z, have been shown to exhibit an exponential dependence on the neutron (N) and proton (Z) numbers of the fragments. This relationship is parameterized in (1) where the ratio of an isotope's yield from two fragments is linked to an exponential function. The α and β in the exponential portion of (1) are related to the chemical potentials and through these the coefficient of the asymmetric portion of the nuclear equation of state (C_{sym}). The relationship between α and C_{sym} given in (2) is well established and has been utilized in experimental investigations of the nuclear symmetry energy[5-9].

$$R_{21}(N,Z) = \frac{Y_2(N,Z)}{Y_1(N,Z)} = Ce^{(N\alpha+Z\beta)} \qquad (1)$$

$$\frac{\alpha}{\Delta} = \frac{4C_{sym}}{T} \quad where \Delta = \left(\frac{Z}{A}\right)_1^2 - \left(\frac{Z}{A}\right)_2^2 \qquad (2)$$

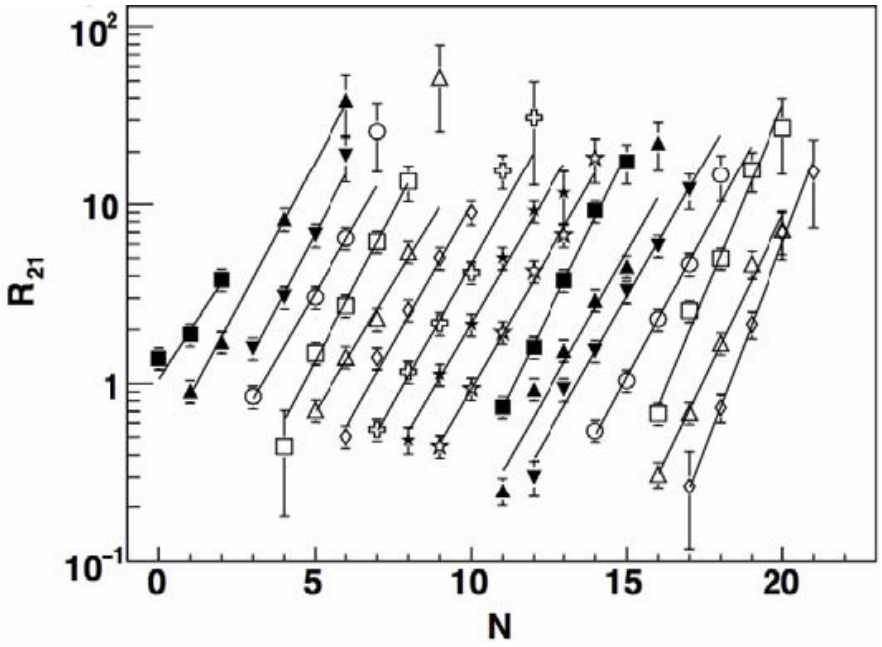

FIG. 1. Isoscaling of Z=1-17 isotopes.

The reconstructed quasi-projectiles from this data set were divided based on the experimentally determined N/Z ratio. The neutron number was obtained event by event from the sum of neutrons bound in charged particles with experimental neutrons obtained from the Neutron Ball [10]. The Z was defined as the sum of protons detected in an event. Two windows in N/Z were taken for the neutron rich and neutron poor sources for isoscaling.

The isoscaling results for Z=1-17 isotopes is plotted in Fig. 1. The lines are individual fits to the isotopic ratios of each element. These fits are parallel and evenly spaced across the range of elements shown in this figure.

The reconstructed quasi-projectiles in this data have been assigned excitation energies through calorimetry [4]. Thus, C_{sym} was studied as a function of E*/A through isoscaling of the data divided into bins of source E*/A.

The same two bins in N/Z used for Figure 1 were used for isoscaling as a function of the source E*/A. The evolution of the isocaling parameter α normalized to the asymmetry of the two source as a function of E*/A is plotted in Fig. 2. The significant decrease in α/Δ seen in this figure may indicate that C_{sym} is decreasing with increasing source excitation energy.

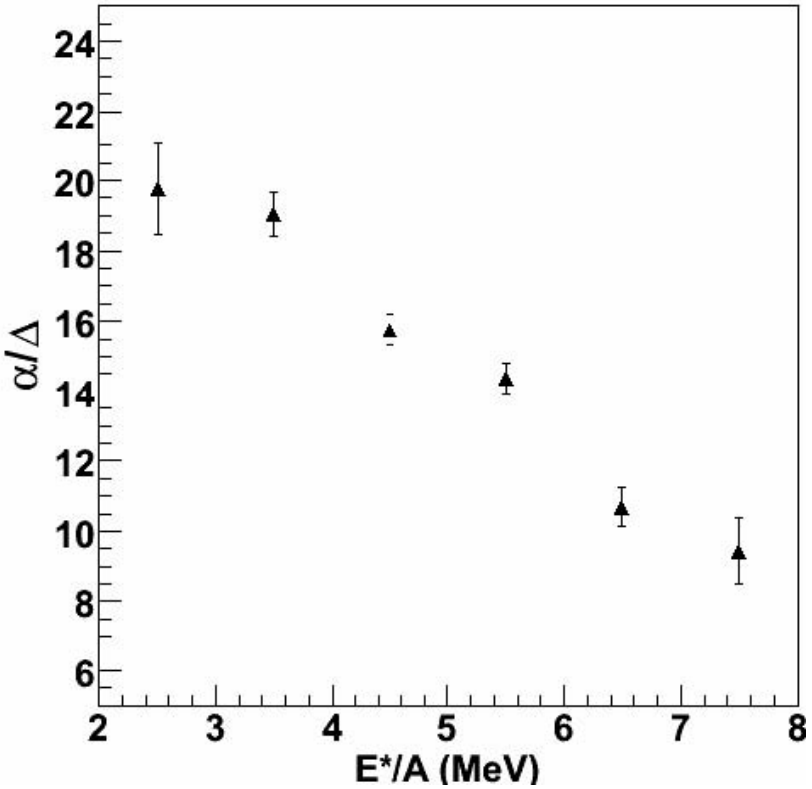

FIG. 2. Isoscaling α/Δ plotted as a function of the E*/A of the reconstructed quasi-projectile sources.

The connection of α/Δ to C_{sym} was made through Eq. 2 with the temperature obtained from the proton momentum fluctuation thermometer [4]. The evolution of C_{sym} with E*/A is plotted in Figure 3 for

constant and evolving temperature. It is clear from this plot that C_{sym} is indeed decreasing as a function of the source E*/A.

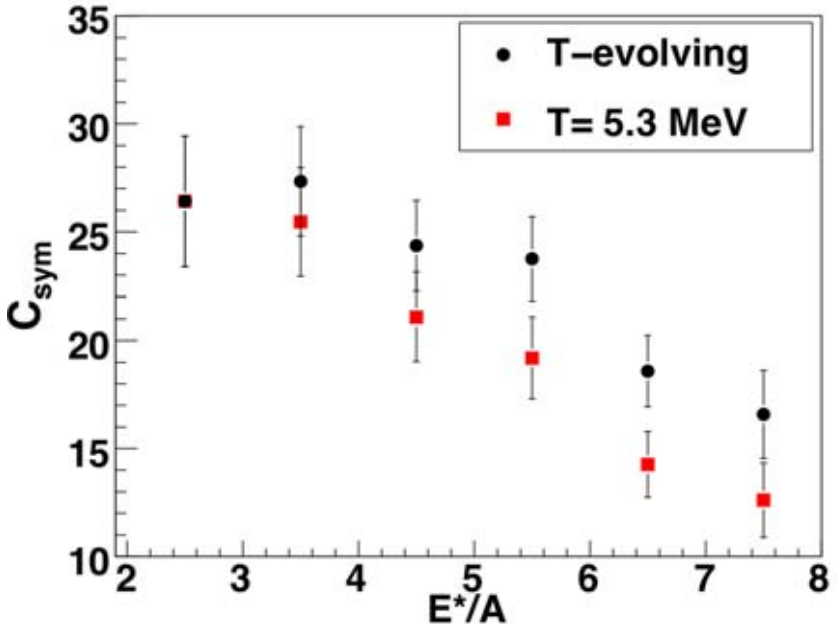

FIG. 3. Csym as a function of the source E*/A. Temperature for this plot was measured using the proton momentum fluctuation thermometer[4].

[1] S. Wuenschel *et al.*, *Progress in Research*, Cyclotron Institute, Texas A&M University (2006-2007), p. II-34.

[2] S. Wuenschel *et al.*, Nucl. Instrum. Methods Phys. Res. **A604**, 578 (2009).

[3] S. Wuenschel *et al.*, *Progress in Research*, Cyclotron Institute, Texas A&M University (2007-2008), p. II-28.

[4] S. Wuenschel *et al.*, *Progress in Reasearch*, Cyclotron Institute, Texas A&M University (2008-2009), – XXXXXX

[5] G. Souliotis, M. Veselsky, D. Shetty, and S. Yennello, Phys. Lett. B **588**, 35 (2004).

[6] M. Tsang *et al.*, Phys. Rev. C **64**, 041603(R) (2001).

[7] M. Tsang *et al.*, Phys. Rev. Lett. **86**, 5023 (2001).

[8] D. V. Shetty, S. J. Yennello, E. Martin, A. Keksis, and G. Souliotis, Phys. Rev. C **68**, 021602 (2003).

[9] G. Souliotis, M. Veselsky, D. V. Shetty, and S. J. Yennello, Phys. Lett. B **588**, 35 (2004).

Isospin dependence of fragmentation

S. N. Soisson, A. S. Botvina, B. C. Stein, G. A. Souliotis, D. V. Shetty, S. Galanopoulos,
S. Wuenschel, Z. Kohley, L. W. May, and S. J. Yennello

In nuclear reactions there is a strong interplay between many nucleons that can lead to fast equilibration of a nuclear system. Multifragmentation reactions provide valuable information about hot nuclei surrounded by other nucleons and nuclei, which provides an environment similar to that of supernova interior as they are highly excited and equilibration properties can be constrained [1]. Understanding how the equation of state behaves in supernova matter is important in constructing the abundances of chemical elements in the universe however current models have used only "average" nuclei as the starting point of the models [2] or only take into consideration long-lived nuclei where neutron rich nuclei are in cold or slightly excited states [3]. Neither of these methods is truly sufficient for the accurate treatment of supernova processes as they distort the true statistical ensemble in many cases.

Using the Forward Array Using Silicon Technology, FAUST, a beam of ^{32}S was reacted with ^{112,124}Sn, ^{nat}Au at 45 MeV/nucleon to probe the isospin dependence of nuclear fragmentation from multi-

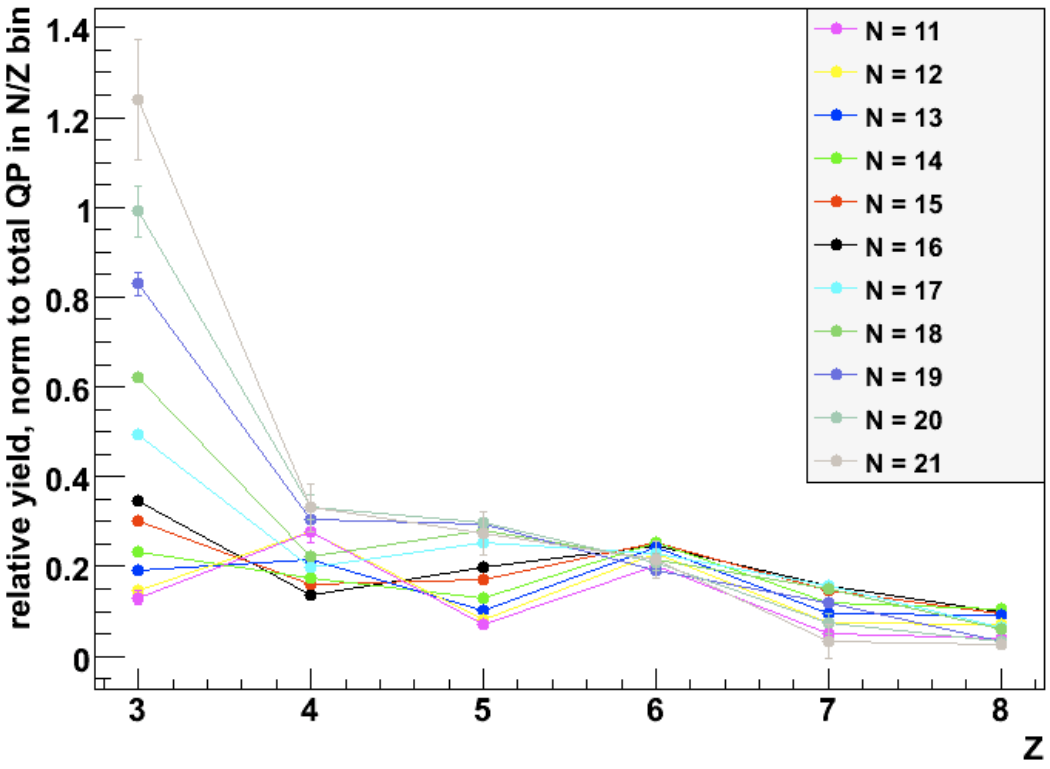

FIG. 1. Charge distribution of fragment for reconstructed quasiprojectile sources wth ∑Z=16 and ∑N= 11, 12,13, 14, 15, 16, 17, 18, 19, 20, 21. The yield of each element is normalized to number of quasiprojectiles in a given source.

fragmentation processes [4,5]. FAUST consists of 68 Si-CsI(Tl) telescopes arranged in 5 concentric rings which span from approximately 1.6 to 45 degrees. The arrangement along with the asymmetry in the size of the projectile and target allows for complete reconstruction of the projectile from the resulting fragments. A reconstructed quasi-projectile is generated for each event by summing the charge and mass collected. Free neutrons are neglected in this process as FAUST does not have the capability to detect free neutrons. Focusing only on the reaction $^{32}S + ^{112}Sn$, the isospin dependence of the fragmentation is currently being studied. Fig. 1 shows the change in the charge distribution as a function of neutron

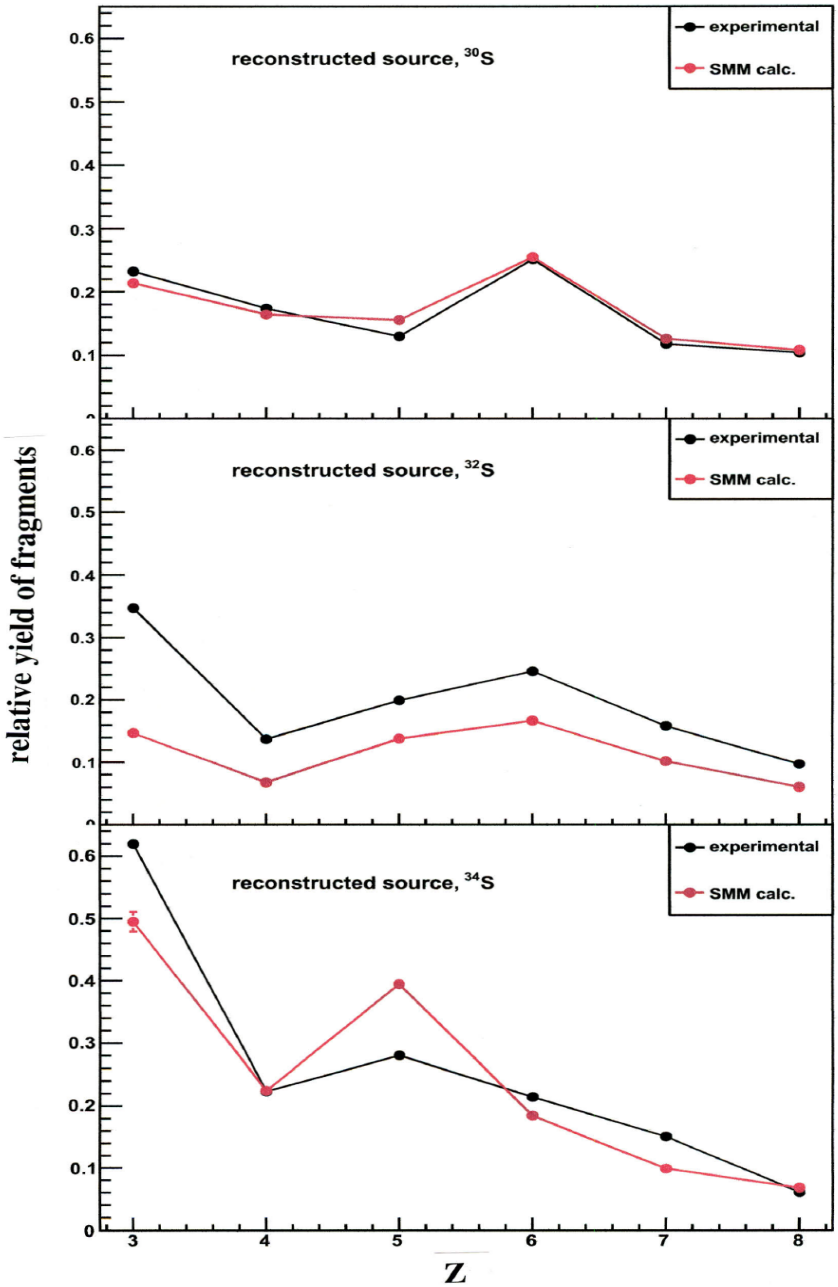

FIG. 2. Charge distributions of fragments from reconstructed quasiprojectile sources 30S (top), 32S (middle), and 34S(bottom) from the experimental data (black) and SMM (red).

content of quasi-projectiles whose charge is that of the beam, 16. The yield of each element is normalized to the number of quasi-projectiles in a given source. For the most neutron poor quasi-projectiles (ex. N = 11) one can see that there is a prominent "zig-zag" behavior which occurs in the range of Z = 3 to 8. As the neutron content increases the "zig-zag" behavior dampens and the resulting shape of the charge distribution becomes more power law like (ex. N = 21). SMM, the Statistical Multifragmentation Model [6], has been used to attempt to model this behavior. The results are presented in Fig. 2 for the quasi-projectiles ^{30}S, ^{32}S and ^{34}S. As one can see, the SMM does a reasonable job at predicting the shape of the charge distribution. For ^{30}S, the shape has a prominent "zig-zag" pattern, ^{32}S the "zig-zag" pattern dampens but the SMM predicts the normalized yield to be lower. In contrast, the ^{34}S has a very different shape to the charge distribution in comparison to the previous examples and the SMM is able to predict that shape reasonably well. From this observation we are beginning to look at the underlying properties of these experimental signatures and constrain the EOS for supernova processes through a better experimental definition of the populated statistical ensemble.

[1] A. S. Botvina and I. N. Mishustin; arXiv:0811.2593v1 [nucl-th]

[2] H. Shen, H. Toki, K. Oyamatsu, and K. Sumiyoshi, Nucl. Phys. **A637**, 435 (1998).

[3] C. Ishizuka, A. Ohnishi, and K. Sumiyoshi, Nucl. Phys. **A723**, 517 (2003).

[4] B. C. Stein, S. N. Soisson *et al.*, *Progress in Research*, Cyclotron Institute, Texas A&M University (2007-2008), p II-30.

[5] F. Gimeno-Nogues *et al.*, Nucl. Instrum. Methods Phys. Res. **A399**, 94 (1997).

[6] J. P. Bondorf *et al.*, Phys. Rep. **257**, 133 (1993).

New heavy element program at Texas A&M University

C. M. Folden III, A. A. al-Harbi, and M. C. Alfonso

A new program to study the heaviest elements has begun at the Texas A&M University Cyclotron Institute. The goals of this program are a better understanding of the production, decay, and chemical properties of the heavy actinide and transactinide elements. These elements are not naturally occurring and must be produced artificially using fusion reactions requiring high-intensity beams, long irradiation times, and efficient separation techniques. This combination of facilities is available at the Institute.

As part of a DOE-sponsored upgrade program, the idle K140 88-Inch Cyclotron is being recommissioned to provide intense, stable beams for experiments in fundamental interactions, rare isotope production, etc. [1]. The new heavy element program will focus on using medium-mass beams from the recommissioned K140 cyclotron for production of actinide and transactinide nuclei in complete fusion, neutron evaporation reactions. Due to the low recoil range of slow, heavy ions, target thicknesses in these experiments are limited to ≈500 μg/cm^2. Transactinide production cross sections are typically nanobarns or smaller (see Fig. 3 in [2]), so beam intensities of >200 pnA with energies of ≈5 MeV/u are required. Table I gives a sample of predicted intensities and energies for several beams from the K140 cyclotron. For those beams with listed energies greater than 5 MeV/u, the actual intensity is likely to be higher due to fewer losses during acceleration. Until the upgrade is complete, beams will be provided by the K500 superconducting cyclotron, which is capable of delivering beam intensities of ≈50 pnA.

Once the fusion reaction has taken place, it is critical to efficiently separate the evaporation

TABLE I. Predicted intensities and energies of sample beam from the K140 cyclotron.

Beam	Energy (MeV/u)	Intensity (pnA)	Beam	Energy (MeV/u)	Intensity (pnA)
^{22}Ne	29	500	^{59}Co	11	900
^{40}Ar	17	1400	^{86}Kr	8.3	600

residues from the unreacted beam, scattered nuclei, and transfer reaction products. The Momentum Achromat Recoil Separator (MARS) [3, 4] will be used for this purpose. It couples a pair of dipole magnets with achromatic focusing to a Wien velocity filter, followed by a final dipole magnet. The velocity of a typical heavy evaporation residue is ≈0.02c (energy ≈ 0.2 MeV/u) and generally a factor of 5 lower than the primary beam; therefore a velocity filter should provide excellent primary beam rejection. Table II shows a comparison of MARS to other separators in use in the heavy elements field. Currently, MARS is used primarily for experiments in nuclear astrophysics and radioactive beam production with primary beam energies of tens of MeV/u. Experiments are planned to characterize the performance of the separator for slow ions using sources of degraded α particles. These experiments will begin in Summer 2009.

TABLE II. Comparison of MARS to other heavy element separators.

Separator	Solid Angle (msr)	$\Delta p/p$	Maximum $B\rho$ (T m)
MARS	9	4%	1.8
SHIP [5, 6]	4	10%	1.2
BGS [7]	45	9%	2.5

First beam experiments will focus on the production of lighter elements ($Z > 70$) to measure the transmission of MARS and compare it to simulations. The residue charge state distribution is the most important factor influencing the transmission, so the distribution will be measured in each case to augment the small amount of data available. Future experiments through 2010 will work to steadily push toward heavier elements, with the eventual goal of producing transactinides. Once this occurs, a broad-based program focused on the study of fusion reactions and chemical properties of these elements will begin.

[1] *A Proposed Facility Upgrade for the Texas A&M University Cyclotron Institute* (College Station, TX, 2001); http://cyclotron.tamu.edu/facility_upgrade.pdf.

[2] S. Hofmann *et al.*, Nucl. Phys. **A734**, 93 (2004).

[3] R. E. Tribble, R. H. Burch, and C. A. Gagliardi, Nucl. Instrum. Methods Phys. Res. **A285**, 441 (1989).

[4] R. E. Tribble, C. A. Gagliardi, and W. Liu, Nucl. Instrum. Methods Phys. Res. B **56/57**, 956 (1991).

[5] H. Ewald *et al.*, Nucl. Instrum. Methods **139**, 223 (1976).

[6] G. Münzenberg *et al.*, Nucl. Instrum. Methods **161**, 65 (1979).

[7] V. Ninov, K. E. Gregorich, and C. A. McGrath, in *ENAM 98: Exotic Nuclei and Atomic Masses*, edited by B. M. Sherrill, D. J. Morrissey, and C. N. Davids (American Institute of Physics, Woodbury, New York, 1998), p. 704.

Thin-target preparation for heavy element experiments

M. C. Alfonso and C. M. Folden III

The heavy element research program at the Cyclotron Institute will utilize low-energy (~5 MeV/u) beams and requires thin targets (~300 μg/cm^2), because the products of complete fusion-evaporation reactions have large masses and low velocities that can be stopped in thick targets. Thin targets also cause less angular straggling. The ability to make thin targets on site would be very beneficial to the future of the heavy element research program.

Physical vapor deposition is often used in the field to make these thin targets; in this method vapors of the target material are deposited on a substrate. The deposition occurs in a vacuum (< 10^{-4} torr) allowing for even deposition and greatly reducing the chance of contamination. The Cyclotron Institute Target Laboratory has a thermal and electron gun evaporator shown in Fig. 1, which could be used to make the needed holmium targets. The reaction ^{165}Ho(^{40}Ar, 6n)^{199}At was chosen due its similar kinematics to ^{208}Pb(^{50}Ti, n)^{257}Rf reaction, which is of future interest. Due to the high melting point of Ho the electron gun evaporator was more suitable. Ho pieces purchased from Alfa Aesar were used and the deposition occurred on an Al foil (~0.8 μm) sandwiched in a Cyclotron Institute standard target frame, covered with a mask. After numerous attempts to make targets it was determined that the cooling system for the gun could not handle the high temperature of the Ho evaporation. Also, the thickness of the deposition could not be monitored in the chamber with the current setup.

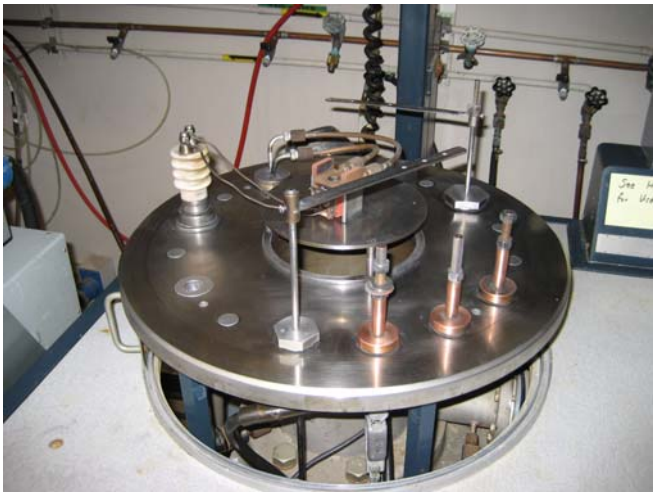

FIG. 1. Close-up of thermal and electron gun evaporator at target lab (bell jar retracted).

The Materials Characterization Facility (MCF) has a newer thermal evaporator, a BOC Edwards Auto 306 Metal Evaporation Chamber shown in Fig. 2, which could be used to make the Ho targets. This instrument could monitor the thickness of the deposition by using a quartz crystal thickness monitor which works by monitoring the change in frequency of a quartz crystal oscillator while the deposition occurs. Typically, the deposition rate fluctuated between 0.1-0.4 nm/s during the deposition. Evaporation of Ho required higher voltages than normal because Ho goes through sublimation instead of melting like most metals used in the thermal evaporator. Though difficult, the necessary targets were successfully prepared. Metals with lower melting temperatures than Ho can be used in the future. The thermal

evaporator at the MCF is a suitable instrument for making thin targets in the future for the heavy element research program here at the Cyclotron Institute.

FIG. 2. Thermal evaporator at MCF.

SECTION III

NUCLEAR THEORY

Effect of medium dependent binding energies on inferring the temperatures and freeze-out density of disassembling hot nuclear matter from cluster yields

S. Shlomo, G. Ropke,[1] J. B. Natowitz, L. Qin, K. Hagel, R. Wada, and A. Bonasera[2]
[1]*University of Rostock, Institut fur Physik, 18051 Rostock, Germany*
[2]*Laboratori Nazionali del Sud, INFN, 95123 Catania, Italy*

The decay of highly excited nuclear matter produced in heavy ion collisions is a complex dynamic process, which needs, in principle, a sophisticated treatment. One simple approach is the freeze-out concept in which the hot and dense matter in the initial stage is assumed to reach thermal equilibrium as long as reaction rates are high. With decreasing density, the reaction rates decrease and the equilibration process becomes suppressed. At that time the nuclear thermal and chemical equilibrium is frozen out. Often the description of the nuclear matter, in particular the distribution of clusters, is calculated within a statistical multifragmentation model assuming nuclear statistical equilibrium (NSE). Under the simplifying assumption that the final reaction product distribution is identical to the cluster distribution at the freeze out point, the thermodynamic parameters such as temperature T and particle number densities, n_n and n_p for neutrons and protons, respectively, can be reconstructed from the observed abundances. A simple method for extracting the temperature of the fragmenting hot system was given by Albergo, Costa, Costanzo and Rubbino (ACCR) [1]. The method is based on selecting double isotope (or isotone) ratios, R_2, such that the nucleon chemical potentials are eliminated leading to a relation between R_2, T and the binding energies of the isotopes (isotones). This method has been used in the analysis of a large number of experiments [2]. We point out [2] that the ACCR method was modified to account for: (i) the screening due to the Coulomb interactions among fragments in the freeze-out volume by using the Wigner-Seitz approximation; (ii) the effect of radial collective flow, and (iii) the effects of post emission decay (secondary decay) processes of particles and, in particular, γ which modify the freeze-out yield ratios. Without these corrections, different double ratios R_2 associated with selected sets of fragments (different thermometers) may result in significantly different temperature T (see a review in Ref. [2]).

If the freeze-out density is not very low the NSE will be modified by medium effects. In this work [3] we explore the abundance of light clusters in nuclear matter at subsaturation density. With increasing density, binding energies and wave functions are modified due to medium effects. The method of ACCR for determining the temperature and free nucleon density of disassembling hot nuclear source from fragment yields is modified to include, in addition to Coulomb effects and flow, also effects of medium modifications of cluster properties, which become of importance when the nuclear matter density is above 10^{-3} fm^{-3}.

Recent progress in the description of clusters in low density nuclear matter [4] enables us to evaluate the abundance of deuterons, tritons and helium nuclei in a microscopic approach, taking the influence of the medium into account. Within a quantum statistical approach to the many-particle system, we determine the single-particle spectral function, which allows calculation of the density of the nucleons as a function of the temperature and the proton's and the neutron's chemical potentials (T, μ_p, μ_n). The main ingredient is the self-energy $\Sigma(1,z)$, which is treated in different approximations. The single-particle

spectral function contains the single-nucleon quasiparticle contribution. Expressions for the single-nucleon quasiparticle energy $E^{qu}(p)$ can be given, for example, by the Skyrme mean-field parameterization. We note that in addition to the quasiparticle contribution, the contribution of the bound and scattering states can also be included in the single-nucleon spectral function, by analyzing the imaginary part of $\Sigma(1,z)$. Within cluster decomposition, A-nucleon T matrices appear in a many-particle approach. These T matrices describe the propagation of the A-nucleon cluster in nuclear matter. In this way, bound states contribute to the EoS, $n_\tau = n_\tau (T, \mu_p, \mu_n)$, see Ref [4]. In the low-density limit, the propagation of the A-nucleon cluster is determined by the energy eigenvalues of the corresponding nucleus. For the nuclei embedded in nuclear matter, an effective wave equation can be derived [4]. The A-particle wave function and the corresponding eigenvalues follow from solving the in-medium Schrodinger equation

$$\left[E^{qu}(1) + \cdots + E^{qu}(A) - E^{qu}_{Avp}(p)\right]\Psi_{Avp}(1 \ldots A) + \Sigma'_{1' \ldots A'} \Sigma'_{i<j}\left[1 - \bar{f}(i) - \bar{f}(j)\right] V(ij, i'j') \prod'_{k \neq i,j} \delta_{kk'} \Psi_{Avp}(1' \ldots A') = 0. \quad (1)$$

This equation contains the effects of the medium in the single-nucleon quasiparticle shifts as well as in the Pauli blocking terms. It can be shown that the EoS can be evaluated as in the non-interacting case, except that the number densities of clusters must be calculated with the quasiparticle energies,

$$n^{qu}(A,Z) = g_{A,Z} \int \frac{d^3p}{(2\pi)^3} f_{A,Z}\left[E^{qu}_{A,Z}(p)\right]. \quad (2)$$

In the cluster-quasiparticle approximation, the EoS reads,

$$n^{qu}_p(T, \mu_p, \mu_n) = \Sigma_{A,Z} Z n^{qu}(A,Z), \quad (3)$$

$$n^{qu}_n(T, \mu_p, \mu_n) = \Sigma_{A,Z} (A - Z) n^{qu}(A,Z), \quad (4)$$

for the total proton and neutron densities, respectively.

Comparing the values of the parameters obtained in the full calculation, with inclusion of medium effects on the yields with those deduced in the ACCR approach, we find that moderate deviations in the temperature arise for densities larger than 0.0001 fm^{-3}. Determination of the densities is more sensitive to the medium effects. We thus conclude that the fragment yields from hot and dense nuclear matter produced in heavy ion collisions can be used to infer temperatures and proton/neutron densities of the early stages of the expanding hot matter. The assumption of thermal equilibrium can be only a first approach to this non-equilibrium process. To determine the yield of the different clusters, a simple statistical model neglecting all medium effects, i.e., treating it as an ideal mixture of non-interacting nuclei is not applicable when the density is larger than 0.0001 fm^{-3}. Self-energy and Pauli blocking will lead to energy shifts, which have to be taken into account to reconstruct the thermodynamic parameters from measured yields. The success of the simple ACCR method to derive the values for the temperature can be understood from a partial compensation of the effect of the energy shifts so that reasonable values

for the temperature are obtained also at relatively high densities. More care must be taken in inferring densities from the data.

[1] S. Albergo, S. Costa, E. Costanzo, and A. Rubino, Nuovo Cimento A **89**, 1 (1985).
[2] S. Shlomo and V. M. Kolomietz, Rep. Prog. Phys. **68,** 1 (2005).
[3] S. Shlomo, G. Ropke, J. B. Natowitz, L. Qin, K. Hagel, R. Wada, and A. Bonasera, Phys. Rev. C **79**, 034604 (2009).
[4] G. Ropke, M. Schmidt, L. Munchow, and H. Schulz, Nucl. Phys. **A399**, 587 (1983).

A new Skyrme type energy density functional

D. C. Fuls and S. Shlomo

Energy density functional (EDF) theory is a powerful tool for the study of many-body problems. The problem in its implementation is to find the EDF itself. The quest for a new and more accurate EDF is one of the major problems in modern nuclear theory.

We aim to build a more effective EDF associated with the Skyrme effective nucleon-nucleon interaction that is able to correctly predict the properties of nuclei at and away from the valley of stability. We have used many different nuclear properties including binding energy, charge rms radii, spin-orbit splitting of single-particle orbits, rms radii for valence neutrons and centroid energies for the isoscalar giant monopole resonance (ISGMR) for many different nuclei ranging from very light ^{16}O to very heavy ^{208}Pb. Traditionally, it has been required that experimental data on the ground state be well reproduced by the mean-field theory. We have made our fit to modified experimental data [1], which takes into account correlation effects, i.e. to go beyond the mean-field.

We have used the simulated annealing method in addition to an advanced least square method to search the hyper-surface of the Skyrme parameter space for the global minima. We have developed a new Skyrme-based EDF, named KDEX. The new interaction better predicts the rms radii of ^{16}O and ^{208}Pb which has been a problem in most previous interactions. The values of the Skyrme parameters for the KDEX interaction are given in Table I together with those of the KDE0 [2] interaction.

TABLE I. Values of the parameters of the Skyrme type interactions.

	KDE0 (HF)	KDEX (HF+CORR)
t_0 (MeV fm^3)	-2526.51 (140.63)	-1419.83 (14.68)
t_1 (MeV fm^5)	430.94 (16.67)	309.14 (8.79)
t_2 (MeV fm^5)	-398.38 (27.31)	-172.96 (3.92)
t_3 (MeV fm$^{3(1+\alpha)}$)	14235.5 (680.73)	10465.4 (133.29)
x_0	0.7583 (0.0655)	0.14741 (0.00437)
x_1	-0.3087 (0.0165)	-0.08527 (0.0046)
x_2	-0.9495 (0.0179)	-0.6144 (0.0159)
x_3	1.1445 (0.0882)	0.02197 (0.00106)
W_0 (MeV fm^5)	128.96 (3.33)	98.90 (2.27)
α	0.1676 (0.0163)	0.4989 (0.0103)

Our future plans include:

i) Improve the fit between theoretical prediction and experimental results by modifying the density dependence of the Skyrme interaction.

ii) Include in the fit of the EDF ISGMR data for more nuclei, which is sensitive to the nuclear matter incompressibility coefficient. Also we would like to include higher multipole data, which is sensitive to symmetry energy density and the effective mass.

[1] P. Klüpfel, P.-G. Reinhard, T. J. Bürvenich, and J. A. Maruhn, arXiv:0804.3385v2 (2008).
[2] B. K. Agrawal, S. Shlomo, and V. Kim Au, Phys. Rev. C **72**, 014310 (2005).

Damping effects on centroid energies of isoscalar compression modes

D. C. Fuls, V. M. Kolomietz,[1] S. V. Lukyanov,[1] and S. Shlomo
[1]*Institute for Nuclear Research, Kiev 03680, Ukraine*

Experimental data for the centroid energies E1 of the isoscalar giant dipole resonance (ISGDR) are significantly smaller than those obtained by the self-consistent Hartree Fock (HF) random phase approximation (RPA) calculations with effective interactions, which reproduce the experimental value of the centroid energy E0 of the isoscalar giant monopole resonance (ISGMR). The experimental value $(E1/E0)_{exp} = 1.60\pm0.1$ exceeds the prediction of the liquid drop (hydrodynamic) model (LDM) and lies below the theoretical results for the ratio E1/E0 obtained in both the RPA and the scaling-like calculations. In this work we study the sensitivity of E0 of the ISGMR and E1 of the ISGDR to the effect of relaxation (collisional damping). We use the semiclassical kinetic approach in phase space. This approach, in contrast to the quantum Hartree-Fock based RPA, ignores the single particle (shell) effects. However, the advantage is that the kinetic theory allows one to take into consideration the relaxation (damping) processes in a transparent way via the collisional integral.

We start from the fluid dynamic equations of motion for the viscous Fermi liquid. Within the fluid dynamic approach (FDA) [1], the eigenfrequency ω of the compression eigenmodes satisfies the dispersion equation

$$\omega^2 - c_0^2(\omega)q^2 + i\omega\gamma(\omega)q^2 = 0, \quad c_0^2(\omega) = [K+12\mu(\omega)/\rho_0]/9m, \quad \gamma(\omega) = 4\nu(\omega)/3\rho_0 m, \qquad (1)$$

where K is the incompressibility coefficient, ρ_0 is the bulk particle density and m is the nucleon mass. The transport coefficients $\mu(\omega)$ and $\nu(\omega)$ in Eq. (1) are due to the Fermi distortion effects [1] and depend on the relaxation time τ. The wave number q in Eq. (1) is due to the boundary conditions on the free surface of the nucleus, which are significantly different for the ISGMR and the ISGDR because the ISGDR appears as the overtone to the spurious mode. We have carried out calculations for the isoscalar monopole and dipole giant resonances in the frameworks of Hartree-Fock based RPA and the semiclassical Fermi liquid approach. We have solved the dispersion Eq. (1) augmented by the corresponding boundary condition for both ISGMR and ISGDR for several nuclei. Since the ISGDR appears as the overtone to the spurious mode, the energy of the ISGDR is shifted to higher energies with respect to the liquid drop model (LDM) prediction because of the Fermi surface distortion effect and it is sensitive to the interparticle collisions. As a result, the energy ratio E1/E0 decreases and approaches the experimental value if the collisional damping is taken into account.

We find [2] that the ratio $(E1/E0)_{FDA}$ depends on the relaxation time $\tau = \hbar\beta/(\hbar\omega/2\pi)^2$ and approaches the experimental value $(E1/E0)_{exp} = 1.60\pm0.1$ in a short relaxation time limit at $\beta = 0.75$. In rare collision regime ($\omega\tau >> 1$), the compression mode energies E0 and E1 are saturated at certain values which correspond to the zero sound velocity $c_0 = [K+(24/5)\varepsilon_F/9m]^{1/2}$ (ε_F is the Fermi energy). In frequent collision regime ($\omega\tau << 1$, small β), the contribution to the sound velocity c_0 from the Fermi surface distortion effect is washed out and both energies E0 and E1 reach the first sound limit (i.e., the LDM

regime) at $c_0 = c_1 = (K/9m)^{1/2}$. We note also the non-monotonic behavior of the widths $\Gamma 0$ and $\Gamma 1$ for the ISGMR and the ISGDR, respectively, which is a consequence of the memory effect (ω-dependence) in the friction coefficient $\gamma(\omega)$ of Eq. (1).

[1] V. M. Kolomietz and S. Shlomo, Phys. Rev. C **61**, 064302 (2000).
[2] D. C. Fuls, V. M. Kolomietz, S. V. Lukyanov, and S. Shlomo, to be published.

Threshold effects in low energy isovctor dipole excitations in nuclei

E. Nica, D. C. Fuls, and S. Shlomo

Calculations of the nuclear response function for the Isovector Giant Dipole Resonance (IVGDR) have been carried out in the past using the discretized Hartree-Fock Random Phase Approximation (HF-DRPA). In many cases they contained violations of self-consistency and a large smearing parameter. Under these conditions, low energy enhancements in the nuclear response function have been interpreted as resonances in some instances. To investigate the validity of these claims we undertook HF- Continuum RPA (HF-CRPA) and scattering phase shift calculations for the asymmetric ^{28}O and ^{60}Ca nuclei. In addition, we also calculated the Free response of the above-mentioned nuclei using a HF-DRPA scheme.

Shown in Fig.1 is the RPA response (top) for isovector dipole excitations for ^{60}Ca, calculated using the HF-CRPA scheme. The points of contention are the enhancements seen in the 5-7.5 MeV region in the RPA response.

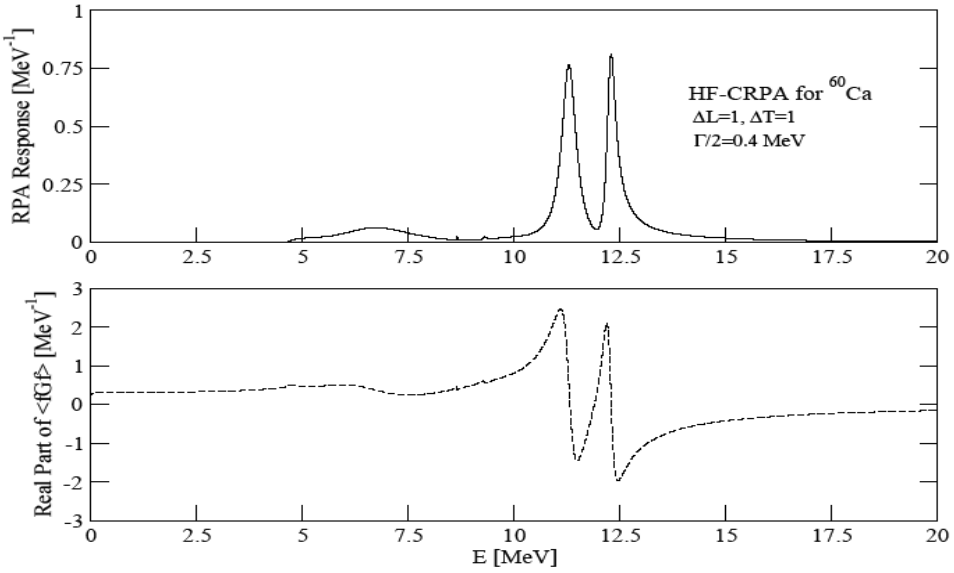

FIG. 1. Isovector Dipole Continuum HF-CRPA for ^{60}Ca with smearing Γ/2=0.4 MeV and a maximum radius of 12 fm. The imaginary part of $\langle fGf \rangle$ (RPA response) is shown on top while the real part of $\langle fGf \rangle$ is shown on the bottom. To better distinguish between the two, the real part of $\langle fGf \rangle$ is dashed.

To understand how these could come about, we illustrate the Free response for ^{60}Ca under dipole transitions calculated according to HF-CRPA theory in Fig.2. Collective excitations in the RPA are built from coherent particle-hole excitations. As such, we expect that resonances in the single-particle transition spectrum contribute the most to resonances in the collective spectrum. For single-particle

resonances within the HF-CRPA theory, the real part of $\langle f G^{(0)} f \rangle$ has a pole. Referring to Fig. 2 we do not notice poles in the real part of $\langle f G^{(0)} f \rangle$ (bottom of figure) in the 5-7.5 MeV excitation energy range. The HF-CRPA scheme therefore does not predict single-particle resonances in this region.

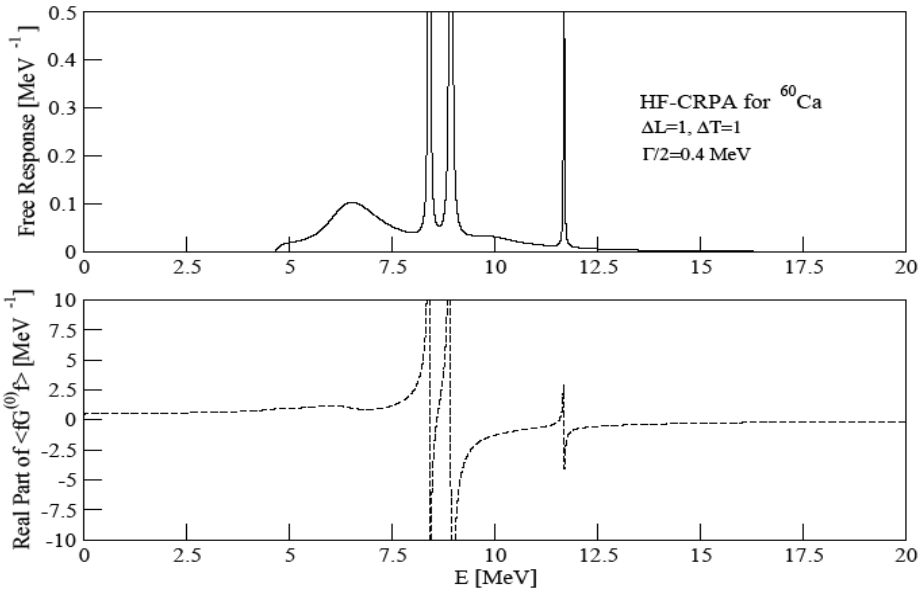

FIG. 2. Isovector Dipole Continuum HF-CRPA Free Response for ^{60}Ca with smearing Γ/2=0.4 MeV and a maximum radius of 12 fm. The imaginary part of $\langle f G^{(0)} f \rangle$ (Free response) is shown on top while the real part of $\langle f G^{(0)} f \rangle$ is shown on the bottom. To better distinguish between the two, the real part of $\langle f G^{(0)} f \rangle$ is dashed

The Free response for ^{60}Ca within the HF-DRPA is shown in Fig. 3. This approach uses a discrete continuum ensuring that all transitions to the latter are given the same aspect as bound-to-bound transitions in the Free response. Because of this, non-resonant transitions to the continuum could be interpreted as resonances. This can be seen in Fig.3 where transitions in the 5-7.5 MeV excitation energy range appear as resonances, in stark contrast to the results shown in Fig. 2.

To check our HF-CRPA results we undertook scattering phase shift derivative calculations for the two nuclei under study. The phase shift derivatives are proportional to the single-particle level densities in the continuum

$$g_{cl}(\varepsilon) = \frac{1}{\pi} 2(2l+1) \frac{d\delta_l(\varepsilon)}{d\varepsilon}. \qquad (3)$$

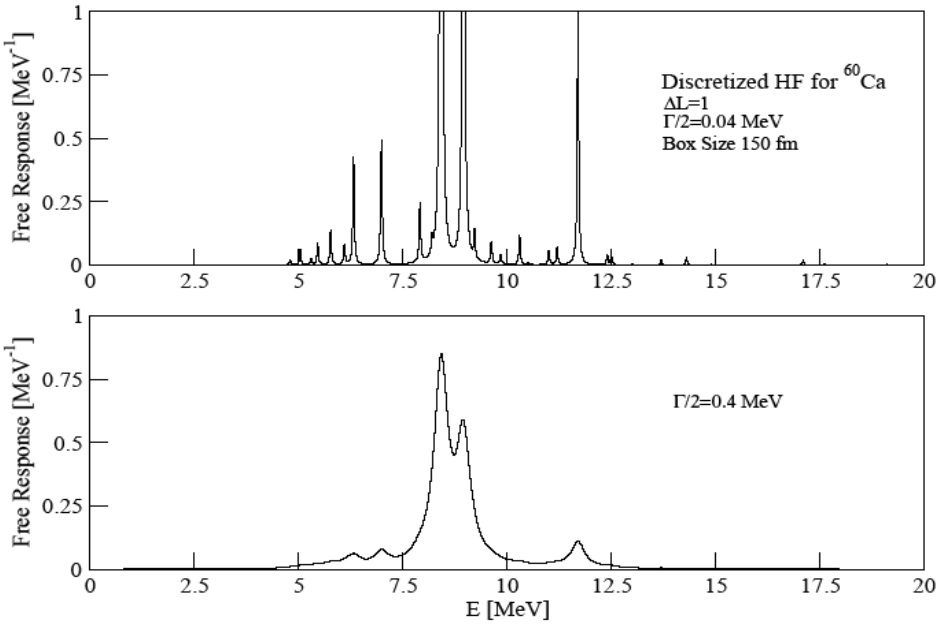

FIG. 3. Isovector Dipole Discretized HF for ^{60}Ca with a box size of 150 fm. The top part shows the Free response with smearing Γ/2=0.04 MeV while the bottom shows the Free response with smearing Γ/2=0.4 MeV.

The phase shift derivatives were calculated by two methods. The first involved the use of the asymptotic form of the solutions to the radial Schrodinger equation. In the second method the scattering phase shift derivatives were calculated using the Green's function method as given by

$$g_l(\epsilon) = \lim_{\alpha\to\infty, R\to\infty} 2(2l+1)\frac{1}{\pi}\int_0^R dr\,[\mathrm{Im}G_l(r,r',\epsilon+i\alpha) - \mathrm{Im}G_{0l}(r,r',\epsilon+i\alpha)]_{r=r'} \quad (4),$$

where G_l and G_{0l} are Green's functions as given in Ref. [1] and which include a proper treatment of the continuum as described in Ref. [2]. The second term G_{0l} is associated with the free Hamiltonian. In both Green's function and the asymptotic form approaches, a resonance is characterized by a peak in the phase shift derivative with the phase shift passing through π/2.

Fig. 4 illustrates the results of the phase shift calculations. From the top, we list the integral of the imaginary part of the Green function with interactions, the integral of the imaginary part of the Green's function associated with the free Hamiltonian and the difference between the two integrals which, according to Eq. (2) is proportional to the phase shift derivative. The result shown in the bottom part is proportional to the scattering phase shift derivative calculated with the first method.

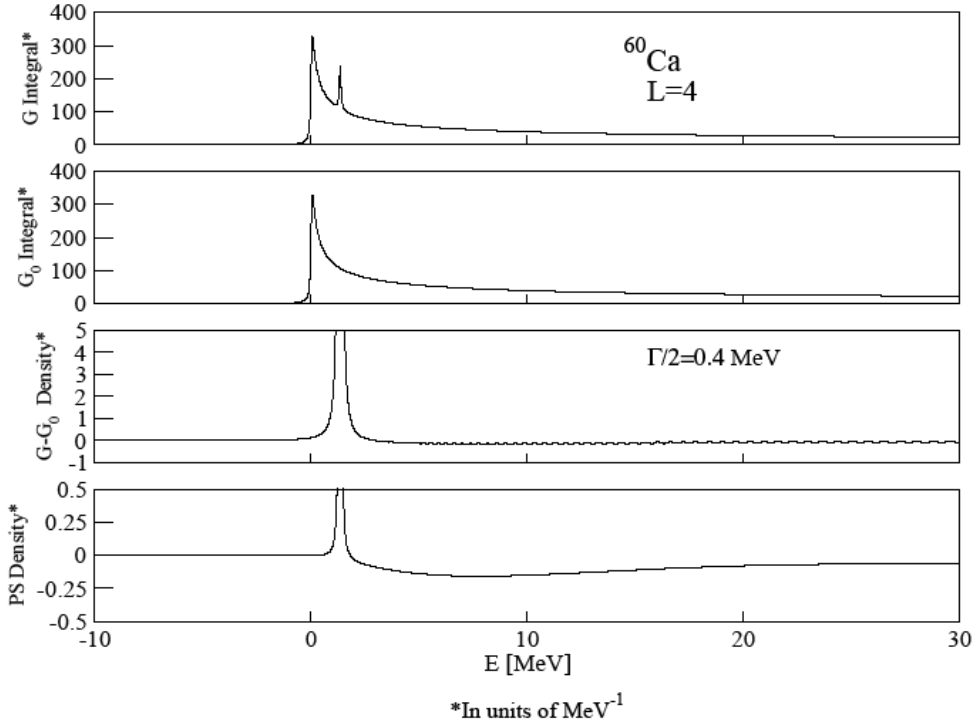

FIG. 4. Single-Particle Level Density for ^{60}Ca, for L=4. The results are plotted as functions of state energy. A resonance at 1.36 MeV is found. A smearing of Γ/2=0.4 MeV was used in the Green's function calculations.

The lowest resonance found in the ^{60}Ca spectrum from the scattering phase shift derivative occurred at 1.36 MeV corresponding to a transition from a neutron 0f bound state with total excitation energy of 9.312 MeV, which is higher than our region of 5-7.5 MeV. This confirmed our HF-CRPA results, which indicated no resonance in the Free response in that particular energy range. The resonance is shown in the bottom two sections of Fig. 4. Similar results were obtained for ^{28}O.

Owing to our HF-CRPA results which show no pole in the real part of the RPA response, and scattering phase shift results, which indicated no single-particle resonances, in the 5-7.5 MeV range, we conclude that the enhancements seen in the collective response of both ^{28}O and ^{60}Ca in the same region are not resonances.

[1] S. Shlomo, V. M. Kolomietz, and H. Dejbakhsh, Phys. Rev. C **55**, 1972 (1997).
[2] S. Shlomo and G. Bertsch, Nucl. Phys. **A243**, 507 (1975).

Trojan horse as indirect technique in nuclear astrophysics

A. M. Mukhamedzhanov, L. D. Blokhintsev,[1] B. F. Irgaziev,[2] A. S. Kadyrov,[3]
M. La Cognata,[4] C. Spitaleri,[4] and R. E. Tribble
[1]*Skobeltsyn Institute of Nuclear Physics, Moscow State University, Russia*
[2]*GIK Institute of Engineering Sciences and Technology,Topi, District Swabi, N.W.F.P.,Pakistan*
[3]*Curtin University of Technology, GPO Box U1987, Perth, WA 6845, Australia*
[4]*DMFCI, Universit di Catania, Catania, Italy and INFN - Laboratori Nazionali del Sud, Catania, Italy*

A general theory of the Trojan Horse (THM) method as indirect technique in nuclear astrophysics has been developed. The kinematics of the THM, the experimental conditions for measurements via the THM are considered and the explanation why the THM works are given.

In the TH method the cross section for the binary process $x + A \rightarrow b + B$ is determined from the TH reaction $a + A \rightarrow y + b + B$, where $a = (yx)$ is the Trojan Horse particle. Projectile a is accelerated to energies higher than the Coulomb barrier in the initial state allowing a to approach the proximity of the target A. After that the binary reaction $x + A \rightarrow b + B$ occurs, while the spectator y carries away the excess of energy of the projectile.

The binary sub-process can be direct and resonant. We address both cases, because they require different approaches. For direct binary reactions the THM amplitude can be approximated by the zero-range DWBA amplitude describing the transfer of particles x into the continuum times the half-off-energy-shell (HOES) amplitude for the binary sub-process $x + A \rightarrow b + B$. For the resonant binary sub-reaction the multi-level, multi-channel R matrix method has been generalized for the $2 \rightarrow 3$ reactions proceeding through isolated or overlapping resonances.

The practical applications of the THM method for different astrophysical reactions are presented and comparisons with direct measurements are done.

Indirect measurement of the $^{18}O(p,\alpha)^{15}N$ reaction rates through the Trojan horse method

M. La Cognata,[1,2] C. Spitaleri,[1] A. M. Mukhamedzhanov, B. Irgaziev, [3] R. E. Tribble, A. Banu, S. Cherubini,[1] A. Coc, [4] V. Crucillá, [1] V. Goldberg, M. Gulino, [1] G. G. Kiss,[1] L. Lamia,[1] J. Mrazek, [5] R. G. Pizzone,[1] S. M. R. Puglia,[1] G. G. Rapisarda,[1] S. Romano,[1] M. L. Sergi,[1,2] G. Tabacaru, L. Trache, W. Trzaska, [6] and A. Tumino [7]

[1]*INFN Laboratori Nazionali del Sud and DMFCI Universit`a di Catania, Catania, Italy*

[2]*Centro Siciliano di Fisica Nucleare e Struttura della Materia, Catania, Italy*

[3]*GIK Institute of Engineering Sciences and Technology Topi, District Swabi, NWFP Pakistan*

[4]*CSNSM CNRS/IN2P3 Universit`e, Paris Sud, Orsay, France*

[5]*Nuclear Physics Institute of ASCR Rez near Prague, Czech Republic*

[6]*Physics Department University of Jyvaskyla, Jyvaskyla, Finland*

[7]*Universit`a Kore, Enna, Italy*

In this paper we have evaluated the impact of the new improved measurement of the 20 keV resonance on the reaction rate of the $^{18}O(p,a)^{15}N$ reaction. For the first time, the strength of the low-lying 8.014 MeV resonance in ^{19}F has been experimentally determined via the indirect THM, while the same measurements have proved elusive or highly uncertain for any direct and indirect approach. The present result turns out to be about 35% larger than the NACRE rate [1] in the region where the effect of the presence of the 20 keV resonance is more intense. On the other hand the accuracy of the data has been improved by a factor ≈ 8.5. These changes reflects on the reaction rate, while no significant change is produced by the THM measurement of the strength of the 8.084 MeV state in ^{19}F. The correct reproduction of the strength of the 90 keV resonance, which has been more accurately determined than the 20 keV one by previous experiments, represents a benchmark of the present approach, making us confident of its validity. The main advantage of the THM approach is the possibility to provide not only a more precise determination of the relevant resonance strength but, more importantly, a much more accurate one. In details, this newly developed approach is based on experimental data in contrast to the previous works, which mainly rely on various kinds of estimates. Moreover, the THM leads to the determination of the strength of the unknown resonance avoiding information about the spectroscopic factors, which are a primary source of systematic errors. Finally, our results are not affected by the electron screening, which can enhance the cross section by a factor larger than about 2.4 at 20 keV, thus spoiling any direct measurement of this resonance. As a next step, the astrophysical consequences of the present work are to be evaluated. These results have to be linked with the recent developments in astrophysical models to provide an up-to-date and consistent picture of AGB star nucleosynthesis. In addition, at higher temperatures, higher energy resonances in the $^{18}O(p,\alpha)^{15}N$ reaction can play a role. These studies will be the subject of forthcoming works. The paper will be submitted to Phys. Rev. C.

[1] C. Angulo *et al.*, Nucl. Phys. **A656**, 3 (1999).

Improved determination of the astrophysical S(0) factor of the $^{15}N(p,\alpha)^{12}C$ reaction

M. La Cognata,[1] V. Z. Goldberg, A. M. Mukhamedzhanov, C. Spitaleri,[1] and R. E. Tribble
[1]*INFN - Laboratori Nazionali del Sud, Dipartimento di Metodologie Chimiche e Fisiche per l'Ingegneria, Universita di Catania, Catania, Italy*

We present new improved R matrix fits of direct data and indirect Trojan Horse data for the $^{15}N(p,\alpha)^{12}C$ reaction and provide a more accurate recommended value of S(0) = 73.0 ± 5.0 MeVb from direct Redder data [1] and S(0) = 70.0 ± 13.5 MeVb from the Trojan Horse data [2]. We also analyze a recent fit by Barker [3] and demonstrate that, when all the uncertainties are taken into account, our results overlap with his S(0)= 82 ±10 MeVb obtained from the fit of the Redder data [1] and 79 ± 13 MeVb from the fit to the direct data [4]. We also provide a fit of the Trojan Horse data that properly takes into account finite residual energy resolution of the data. In Fig. 1 the S(0) factors obtained by extrapolation of direct measurements [1,4,5] are compared with the measured indirect value [2] and the full R matrix extrapolation [3], and with the recommended values in the most recent compilations, namely NACRE [6] and Adelberger *et al.* [7]. Fig. 1 demonstrates that all the experimental values are in agreement with each other within the experimental uncertainties, resulting in S(0)= 62 MeVb [5], S(0) = 78 ±13 MeVb [4], S(0) = 65 ± 4.0 MeVb [1] and S(0) = 68 ± 11 MeVb [2]. The compilations by NACRE [6] and Adelberger *et al.* [7] recommended S(0) = 65±7 MeVb and S(0) = 67.5 ± 4.0 MeVb, correspondingly, relying on the results from [4]. The paper has been published to Phys. Rev. C **80**, 012801 (R) (2009).

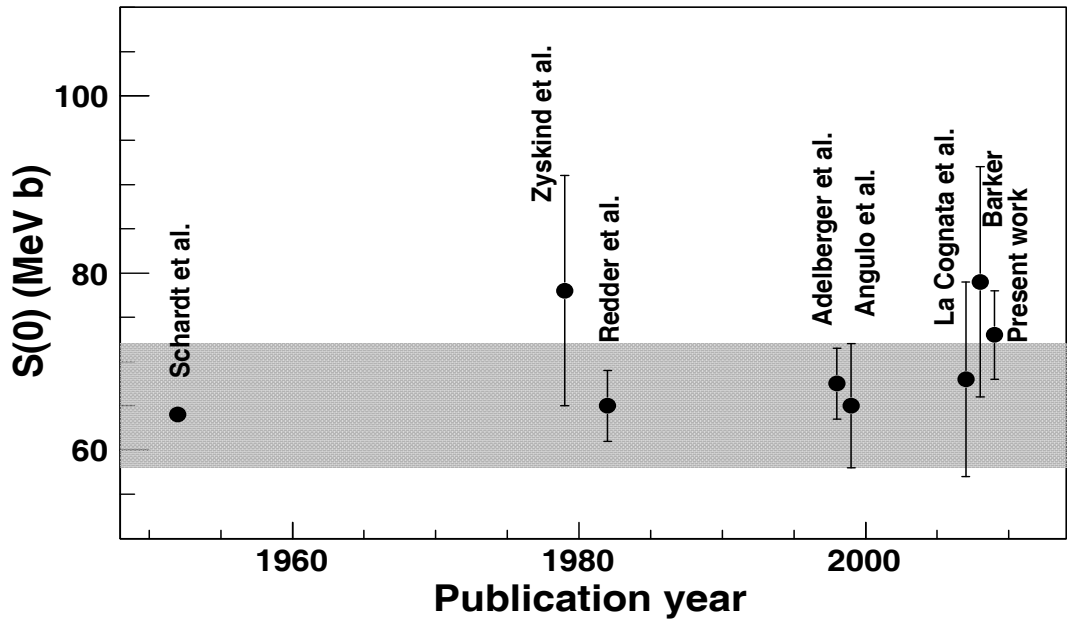

FIG. 1. Summary of the available astrophysical S(0) factors of the $^{15}N(p,\alpha)^{12}C$ reaction.

[1] A. Redder *et al.*, Z. Phys. A **305**, 325 (1982).
[2] M. La Cognata *et al.*, Phys. Rev. C **76**, 065804 (2007).
[3] F. C. Barker, Phys. Rev. C **78**, 044611 (2008).
[4] J. L. Zyskind and P. D. Parker, Nucl. Phys. **A320**, 404 (1979).
[5] A. Schardt *et al.*, Phys. Rev. **86**, 527 (1952).
[6] C. Angulo *et al.*, Nucl. Phys. **A656**, 3 (1999).
[7] E. G. Adelberger *et al.*, Rev. Mod. Phys. **70**, 1265 (1998).

Surface-integral formulation of scattering theory

A. S. Kadyrov,[1] A. M. Mukhamedzhanov, I. Bray,[1] and A. T. Stelbovics[1]
[1]*Curtin University of Technology, GPO Box U1987, Perth, WA 6845, Australia*

We formulate scattering theory in the framework of a surface-integral approach utilizing analytically known asymptotic forms of the two-body and three-body scattering wavefunctions. This formulation is valid for both short-range and long-range Coulombic interactions.

New general definitions for the potential scattering amplitude are presented. For the Coulombic potentials, the generalized amplitude gives the physical on-shell amplitude without recourse to a renormalization procedure. New post and prior forms for the Coulomb three-body breakup amplitude are derived. This resolves the problem of the inability of the conventional scattering theory to define the post form of the breakup amplitude for charged particles. The new definitions can be written as surface integrals convenient for practical calculations. The surface-integral representations are extended to amplitudes of direct and rearrangement scattering processes taking place in an arbitrary three-body system. General definitions for the wave operators are given that unify the currently used channel-dependent definitions. This work has been published as review in Annals of Physics March 2009, online address: doi:10.1016/j.aop.2009.02.003.

Coulomb breakup problem

A. S. Kadyrov,[1] A. M. Mukhamedzhanov, I. Bray,[1] and A. T. Stelbovics[1]
[1]*Curtin University of Technology, GPO Box U1987, Perth, WA 6845, Australia*

Scattering in a few-body system is one of the central subjects of quantum mechanics. However, conventional scattering theory is formally valid only when the particles interact via short-range potentials. For charged particles with the long-range Coulomb interactions the theory requires modification. In the time-dependent formulation, formal scattering theory is generalized to include Coulomb potentials by choosing appropriately modified time evolution operators. This is equivalent to various forms of screening and renormalization in the time independent formulation. The renormalization method leads to the correct cross sections for the two-body problem; however, the results from this procedure cannot be regarded as completely satisfactory. For instance, different ways of screening lead to different asymptotic forms for the scattering wave function. Recently we have demonstrated that there was a general approach to the two body collision problem [1] that did not lead to the aforementioned formal difficulties and did not require renormalization. The situation in a few-body system is even more complicated. Rigorous scattering theory for a system of three particles valid for short-range potentials was given by Faddeev [2]. A renormalization method was implemented for the three-body problem when only two particles are charged [3].

In this work [4] we present a surface-integral approach to formulating scattering theory. We use the recently derived analytic results for total scattering wave functions in asymptotic domains to develop a well-defined prior and post forms of the breakup amplitude valid for short-range and Coulomb potentials. These new definitions do not require screening and renormalization or any regularization as they are exact and divergence-free. We have derived for the first time post and prior forms of the breakup amplitude for a three-body system that are valid for both short-range and Coulomb potentials. This was made possible by the recently obtained analytic forms of the asymptotic wave functions combined with a surface integral approach to the scattering theory. This work published in Phys. Rev. Lett. **101**, 230405 (2008).

[1] A. S. Kadyrov, I. Bray, A. M. Mukhamedzhanov, and A. T. Stelbovics, Phys. Rev. A **72**, 032712 (2005).
[2] L. D. Faddeev, Tr. Matem. Inst. V. A. Steklova, Akad. Nauk. SSSR **69**, 1 (1963).
[3] E. O. Alt, W. Sandhas, and H. Ziegelmann, Phys. Rev. C **17**, 1981 (1978).
[4] A. S. Kadyrov, A. M. Mukhamedzhanov, I. Bray, and A. T. Stelbovics, Phys. Rev. Lett. **101**, 230405 (2008).

Effects of distortion on the intercluster motion in ^{2}H, ^{3}He, ^{3}H, ^{6}Li and ^{9}Be on Trojan horse applications

R. G. Pizzone,[1] C. Spitaleri,[1] C. Bertulani,[2] L. D. Blokhintsev,[3] A. M. Mukhamedzhanov, B. F. Irgaziev,[4] S. Cherubini,[1] M. La Cognata,[1] L. Lamia,[1] S. Romano,[1] and A. Tumino[5]

[1]*INFN - Laboratori Nazionali del Sud, Dipartimento di Metodologie Chimiche e Fisiche per l'Ingegneria, Universita di Catania, Catania, Italy*

[2]*Physics Department, Texas A&M University-Commerce, Commerce, Texas*

[3]*Institute for Nuclear Research, Moscow State University, Moscow, Russia*

[4]*IGIK Institute of Engineering Sciences and Technology, Topi, District Swabi, N. W. F. P., Pakistan*

[5]*Universit´a KORE Enna, Enna, Italy*

Deuteron induced quasi-free scattering and reactions have been extensively investigated in the past few decades as well as ^{6}Li, ^{3}H, ^{3}He and ^{9}Be induced ones. This was done not only for nuclear structure and reaction mechanisms investigation but also for important astrophysical implications (Trojan Horse Method). In particular the width of the spectator momentum distribution in several nuclei which have been used as Trojan Horse ones have been obtained as a function of the transferred momentum. Trojan Horse method applications is also discussed because the momentum distribution of the spectator particle inside the Trojan horse nucleus is a necessary input for this method. This gives us hints on distortion effects at low energies as well as implications for nuclear astrophysics. It is the goal of the present work to estimate the distortion of the momentum distribution of the spectator based on the experimental data obtained in the previous publications. This is performed by comparing the momentum distribution extracted in the Plane Wave Impulse Approximation (PWIA) from experimental data with the theoretical calculation.

What is clear from our analysis is that as far as the energies of the ejectiles are large enough the momentum distribution of the spectator extracted from the experimental data using the PWIA agrees with the theoretical prediction calculated using the Fourier transform of the bound state wave function of the Trojan Horse nucleus. We find that the deviation of the theoretical momentum distributions from the experimental one is correlated with the transfer momentum from the projectile to the ejectiles. When the average transferred momentum is large compared to the bound state wave number the experimental FWHM reaches the theoretical one. The application of the THM should take into account the distortions caused by the interaction of the spectator with the fragments from the sub-reaction; they can be taken into account by adopting the ”distorted” FWHM extracted from the experimental data instead of the theoretical one. The paper has been submitted to Phys. Rev. C.

Gravitational interaction of nucleons with mini black holes

A. M. Mukhamedzhanov and L. Greenspan

We analyzed the interaction of the nonreltivistic nucleons with mini black holes (MBH). MBH are hypothetical objects having enormous mass density. The mass of the MBH (in g) can be estimated from equation

$$M = 6.74\times 10^{27} R\ g\,, \tag{1}$$

where its radius R is expressed in cm. For example, for $R = 10^{-13}$ we get $M = 6.74\times 10^{14}$ g. Such a gigantic mass curves the space around. In this work we consider the gravitational interaction of the MBHs with non-relativistic nucleons. Evidently that requires derivation of the equation for the wave function in a curved space. To do it we start from the Klein-Gordon equation, which is written in the covariant form in the general relativity:

$$\hbar^2 \frac{1}{\sqrt{-g}} \frac{\partial}{\partial x^\mu} \sqrt{-g}\, g^{\mu\nu} \frac{\partial}{\partial x^\nu} \Psi = -m^2 c^2 \Psi\,. \tag{2}$$

Here, $g^{\mu\nu}$ is the contravariant metric tensor, g its determinant, m is the nucleon mass, Ψ its wave function. The Schwarzschild metric tensor is the most common used, but its spatial part has singularity at $r = r_s$, where r_s is the Schwarzschild radius. To remove this singularitywe use Eddington-Filkenstein metric tensor.

$$g^{\mu\nu} = \begin{pmatrix} 1+\frac{r_s}{r} & -\frac{r_s}{r} & 0 & 0 \\ -\frac{r_s}{r} & -(1-\frac{r_s}{r}) & 0 & 0 \\ 0 & 0 & -\frac{1}{r^2} & 0 \\ 0 & 0 & 0 & \frac{1}{r^2 \sin^2\theta} \end{pmatrix} \tag{3}$$

Here, r_s is the Schwarzschild radius, writing down the Klein-Gordon equation in the Eddington-Filkenstein metrics and taking nonrelativistic limit we get the Schrödinger equation in the curved space.

$$\psi(t, \mathbf{r}, \theta, \varphi) = \mathrm{e}^{-i\frac{E}{\hbar}t}\, \psi(\mathbf{r}, \theta, \varphi) \tag{4}$$

After that using the standard transformation, we derive the stationary Schrödinger equation in a curved space created by the MBH

$$\left[-\frac{\hbar^2}{2m}\frac{\partial^2}{\partial r^2}+\widetilde{V}_1(r)+\widetilde{V}_2(r)+V^N(r)+\frac{l(l+1)}{2\mu r^2}\right]U_l(k,r)=E_pU_l(k,r), \quad (5)$$

where $\psi_l(k,r)=\dfrac{U_l(k,r)}{kr}$, k is the nucleon momentum,

$$V_N=-\frac{GMm}{r},$$

$$\widetilde{V}_1(r)=i(\hbar c)r_s\left[-\frac{1}{2r^2}+\frac{1}{r}\frac{\partial}{\partial r}\right], \quad (6)$$

$$\widetilde{V}_2(r)=\frac{1}{2}\frac{(\hbar c)^2}{mc^2}\frac{r_s}{r}\left[\frac{1}{r^2}-\frac{1}{r}\frac{\partial}{\partial r}+\frac{\partial^2}{\partial r^2}\right].$$

Due to the imaginary potential $\widetilde{V}_1(r)$, which is generated by a curved space, the absorption cross section of nucleons is non-zero and can be written as

$$\sigma=i\frac{4m}{\hbar^2k}(4\pi)^2\sum_{l=0}^{\infty}\frac{2l+1}{4\pi}\int_{r>r_s}^{\infty}dr\cdot r^2\frac{U_l(k,r)}{kr}\left(-i\hbar\left[\frac{cr_s}{r}\frac{\partial}{\partial r}+\frac{r_sc}{2r^2}\right]\frac{U_l(k,r)}{kr}\right). \quad (7)$$

Using Eq. (7) we calculated the mass gain by the MBH when it passes through sun.

Atomic overlap correction to the statistical rate function

I. S. Towner and J. C. Hardy

In nuclear β decay, the transition rate depends on the statistical rate function, *f*, an integral over phase space,

$$f = \int_1^{W_0} pW(W_0 - W)^2 F(Z,W) S(Z,W)\ dW, \tag{1}$$

where *W* is the total energy of the electron in electron-rest-mass units; W_0 is the maximum value of W; $p = (W^2 - 1)^{1/2}$ is the momentum of the electron; *Z* is the atomic number of the daughter nucleus; *F(Z,W)* is the Fermi function and *S(Z,W)* is the shape-correction function. What we address here is the inclusion of an additional factor in Eq. (1) to account for the mismatch in the initial and final *atomic* states in the β decay. Since the nucleus changes charge by one unit in beta decay, the final atomic state does not overlap perfectly with the initial atomic state, an effect that leads to a slight inhibition in the beta-decay rate. In the past, this effect has justifiably been considered too small to be of practical concern but, with the advent of Penning-trap mass measurements, the experimental uncertainties in transition *Q*-values have been reduced so much that they are now comparable to the effects of the imperfect atomic overlap.

We begin by writing

$$f = \int_1^{W_0} pW(W_0 - W)^2 F(Z,W) S(Z,W) r(Z,W)\ dW, \tag{2}$$

where *r(Z,W)* is the atomic overlap correction we are seeking. We then follow the method of Bahcall [1] by expressing *f* as a double integral with an energy-conserving delta function:

$$f = \int\int pWq^2 F(Z,W) S(Z,W) \sum_{A'} |\langle A'|G\rangle|^2 \delta(E_f - E_i)\ dW dq, \tag{3}$$

where *q* is the neutrino momentum. We have introduced into this equation an overlap of the initial and final atomic electron configurations: $|G\rangle$ is the state vector for the initial neutral atom with *(Z+1)* electrons, and $|A'\rangle$ is the state vector for the final *ionized* atom with *(Z+1)* electrons but only charge *Z* in the nucleus. There are many such possible final states, so a sum over A' is included.

The energy difference in the delta function is

$$E_f - E_i = q + W - W_0 + [B(G') - B(A')], \tag{4}$$

where *B(G')* is the total electron binding energy for the *neutral* atom of charge *Z* in the atomic ground-state configuration. For the energy-conserving delta function we now make a Taylor series expansion about the value $q + W - W_0$:

$$\delta(E_f - E_i) = \delta(q + W - W_0) + \delta'(q + W - W_0)[B(G') - B(A')] + \ldots \tag{5}$$

If the first term in this expansion is inserted into the double integral, Eq. (3), then the expression for f reduces to the original form Eq. (1) since the atomic overlap factor is unity under the assumption that the sum over electronic configurations A' can be completed by closure: *i.e* $\sum_{A'}\left|\langle A'|G\rangle\right|^2 = \sum_{A'}\langle G|A'\rangle\langle A'|G\rangle = \langle G|G\rangle = 1$. The second term in Eq. (5) involves a derivative of a delta function. This is handled by an integration by parts, in which the rest of the integrand is differentiated with respect to q. No boundary terms survive as the integrand vanishes at the boundaries. Thus the atomic overlap correction becomes

$$r(Z,W) = 1 - \frac{2}{W_0 - W}\sum_{A'}\left|\langle A'|G\rangle\right|^2 \left[B(G') - B(A')\right]$$

$$= 1 - \frac{1}{W_0 - W}\frac{\partial^2}{\partial Z^2}B(G). \qquad (6)$$

A derivation of this latter expression is given in our recent survey [2].

TABLE I. Comparison of statistical rate functions calculated without the atomic overlap correction, $f_{without}$, those calculated with it included, f_{with}. The change in the Q_{EC} value that would lead to the same change in f is given in the last column.

Parent	$f_{without}$	f_{with}	$df/f(\%)$	$dQ/Q(\%)$	$dQ(eV)$
^{10}C	2.30089	2.30039	0.02178	0.00436	83
^{14}O	42.7779	42.7724	0.01277	0.00255	72
^{22}Mg	418.423	418.386	0.00877	0.00175	72
^{26m}Al	478.279	478.237	0.00880	0.00176	75
^{34}Ar	3414.68	3414.46	0.00647	0.00129	78
^{34}Cl	1996.10	1995.96	0.00711	0.00142	78
^{38m}K	3298.10	3297.88	0.00663	0.00133	80
^{42}Sc	4472.52	4472.24	0.00643	0.00129	83
^{46}V	7211.63	7211.20	0.00598	0.00120	84
^{50}Mn	10746.6	10746.0	0.00565	0.00113	86
^{54}Co	15767.5	15766.6	0.00537	0.00107	89
^{62}Ga	26401.6	26400.2	0.00557	0.00111	102
^{74}Rb	47296.9	47294.5	0.00523	0.00105	109

It remains to estimate the second derivative of the electronic binding energy of neutral atoms in their ground-state configuration. For this we use binding-energy values from the tables of Carlson *et al*. [3], which were obtained from self-consistent Hartree-Fock calculations and have been demonstrated to

agree with experimental values to within 5%. We performed a fit to these tabulated values using a fitting function, aZ^b, in three ranges of Z values, with the following results:

$$\mathrm{B(G)} = \begin{cases} 13.080\, Z_i^{2.42}\ \mathrm{eV}, & 6 \le Z_i \le 10 \\ 14.945\, Z_i^{2.37}\ \mathrm{eV}, & 11 \le Z_i \le 30 \\ 11.435\, Z_i^{2.45}\ \mathrm{eV}, & 31 \le Z_i \le 39, \end{cases} \qquad (7)$$

where Z_i is the charge of the parent atom in the beta-decay process. It is conventional to use Z as the charge of the daughter nucleus in beta decay; thus for positron decay $Z_i = Z+1$. The second derivative is easily obtained from these expressions.

We have re-computed the statistical rate function f, and some sample results are listed in Table I. Those results obtained without the atomic overlap correction, Eq. (1), are given under the heading $f_{without}$, while those with the correction, Eqs. (2) and (6), are labelled f_{with}. The fractional difference between f_{with} and $f_{without}$ in percent is given in column 4 and is of order 0.01%, decreasing with increasing mass value. This is a very small correction. Furthermore, the statistical rate function depends on the Q-value to the fifth power, so the fractional change in Q that would lead to a change in f of the same size as that induced by the atomic overlap correction is even smaller: $1/5 \times df/f$. This percentage change is given in column 5 of Table I. As small as this effect is, it can be seen from the last column of the table that the equivalent change in Q-value ranges from 70 to 110 eV, an amount that is similar to the experimental uncertainties on the most precisely measured Q-values.

[1] J. N. Bahcall, Phys. Rev. **129**, 2683 (1963).
[2] J. C. Hardy and I. S. Towner, Phys, Rev. C **79**, 055502 (2009).
[3] T. A. Carlson, C. W. Nestor, N. Wasserman, and J. D. McDowell, At. Data **2**, 63 (1970).

New Hartree-Fock calculations for isospin-symmetry breaking correction in nuclear beta decay

I. S. Towner and J. C. Hardy

For accurate work, an isospin-symmetry breaking correction of between 0.5% and 1.5% is applied to *ft* values of nuclear beta decay. The correction is nucleus dependent and its evaluation dependent on nuclear-structure models. Conveniently the correction is divided into two components: $\delta_C = \delta_{C1} + \delta_{C2}$, where δ_{C1} arises from inserting charge-dependent terms into the Hamiltonian employed in a shell-model calculation, while δ_{C2} depends on radial-function differences between the initial-state proton and final-state neutron involved in the beta transition. These radial functions are taken to be eigenfunctions of either a Saxon-Woods (SW) or a mean-field Hartree-Fock (HF) potential with adjustments to ensure the radial functions have the appropriate asymptotic behaviour. It has been found in the past that the results for δ_{C2} obtained with SW were systematically larger than those of HF and this difference is included in the error analysis.

Until now, the HF calculations were all performed by Ormand and Brown [1-3]. This past year, we decided to examine the HF method and came upon an inconsistency, which when fixed considerably reduced the difference between the HF and SW δ_{C2} values. To be clear about the procedure, we illustrate it for the specific case of the decay of ^{34}Cl to ^{34}S. The decaying nucleus has $Z + 1 = 17$ protons; the daughter nucleus has $Z = 16$ protons. In the SW approach, the proton radial wave functions are taken to be eigenfunctions of a potential defined for a nucleus of mass A and charge Z+1 as follows:

$$V(r) = -V_0 f(r) - V_s g(r) \mathbf{l}.\boldsymbol{\sigma} + V_C(r), \qquad (1)$$

where V_0 and V_s are strengths of the central and spin-orbit terms, $f(r)$ is a Saxon-Woods radial function, $g(r)$ is its derivative, and $V_C(r)$ is a Coulomb term, whose asymptotic form is $V_C(r) \rightarrow Ze^2/r$ for large r. In our calculations [4] most of the parameters were fixed at standard values, with the well depth V_0 being adjusted case by case so that the binding energy of the eigenfunction being computed matched the separation energy to the corresponding parent state – in ^{33}S, for our example. Likewise the neutron radial functions were taken to be eigenfunctions of an similar potential but with the Coulomb term omitted.

The HF procedure is similar. For our illustrative example, a HF calculation is first mounted for ^{34}Cl, which would yield a mean field with central, spin-orbit and Coulomb terms. The required proton radial functions would then be taken as eigenfunctions of this mean field with the strength of the central term readjusted case by case so that the computed binding energy matched the appropriate separation energy. A second HF calculation is then mounted for ^{34}S, from which the neutron radial functions would be similarly determined in the mean field, but without the Coulomb term. However, under these circumstances, if the Coulomb terms in the HF mean-field potential were to be compared with those in the SW potential, a very significant difference would emerge. In the HF case, the Coulomb term is

$$V_C(\mathbf{r}) = \int d^3\mathbf{r}' \, \frac{e^2}{|\mathbf{r}-\mathbf{r}'|}\rho_p(\mathbf{r}') - \frac{3e^2}{2}\left[\frac{3}{\pi}\rho_p(\mathbf{r})\right]^{1/3}, \qquad (2)$$

which depends on the proton density (of ^{34}Cl in our example) that is generated as part of the HF procedure. The two terms in Eq. (2) are called the direct and exchange terms respectively. If we take the asymptotic limit of the direct term for large *r*, we obtain

$$V_C^{\rm dir}(\mathbf{r}) = \int d^3\mathbf{r}' \frac{e^2}{|\mathbf{r}-\mathbf{r}'|}\rho_p(\mathbf{r}') \stackrel{r\to\infty}{\longrightarrow} \frac{e^2}{r}\int d^3\mathbf{r}'\rho_p(\mathbf{r}') = \frac{(Z+1)e^2}{r}. \qquad (3)$$

Since the HF proton density is normalized to *(Z+1)* protons in ^{34}Cl, the asymptotic form of the Coulomb potential tends to $(Z+1)e^2/r$. However, this disagrees with the equivalent SW calculation, which has the form Ze^2/r.

This discrepancy is important and constitutes a flaw in the HF calculations of the radial-mismatch factors. Since a proton removed from a nucleus of charge *Z+1* leaves behind *Z* protons, its asymptotic interaction is with charge *Z* -- as described by the SW potential -- and not with charge *Z+1*. This deficiency in HF would be cured in principle by the Coulomb exchange term. However, in Skyrme-Hartree-Fock calculations it is not possible to compute the exchange term exactly without sacrificing the simplicities that come with use of zero-range Skyrme interactions. The exchange term appearing in Eq. (2) is a commonly used local approximation, which might well be appropriate for the nuclear interior and for the computation of bulk properties such as binding energies and radii, but it does not do the job asymptotically, which is the region of greatest importance to our calculations.

To circumvent this difficulty, we have chosen to alter the HF protocol. Instead of mounting two HF calculations -- for ^{34}Cl and ^{34}S -- as just described, we mount a *single* calculation for the nucleus with *(A-1)* nucleons and *Z* protons -- ^{33}S in our example. We then use the proton mean field from this calculation to generate the proton eigenfunctions and the neutron mean field from the same calculation to generate the neutron eigenfunctions. In this procedure, the Coulomb interaction automatically has the correct asymptotic form. Calculations of δ_{C2} with this new HF protocol yields results larger than those obtained with the conventional protocol by between 10% and 40% depending on the Skyrme interaction used and the nucleus under study. This change of protocol goes a long way in reducing the systematic error between SW and HF calculations.

The results from our HF calculations for δ_{C2} are listed in column 3 of Table I. For each transition, the central value is an average of the results obtained with the three choices of Skyrme interactions. To assign an uncertainty, we have examined the spread in results obtained with the different Skyrme interactions and with different shell-model effective interactions and model spaces. Observe that these new results of ours are systematically larger than those computed by Ormand and Brown (given in column 2) and are much closer to the SW values (column 4).

TABLE I. Isospin-symmetry-breaking corrections, δ_{C2} in percent units, and their assigned uncertainties obtained from HF calculations. Also listed are earlier results obtained with HF (column 2) and SW (column 4) eigenfunctions.

	Hartree-Fock		Saxon-Woods
Nucleus	OB95[a]	This work	TH08[b]
^{10}C	0.11	0.215(35)	0.165(15)
^{14}O	0.14	0.255(30)	0.275(15)
^{22}Mg	0.19	0.250(55)	0.370(20)
^{26}Al	0.29	0.410(50)	0.280(15)
^{34}Ar	0.37	0.510(60)	0.635(55)
^{34}Cl	0.51	0.595(55)	0.550(45)
^{38}K	0.48	0.640(60)	0.550(55)
^{42}Sc	0.31	0.620(55)	0.645(55)
^{46}V	0.29	0.525(55)	0.545(55)
^{50}Mn	0.33	0.575(55)	0.610(50)
^{54}Co	0.40	0.635(55)	0.720(60)
^{62}Ga	0.89	0.93(16)	1.20(20)
^{74}Rb	0.83	1.29(16)	1.50(30)

[a]Ref. [3]
[b]Ref. [4]

[1] W. E. Ormand and B. A. Brown, Nucl. Phys. **A440**, 274 (1985).

[2] W. E. Ormand and B. A. Brown, Phys. Rev. Lett. **62**, 866 (1989).

[3] W. E. Ormand and B. A. Brown, Phys. Rev. C **52**, 2455 (1995).

[4] I. S. Towner and J. C. Hardy, Phys. Rev. C **77**, 025501 (2008).

Nuclear modification factor of non-photonic electrons in heavy-ion collisions and the heavy-flavor baryon to meson ratio

Y. Oh and C. M. Ko

The nuclear modification factor R_{AA} of non-photonic electrons in Au+Au collisions at $s_{NN}^{1/2}$ = 200 GeV has been studied by considering the decays of heavy-flavor hadrons produced in a quark coalescence model [1]. Although an enhanced Λ_c/D_0 ratio is predicted by the coalescence model, it is peaked at small transverse momenta (~ 2 GeV) due to the large difference between heavy and light quark masses. As a result, the enhanced Λ_c/D_0 ratio, which is expected to suppress the electron R_{AA} as the branching ratio of Λ_c decay into electrons is smaller than that of D_0, does not lead to additional suppression of the electron R_{AA} at large transverse momenta (> 5 GeV), where the suppression is mainly due to heavy quark energy loss in produced quark-gluon plasma. Also, the enhanced Λ_b/B_0 ratio predicted by the coalescence model has even smaller effect on the non-photonic electron R_{AA} as bottom baryons and mesons have similar branching ratios for semi-leptonic decays into electrons.

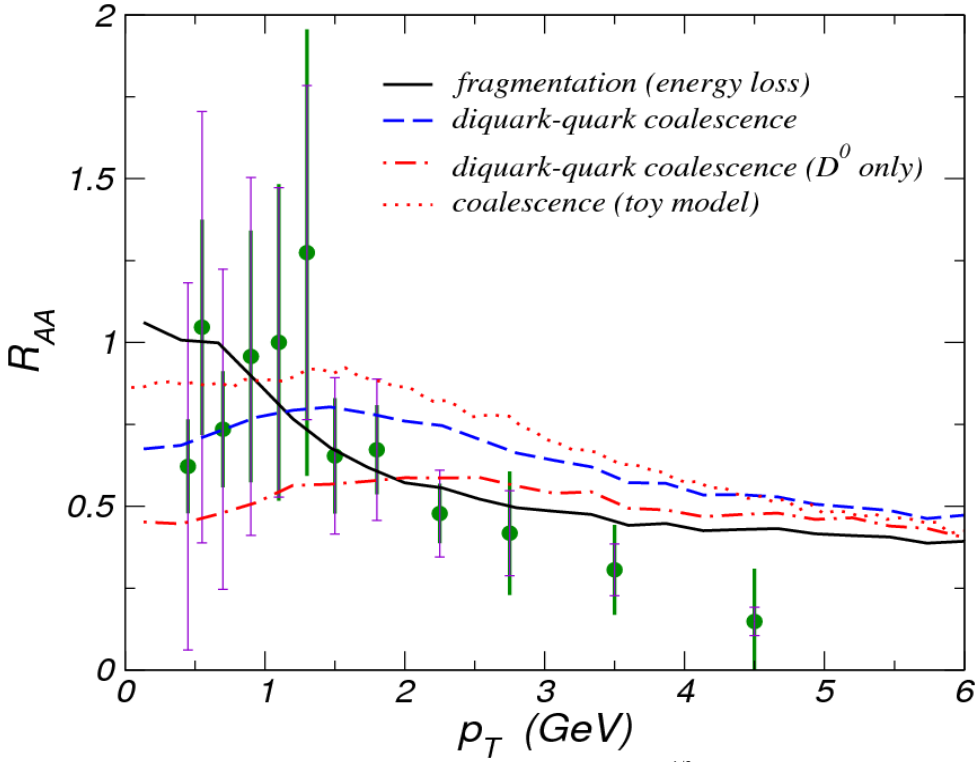

FIG. 1. The electron R_{AA} in central Au+Au collisions at $s_{NN}^{1/2}$ = 200 GeV from charmed hadrons. The solid line includes only fragmentation of charm quarks. The dashed and dot-dashed lines are the results of the three-quark and the diquark-quark coalescence model, respectively, while the dotted line is obtained with D_0 meson only in the diquark-quark coalescence model. The experimental data are from Ref.[2].

[1] Y. Oh and C. M. Ko, arXiv: 0903.4166; Phys. Rev. C (submitted).

[2] A. Adare *et al.*(PHENIX Collaboration), Phys. Rev. Lett. **98**, 162301 (2007).

Deuteron spectrum and elliptic flow in relativistic heavy ion collisions

Y. Oh, C. M. Ko, and Z. W. Lin[1]

[1]*Physics Department, East Carolina University, Greenville, North Carolina 27858*

We have extended the hadronic transport model ART [1] to include the production and annihilation of deuterons via the reaction NN→dπ and its inverse reaction as well as the elastic scattering of deuterons with both mesons and baryons in the hadronic matter. The cross sections for these reactions are taken to be those available empirically. Using initial hadron distributions from a blast wave model with temperature T=170 MeV, same as the phase transition temperature between the quark-gluon plasma and hadronic matter, and a flow velocity parameterized in such a way that the final transverse momentum spectrum and elliptic flow of protons in midrapidity from minimum biased Au+Au collisions at $s_{NN}^{1/2}$ = 200 GeV reproduce those measured in experiments at RHIC by the PHENIX [2] and STAR [3] Collaborations, we have studied the effects of hadronic rescattering on the transverse momentum spectrum and elliptic flow of deuterons produced in these collisions. As shown in Fig.1, the resulting transverse momentum spectrum of deuterons agrees reasonably with the experimentally measured one. The elliptic flow of deuterons are also consistent with the experimental data for most transverse momenta

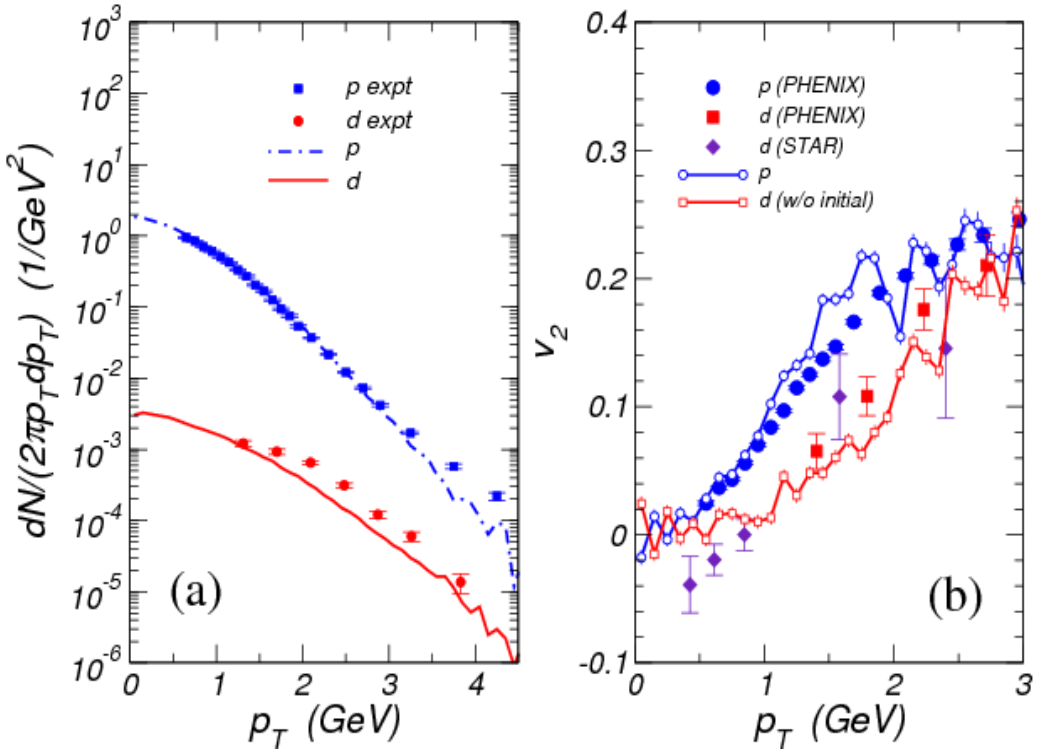

FIG. 1. Transverse momentum spectra (a) and elliptic flow (b) of protons and deuterons in minimum biased Au+Au collisions at $s_{NN}^{1/2}$ = 200 GeV.

except below 1 GeV/c, where the elliptic flow of deuterons is negative in the data but remains positive in our model study. Study is being continued to understand the mechanism for the appearance of negative deuteron elliptic flow at low transverse momentum. Also, the relation between the results from the hadronic transport model and those from the coalescence model [4] is being investigated.

[1] B. A. Li and C. M. Ko, Phys. Rev. C **52**, 2037 (1995).
[2] S. Afanasiev *et al.* (PHENIX Collaboration), Phys. Rev. Lett. **98**, 162301 (2007).
[3] H. Liu (STAR Collaboration), J. Phys. G **34**, S1087 (2007).
[4] Y. Oh and C. M. Ko, Phys. Rev. C **76**, 054910 (2007).

Ratios of heavy baryons to heavy mesons in relativistic nucleus-nucleus collisions

Y. Oh, C. M. Ko, S. H. Lee,[1] and S. Yasui[2]

[1]*Institute of Physics and Applied Physics, Yonsei University, Seoul 120-749, Korea*

[2]*High Energy Accelerator Research Organization (KEK), Tsukuba, Ibaraki, 302-0801, Japan*

We have studied heavy baryon/meson ratios Λ_c/D_0 and Λ_b/B_0 in relativistic heavy ion collisions in the quark coalescence model [1]. For heavy baryons, we include production from coalescence of heavy quarks with free light quarks as well as with bounded light diquarks [2] that might exist in the strongly coupled quark-gluon plasma produced in these collisions. As shown in Fig. 1 and Fig. 2, the resulting Λ_c/D_0 and Λ_b/B_0 ratios, including the contribution from decays of heavy hadron resonances and also that due to fragmentation of heavy quarks that are left in the system after coalescence, in central Au+Au collisions at $s_{NN}^{1/2}$= 200 GeV are about a factor of five and ten, respectively, larger than those given by the thermal model, and about a factor of ten and twelve, respectively, larger than corresponding ratios in the PYTHIA model for pp collisions. These ratios are reduced by a factor of about 1.6 if there are no diquarks in the quark-gluon plasma. The momentum dependence of the heavy baryon/meson ratios is found to be sensitive to the heavy quark mass, with the Λ_b/B_0 ratio being much flatter than the Λ_c/D_0 ratio, which peaks at the transverse momentum $p_T \sim 0.8$ GeV but the peak shifts to $p_T \sim 2$ GeV in the absence of diquarks.

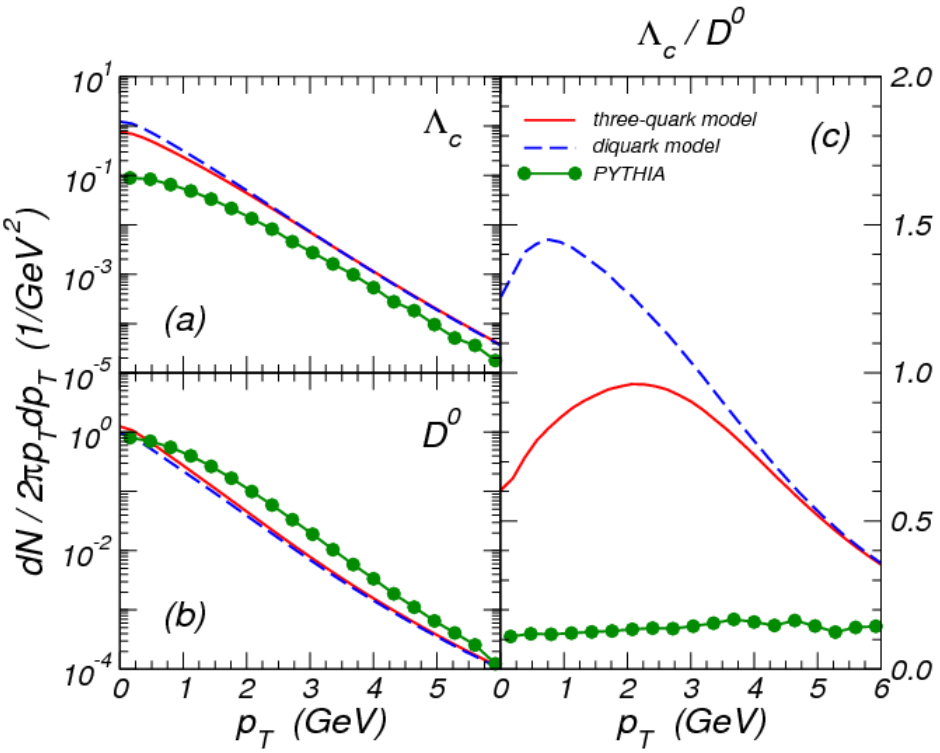

FIG. 1. Spectra of (a) Λ_c and (b) D_0 as well as (c) the ratio Λ_c/D_0. Solid lines are for the three-quark model and dashed lines are for the diquark model. Results from the PYTHIA model are shown by filled circles.

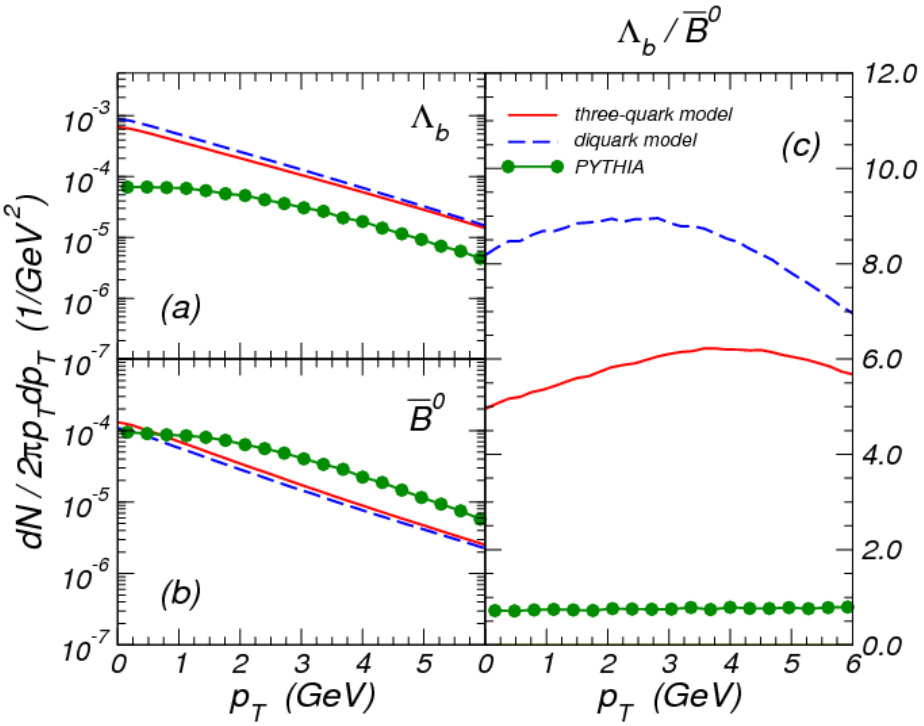

FIG. 2. Same as Fig.1 for (a) Λ_b and (b) B_0 spectra, and (c) the Λ_b/B_0 ratio.

[1] Y. Oh, C. M. Ko, S. H. Lee, and S. Yasui, Phys. Rev. C **79**, 044905 (2009).

[2] S. H. Lee, K. Ohnishi, S. Yasui, I. K. Yoo, and C. M. Ko, Phys. Rev. Lett. **100**, 222301 (2008).

High-order effects on the incompressibility of isospin asymmetric nuclear matter

L. W. Chen,[1] B. J. Cai,[1] C. M. Ko, B. A. Li,[2] C. Shen,[1] and J. Xu
[1]*Department of Physics, Shanghai Jiao Tong University, Shanghai 200240, China*
[2]*Department of Physics, Texas A&M University-Commerce, Commerce, Texas 75429*

We have derived the analytical expressions for the saturation density as well as the binding energy and incompressibility at the saturation density of asymmetric nuclear matter exactly up to 4th-order in the isospin asymmetry $\delta=(\rho_n-\rho_p)/(\rho_n+\rho_p)$ using 11 characteristic parameters defined at the normal nuclear density ρ_0 by the density derivatives of the binding energy per nucleon of symmetric nuclear matter, the symmetry energy $E_{sym}(\rho)$ and the 4th-order symmetry energy $E_{sym,4}(\rho)$ [1]. Using an isospin- and momentum-dependent modified Gogny (MDI) interaction and the Skyrme-Hartree-Fock (SHF) approach with 63 popular Skyrme interactions, we have systematically studied the isospin dependence of the saturation properties of asymmetric nuclear matter, particularly the incompressibility $K_{sat}(\delta)=K_0+K_{sat,2}\delta^2+K_{sat,4}\delta^4+O(\delta^6)$ at the saturation density. Our results show that the magnitude of the high-order $K_{sat,4}$ parameter is generally small compared to that of the $K_{sat,2}$ parameter. The latter essentially characterizes the isospin dependence of the incompressibility of asymmetry nuclear matter at the saturation density and can be expressed as $K_{sat,2}=K_{sym}-6L-(J_0/K_0)L$, where L and K_{sym} represent, respectively, the slope and curvature parameters of the symmetry energy at ρ_0 while J_0 is the third-order derivative parameter of symmetric nuclear matter at ρ_0. Furthermore, we have constructed a phenomenological modified Skyrme-like (MSL) model which can reasonably describe the general properties of symmetric nuclear matter and the symmetry energy predicted by both the MDI model and the SHF approach. The results indicate that the high-order J_0 contribution to $K_{sat,2}$ generally cannot be neglected. In addition, it is found that there exists a nicely linear correlation between K_{sym} and L as well as between J_0/K_0 and K_0. These correlations together with the empirical constraints on K_0, L, $E_{sym}(\rho_0)$ and the nucleon effective mass lead to an estimated value of $K_{sat,2} = -370 \pm 120$ MeV.

[1] L. W. Chen, B. J. Cai, C. M. Ko, B. A. Li, C. Shen, and J. Xu, arXiv:0905.4323; Phys. Rev. C (submitted).

Isospin physics with heavy-ion reactions

B. A. Li,[1] L. W. Chen, [2] and C. M. Ko
[1]*Department of Physics, Texas A&M University-Commerce, Commerce, Texas 75429-3011*
[2]*Department of Physics, Shanghai Jiao Tong University, Shanghai 200240, China*

The ultimate goal of studying isospin physics via heavy-ion reactions with neutron-rich, stable and/or radioactive nuclei is to explore the isospin dependence of in-medium nuclear effective interactions and the equation of state of neutron-rich nuclear matter, particularly the isospin-dependent term in the equation of state, i.e., the density dependence of the nuclear symmetry energy. Because of its great importance for understanding many phenomena in both nuclear physics and astrophysics, the study of the density dependence of the nuclear symmetry energy has been the main focus of the intermediate-energy heavy-ion physics community during the last decade, and significant progress has been achieved both experimentally and theoretically. In particular, a number of phenomena or observables have been identified as sensitive probes to the density dependence of the nuclear symmetry energy. Experimental studies have confirmed some of these interesting isospin-dependent effects and allowed us to constrain relatively stringently the symmetry energy at sub-saturation densities [1]. The impacts of this constrained density dependence of the symmetry energy on the properties of neutron stars have also been studied, and they were found to be very useful for the astrophysical community. With new opportunities provided by the various radioactive beam facilities being constructed around the world, the study of isospin physics is expected to remain one of the forefront research areas in nuclear physics. We have published an comprehensive review on the major progress achieved during the last decade in isospin physics with heavy ion reactions and discuss future challenges to the most important issues in this field [2].

[1] L. W. Chen, C. M. Ko, B. A. Li, and G. C. Yong, Int. J. Mod. Phys. **17**, 1825 (2008).
[2] B. A. Li, L. W. Chen, and C. M. Ko, Phys. Rep. **464**, 113 (2008).

Isospin-dependent pion in-medium effects on charged pion ratio in heavy ion collisions

J. Xu, C. M. Ko, and Y. Oh

The spectral functions of pions in asymmetric nuclear matter become dependent on their charges. Using those determined from the couplings of pions to the delta-resonance nucleon-hole excitations in nuclear matter, we have studied in a thermal model their effects on the ratio of negatively charged to positively charged pions [1]. In the neutron-rich matter formed in heavy ion collisions, this ratio is enhanced by the isospin-dependent pion in-medium effects, and the effect is comparable to that due to the uncertainties in the theoretically predicted stiffness of the nuclear symmetry energy at high densities. As shown in Fig.1, the measured π^-/π^+ ratio of about 3 with a large error bar by the FOPI Collaboration [2], shown by the dash-dotted line, which without the pion in-medium effects favors a nuclear symmetry energy softer than the one given by x=1, is now best described by the latter. Therefore, it is of great interest to include the pion in-medium effects in the transport model [3], which takes into account possible non-thermal effects, to extract more reliably the nuclear symmetry energy at high density from the measured π^-/π^+ ratio in high energy heavy ion collisions.

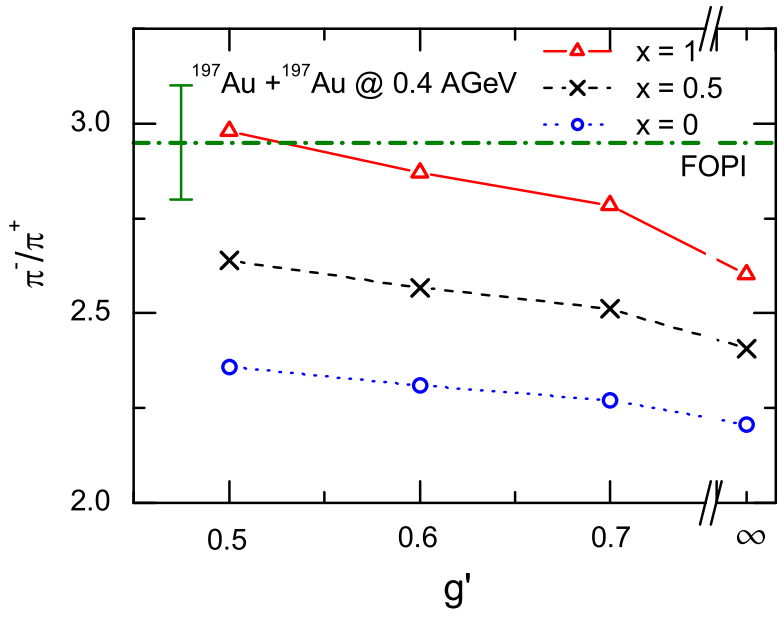

FIG. 1. The π^-/π^+ ratio in Au+Au collisions at the beam energy of 0.4 AGeV for different values of nuclear symmetry energy (x=0, 0.5, and 1) and the Migdal parameter g=0.5, 0.6, and 0.7. Results for g = ∞ correspond to the case without the pion in-medium effects.

[1] J. Xu, C. M. Ko, and Y. Oh, arXiv:0906.1602, Phys. Rev. Lett. (submitted).
[2] W. Reisdorf *et al.*(FOPI Collaboration), Nucl. Phys. **A781**, 459 (2007).
[3] Z. G. Xiao, B. A. Li, L. W. Chen, G. C. Yang, and M. Zhang, Phys. Rev. Lett. **102**, 062502 (2009).

Resonance recombination of quarks in the quark-gluon plasma

L. Ravagli, H. van Hees, and R. Rapp

A theoretical description of the hadronization process, converting quarks and gluons, as produced in hadronic or electromagnetic interactions, into colorless hadrons, remains a formidable challenge to date. For partons with large transverse momentum, p_t, the factorization theorem of QCD allows to factorize the hadronization process into universal fragmentation functions which, in principle, can be determined empirically. At low momenta the factorization breaks down and other hadronization schemes are expected to become relevant. The quark-coalescence model (QCM) assumes that constituent quarks, produced in a reaction, can recombine to form hadrons. In elementary hadron-hadron collisions (pN, πN), this approach has been successfully applied to describe flavor asymmetries in kaon and charmed-hadron spectra as a consequence of recombining valence and/or sea quarks in both target and projectile.

In heavy-ion collisions at the Relativistic Heavy-Ion Collider (RHIC) hadronization via quark coalescence from a thermalized Quark-Gluon Plasma (QGP) provides an intuitive and economic explanation for the observed enhancement in the baryon-to-meson ratio and for the constituent-quark number scaling (CQNS) of the elliptic flow of different hadron species, $v_2(p_T)=n_q v_{2,q}(p_T/n_q)$; here, p_T denotes the hadron's transverse momentum, v_2 its elliptic flow, and n_q the number of constituent quarks in the hadron. The universal function $v_{2,q}$ is interpreted as the underlying quark elliptic flow at the time of hadronization.

The commonly applied rather simple version of quark coalescence models is empirically very successful, but subject to limitations. E.g., the collinearity of quark transverse momenta imposed on the coalescence process implies the violation of energy conservation, restricting the QCM's applicability to sufficiently large momenta, 2 GeV<p_T<6 GeV (the upper bound is set by the onset of fragmentation dominance). Furthermore, it is not obvious how the resulting hadron multiplicities relate to the thermodynamic limit. To remedy these problems, two of us [1] have suggested a reinterpretation of quark coalescence as the formation of hadron-like resonances in the QGP close to the phase transition, using a kinetic-theory approach based on the Boltzmann equation (the so-called resonance recombination model = RRM). By construction, the corresponding hadron formation process satisfies both energy-momentum conservation and the correct thermodynamic limit. In the stationary limit (characterized by the equality of gain and loss terms), the Boltzmann equation can be used to extract the equilibrium form of the meson distribution function as

$$f_M^{\rm eq}(\vec{p}) = \frac{\gamma_p}{\Gamma} g(\vec{p}) \ ,$$

where γ_p is a Lorentz time-dilation factor and Γ the resonance width (reaction rate) corresponding to the formation reaction $q+qbar \leftrightarrow M$ (M: meson). The gain term, g, is given by the phase-space distributions

$$g(\vec{p}) = \int \mathrm{d}^3x \beta(\vec{x},\vec{p}) = \int \frac{\mathrm{d}^3p_1 \mathrm{d}^3p_2}{(2\pi)^6} \int \mathrm{d}^3x \ f_q(\vec{x},\vec{p}_1) \ f_{\bar{q}}(\vec{x},\vec{p}_2) \ \sigma(s) \ v_{\rm rel}(\vec{p}_1,\vec{p}_2) \ \delta^{(3)}(\vec{p}-\vec{p}_1-\vec{p}_2)$$

of quarks and anti-quarks, where σ denotes the resonance-formation cross section and v_{rel} the relative velocity of the recombining quark-anti-quark pair. In simplistic QCMs a successful description of CQNS resides on a factorization of the space and momentum dependencies in the quark and anti-quark phase-space distributions. However, space-momentum correlations are at the heart of anisotropic (elliptic) flow as a collective phenomenon in the fireball expansion of heavy-ion collisions (as, e.g., encoded in hydrodynamic simulations). It has turned out to be difficult to reconcile space-momentum correlations with CQNS within QCMs.

In the present work [2] we utilize the RRM by implementing quark phase-space distributions generated from relativistic Langevin simulations of heavy-quark diffusion in the QGP. The Langevin approach is based on in-medium resonance interactions of quarks and anti-quarks [3] in an elliptically expanding QGP fireball, as applied earlier in calculations of p_T spectra and elliptic flow for "non-photonic" single-electron spectra arising from the decay of charm and bottom mesons at RHIC [4]. We furthermore extend our calculations to strange quarks. At the quark level, the resonance interaction strength in the QGP is adjusted to obtain a maximal elliptic flow leveling off at about 7-8%, consistent with experiment [5]; when plotted as a function of kinetic quark energy, KE_t, the resulting charm- and strange-quark distributions exhibit approximate scaling behavior, see left panel of Fig. 1. Upon applying the RRM to form ϕ and J/Ψ mesons, we find the following [2]: (i) CQNS is recovered for each meson separately, $v_2(p_T)=n_q v_{2,q}(p_T/n_q)$ from p_T=0 to at least 5 GeV; (ii) the meson-v_2 is found to be "universal" (for ϕ and J/Ψ mesons) but only as a function of transverse kinetic energy, KE_T (not p_T), of the meson (cf. Fig. 1 right), in line with the experimental observations [5]. These are rather nontrivial results in view of: (a) the energy-conserving coalescence formalism (essential for applications at low p_T) ,and (b) the implementation of space-momentum correlations (essential for a realistic description of elliptic flow).

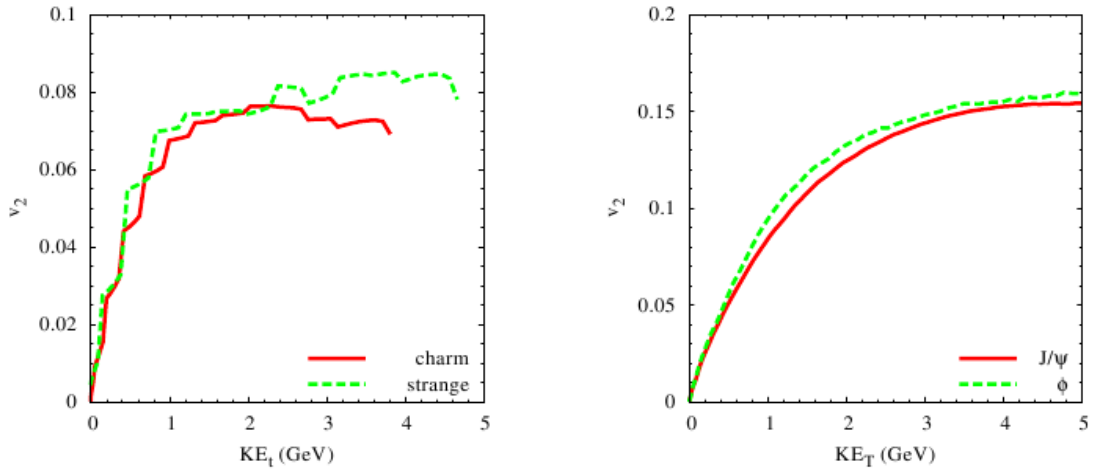

FIG. 1. Charm- and strange-quark elliptic flow, v_2, generated by Langevin simulations employing resonance interactions with light quarks and anti-quarks in the QGP (left panel) and the resulting v_2 of J/ψ and ϕ mesons after application of the resonance-recombination model for hadronization.

[1] L. Ravagli, R. Rapp, Phys. Lett. B **655**, 126 (2007).

[2] L. Ravagli, H. van Hees, and R. Rapp, Phys. Rev. C **79**, 064902 (2009).
[3] H. van Hees, V. Greco, and R. Rapp, Phys. Rev. C **73**, 034913 (2006).
[4] H. van Hees, R. Rapp, Phys. Rev. C **71**, 034907 (2005).
[5] A. Adare *et al.* (PHENIX Collaboration), Phys. Rev. Lett. **98**, 162301 (2007) ; B.I. Abelev *et al.* (STAR Collaboration), Phys. Rev. C **75**, 054906 (2007).

Medium effects in rho-meson photo-production

F. Riek, R. Rapp, T. S. H. Lee, and Y. Oh

Medium modifications of hadron properties in hot and/or dense matter are of fundamental interest in connection with the chiral and deconfinement phase transition(s) in QCD. E.g., dilepton spectra measured in high-energy heavy-ion collisions are consistent with a strong broadening of the ρ-meson spectral function in hot and dense hadronic matter [1]. The prevalent medium effects on the ρ are attributed to the baryonic component of the medium, but the rapid expansion of the fireball formed in heavy-ion reactions implies a rather large range of temperatures and densities contributing to the total dilepton spectrum. It is therefore desirable to test medium effects in a static environment, such as provided by ground-state nuclei. Dileptons are of special interest due to their negligible final-state interactions. In the present work [2] we evaluate dilepton spectra resulting from photon-induced ρ-production off nuclei. Toward this goal we combine a previously constructed model for the elementary photo-production process on the nucleon [3] with an in-medium ρ spectral function [4] which has been successfully applied to dilepton spectra in heavy-ion collisions.

The ρ-meson spectral function of Ref. [4] has been calculated within hadronic many-body theory. It includes medium modifications of the pion cloud and direct couplings of the ρ-meson to resonances on pions, nucleons, etc. Constraints on the interaction vertices from hadronic and radiative decays (as well as from total photo-absorption cross sections) lead to rather soft hadronic formfactors which, in turn, induce a considerable 3-momentum dependence of the spectral function: The medium effects are significantly larger at low momentum than at high momentum.

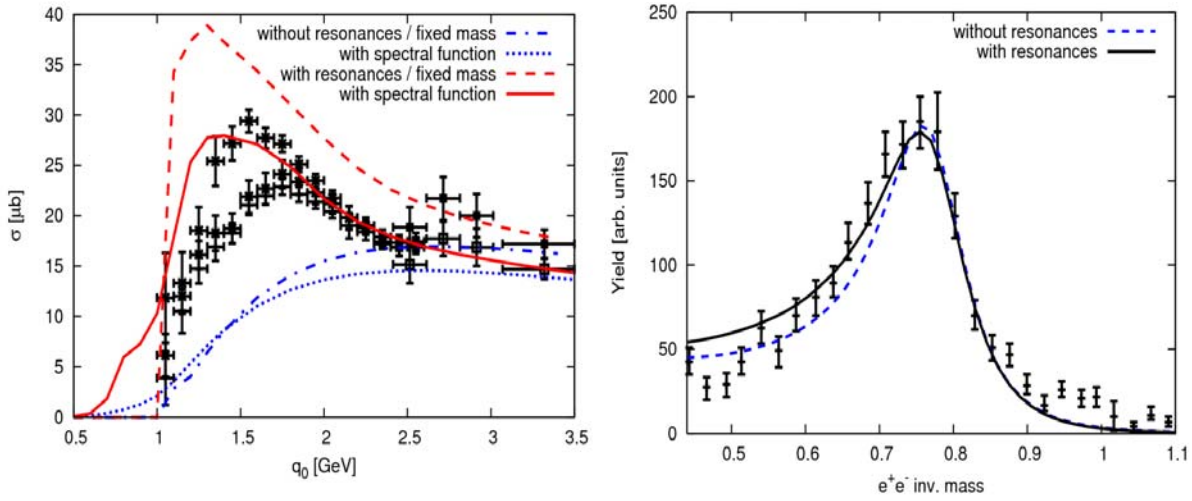

FIG. 1. Left panel: Total cross section for γ p →p ρ^0 as a function of incident photon energy in the laboratory frame. The calculations are based on either a fixed ρ-mass of 770 MeV (dash-dotted and dashed line) or a full vacuum spectral function (dotted and solid line). Right panel: Dilepton invariant-mass spectrum for ρ photo-production off deuterium compared to CLAS data after subtraction of ω- and ϕ-decay contributions [5].

The ρ photo-production model by Oh and Lee [3] is based on *t*-channel meson-exchange as well as *s*- and *u*-channel nucleon-exchange; it provides a good description of experimental data for photon energies above ~2 GeV. Here, we additionally include baryon-resonance contributions precisely corresponding to the resonance-hole excitations in the ρ spectral function, with identical formfactors but relativistic vertex functions (requiring a slight adjustment in the coupling constants to recover the same decay branching ratios). This establishes consistency between the elementary production amplitude and the in-medium spectral function. Without further readjustments, experimental data for total ρ photo-production cross sections on the nucleon and dilepton invariant-mass spectra on the deuteron are rather well reproduced, cf. Fig. 1. The baryon resonance contributions provide the required low-energy strength which is not accounted for by *t*-channel exchange processes.

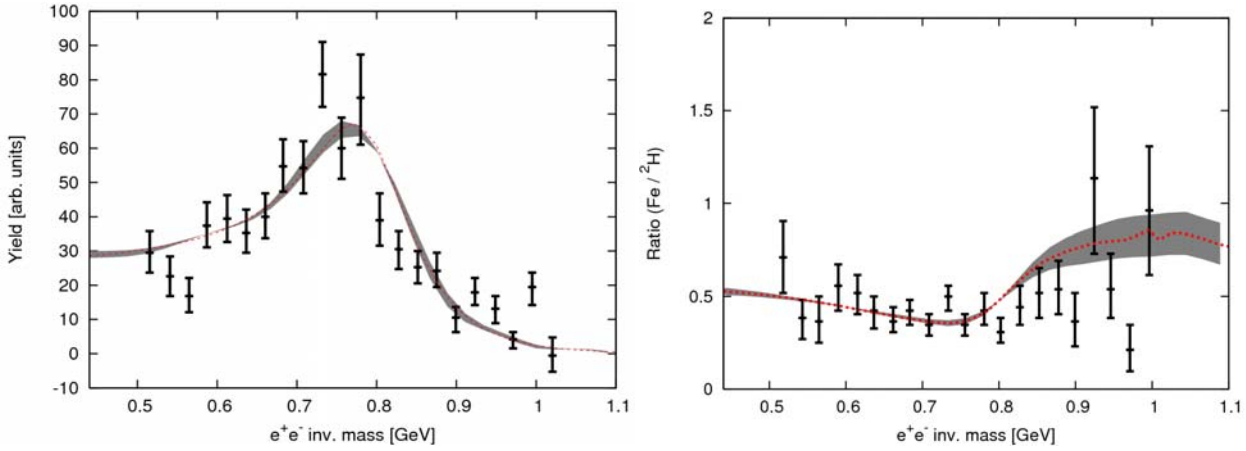

FIG. 2. Left panel: Calculated dilepton invariant-mass spectra resulting from ρ photo-production off iron for a nuclear density range $\rho_N=(0.4\text{-}0.6)\rho_0$, normalized and compared to CLAS data (where ω and ϕ decays have been subtracted) [5]. Right panel: iron-to-deuteron ratio of the dilepton spectra.

Turning to nuclear photo-production, it is important to note that the ρ is produced with appreciable 3-momentum relative to the nucleus, enhancing the probability for its decay outside the nucleus. It is thus mandatory to properly evaluate the effective densities probed. For incoming photon energies of ~1.5-2.5 GeV we estimate [2] the average density at the decay point to be $(0.5\pm0.1)\rho_0$ for an iron target.

Our results for dilepton invariant-mass spectra are compared to the corresponding ``excess" spectra measured by the CLAS collaboration at Jefferson Lab [5] in Fig. 2. In the absence of an absolute normalization of the data, the calculations are normalized to the same integrated strength as the data. We find fair agreement for both iron and carbon targets (the latter are not shown), with a χ^2 per data point of $\chi^2/N=1.35$ (or 1.29 with a normalization which minimizes χ^2). The extracted ``average" in-medium width of the ρ-meson amounts to ~200 MeV, moderately enhanced over its vacuum value. This is to be compared to ~(350-400) MeV as recently extracted [1] from NA60 data in In(158AGeV)-In collisions at the CERN-SPS [6], employing the same underlying model for the in-medium ρ spectral function [4]. Thus, the rather pronounced 3-momentum dependence of the latter turns out to be an important ingredient in the consistent understanding of dilepton spectra in photo-nuclear and heavy-ion reactions.

[1] R. Rapp, J. Wambach, and H. van Hees, LANL arXiv:0901.3289[hep-ph], Landolt-Börnstein (to be published).
[2] F. Riek, R. Rapp, T. S. H. Lee, and Y. Oh, Phys. Lett. B **677**, 116 (2009).
[3] Y. Oh and T. S. H. Lee, Phys. Rev. C **69**, 025201 (2004).
[4] R. Rapp and J. Wambach, Eur. Phys. J. A **6**, 415 (1999).
[5] R. Nasseripour *et al.*, Phys. Rev. Lett. **99**, 262302 (2007); M.H. Wood *et al.*, Phys. Rev. C **78**, 015201 (2008).
[6] R. Arnaldi *et al.*, Phys. Rev. Lett. **96**, 162302 (2006).

SECTION IV

ATOMIC, MOLECULAR AND MATERIALS SCIENCE

Energy systematics of vanadium Kα x-ray satellites and hypersatellites

R. L. Watson, V. Horvat, and Y. Peng

Vanadium K x-ray spectra excited by 15 MeV/u Ne, Ar, Kr, Ag, and Ho ion collisions were described in last year's progress report [1]. Further analysis has been performed to investigate the dependence of the Kα satellite and hypersatellite energies on projectile atomic number and to compare them with the results of Dirac-Fock calculations.

Comparison of the vanadium x-ray energies measured with each target (V metal, VO, V_2O_4, and V_2O_5), excited by the same projectile indicated that chemical shifts must be quite small, as evidenced by the root-mean-square deviations obtained for each peak. However, the energy of a given peak steadily increases with the projectile atomic number. In the past, this latter effect has been attributed to outer-shell ionization.

The average energy shifts of the Kα satellite peaks relative to the average $K\alpha_{12}$ diagram energy (4949.7 eV) are compared for each projectile in Fig. 1. Here, it is shown that the energy shifts observed with the different projectiles range between the energy shifts predicted by average-of-configuration Dirac-Fock calculations using the Desclaux program [2] for the outer shell electrons all present (dashed

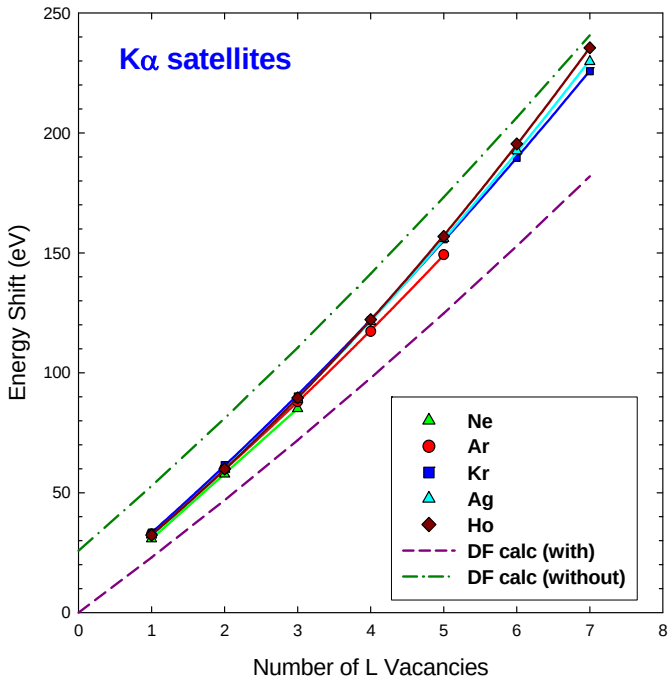

FIG. 1. The Kα satellite average energy shifts measured relative to the average $K\alpha_{1,2}$ diagram peak energy. The dashed (purple) and dot-dashed (green) curves show the average Dirac-Fock energy shifts calculated for a vanadium atom with all outer-shell electrons present and absent, respectively

purple curve) and all absent (dot-dashed green curve). The same kind of graph is shown for the average energy shifts of the Kα hypersatellite peaks relative to the average $K\alpha_{12}$ energy in Fig. 2. In the present work, the average Dirac-Fock energy shifts were obtained by averaging the calculated $K\alpha_1$ and $K\alpha_2$ transition energies;

$$\overline{E}(K\alpha_{1,2}) = \frac{E(K\alpha_1) + RE(K\alpha_2)}{1 + R} \quad , \tag{1}$$

where R is the $K\alpha_2/K\alpha_1$ intensity ratio. In the case of the satellites, the value of R is expected to be close to the statistical value of 0.5 because a large number of transitions is possible for electron configurations containing a single K plus additional L vacancies. The same holds true for the hypersatellites with n > 0. However, the K^2L^0 initial state configuration is a special case since, in the limit of LS-coupling, only transitions to the $^1P_1$ final state are allowed. Hence, the $K\alpha_2$ transition is expected to be heavily favored. In the present analysis, the average energy for the K^2L^0 hypersatellite was computed using a theoretical R value of 10.1, from the calculations of Costa et al. [3].

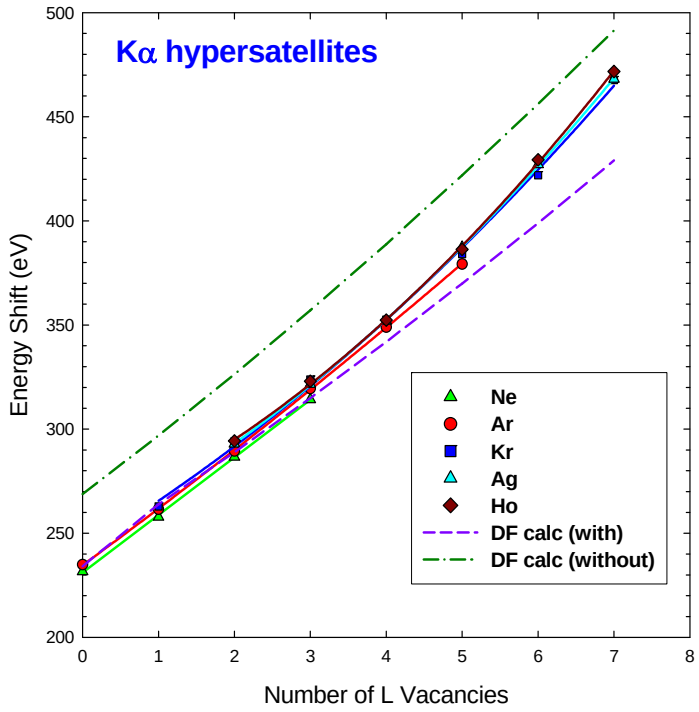

FIG. 2. The Kα hypersatellite average energy shifts measured relative to the average $K\alpha_{1,2}$ diagram peak energy. The dashed (purple) and dot-dashed (green) curves show the average Dirac-Fock energy shifts calculated for a vanadium atom with all outer-shell electrons present and absent, respectively.

It is reasonable to expect that the degree of outer-shell ionization should be related to the degree of inner-shell ionization, in which case the Kα satellite and hypersatellite energy shifts should correlate with p_L^x (the average fraction of L vacanies at the time of K x-ray emission). This was verified in Ref [4] for a variety of targets and projectiles. Plots of the satellite and hypersatellite energy shifts as a function of p_L^x using the current vanadium data are shown in Figs. 3 and 4, respectively. In the present work, the straight line least-squares fits displayed in these figures were extrapolated to predict the limiting energy shifts as p_L^x approaches zero. These energy shifts (ΔE_0) are presumed to be the energy shifts that would be observed if all outer-shell electrons were present. The calculated energy shifts for vanadium atoms with all outer-shell electrons present are shown by the diamond shaped points in Figs. 3 and 4. As may be seen from Fig. 3, the calculated energy shifts for the Kα satellites are systematically smaller (by 12 to 34%) than the experimental energy shifts. On the other hand, (as may be seen in Fig. 8) the agreement between the calculated (average-of-configuration Dirac-Fock) and experimental energy shifts is much better for the hypersatellites, with differences ranging from 2.8% to −1.0%.

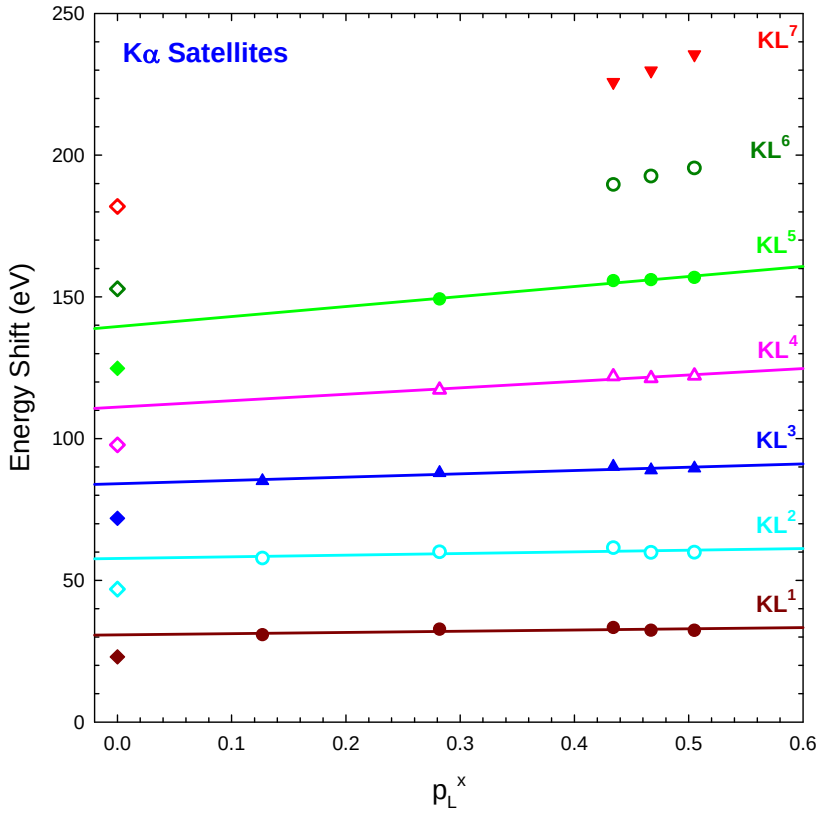

FIG. 3. The Kα satellite average energy shifts as a function of p_L^x. The results of straight line least-squares fits are shown by the solid lines and the average Dirac-Fock energy shifts calculated for vanadium atoms with all outer shell electrons present are shown by the diamond shaped data points at $p_L^x = 0$.

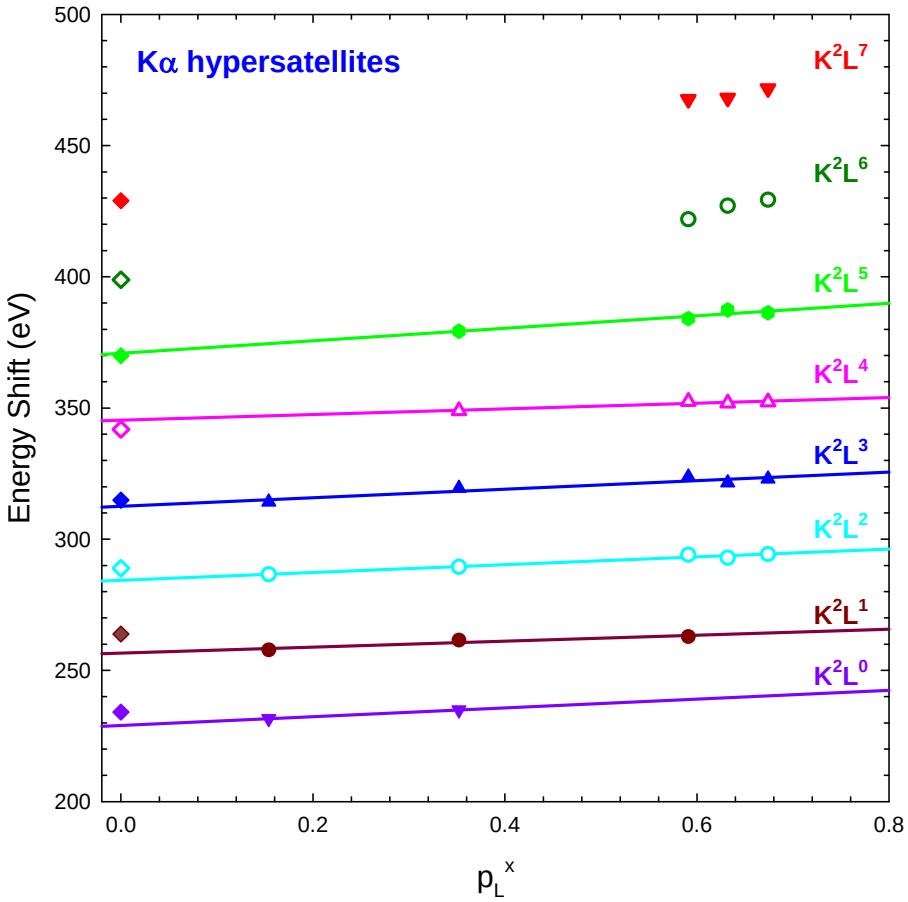

FIG. 4. The Kα hypersatellite average energy shifts as a function of p_L^x. The results of straight line least-squares fits are shown by the solid lines and the average Dirac-Fock energy shifts calculated for vanadium atoms with all outer shell electrons present are shown by the diamond shaped data points at $p_L^x = 0$.

The $K^2\alpha L^0$ hypersatellite is of particular interest since several authors have performed calculations for this case that take into account the Breit interaction [3, 5] and include radiative corrections from the most recent QED calculations [3]. The experimental value of the $K^2\alpha L^0$ hypersatellite energy shift is 229.0 ± 1.2 eV, which is in good agreement with the theoretical value of 228.0 eV[3].

[1] R. L. Watson, V. Horvat, and Y. Peng, *Progress in Research,* Cyclotron Institute, Texas A&M University (2007-2008), p. IV-7.
[2] J. P. Desclaux, Comput. Phys. Commun. **9**, 31 (1975).
[3] A. M. Costa, M. C. Martins, J. P. Santos, P. Indelicato, and F. Parente, J. Phys. B **40**, 57 (2007).
[4] V. Horvat, R. L. Watson, and Y. Peng, Phys. Rev. A **74**, 022718 (2006).
[5] M. H. Chen and B. Crasemann, Phys. Rev. A **25**, 391 (1982).

Energy and charge state dependence of electron capture and loss cross sections for Kr ions traveling in He

R. L. Watson, V. Horvat, and D. J. Morrissey[1]

[1]*Department of Chemistry, Michigan State University, East Lansing, MI 48824*

Efforts are currently under way at the National Superconducting Cyclotron Laboratory to develop a cyclotron gas stopper that will enable the stopping and collection of rare isotopes produced by projectile fragmentation prior to use in "stopped-beam" experiments or re-acceleration [1]. This project requires a detailed understanding of the interactions of fast heavy ions with the stopping medium, which in turn relies upon knowledge of the cross sections for electron exchange between projectiles and the media through which they travel. Because these cross sections depend on many variables (e.g., projectile charge, energy, atomic number, and target atomic number), it is not practical to experimentally measure them for all combinations of interest. Therefore, it is necessary to develop theoretical or semi-empirical methods for their prediction.

A procedure that utilizes various computer codes, such as Charge and Global [2], and Etacha [3], together with the semi-empirical formulas of Schlachter et al. [4], Franzke [5], and Schiwietz and Grande [6], has been devised to calculate electron capture and loss cross sections over a wide range of projectile energies [1]. The present measurements were performed for the purpose of testing the accuracy of this calculation procedure.

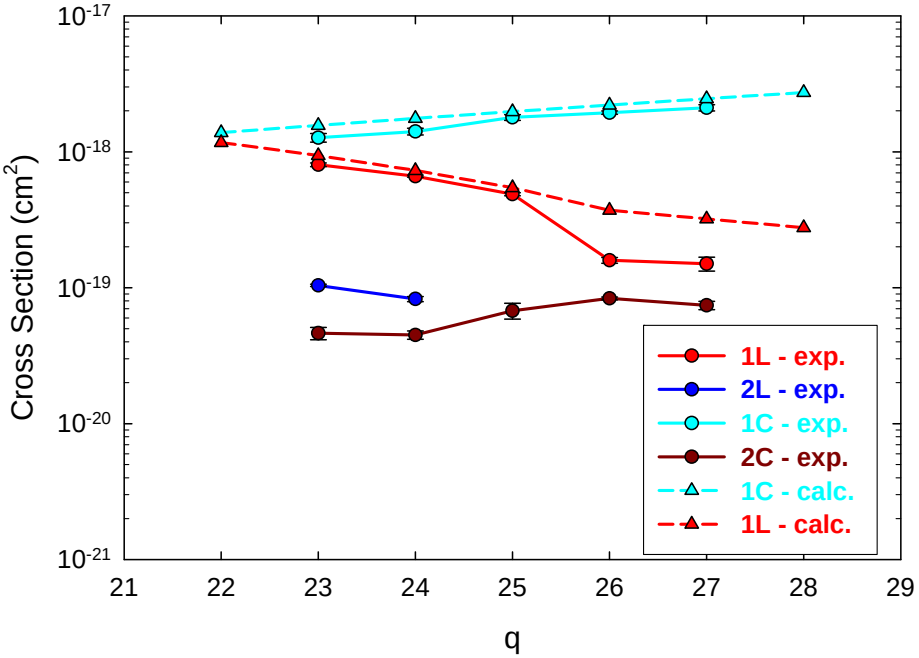

FIG. 1. Cross sections for electron capture and loss by 2.5 MeV/amu Kr^{q+} ions traveling in helium.

Beams of 2.5 MeV/u Kr^{8+}, 7.5 MeV/u Kr^{13+}, and 15 MeV/u Kr^{17+} passed through a 5 μg/cm^2 carbon foil located in front of a (horizontal) bending magnet, which was used to select individual projectile charge states. Each beam was then collimated to a diameter of 1 mm and directed through a windowless, differentially pumped gas cell having an effective path length of 2.08 cm. After emerging from the gas cell, the beams passed through a second (vertical) bending magnet into a 10 x 1.5 cm one-dimensional position-sensitive microchannel plate detector. The pressure of the He target gas was monitored by a Baratron pressure transducer and the gas flow was regulated by means of an automated control valve and flow controller. Additional details of the experimental setup are described in Ref. [7]. Charge distributions were measured for each selected incident charge state at five pressures ranging from 0 to 394 mTorr. The variation of the charge fractions versus pressure were found to be linear over this pressure range. Consequently, the cross sections for electron capture or loss in single collisions were obtained from the slopes of straight lines fitted to the data.

The experimental results are shown in Figs. 1-3. Also shown in these figures are the single-electron capture and loss cross sections (dashed curves) obtained using the calculation procedure. Overall, the calculated single-electron cross sections agree reasonably well with the experimental cross sections.

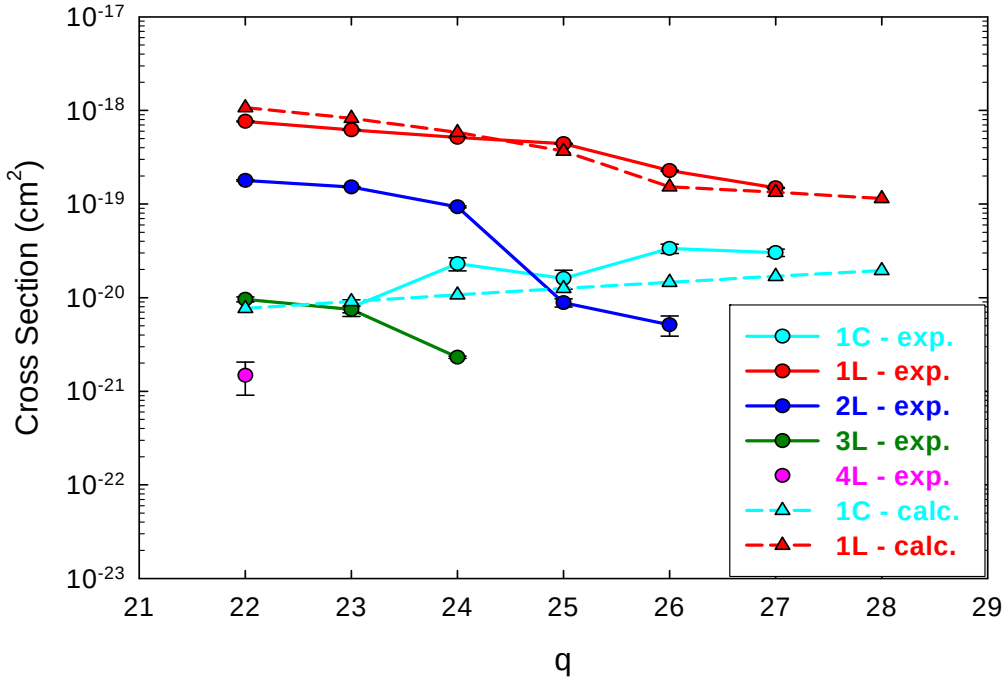

FIG. 2. Cross sections for electron capture and loss by 7.5 MeV/amu Kr^{q+} ions traveling in helium.

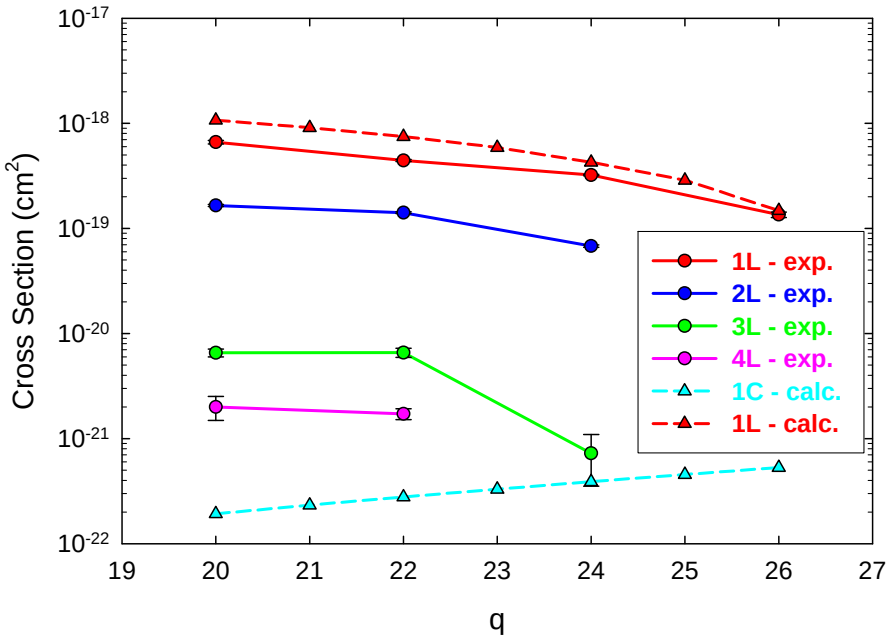

FIG. 3. Cross sections for electron capture and loss by 15 MeV/amu Kr^{q+} ions traveling in helium.

[1] G. Bollen, C. Campbell, S. Chouhan, C. Guénaut, D. Lawton, F. Matri, D. J. Morrissey, J. Ottarson, G. Pang, S. Schwarz, A. F. Zeller, and P. Zavodszky, Nucl. Instrum. Methods Pyys. Res. **B266**, 4442 (2008).

[2] C. Scheidenberger, Th. Stöhler, W. E. Meyerhof, H. Geissel, P. H. Mokler, and B. Blank, Nucl. Instrum. and Methods Phys, Res. **B142**, 441 (1998).

[3] J. P. Rozet, C. Stéphan, and D. Vernhet, Nucl. Instrum. Methods Phys. Res. **B107**, 67 (1996).

[4] A. S. Schlachter, J. W. Stearns, W. G. Graham, K. H. Berkner, R. V. Pyle, and J. A. Tanis, Phys. Rev. A **27**, 3372 (1983).

[5] B. Franzke, CERN Yellow Report 92-10, 100 (1992).

[6] G. Schiwietz and P. L. Grande, Nucl. Instrum. and Methods Phys. Res. **B175**, 125 (2001).

[7] R. E. Olson, R. L. Watson, V. Horvat, and K. E. Zaharakis, J. Phys. B **35**, 1893 (2002).

Cross sections for charge change of 4 MeV/u argon ions traveling in argon

V. Horvat and R. L. Watson

The ionization and electron transfer mechanisms that determine the charges of energetic ions passing through matter have been of continuing interest since the discovery of natural radioactivity. The close connection between the charge of an ion and the strength of its Coulomb interaction with atoms of the medium makes it one of the most important factors in determining the rate of energy loss or stopping power. Consequently, new information pertaining to the fundamental atomic collision processes responsible for the evolution of fast-projectile charge-state distributions is of potential interest to many areas of basic and applied research. We have measured the cross sections for single and multiple electron capture and loss for 4 MeV/u argon ions traveling in argon gas as a function of incident charge state. The measurements covered all incident charge states between 5+ and 18+. The results of this case study will be used to test the predictions of various theoretical models and to determine the evolution of the projectile charge distribution and its parameters as a function of distance traveled through the target gas.

In the experiment, an electron cyclotron resonance ion source was used to produce Ar^{5+} ions which then were injected into the Texas A&M K500 superconducting cyclotron, accelerated to an energy of 4 MeV/u, and directed to an analyzing magnet located upstream from the target chamber. Before entering the magnet, the beam was allowed to pass through either a carbon stripper foil, an aluminum stripper foil, or a high residual gas pressure region in the vicinity of the magnet to produce a distribution of projectile charge states. Ions having the desired charge state (q_i) were then selected using the analyzing magnet and passed through a series of four collimators before entering a windowless, differentially pumped gas cell containing Ar gas. Projectiles that exited the gas cell passed through a collimator and then between the poles of a vertical charge dispersing magnet (producing a horizontal magnetic field) before stopping in a one-dimensional position-sensitive microchannel plate detector. Signals from the detector were used to determine the height of the projectile at impact, which in turn was used to identify the charge state (q_f) of the ion when it emerged from the gas cell. The pressure of Ar gas inside the cell was monitored by a Baratron pressure transducer and the gas flow was regulated using an automatic control valve and a flow controller. The charge state distribution of the ions emerging from the gas cell was measured at nominal target gas pressures (p) of 0, 2, 4, 8, 16, 32 and 64 mTorr for each of the fourteen incident projectile charge states. Some typical charge state spectra are shown in Fig. 1 (for q_i = 5, 13, 18 and p = 64 mTorr).

After the fractions of detected ions in each charge state were determined as a function of target gas pressure, the cross sections for charge change in a single collision were determined using the well-known growth rate method [1]. A representative set of growth curves (for q_i = 13) is shown in Fig. 2, while the preliminary results for selected cross sections are shown in Fig. 3 as a function of charge change ($\Delta q = q_f - q_i$).

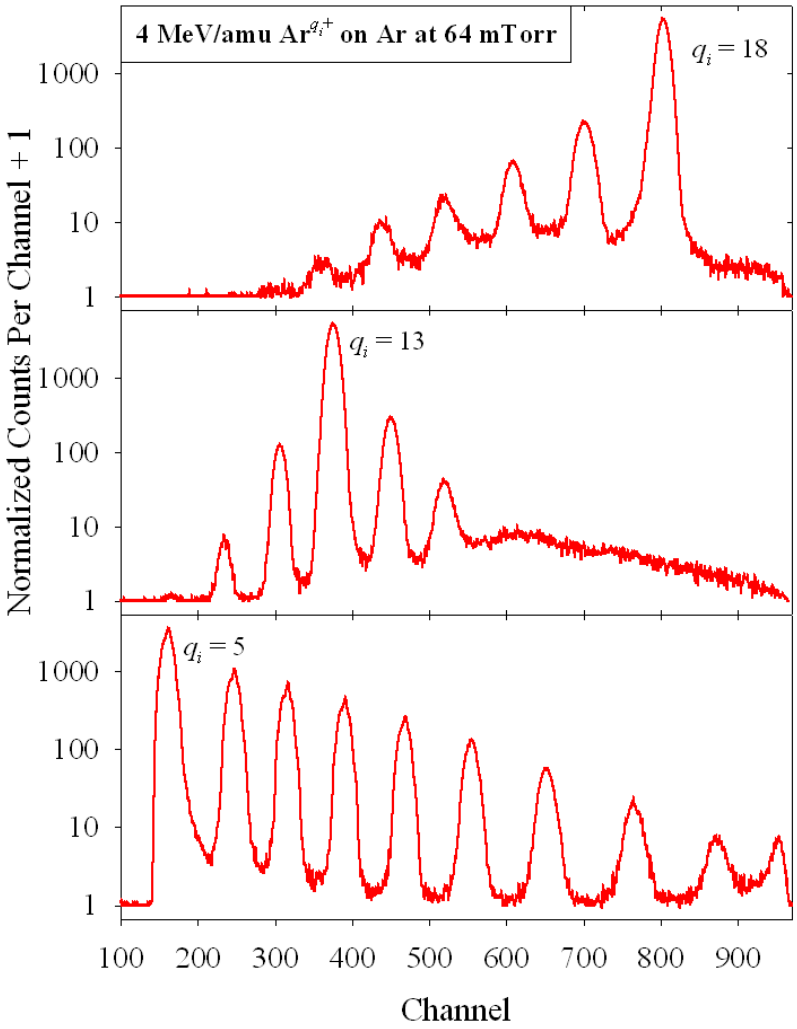

FIG. 1. Charge state spectra of 4 MeV/u Ar(q_i+) ions (q_i = 5, 13, 18) in Ar gas at the pressure of 64 mTorr.

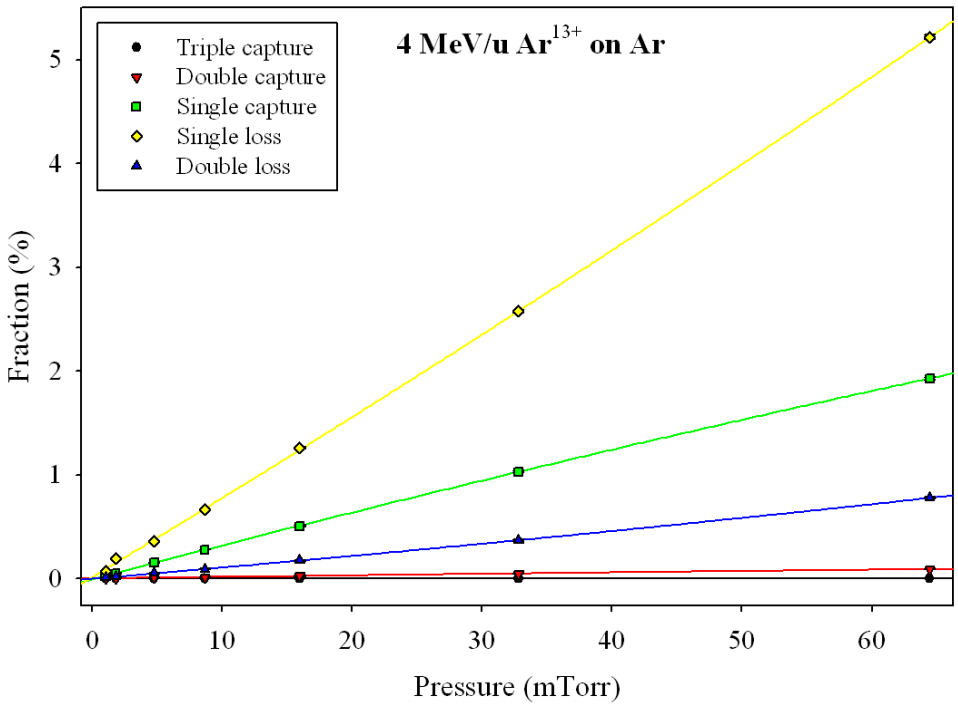

FIG. 3. Growth curves for 4 MeV/u Ar^{13+} ions in Ar gas.

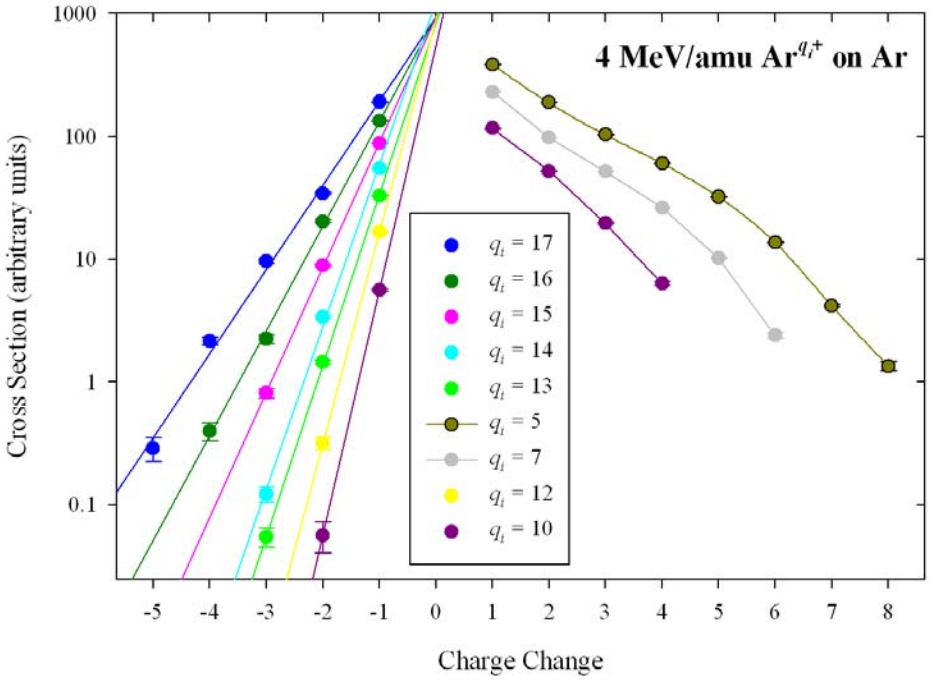

FIG. 2. Cross sections for charge change (in arbitrary units) of 4 MeV/u Ar ions in Ar gas.

[1] H. Tawara and A. Russek, Rev. Mod. Phys. **45**, 178 (1973).

SECTION V

SUPERCONDUCTING CYCLOTRON, INSTRUMENTATION, AND RIB UPGRADE

K500 operations and development

D. P. May, G. J. Kim, H. L. Clark, and F. P. Abegglen

Introduction

During the 2008-2009 reporting period a total of 30 different beams, including 10 newly developed beams, were used for experiments, and there were a total of 34 beam tunings for these experiments. In addition, seven new beams were developed for the SEE program. The SEE program will be treated separately.

Ion Sources

During the January shut-down ECR1 was opened for examination and cleaning. There was no further deterioration in the damaged spot that had previously developed over a plasma flute on the aluminum wall. In January of 2008 the axial field of the source had been reversed to move the bulk of the plasma heating away from this spot.

The method for sputtering isotopic titanium foil into ECR1 was improved with the development of an aluminum holder that serves as a clamp to the foil. Aluminum was chosen because it seems to be impervious to sputtering at the voltages that are applied, and several kilovolts are required in order to sputter a significant amount of the titanium sample. A stainless-steel holder tends to be sputtered into the plasma more than the titanium. The aluminum is emissive, however, and several milliamps of current are drawn from the aluminum. This causes heating of the holder, and the subsequent out-gassing increases the conditioning time to several hours as opposed to the usual minutes which are usually required. After conditioning this method works much better than other methods using foil samples spot-welded onto stainless-steel supports.

Cyclotron Beams

New beams of ^{4}He at 15 and 24.8 AMeV, ^{7}Li at 20 AMeV, ^{14}N at 15, 24.8, 38 and 40 AMeV, ^{15}N at 15 AMeV, ^{16}O at 40 AMeV, ^{20}Ne at 25 AmeV, ^{40}Ca at 10, 25 and 35 AMeV, ^{47}Ti at 32 AMeV, ^{64}Ni at 35 AMeV, ^{64}Zn at 35 AMeV and ^{70}Zn at 35 AMeV were developed.

Operations

For the period April 1, 2008 through March 31, 2009, the operational time is summarized in Table I, while Table II lists how the scheduled time was divided. There were five major repairs that caused significant loss of time. The helium refrigerator contamination problem from the last reporting period was finally resolved after the loss of the month of April and half of the month of May in the new period. Finally, on May 15 a beam was extracted from the K500. Then again in the month of June over

five days were lost to a failure of the helium expansion engine. In September and October more than eleven days were lost first to the failure of the rf "B" amplifier and then to the vacuum failure of the rf lower "A" insulator. Finally, in March over a week was lost to the failure of one of the three E1 deflector insulators. As a consequence, the unscheduled maintenance for this year represents a much higher percentage of time than for previous years.

TABLE I. 2008-2009 Operational Time

Time	Hrs.	%Time
Beam on target	5461.75	**72.0**
Tuning, optics, set-up	40.00	**0.5**
Beam development	604.50	**8.0**
Scheduled maint.	11.00	**0.1**
Unscheduled maint.	1474.75	**19.4**
Idle time	0.00	**0.0**
Total	**7592.00**	**100.0**

TABLE II. 2007-2008 Scheduled Beam Time.

Time	Hrs.	%Time
Nuclear physics	1601.50	**24.9**
Nuclear chemistry	1103.50	**17.2**
Atomic physics	144.00	**2.3**
Outside collaboration	13.00	**0.2**
Outside users	3198.50	**49.8**
Beam development	361.00	**5.6**
Total	**6421.50**	**100.0**

Texas A&M cyclotron radiation effects facility

H. L. Clark, J. Brinkley, G. Chubarian, V. Horvat, B. Hyman, G. Souliotis, and G. Tabacaru

The activity of the Radiation Effects Facility (REF) increased over the previous reporting year. In this reporting period, the facility was used for *a record* 2,600 hours, which is a ~10% increase over the 2,373 hours used in the 2007-2008 reporting period. Users of the facility (and hours used) over the past year were: NASA GSFC (308.5), Xilinx Corp. (274), NASA JPL (200.5), Boeing Seattle (163.25), SEAKR Engineering (143), Ball Aerospace (142.25), Aeroflex Corp. (135.25), International Rectifier (129.5), BAE Systems (120.75), Cisco Corp. (106), Intersil (88), General Dynamics (77.5), Honeywell (64), Northrop Grumman (61), European Space Agency (48), NAVSEA (48), VPT Inc (46.5), Sandia National Laboratory (40), University of Idaho (39.5), Intel Corp. (38), Lockheed Martin (31.75), Air Force (24), AMTEC Corp. (24), Georgia Tech University (24), Harris Corp. (24), Shoga(independent) (24), Vanderbilt University (23.75), Silicon Turnkey Solutions (23.5), Maxwell Corp. (22), L3 Communications (16), NASA JSC (16), National Semiconductor (16), Vitesse Semiconductor (16), Raytheon Corp (13.5), Silicon Space Technologies (11.75), Space Micro Inc (8) and Sun Tronics (8). New users included European Space Agency, L3 Communications, National Semiconductor, Shoga, Silicon Space Technologies, Silicon Turnkey Solutions, Space Micro Inc, Sun Tronics, University of Idaho, Vanderbilt University and Vitesse Semiconductor.

TABLE I. Radiation Effects Facility usage by commercial and government customers for this and previous reporting years.

Reporting Year	Total Hours	Commercial Hours (%)	Government Hours (%)
2008-2009	2,600	1,828 (70%)	772 (30%)
2007-2008	2,373	1,482 (62%)	891 (38%)
2006-2007	2,498	1,608 (64%)	890 (36%)
2005-2006	2,314	1,314 (57%)	1,000 (43%)
2004-2005	2,012	1,421 (71%)	591 (29%)
2003-2004	1,474	785 (53%)	689 (47%)
2002-2003	1,851	1,242 (67%)	609 (33%)
2001-2002	1,327	757 (57%)	570 (43%)
2000-2001	1,500	941 (63%)	559 (37%)
1999-2000	548	418 (76%)	131 (24%)
1998-1999	389	171 (44%)	218 (56%)
1997-1998	434	210 (48%)	224 (52%)
1996-1997	560	276 (49%)	284 (51%)
1995-1996	141	58 (41%)	83 (59%)

Table I compares the facility usage by commercial and government customers. The ratio from this reporting year (70% to 30%) is similar to the trend seen in previous reporting periods and commercial hours still dominate. Commercial hours increased by 23% and government hours increased by 13% over hours from 2007-2008. Much of the testing conducted at the facility continues to be for defense systems by both government and commercial agencies. It is expected that the high usage of facility will continue

Table II lists the beams used this year and the number of times each was requested. In total, 485 beams were run this year which is identical to the previous year. 15 and 25 MeV/u Kr and Xe were most utilized as well as 15 MeV/u Au. New beams of 15A MeV ^{4}He, ^{14}N, 25A MeV ^{4}He, ^{14}N and 40A MeV ^{3}He were added to SEELine users list.

TABLE II. Beams used and the number of times requested for this reporting year and previous years. 485 beams were run this year.

Particle Type	A MeV	2000-2001	2001-2002	2002-2003	2003-2004	2004-2005	2005-2006	2006-2007	2007-2008	2008-2009
^{4}He	15	N/A	N/A	N/A	N/A	N/A	N/A	N/A	N/A	1
^{14}N	“	N/A	N/A	N/A	N/A	N/A	N/A	N/A	N/A	0
^{20}Ne	“	1	13	19	15	23	36	39	37	41
^{40}Ar	“	4	24	43	46	51	56	60	57	63
^{63}Cu	“	N/A	N/A	5	14	22	23	25	24	19
^{84}Kr	“	6	26	55	47	49	75	81	77	63
^{109}Ag	“	N/A	N/A	6	18	15	26	28	28	34
^{129}Xe	“	5	18	43	51	50	78	84	84	48
^{141}Pr	“	N/A	N/A	2	2	1	4	4	4	4
^{165}Ho	“	3	11	17	7	8	22	24	24	13
^{181}Ta	“	4	5	4	3	5	3	3	3	3
^{197}Au	“	12	9	23	34	34	46	50	49	44
^{4}He	25	N/A	N/A	N/A	N/A	N/A	N/A	N/A	N/A	2
^{14}N	“	N/A	N/A	N/A	N/A	N/A	N/A	N/A	N/A	1
^{22}Ne	“	27	13	19	6	15	21	23	20	21
^{40}Ar	“	31	20	32	16	25	31	33	35	28
^{84}Kr	“	32	20	35	26	33	40	43	45	47
^{129}Xe	“	25	18	24	15	25	34	37	40	37
H-D	40	1	8	10	4	7	4	4	5	2
^{3}He	“	N/A	N/A	N/A	N/A	N/A	N/A	N/A	N/A	0
^{14}N	“	N/A	N/A	N/A	N/A	N/A	N/A	N/A	3	2
^{20}Ne	“	5	3	5	6	11	2	2	3	4
^{40}Ar	“	12	8	10	7	13	7	8	9	6
^{78}Kr	“	13	9	6	5	10	3	3	3	2
Total		192	207	360	324	399	511	552	550	485

Cyclotron computing

R. Burch and K. Hagel

This past year we increased the Cyclotron Institute's computing capacity and infrastructure. We continued the migration from SL 4.x (Scientific Linux 4.x) to SL 5.x, added three computational servers, two file servers allowing us to decoupling the data directories from the home directories, added server room cooling capacity and a computerized temperature warning system with automated server shutdown facilities. Our goal is to provide the Institute's personnel the computational and network resources necessary to allow them to carry out their research programs and the Institute's mission.

Last year we started the process of migrating administrative servers from SL 4.x to SL 5.x [1], developing disaster recovery plans as we went. We nearly finished the process with the AAA (Authentication, Authorization, and Accounting) servers, firewall servers and mail server still to be migrated. We will continue to run SL 4.x on all computational servers till a migration is required for security or compatibility reasons and run SL 5.x on any new administrative servers acquired. We added a configuration file synchronization system, PUPPET, which enables us to push out changes in configuration files from a central server, rather then logging on to each server and changing each file by hand.

This past year we added three new computational server, Dell PowerEdge 1950 with two Xeon 3.16GHz Quad Core processors, one for the lab and two for SJY-Group. We also relocated the 8-drive SATA enclosure [1], with it's drive slots now full and totaling 6T Bytes of data, from the main file server to its own server, a reallocated Dell PowerEdge computer. Seperating the SATA data drives from the home drives allowed us to reduce the main file server's down time due to data drive issues which has impacted the lab at large. This also allowed us to migrate the main file server to SL 5.x and replace aging home drives with larger faster drives running in a RAID 5 configuration. Doing so, we doubled our home directory capacity, enhanced performance and increased storage reliability. Additionally we purchased a 12 drive slot SATA enclosure with 2TBytes of data and a new Dell PowerEdge R610 to augment our data serving capacity and also installed a 12 drive slot SATA enclosure with 3TBytes of data onto a reallocated Dell PowerEdge computer for SJY-Group.

This past year we suffered several server room cooling failures. In an effort to mitigate issues due to cooling loss, we added an air circulation system to pull cooler air from the subbasement and implemented an automated staged server shutdown system.

In an effort to supply the Institute the resources it needs to execute its mission, we have migrated additional administrative servers to SL 5.x, installed a file synchronization system, added computations servers, grown our data serving capacity, and finally to protect out investment, added a emergency cooling system with automated server shutdown.

[1] R. Burch and K. Hagel, *Progress in Research*, Cyclotron Institute, Texas A&M University (2006-2007), p.V-5.

Cyclotron Institute upgrade project

H. L. Clark, F. Abegglen, G. Chubarian, G. Derrig, G. Kim, D. May, G. Souliotis
and G. Tabacaru

On January 3, 2005 the Cyclotron Institute Upgrade Project (CIUP) began with the approval of the CIUP management plan by the Department of Energy Nuclear Physics Office. The project will extend to the first quarter of calendar year 2011. When completed, the upgraded facility will provide high-quality re-accelerated secondary beams in a unique energy range in the world. Funding for the upgrade comes from several sources: the Department of Energy, matching support from TAMU, the Robert A. Welch Foundation and beam time sales for testing electronics components at the Cyclotron Institute.

The CIUP is divided into three major tasks: (1) Re-commission of the existing K150 (88") cyclotron and refurbish beam lines; (2) Construct light-ion and heavy-ion guides and produce 1+ radioactive ions; (3) Transport and charge boost radioactive ions and accelerate in the K500 cyclotron.

As detailed in the Management Plan, the effort made during this year on Task 1 included,

- Procurement and installation of equipment for the K150 high vacuum system,
- Fabrication of the dee inserts for the central region of the cyclotron,
- Development of high intensity 30 MeV Proton beams (design study with H- beams),
- Fabrication and assembly of K150 beam lines, and
- Evaluation of the radiation shielding system of the K150 cyclotron.

Progress was also made on Tasks 2 and 3. This included,

- Procurement of material for the ion guide beam dump,
- Installation and development of phase 2 of the Light Ion Guide system (connecting the light ion guide to the CB-ECR ion source),
- Development and design of the Heavy Ion Guide system and beam diagnostic systems,
- Installation and testing of the CB-ECR ion source, and
- Procurement, assembly and installation of the n+ transport system. Below we report on a few of the accomplishments listed above.

Central Region Calculations

Following the Berkeley design, a first set of dee inserts (made from titanium) and mounting mechanisms have been constructed and are ready for installation, see Fig 1. From the mirror inflector at the center of cyclotron, the acceleration process starts with the help of the Berkeley designed dee inserts or "batwings". One dee insert is attached to the active dee and the other to the dummy dee. The dee inserts are installed around the inflector housing and provide a well-defined electric field near the center of the cyclotron. The horizontal gap between the two dee inserts is 0.25", and the extent of the dee inserts (along the dee lip) is only a few inches. The nominal gap between the dee and the dummy dee is 2". Center region calculations were undertaken to study the effectiveness of the batwings.

These calculations involve tracking the beam particles through the combined RF electric field and the magnetic field at the center of the cyclotron – along the critical first few turns of the acceleration. The tracking is carried out with the MSU program called Z3Cyclone. Tracking the beam can answer some basic questions such as whether the particles can negotiate all the obstacles in the center, the mirror housing and the dee insert structures. Other important questions such as the RF voltage requirements, the RF phase acceptance, the electrical vertical focusing properties for the first few turns, and the centering of the beam orbits after several turns can also be studied.

FIG. 1. Berkeley designed dee inserts. They mount onto the dee and dummy dee; the bottom one with an opening for the beam entry attaches to the dummy dee side.

To perform the calculations, a 3-dimensional electric field map in the center region and a 2-dimensional magnetic field map of the cyclotron median plane are needed. A 3-D electric field map can be generated with a number of programs such as Relax3d. However, due to time constraint, a 2-D map has been use to simulate a 3-D field map, which is valid only near the center of the cyclotron. The 2-D electric potential map (looking from above) of the dee inserts together with the circular, grounded inflector housing at the center of the cyclotron is shown in Fig. 2. The beam particles are injected into the cyclotron from the inflector into the dummy dee side, through an opening in the dummy dee insert. The figure shows that the electric field is shielded away in the region between the inflector housing and the dummy dee insert. Another 2-D electric map can be obtained by looking at the dee inserts from the side, see Fig. 3. This 2-D map was used in the tracking calculations, as this map provided a more realistic electric field for the beam particles in crossing the electric gaps. Since this 2-D map completely ignores the inflector at the center of cyclotron, the beam particles had to be transported away from the mirror

inflector before the integration of the particles over the field maps can begin with the Z3Cyclotron program. As for the magnetic field map, a simple flat uniform field was used since we were only interested in the first few turns for this initial center region study.

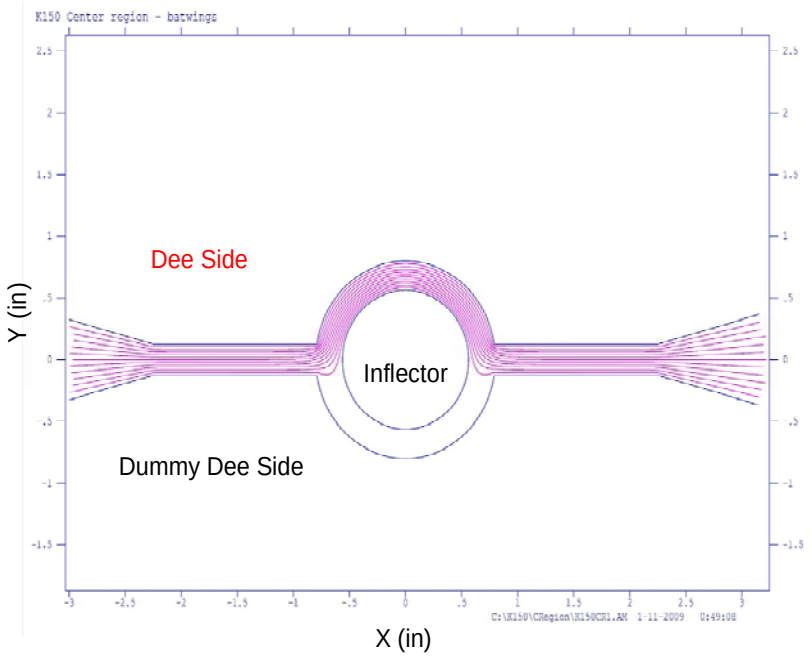

FIG. 2. Two dimensional Poisson calculation of the batwings and the grounded inflector housing looking from the top.

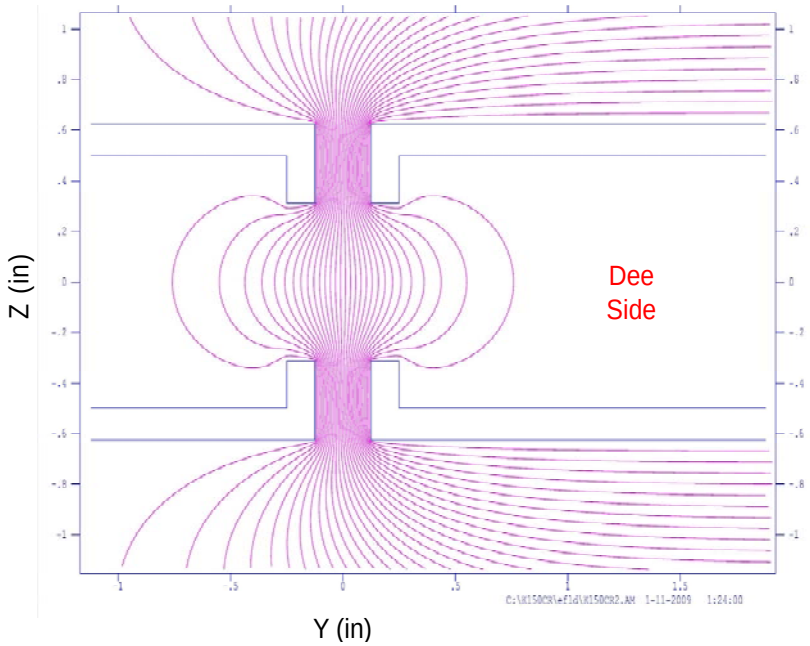

FIG. 3. Two dimensional Poisson calculation of the batwings looking from the side.

The first results of the center region calculations are shown in Fig. 4. The particle tracking started just above the mirror inflector at the center of cyclotron. Using analytical formulas it was tracked through the inflector and then followed into the dummy dee insert. Then, the Z3Cyclone program was used to track through the first few turns of the acceleration. Using 64 kV on the dee, the beam safely negotiated the first turn and led to well-centered orbits, as shown in Fig. 4. With the maximum of 64 kV on the dee, about 500 turns are needed to reach full energy in the cyclotron.

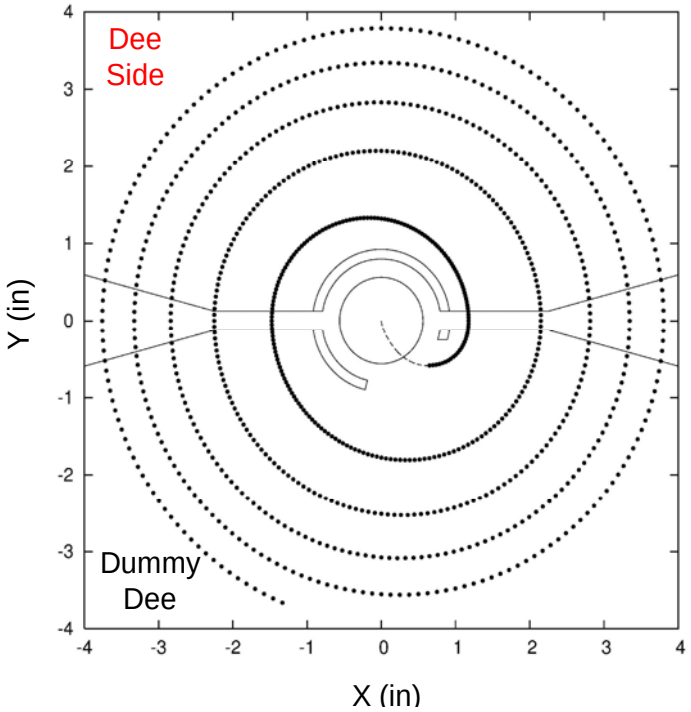

FIG. 4. First few turns of the acceleration in the K150 Cyclotron with a mirror inflector and dee inserts.

Beam Lines

Of the four new beam lines planned for the K150 cyclotron, the lines to the MARS cave and to the Maryland magnet, which in turn connects to the MDM and NIMROD caves, have been installed, and are under vacuum. On Jan 21, 2009, we accelerated and extracted a beam of 20 MeV protons from the K150 cyclotron, and transported the beam around the 160 degree analysis magnet for the first time. In order to complete the beam line installation, we had to move a quadrupole doublet in the BAS line (a K500 beam line) by 13" upstream into the concrete wall. Also, a 2-foot diameter and 10-feet long hole was bored through the concrete wall from the K150 vault to the cave 2 in order to make K150 beams available in the MARS cave. Of course earlier, we replaced the beam switching dipole magnet, located upstream of MARS, with a large 42.5-in circular pole magnet, which we had obtained free from Indiana University several years back. This freed up the Scanditronix dipole magnet, which has been moved to

K150 cyclotron vault and placed between K150 and the analysis magnet, to switch the beams to the Light Ion Guide (LIG) and Heavy Ion Guide (HIG). The two beam lines to LIG and to HIG have been designed, and they will be installed over the next year as we make progress with LIG and HIG installations in the cave north of the cyclotron.

The layout of the K150 beam lines is shown in Fig. 5. After the beam is extracted and collected with the help of the first pair of the quadrupoles, the beam optics for all the beam lines starts from the object slits located in the first beam box. The biggest challenge for the K150 beam lines is how to handle the much larger beam emittance from the K150 as compared to the K500 beams (about 5 π-mm-mrad for K500 beams to 24 π-mm-mrad or larger for K150 beams).

In order to control the size of the beam in both x and y transverse directions, using symmetric quadrupole triplets would have been ideal, however that was not possible due to space limitations. Therefore, we used instead closely-spaced quadrupole doublets to function in the point-to-parallel and then parallel-to-point scheme along the beam lines. The spacing between the quadrupoles for a doublet has been shortened in order to control the beam divergences, and at the same time taking advantage of the smaller beam rigidity from the K150 as compared to the K500.

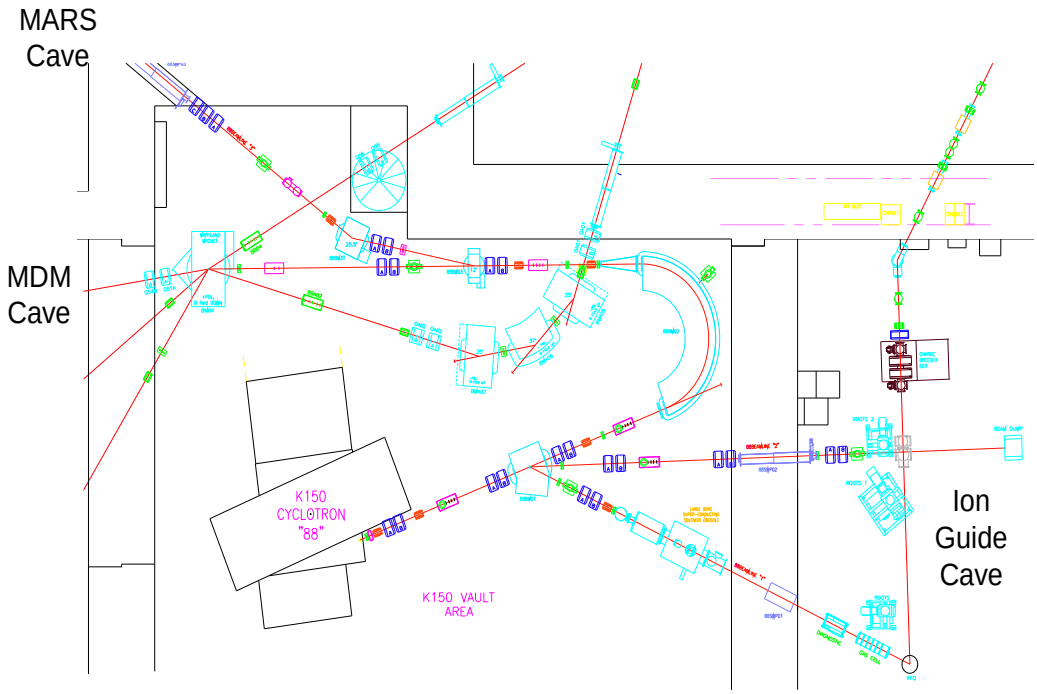

FIG. 5. New K150 beam lines.

H- Acceleration

One of the concerns for the project is the extraction efficiency of high intensity light ions from the cyclotron. Poor extraction efficiency may cause radiation damage to and high activation of the

cyclotron deflector. One solution is to accelerate H- ions and then strip to H+ near extraction. At other cyclotron labs this technique has shown to have extraction efficiencies of nearly 100% and greatly diminishes interior activation problems. Simple ray tracing calculations show that such as system could physically fit into and operate within the vacuum space of the K150 cyclotron. With the deflector pulled back from the extraction channel (but not removed from the cyclotron), H- ions could be accelerated to 38-40" and then stripped to H+. Upon exit, the trajectory of the H+ ions would then be steered along the normal beam line with a dipole magnet (see Fig 6).

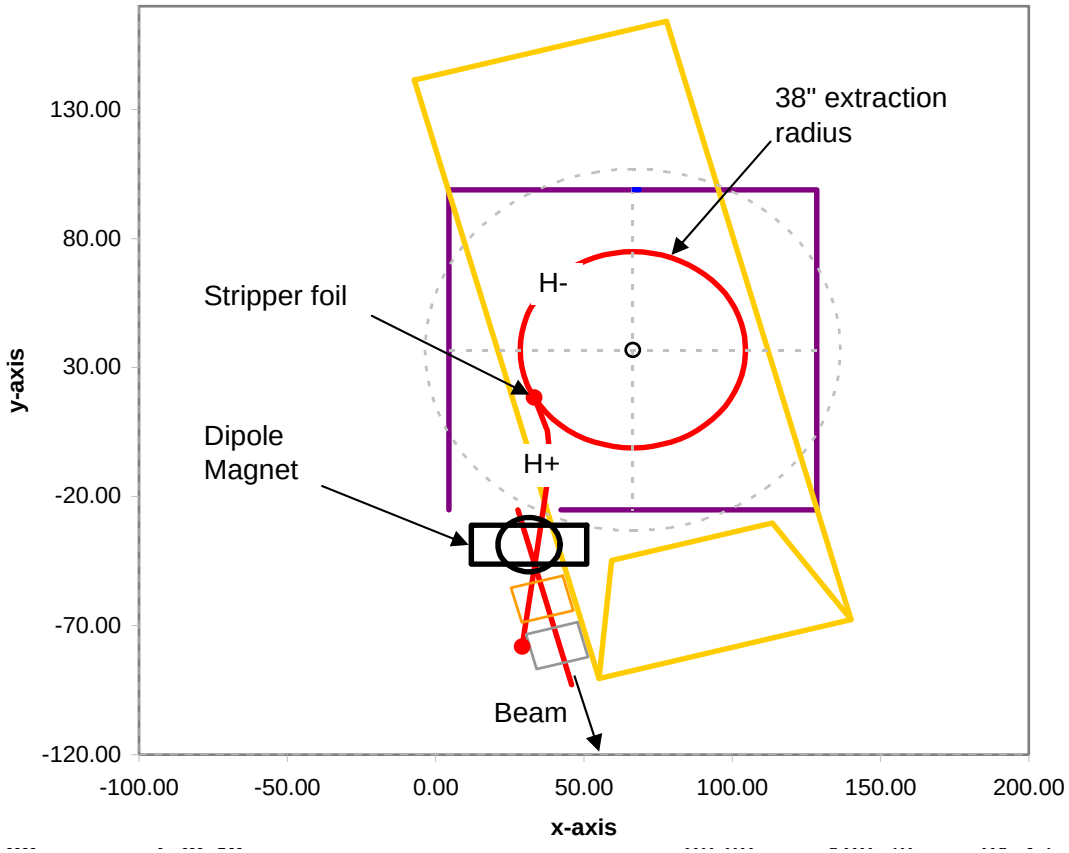

FIG. 6. Raytracing calculations for H- stripping at the exit of the K150 cyclotron.

The cyclotron laboratory in Jyväskylä, Finland (JYFL) has had great success with a multi-cusp source that was built by them with help from the TRIUMF lab in Vancouver, Canada. The experience of JYFL is that their source LIISA (Light-Ion Ion Source Apparatus) produces over 5 mA of H- at the 5.9 kV extraction voltage suitable for their fixed center region geometry for 30 MeV. This results in a proton beam out of the cyclotron of 60 eμA. JYFL has offered to loan their prototype negative ion source to us in an MOU for 8 years. This ion source has a shorter plasma chamber than LIISA, but is capable of producing at least 1 mA of H- which is suitable for our project (14 μA extracted from the K150 cyclotron). To become fully functional, the source requires new power supplies, a gas system and beam line elements. Our plan is to attach the H- source assembly to the existing vertical flange of the 90°

magnet on the ECR2 injection line. The layout of the H-source of the ECR2 injection line is shown below in Fig. 7.

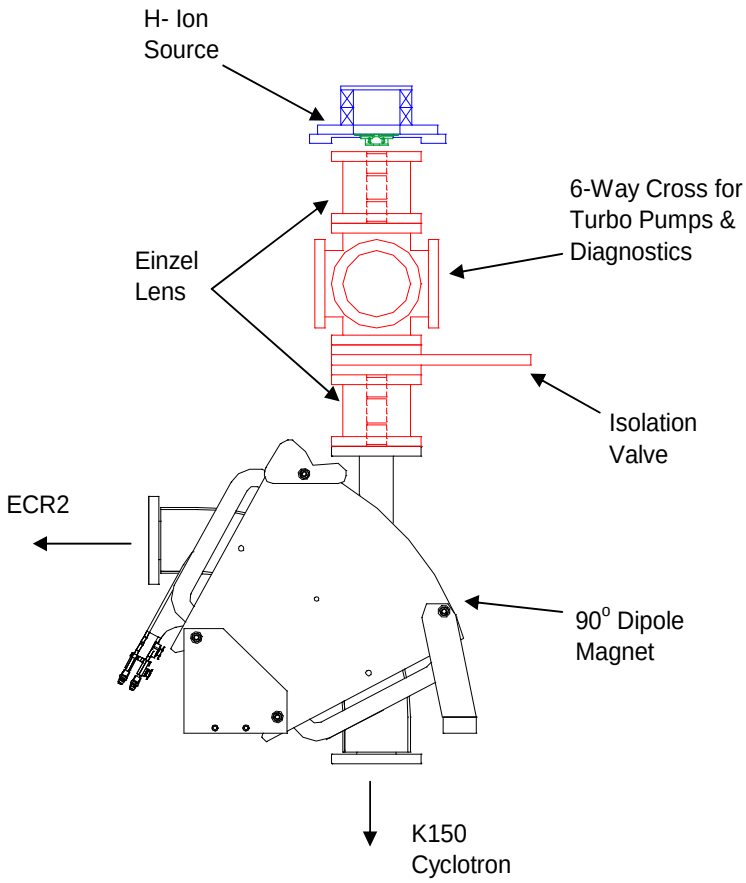

FIG. 7. Layout of the H- LIISA ion source on the ECR2 injection line of the K150 cyclotron.

Radiation Shielding Evaluation of the K150 Cyclotron Vault

The radiation shielding system of the K150 cyclotron vault was studied with the same computer codes/models (PHITS, MORTIZ and MCNPX) that were used to study the ion guide beam dump and radiation shielding system. Prompt radiation created by protons at 50 MeV, deuterons at 50 MeV and alpha particles at 127 MeV on thick targets of Pb, Cu, C and Ta placed at various locations inside the K150 vault was studied (see Fig 8).

The calculations show that the thick concrete walls and double-layered roof system provide adequate protection by showing zero dose levels outside the vault. One area of concern is region above the center of the cyclotron where the roof planks are arranged to allow a hole through the shielding for the vertical injection line equipment. At 1 meter from the hole, the calculated neutron dose is ~200 mrem/hour however the dose decreases rapidly to ~10 mrem/hour at a distance of 2 meters. It is clear that

this area will need additional shielding and an interlock safety system similar to the system used for region above the K500 cyclotron. Additional calculations for the estimates for "sky-shine" radiation above the opening are now underway.

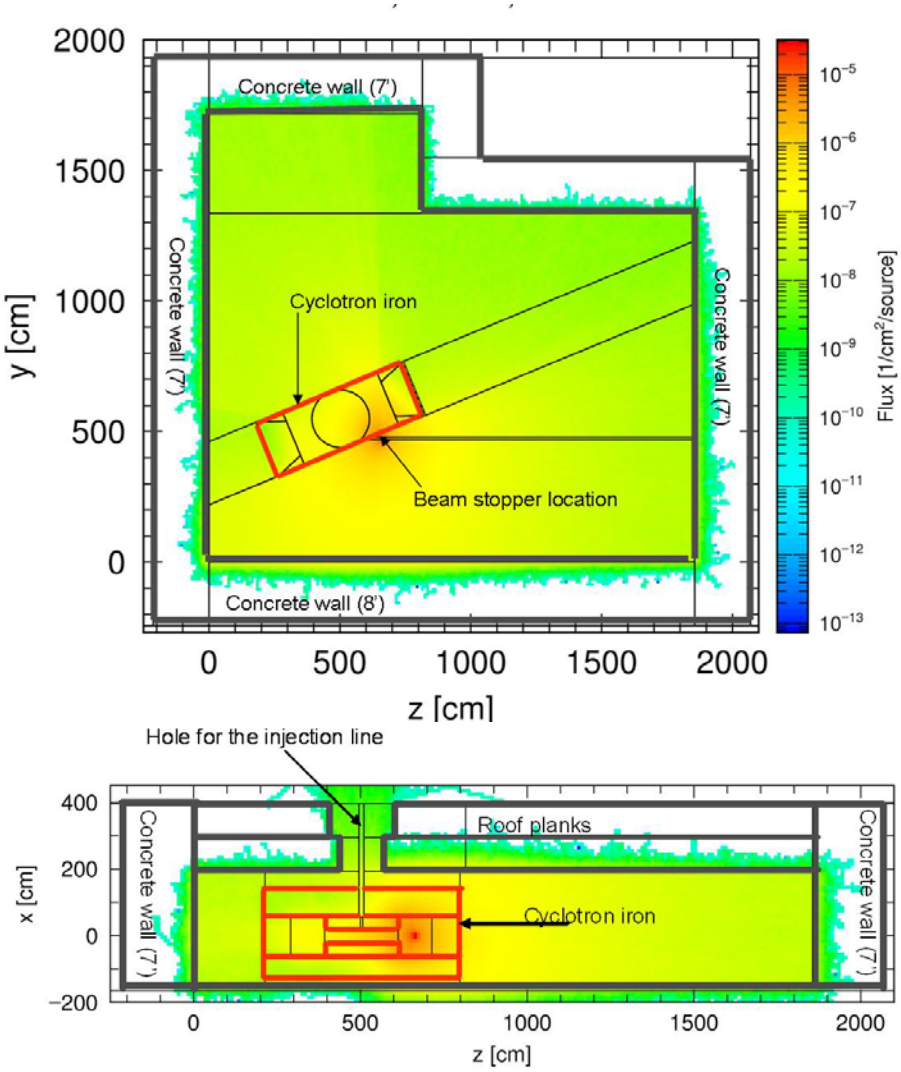

FIG. 8. Top (above) and side (bottom) views of the cyclotron iron, vault walls, roof system and beam target location. All neutrons and gamma rays produced by the 20 μA, 50 MeV proton beam are contained by the shielding system except for the opening above the cyclotron.

Charge Breeding ECR Ion Source

The CB-ECR ion source was delivered in September 2007 and assembled by Wayne Cornelius in October 2007. All of the equipment needed to complete the CB-ECR ion source has been procured and installed including both coil power supplies, the turbo pumping systems, microwave transmitters and control equipment. The analyzing magnet for the CB-ECR ion source has been constructed and is currently being installed.

The CB-ECR ion source was turned on for a short period of time. The TWT transmitter was turned on and plasma was created successfully. The extraction plate was removed and the star shape carbon coating by the hexapole field (see Fig 9) was observed. An extraction current of about 300 μA at 50 V extraction voltage was collected on a Faraday cup.

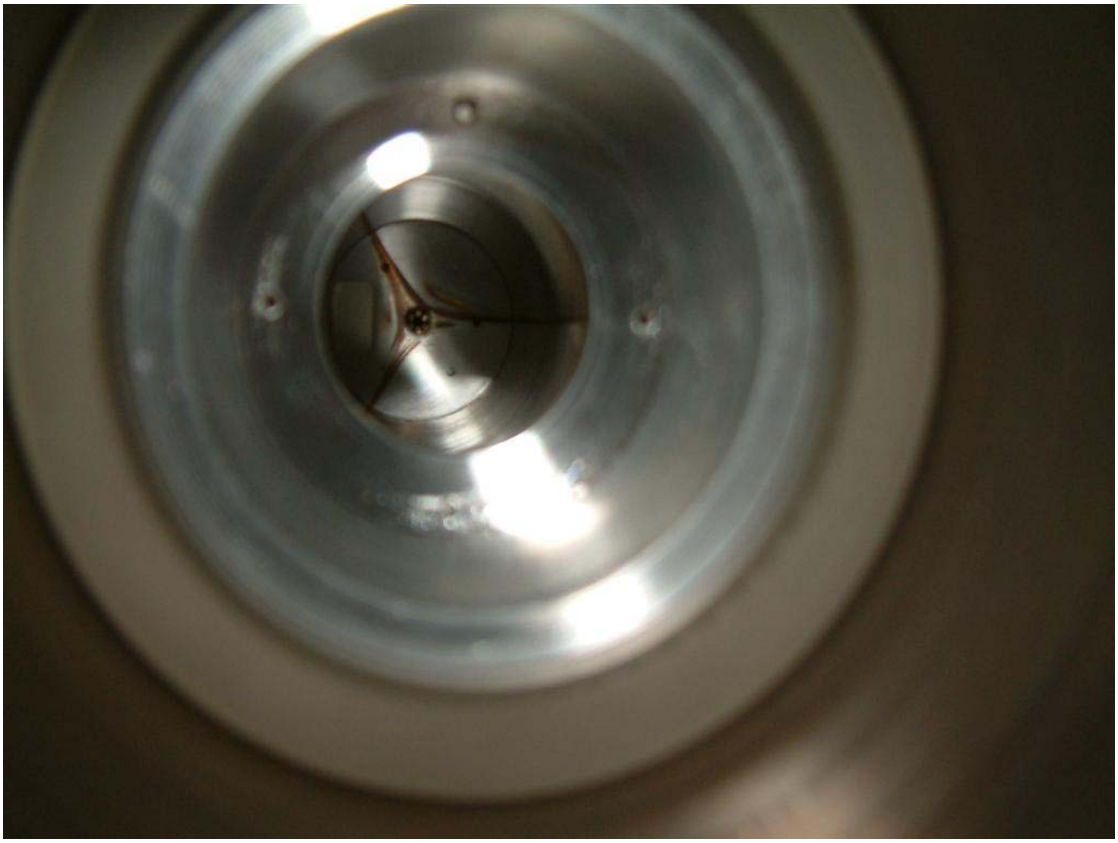

FIG. 9. The extraction plate of the CB ECR ion source after initial testing with the TWT transmitter. Note the star shape carbon coating by the hexapole field is observed.

The light ion guide project

G. Tabacaru, J. Arje, G. Chubaryan, H. L. Clark, G. J. Kim, and D. P. May

In the previous progress report [1], details about and a description of the evolution of the Light Ion Guide (LIG) project were given. Last year, a major piece of equipment was added to the project: the new Charge Breeding ECRIS (CB-ECRIS) built by Scientific Solution, San Diego, California [2]. The CB-ECRIS was turned on and plasma was ignited; details can be found elsewhere in this progress report. The main directions followed last year in the development of the LIG, were: the lengthening of the rf-only hexapole in order to reach the CB-ECRIS's plasma chamber and the development of the ^{228}Th open-source operation.

As explained in the previous progress reports, the device was initially developed with ionized gas created by two high-voltage spark electrodes inside the gas cell. We were able to produce a few mA of current, mainly ionized helium and ionized impurities. The transported current (a few nA) was measured at the end of the rf-only hexapole on a Faraday cup. The discharge voltage and current were 227 V and about 3.5 mA, respectively. The production of the ions via the spark method has drawbacks: the high voltage needed to ignite the spark accelerates the ions, and at the end of the rf hexapole the ions gain about 180 eV in energy. This energy is too high for the injection into the CB-ECRIS.

In order to eliminate the described feature, and reproduce more closely the future on-line operation, we decided to use an open radioactive source (^{228}Th) as the recoil-ion source. An effort to use a heated alkali source was unsatisfactory due to the fact that the continuous flow of helium in the gas cell prevents attaining the temperature where the alkali source will start releasing the products.

Inside the gas cell the daughters from ^{228}Th are released continuously and they are thermalized by the helium gas. In order to have maximum stopping efficiency of the radioactive products, a pressure of 30 mbar of helium was used. The daughters are injected into the rf-only hexapole within helium flow by applying a small (approx. 10 - 50 V) acceleration (guiding) voltage between the cell exit and the hexapole inlet. The same voltage will control the injection energy of the recoil ions into CB-ECRIS plasma chamber. In this preliminary experiment the recoil ions were transported to a collector plate (aluminized mylar), placed at the inlet of the CB-ECRIS plasma chamber. The collector plate is backed by a silicon detector. The alpha particles coming from the products pass through the collector plate and are detected with the Silicon detector. The decay series of ^{228}Th include ^{216}Po with a half life of 145 ms. This is an excellent candidate to test our device: the half-life is short enough to provide a reasonable counting rate and is long enough to be charged boosted in the CB-ECRIS. The first tests, without CB-ECRIS plasma, were successful: we were able to measure about 50 alphas/sec coming from the ^{216}Po. We measured also the energy of the ^{216}Po ions, and found that the energy spread is only around 1 eV (see Figure 1). This extra energy will have to be taken into account for stopping the products in the plasma of the CB-ECRIS. The extraction of radioactive highly-charged ions will be attempted in future experiments after the CB-ECRIS becomes fully operational.

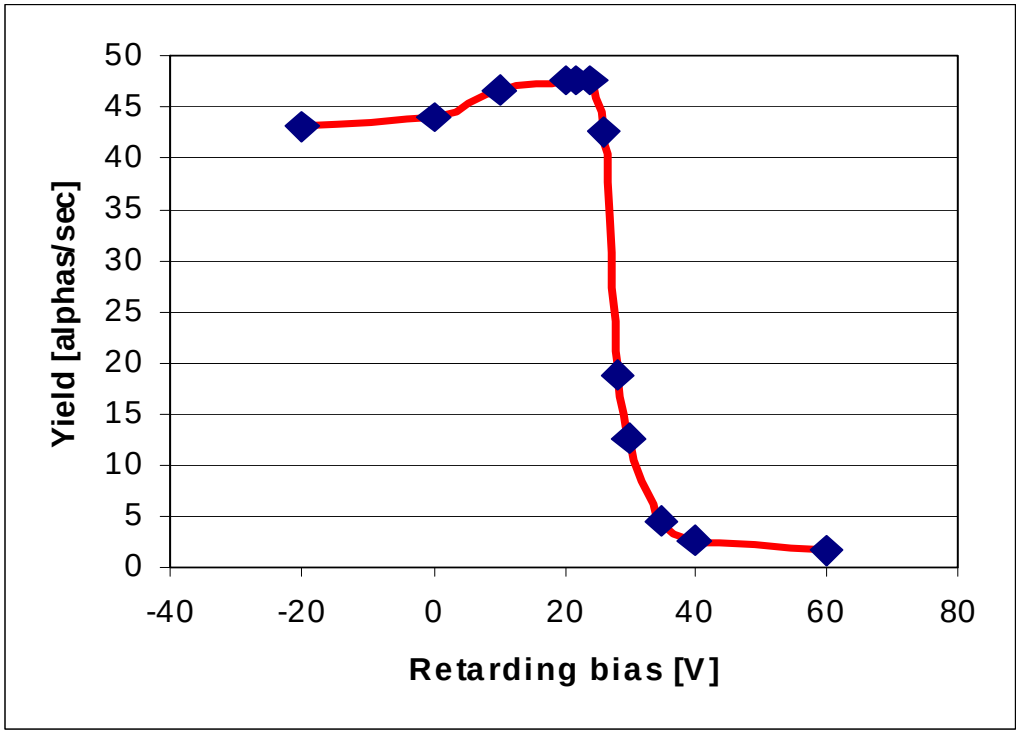

FIG. 1. The retarding bias is a measure of the energy of the ions. The radioactive products exhibit an energy of 20-25 eV approximately. The acceleration voltage was 24 V.

[1] G. Tabacaru *et al.*, Progress in Research, Cyclotron Institute, Texas A&M University (2007-2008), p V-12; http://cyclotron.tamu.edu/2008 Progress Report/5 Superconducting Cyclotron and Instrumentation/V_12_progress on light ion guide.pdf

[2] W. D. Cornelius, ECRIS 2008, 18th International Workshop on ECR Ion Sources, Chicago, Illinois USA, http://cern.ch/AccelConf/ecris08/papers/weco-b01.pdf.

Prompt gamma-ray measurement as method of monitoring changes in tissue undergoing proton irradiation

M. McCleskey, A. Spiridon, J. C. Polf,[1] B. Roeder, G. Tabacaru, S. Peterson,[1]
S. Beddar,[1] E. Simmons, A. Banu, and L. Trache
[1]*MD Anderson Cancer Center, University of Texas, Houston, Texas*

It has been proposed that measuring prompt gamma-ray emission from patients during proton therapy may be a useful tool to determine dose delivery during proton irradiation therapy. The energies of gammas emitted from the irradiated tissue are characteristic of the elemental composition of the tissue and the intensities of the lines are a function of elemental concentration and density. Observing prompt gamma rays could also be used to monitor changes in the composition of tissue that may take place during the irradiation. Monte Carlo simulations have been performed [1] that demonstrate these effects and the possibility of developing a method of "prompt gamma-ray imagining."

Work at TAMU:

Two experiments have been performed at the TAMU Cyclotron Institute using proton beams on the SEE line. For these measurements, a 40 MeV proton beam accelerated by the K500 cyclotron was impinged, in air, on tissue-equivalent phantom targets. The resulting prompt gamma rays were measured. In the first experiment in December 2008, bone- and tissue-equivalent targets were irradiated and the gamma spectrum was measured using a 70% efficiency HPGe detector surrounded by a passive lead shield. Gamma emission lines from the elemental components of the samples were identified and the intensities of these lines were demonstrated to be dependent on the composition and density of the sample. The Monte Carlo simulation, using the experimentally determined efficiency curve, very well reproduced the spectrum measured.

In the second measurement, performed in April 2009, a bismuth germanate oxide (BGO) shield was employed to allow for active Compton suppression. The Compton suppression was done in software, such that the BGO could be used as both a passive and active shield, and the results could be compared to determine whether active suppression would be desirable for future measurements. A narrow (4mm) slit was used and the detector was setup perpendicular to the beam path. The sample was then moved along the beam direction and a radiation depth profile was measured. As the high-energy gamma-ray lines from the inelastic excitation of ^{12}C and ^{16}O in probe were dominant, the addition of Compton suppression was beneficial to decrease the background and diminish the escape peaks (Figs. 1 and 2). Detailed analysis continues.

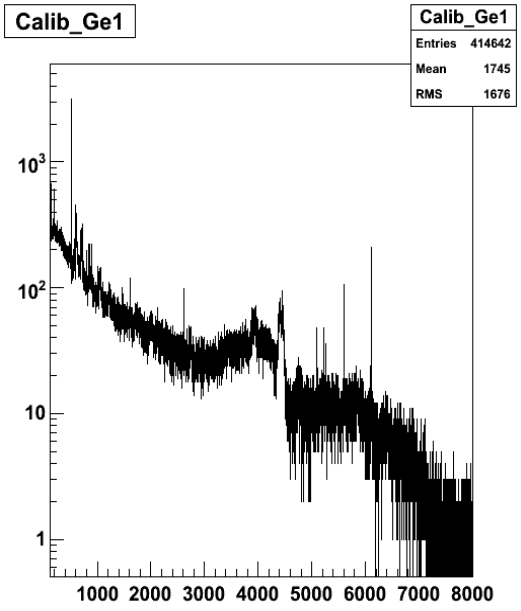

FIG. 2. Gamma spectrum from irradiated Lucite target without BGO Compton suppression. Calibration is 1 keV/channel.

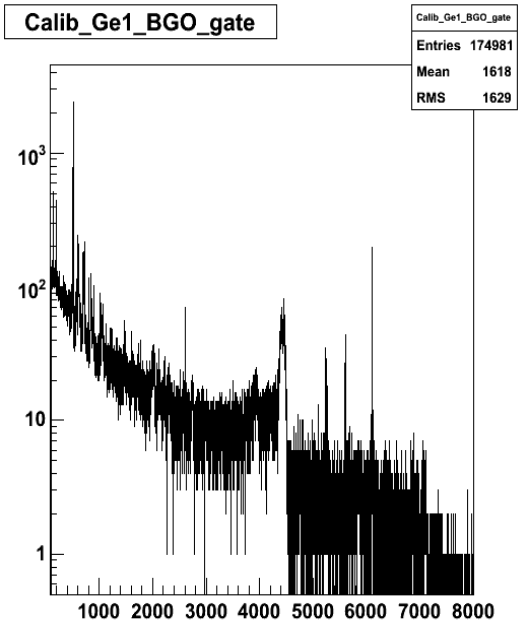

FIG. 1. Gamma spectrum from irradiated Lucite target with Compton Suppression.

[1] J. C. Polf *et al.*, Phys. Med. Biol. **54**, 731 (2009).

Production cross-sections studies of residual radionuclides from proton induced nuclear reactions on ^{nat}Mo up to 40 MeV

A. A. Alharbi,* M. McCleskey, G. Tabacaru, B. Roeder, A. Banu, A. Spiridon,
E. Simmons, L. Trache, and R. E. Tribble

The productions of radioisotopes by cyclotrons play a vital role in nuclear medicine for diagnostic studies via emission tomography, viz. single photon emission computed tomography (SPECT) and positron emission tomography (PET). Since these radioisotopes are mostly neutron deficient, they cause relatively low radiation dose to the patient. The excitation function measurements of charged particle induced reactions are needed to improve and study the ideal way for medical radioisotope production. The optimization of nuclear reaction for the production of radioisotope at a cyclotron involves a selection of the projectile energy range (the energy interval between the energy incident on the thick target and the energy at the end of it) that will maximize the yield of the product and minimize that of radionuclide impurities [1].

[1]In this study, the activation technique has been used to measure the excitation function of proton-induced nuclear reactions on ^{nat}Mo up to 40 MeV. The proton beam from the K500 superconducting cyclotron of the Texas A&M Cyclotron Institute was used in the SEE beam line and target chamber. Thin foils of molybdenum with natural isotopic composition of (^{92}Mo 14.84%, ^{94}Mo 9.25%, ^{95}Mo 15.92%, ^{96}Mo 16.68%, ^{97}Mo 9.55%, ^{98}Mo 24.13%, ^{100}Mo 9.63%) were used as targets. A stack was made from several groups of targets (^{nat}Mo, 50 μm) and monitor foils (^{nat}Al, 125 μm and ^{nat}Cu,

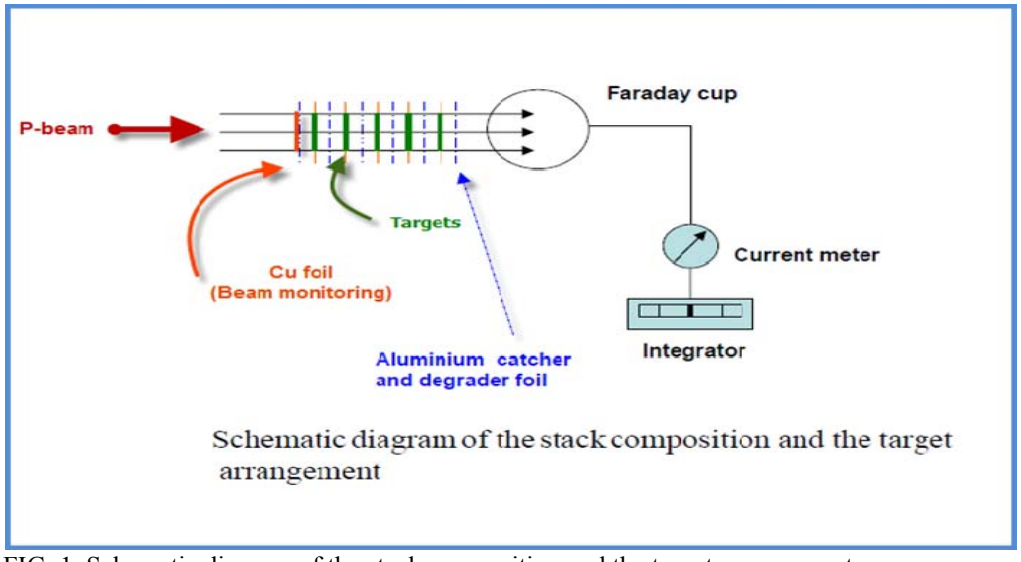

FIG. 1. Schematic diagram of the stack composition and the target arrangement.

* Fulbright Fellow 2009, On leave from Physics Department, Faculty of Sciences, Princess Nora Bint Abdul Rahman University, Riyadh, Saudi Arabia.

125 μm) that acted also as beam degraders (Fig. 1**)**, and placed in a special aluminum target holder which was the Faraday cup to measure the beam intensity (Fig. 2**)**. The Al and Cu monitor foils were inserted into the stack to measure the excitation functions of the well known cross-sections monitor reactions $^{27}Al(p,x)^{24}Na$ [2] and $^{nat}Cu(p,x)^{62}Zn$ [3] simultaneously with the reactions induced on the targets and were measured with the same detector and in a comparable geometry as the targets to confirm the beam intensity and energy. The stacked targets were irradiated by the 40 MeV accelerated protons at a beam current 1 nA for 65 min. The beam hits the target through an aluminum collimator of 8 mm diameter. The target foils of 10 mm diameter were sufficiently larger than the proton beam diameter (Fig. 3**)**. Cares was taken to ensure that equal areas of the monitor and the target foils intercepted the beam. The irradiation geometry used guaranteed that practically the whole beam passed through every foil.

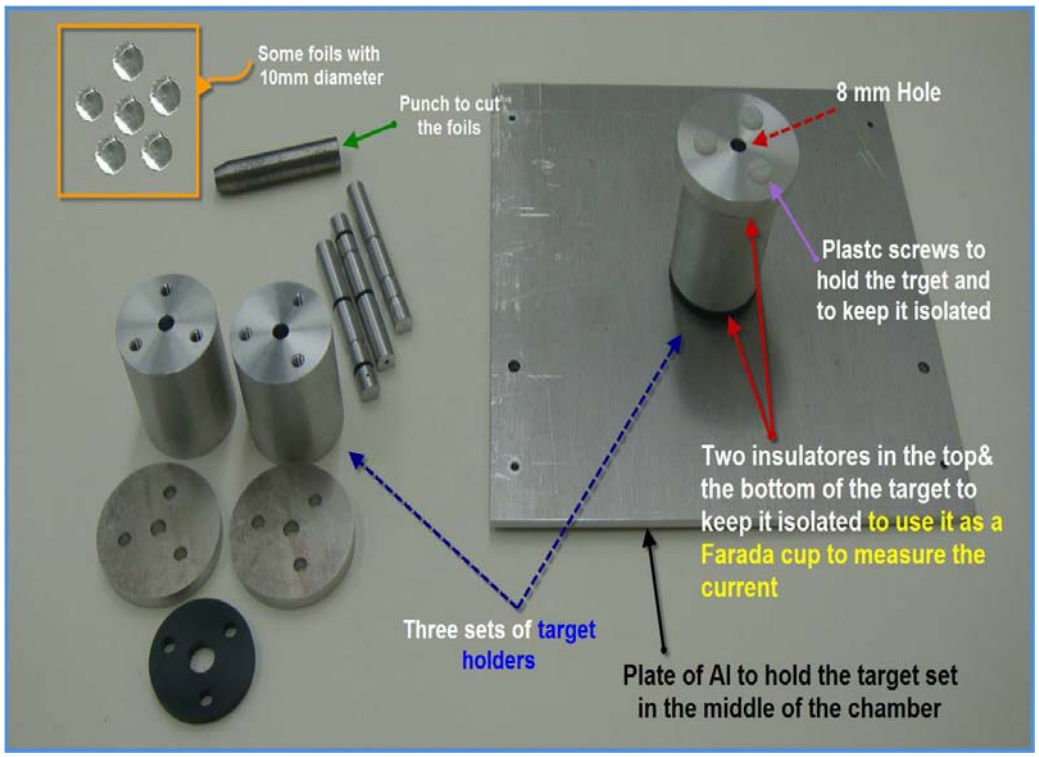

FIG. 2. A photograph for foils and the special aluminum target holders used in the experiment.

The secondary effect of the background neutrons on the molybdenum targets was checked by foils placed in the stack far behind the range of the fully stopped proton beam.

The computer program SRIM-2003 calculated the energy loss in the sample foils, as well as in the degraders [4]. The radioactivity of the residual nuclei in the activated foils was measured nondestructively using one HPGe γ-ray detector (70% relative efficiency). Each foil was recounted 2-3 times to avoid disturbance by overlapping γ-lines from undesired sources and in order to accurately evaluate cross-sections for cumulative formation of the corresponding longer-lived daughter radionuclide.

The detector-source distance was kept large enough to keep the dead time below 5% and to assure the same geometry. Several γ-lines for a nuclide will be considered to minimize the relative errors of calibration, wherever possible. Fig. 4 shows one of the measured calibrated spectrums with identified γ-lines.

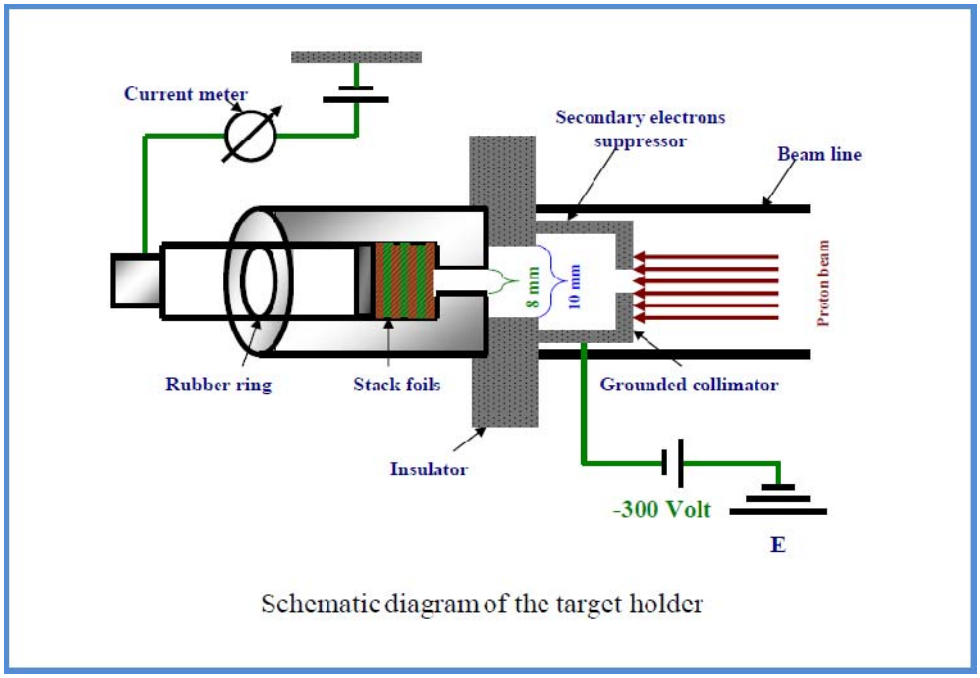

FIG. 3. Schematic diagram of the target holder setup and the faraday cup.

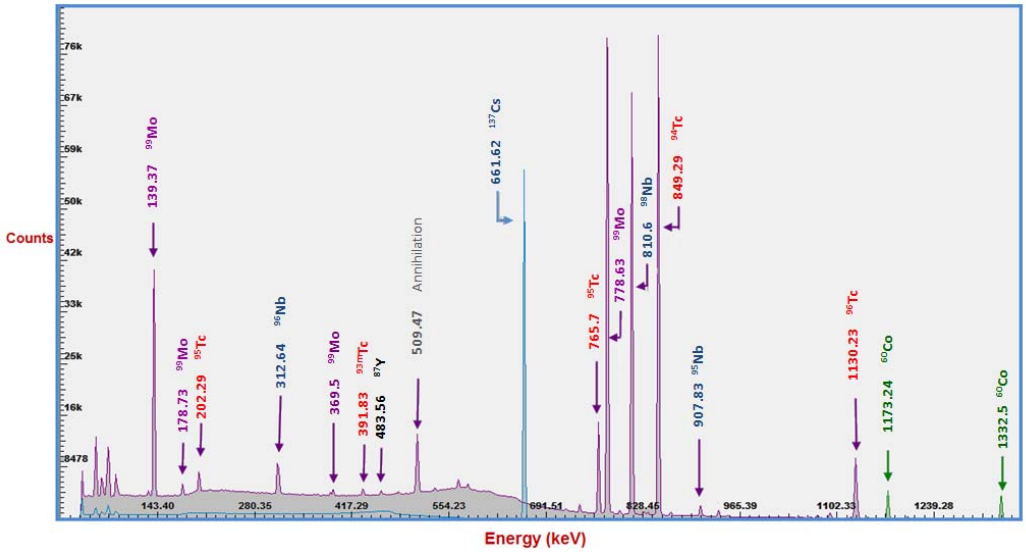

FIG. 4. A calibrated Gamma ray spectrum with identified γ-lines.

The decay data for some of the investigated radionuclides are shown in Table I. From the decay rates of the radioactive products and the measured beam current, the cross sections for the nuclear reactions ^{nat}Mo(p,X) will be determined using the usual activation formula. Then the determined excitation functions will be compared with the available previous published research and with the ALICE-IPPE precompound-hybrid model simulated calculations.

The integral yield of the ^{nat}Mo(p,X) nuclear reactions will be deduced using the excitation functions and the stopping power of ^{nat}Mo by summing the differential yield in a small energy interval (0.1 MeV) over the whole energy range [5]. It will be expressed as MBq $\mu A^{-1}h^{-1}$, i.e. for an irradiation of 1h at a beam current of 1 μA.

We will continue the program with further irradiations using 25 MeV/u alpha particles in a new location, with a chamber specially adapted for our purpose and using simultaneously two HPGe detectors for deactivation measurements.

TABLE I. Decay data of some ^{nat}Mo(p,X) produced radionuclides, Q-value and contributed reactions

Nuclides	Half life	Gamma-ray energy (keV)	Branching ratio (%)	Decay mode	Contributing reactions	Q-value (MeV)
^{93m}Tc	43.5 min	391.83	57.6	EC(23.3%)	^{93}Mo(p,γ)	4.08654
^{93g}Tc	2.75 h	1362.94	66.2	EC(100%)	^{94}Mo(p,2n)	-13.6611
		1520.28	24.4		^{95}Mo(p,3n)	-21.0302
					^{96}Mo(p,4n)	-30.1845
					^{97}Mo(p,7n)	-37.0058
^{94m}Tc	52.0 min	1868.68	5.75	EC(100%)	^{94}Mo(p,n)	-5.0381
		871.05	94.2	IT(0.1%)	^{95}Mo(p,2n)	-12.4072
					^{96}Mo(p,3n)	-21.5616
					^{97}Mo(p,4n)	-28.3827
					^{98}Mo(p,5n)	-37.0253
^{90}Mo	5.67 h	257.34	77.7	EC(100%)	^{92}Mo(p,t)	-14.2985
		122.37	64.2		*^{92}Mo(p,nd)*	*-20.5558*
					^{92}Mo(p,2np)	-22.7803
					^{94}Mo(p,2nt)	-32.0461
					^{94}Mo(p,3nd)	-38.3034
					^{95}Mo(p,3nt)	-39.4152
^{89m}Nb	1.18 h	1627.2	3.4	EC(100%)	^{92}Mo(p,α)	-1.363
^{89g}Nb	1.9 h	588	99.5	EC(100%)	^{92}Mo(p,n^{3}He)	-21.9408
					^{92}Mo(p,2d)	-25.2097
					^{92}Mo(p,2n2p)	-29.659
					^{94}Mo(p,2nα)	-19.1107
					^{94}Mo(p,2t)	-30.4428
					^{94}Mo(p,ndt)	-36.7001
					^{94}Mo(p,2npt)	-38.9247
					^{95}Mo(p,3nα)	-26.4798
					^{95}Mo(p,n2t)	-37.8119
					^{96}Mo(p,4nα)	-35.6341

[1] S. M. Qaim, Rad. Phys. and Chem. **71**, 917 (2004).

[2] F. Tarkanyi *et al.*, *Beam Monitor Reactions*, IAEA-TECDOC-1211, (IAEA, Vienna, 2001) p. 49; www-nds.iaea.or.at/medical

[3] F. S. Al-Saleh, A. A. Al-harbi, and A. Azzam, Radiochimica Acta, **94**, 391 (2006).

[4] J. F. Ziegler *et al.*, SRIM 2003 code, *The Stopping and Range of Ions in Solids*, (Pergamon, New York, 2003).

[5] F. Helus and Lelio G. Colombetti, *Radionuclides Production*, (CRC Press Inc., Boca Raton, Florida, 1980).

The Texas-Edinburgh-Catania Silicon Array (TECSA): a status report

L. Trache, B. T. Roeder, A. Banu, S. Cherubini,[1] T. Davinson,[2] V. Goldberg,
M. McCleskey, C. Spitaleri,[2] R. E. Tribble, and P. J. Woods[2]
[1]*INFN Laboratori Nazionali del Sud & DMFCI Università di Catania, 95123 Catania, Italy.*
[2]*School of Physics and Astronomy, University of Edinburgh, Edinburgh EH9 3JZ, United Kingdom.*

A memorandum of understanding was signed in June 2008 between three groups from Texas A&M University, the University of Edinburgh and the University of Catania to pool our resources and build TECSA (Texas-Edinburgh-Catania Silicon Array), a multi-detector system for use with radioactive nuclear beams. It is made of an array of up to 16 Micron Semiconductor type YY1-300 annular silicon strip detectors. The detectors are composed of 16 annular rings each, and are about 300 μm thick. Detectors of this type have been employed previously to construct high-efficiency detector arrays with large solid angle coverage at Louvain-la-Neuve [1], TRIUMF [2], and elsewhere. The development of TECSA will improve our capability to study reactions induced by rare isotope beams from MARS or from the new upgraded facility at TAMU, with a focus on those relevant for nuclear astrophysics. For example, TECSA will allow for the measurement of Asymptotic Normalization Coefficients (ANC) [3] for reactions such as ^{2}H(^{14}C, p)^{15}C$_{g.s.}$, and multi-particle breakup reactions such as ^{9}C→ ^{8}B+p.

The MSL-YY1 detectors arrived at TAMU from INFN-Catania in August 2008. First, the detectors were tested with a ^{228}Th source to check their resolution. The resolution for a typical detector was approximately 150 keV (Fig. 1) with 6 μs shaping time. It is expected that the resolution will be improved with the dedicated electronics for these detectors. These electronics include power supplies, pre-amplifiers and shaper-amplifiers from the University of Edinburgh. The electronics have recently arrived from Edinburgh and will be tested with the MSL-YY1 detectors in the near future.

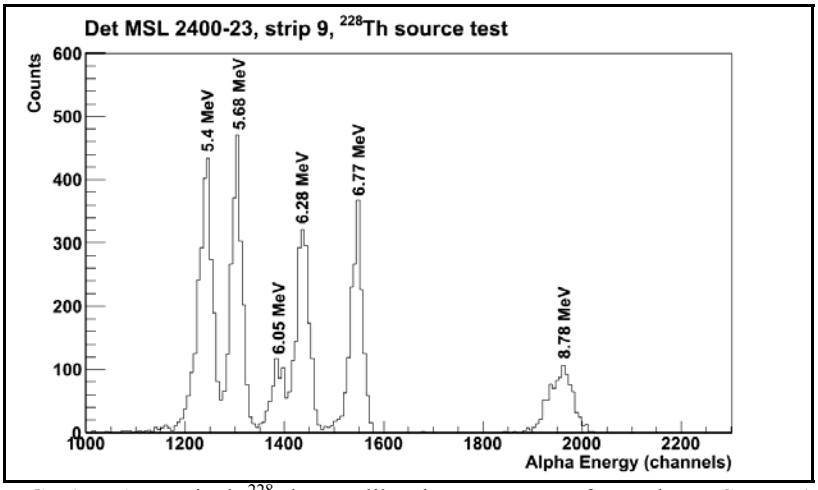

FIG. 1. A Typical ^{228}Th α-calibration spectrum from the MSL-YY1 detector tests

It was found during the testing of the detectors that some of the detectors had damaged wire bonding connections between the silicon strips and the PC board mount. This resulted in non-functional detector strips in 11 of the 16 detector sectors. To repair the damaged wire bondings, the MSL-YY1 detectors were taken to the National Superconducting Cyclotron Laboratory at Michigan State University (NSCL), where we reconnected the silicon strips to the PC board with a West-Bond wire-bonding machine [4]. After these repairs, 15 of the 16 detector sectors have all 16 silicon strips functional. The 16^{th} detector has a damaged PC board in addition to the damaged wire bondings, and will be sent to Micron Semiconductor for further repairs.

Monte-Carlo simulations of envisioned detector array arrangements for TECSA have been carried out with the GEANT4 toolkit [5]. The detector array response for the "flat, annular" ring and "lamp" arrangements as described in Ref. [1] were simulated for the $^{2}H(^{14}C, p)^{15}C$ reaction at 12 MeV/u. The detector arrangements used in the GEANT4 simulation are shown in Fig. 2. In inverse kinematics, the cross section is expected to be largest for backward scattering angles. The goal of these simulations was to observe if it was possible to separate the ^{15}C ground state from the first excited state at 740 keV such that a measurement of the ANC for the $^{15}C_{g.s.}$ can be made. The best energy and angular resolution were obtained with the flat, annular arrangement (Fig. 3). However, as shown in Table IV of Ref. [1], it is possible to cover a larger solid angle with the "lamp" configuration at the cost of both energy and angular resolution. In experiments where the count rate is low and energy and angular resolution are not as critical, the "lamp" configuration may be preferable.

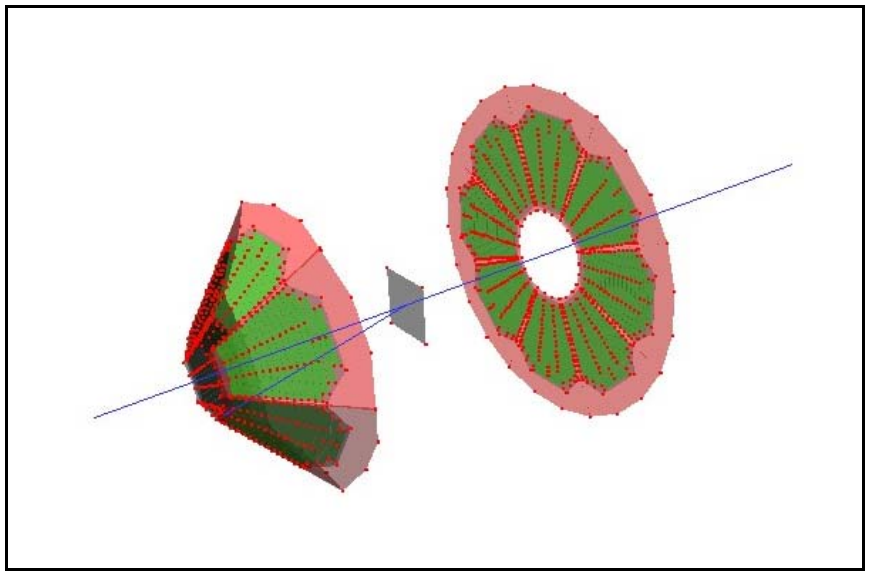

FIG. 2. GEANT4 simulated YY1 detector arrangements for TECSA. The "flat, annular" configuration is shown at forward angles and the "lamp" configuration is shown at backward angles.

The electronics, previously used at LEDA, arrived from Edinburgh in May 2009 and will be tested with the detectors in July 2009 to determine a grounding scheme that minimizes electronic noise in the detector array. The most likely configuration will involve mounting the detector pre-amplifiers

directly to the outer wall of the scattering chamber such that the connectors are covered by the pre-amplifier box. This arrangement will simultaneously create a good ground for the electronics and eliminate RF pick-up noise in the ribbon cables.

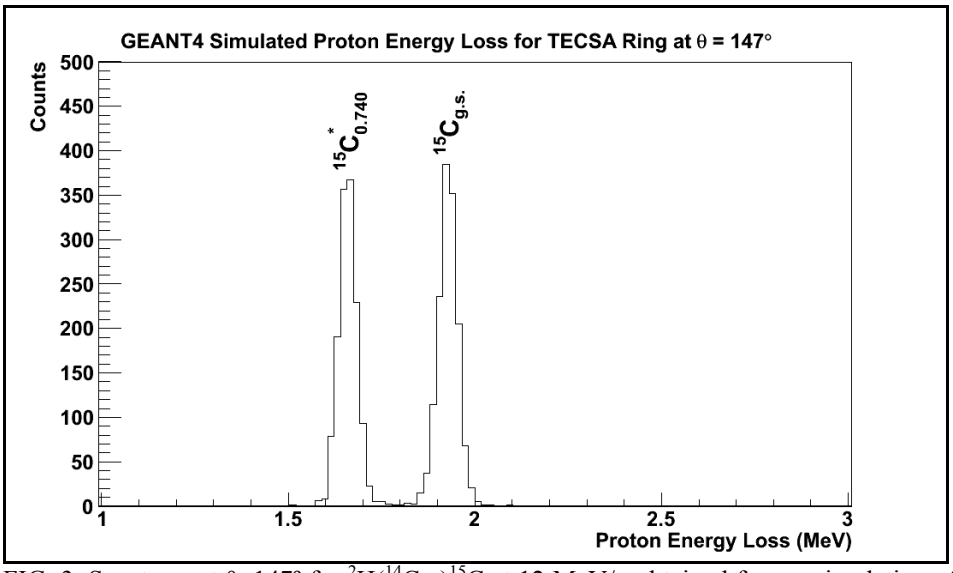

FIG. 3. Spectrum at θ=147º for ^{2}H(^{14}C,p)^{15}C at 12 MeV/u obtained from a simulation of the "flat, annular" configuration. The ground state is clearly separated from the first excited state.

The design of the scattering chamber will be completed within the next few months. Upon completion of the chamber, the first experiments with the TECSA array are envisioned for early 2010.

[1] T. Davinson *et al.*, Nucl. Instrum. Methods Phys. Res. A**454**, 350 (2000).

[2] A. St. J. Murphy *et al.*, Phys. Rev. **C 73**, 034320 (2006).

[3] R. E. Tribble, Nucl. Instrum. Methods Phys. Res. **B241**, 204 (2005).

[4] http://www.westbond.com

[5] S. Agostinelli *et al.*, Nucl. Instrum. Methods Phys. Res. **A506**, 250 (2003).

New Mesytec 32-channel VME ADCs: a status report

B. T. Roeder, A. Banu, K. Hagel, E. Simmons, and L. Trache

In an effort to upgrade the electronics for detector readout and digitization we have purchased five 32-channel VME ADCs model MADC-32 from Mesytec [1]. Their specifications show that they have many desirable features such as: readout as one 32-channel ADC or two 16-channel ADCs (with separate gates), multiple voltage input modes (4V, 8V or 10V pulse ranges), multiple resolution settings (2k, 4k, or 8k channels), fast analog to digital conversion times (800 ns in 2k mode, 1.6 μs in 4k mode, and 6.4 μs in 8k mode), and especially lower power consumption when compared with other VME ADCs. The ADCs arrived in August 2008 from Mesytec, and we have tested and later used them in several experiments. Until now, these MADCs have been used to digitize signals from silicon detectors in exotic beam production tests with MARS, and in recent β-delayed proton-decay experiments. They will also be employed for experimental setups where large numbers of channels are needed, such as for the TECSA array.

The ADCs we have purchased were among the first to be produced after the prototype was released, and had a few problems. In the early tests, we found that when they were used with a CAEN 16-channel shaper model 568B, and connected by ribbon cables, they returned data "overflows" (= data in channel 3750 or above with "overflow" bit in data stream = 1) in channels that did not have signal in them. For example, a pulser signal in one channel, shaped by the CAEN shaper and then connected to the ADC via ribbon cable returned the correct data in the channel connected to the pulser, but would also return as many as 8 other channels with "overflow" readings. Similar results were observed when a Mesytec model MSCF-16 shaper was used in place of the CAEN shaper. These "overflows" were undesirable because not only they generated additional deadtime in the data acquisition system, but they also made analysis of the resulting data more difficult for cases where hit multiplicity was important.

To overcome this "overflow" problem, Mesytec has made changes in the hardware and upgraded the firmware in a few iterations. Four of these upgraded MADC-32 modules were replaced in May 2009 and have recently been tested under similar conditions to those above. With this upgraded hardware (V121-4508E and later) and new firmware (v1.26 and later) the ADCs function normally with ribbon cables and both the CAEN N568B and Mesytec MSCF-16 shapers, without presenting the "overflow" problem.

We have also tested the MADC-32 for resolution and linearity. We chose to conduct the tests using a germanium detector with a well-known linear electronics chain behind and a ^{152}Eu gamma-ray source. During the tests, we observed that even though the M-ADC is a "peak-sensing" ADC, in order to obtain good resolution, the "peak" of the shaped signal needed to be within 2 μs of when the signal gate opened. An example of a "good" versus a "bad" resolution spectrum for a ^{152}Eu source is shown in Fig. 1. As is clearly seen in the figure, if the peak of the signal was placed >2 μs after the signal gate is opened (top panel), the resolution was poor and the peaks in spectrum became asymmetric. Good resolution was restored simply by placing the peak of the signal earlier in the gate (bottom panel). Further tests with the M-ADCs revealed that this problem arose because of "the internal gate generator" feature of the ADCs

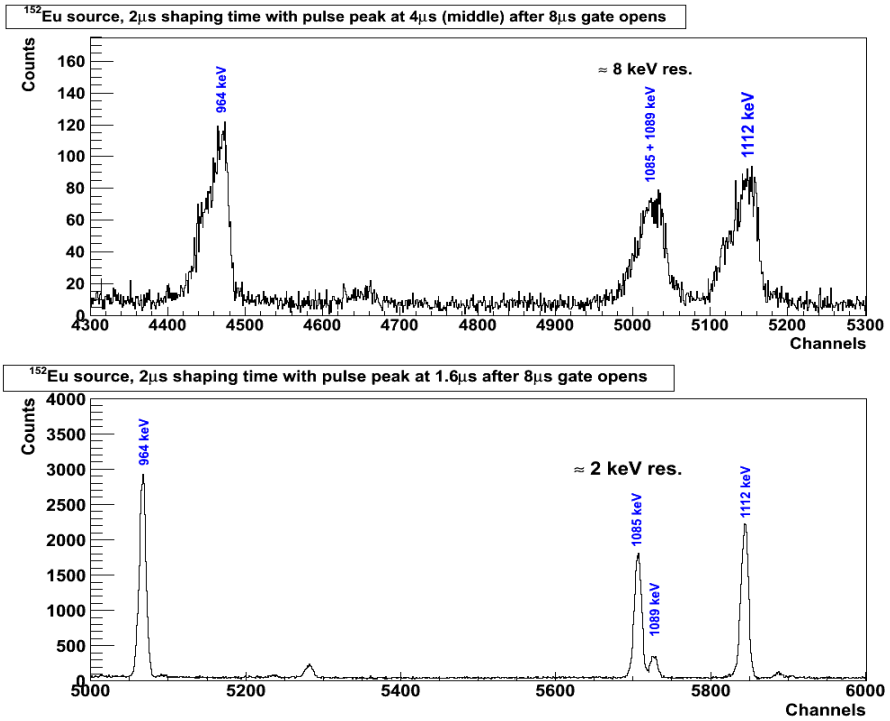

FIG. 1. Comparison of M-ADC generated spectra for different signal positions in the gate. When the M-ADC internal gate generator is used and gate width is not set up properly (see text for explanation).

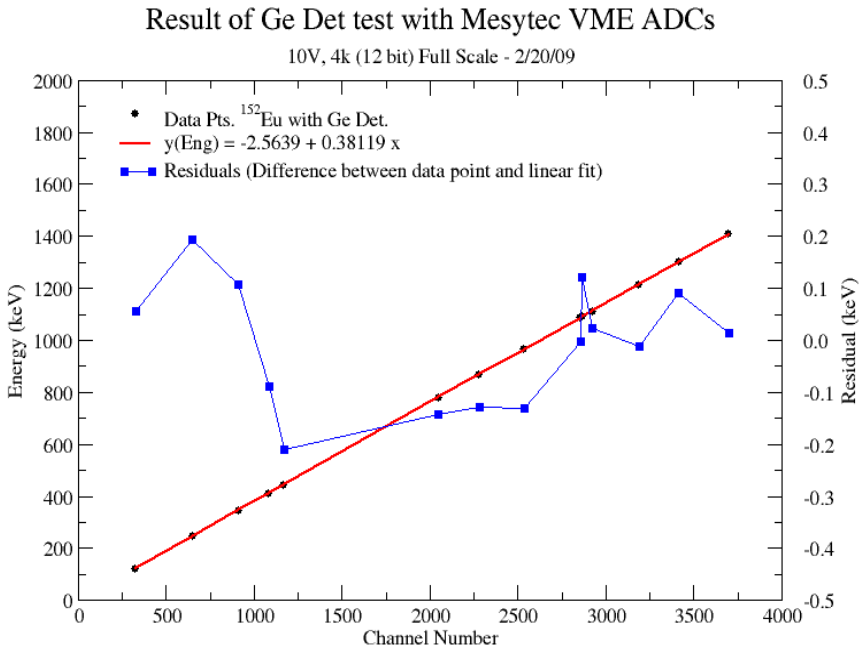

FIG. 2. Energy vs. channel (left scale) and the residues after linear fit (right scale) from the MADC-32 linearity test with a ^{152}Eu source and a germanium detector. The 10V input, 4k hi-resolution mode was used in this test. Overall, the non-linearity was observed to be < 0.1% for this test.

was enabled by default in the software and was not set up correctly. As a result, when the "peak" of the electronics signal came later in the signal gate as in the top panel of Fig. 1, the "peak" of the signal was actually outside the signal gate observed by the M-ADC internal gate generator. Thus, the good peak resolution of the bottom panel in Fig. 1 is restored by a) disabling the internal gate generator (now the default software setting or b) giving the internal gate generator a gate of proper width as described in the M-ADC manual. Note that if the internal gate generator is used one still must send the M-ADC a trigger pulse to start the gate generator.

The specifications of the M-ADC claim that the differential non-linearity (DNL) is < 1% over the entire range of channels regardless of the voltage input or resolution mode used [1]. The worst non-linearity observed during the test was 0.4% in the 10 V input, 8k low-resolution mode, while typical non-linearity over the entire range of data channels was observed to be < 0.1%. The results of the linearity tests of the M-ADCs for in 10V input, 4k high-resolution mode with the Germanium detector and the ^{152}Eu source are shown in Fig. 2.

There were a few problems with the new M-ADCs related to hardware and firmware problems. These problems with phantom "overflows" in the data stream and spectrum resolution have been largely overcome. As a result of these tests, the M-ADCs are now available at the Cyclotron Institute for use in future experiments.

[1] M-ADC manual: http://www.mesytec.com/datasheets/MADC-32.pdf

Assembly and test run of decay detector for ISGMR study

J. Button, R. Polis, Y. Tokimoto, D. H. Youngblood, Y. -W. Lui, Krishichayan

1. ΔE- ΔE - E Plastic Scintillator Array Decay Detector

In order to study the Isoscalar Giant Monopole Resonance in unstable nuclei, we have designed and are in the process of building and testing a ΔE- ΔE - E decay detector composed of plastic scintillator arrays. The measurement of the ISGMR in unstable nuclei will be done using inverse kinematics, with a 40 MeV per nucleon beam of the unstable nucleus incident on a ^{6}Li target. Xinfeng Chen studied the viability of this approach, taking data for elastic scattering and inelastic scattering to low-lying states and giant resonances of 240 MeV ^{6}Li ions on ^{24}Mg, ^{28}Si, and ^{116}Sn [1]. Nuclei excited to the ISGMR region are particle unstable, and will decay by p, α or n decay shortly after excitation. To reconstruct the event it is necessary to measure the energy and angle of the decay particle (with the plastic scintillator array) and of the residual heavy ion (in the focal plane of the MDM spectrometer). In many lighter nuclei a few nucleons off stability, and in light proton rich nuclei, the neutron threshold is above the region of interest.

The decay detector (Figs. 1 and 2) is placed in the MDM target chamber and subtends 70^{o} in Δθ and Δφ. It is composed of 30 - 1 mm thick strips of BC408 plastic scintillator (14 horizontally aligned and 16 vertically aligned, forming the ΔE- ΔE arrays) and 5 blocks of BC408 plastic scintillator (E detector array). Placed back to back, the vertical and horizontal strips overlap to give 1 cm^{2} pixels, providing an approximately 4^{o} x 4^{o} angular resolution. Particle identification can be done using horizontal and vertical strips within the energy range (MeV/amu) 7 < E/A < 11. For 11 < E/A < 75, the strips (ΔE) and the block scintillator (E) can be used for particle identification.

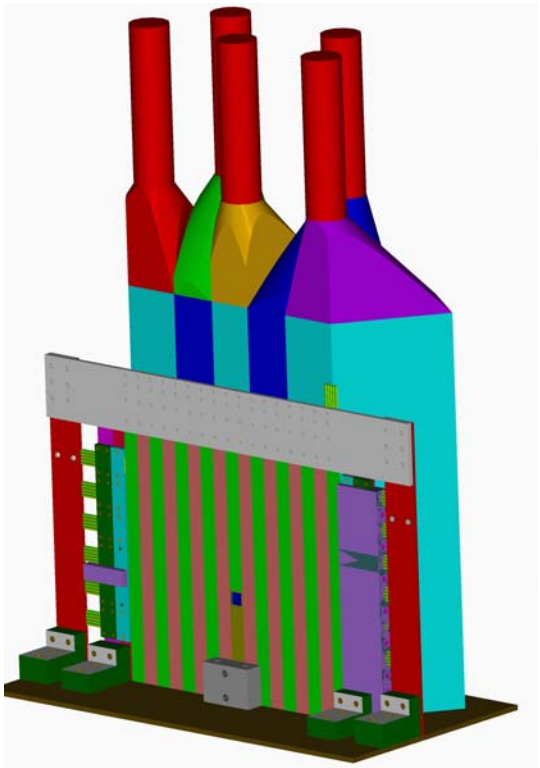

FIG. 1. Schematic of decay detector. The front of the block scintillator array (E) is flat and lies parallel to the scintillator strips (ΔE). Each block covers Δθ~14º relative to the target.

Each strip is bonded to a bundle comprised of 19 optical fibers (1 mm diameter x 50 cm length) manufactured by Saint-Gobain. One end of the fiber bundle is cemented (optical cement BC600 Saint-Gobain) into a rectangular form, and the other end is cemented into an acrylic cyclindrical sleeve. The rectangular end is then cemented to the 1 mm x 1 cm end of

the strip scintillator. The other end is mated with a 1 cm diameter Hamamatsu photomultiplier tube. The strips are wrapped in aluminum foil for light reflection and to eliminate cross-talk between scintillators.

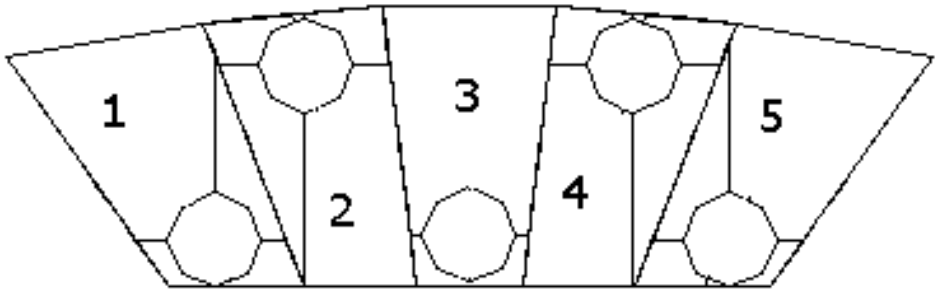

FIG. 2. Drawing of scintillator block array. The lines inside each 4-sided block show how the corresponding light guides taper to 1 in. diameter

2. Test Run

A partial assembly of the decay detector shown in Fig. 3 was used for the purpose of testing and calibration. It consists of 7 strip scintillators (4 horizontal and 3 vertical), with the vertical strips aligned

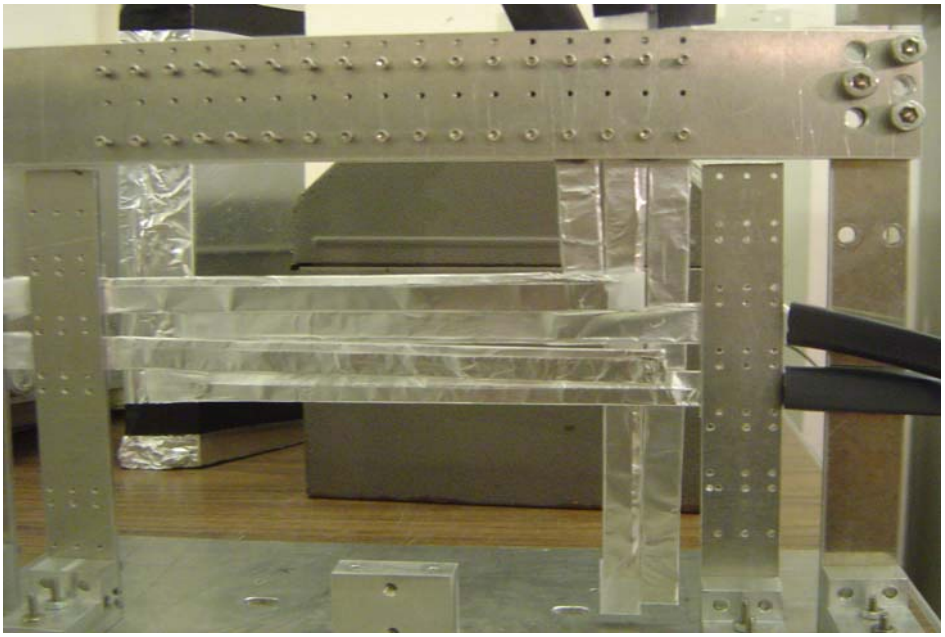

FIG. 3. Photo of partially assembled strip scintillator frame. The scintillators are wrapped in aluminum foil, and the fiber optic bundles are covered in black sheath (heat shrink tubing).

to the rightmost side relative to the beam. A single block scintillator (block 4 from Fig. 2) was used to obtain the E-signal. The block was rotated counter-clockwise so that the face nearest to the strip scintillators effectively overlapped the area of the vertically aligned strips (see Fig. 4).

FIG. 4. Photo of Single Block Scintillator, coupled to odd-shaped and cyclindrical light guides by optical cement (BC600). 1.5 mm Aluminum plate is fixed to the ion accepting side of the block scintillator.

The test run was conducted to assess the suitability of methods employed for making the optical connections between strip scintillators and optical fiber bundles, between fiber bundles and small PMTs, between block scintillators and light guides, and between light guides and large PMTs. This assessment was made by examining and comparing signal strength output from each PMT in the detector array. The optical connection between strip scintillators and fiber bundles presented the greatest concern. Attempts to bond the two parts with optical cement by clamping proved very difficult because each has a small, thin surface area (1 mm x 1 cm), and the fiber bundles are not rigid objects, and plastic scintillators are very easily damaged when subjected to physical stress. As a result, a number of strip scintillators were rendered useless prior to or during the test run. Alternative methods for making this optical bond are being investigated.

Data were taken using beams of 108 MeV α particles and 40 MeV protons on a ^{12}C target. Coincidences between 1 horizontal scintillator (ΔE1) and the block (E), between 1 vertcial scintillator (ΔE2) and the block and triple coincidences between the horizontal and vertical strips and the block were

recorded. Also, singles were collected from the three signals (ΔE1, ΔE2, E). Data for accidental coincidences (ΔE1 + E) were also collected.

During the test run, the ΔE1-E two-dimensional plot for the 40 MeV proton beam showed two overlapping regions of peak intensity along the E axis (Fig. 5), and the projections to ΔE and E axes are shown in Fig. 6. A 1.5 mm thick aluminum plate was subsequently fixed to the front of the block scintillator (Fig. 4) in order to shift these regions to the left along the E axis and yield additional information for the calibration and characterization of the scintillator light output (Table I). For NE-102, which is similar in composition to BC-408, light output is expected to be proportional to the ion range for the energies inside the range $0.5 \leq E/A \leq 15$ (MeV/amu) [4]. Protons entering the E scintillator have a minimum energy of 32 MeV. However, values obtained from this relationship are given in Table I and are in fair agreement with the data. This confirms that the two overlapping regions of peak intensity found in Fig. 5 are the result of protons passing through one ΔE strip and two ΔE strips respectively.

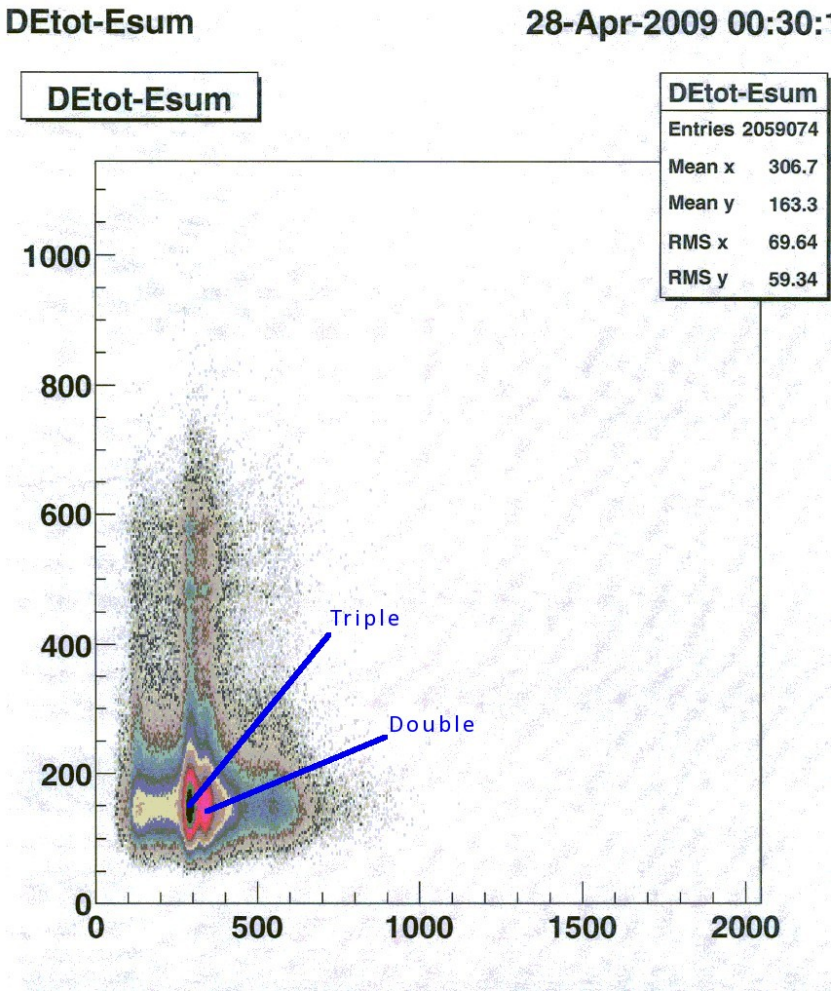

FIG. 5. Two-dimensional ΔE1 vs. E plot (both axes in arbitrary units). Aluminum plate is fixed to E block scintillator. Data are collected with the requirement that signals from ΔE1 and E coincide. "Triple" refers to region of peak intensity in plot believed to be due to protons passing through two strip scintillators before being absorbed by the block scintillator. "Double" refers to protons passing through one strip scintillator before being absorbed by the block scintillator.

TABLE I. Relative pulse height output for the E block scintillator, with and without the 1.5 mm thick aluminum plate attached, for 40 MeV protons. The expected light output is calculated by taking the light output to be proportional to the ion range in BC-408. Range data was taken from the SRIM tables[3].

40 MeV proton in E block Scintillator	Energy absorbed by block scintillator (MeV)	Ion range in BC-408 for proton energy absorbed by block scintillator	Expected relative light output difference (± 11)	Measured relative pulse height difference (± 5)
Double, No Plate	38	1.32	+36%	+45%
Triple, No Plate	36	1.20	+23%	+23%
Double, w/ Plate	34	1.08	+11%	+15%
Triple, w/ Plate	32	.97	0	0

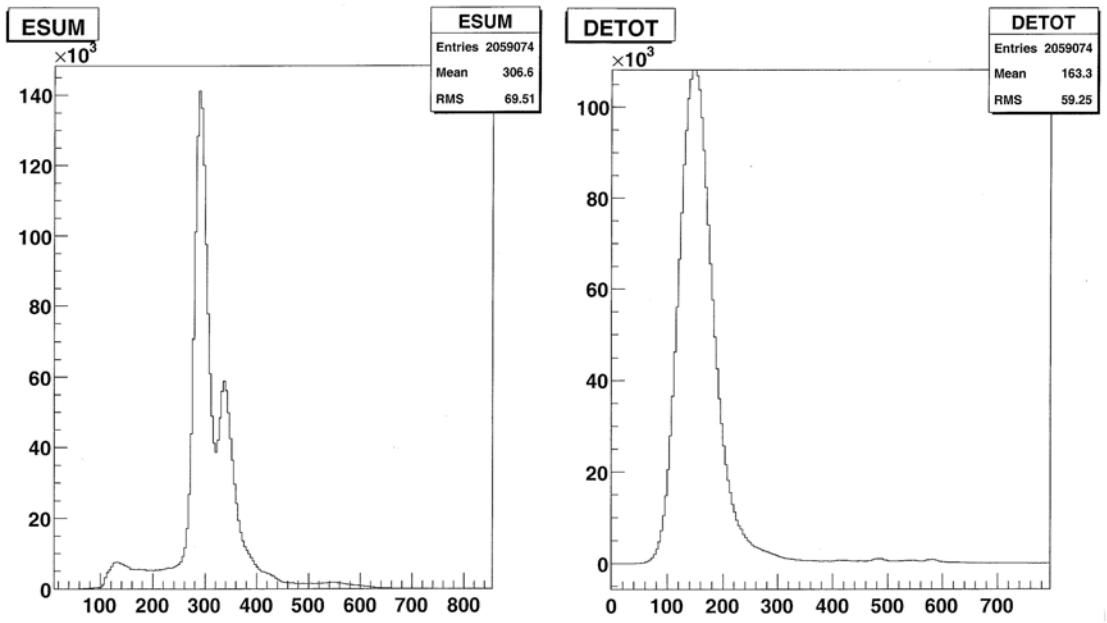

FIG. 6. The number of counts vs. light output for the block scintillator(left) and a strip scintillator (right) for 40 MeV protons incident on the detector.

3. Results

The test run demonstrated that the optical connections used to transmit light produced by the scintillator strips and block to the photomultiplier tubes are adequate. In order to complete construction of the detector array, significant improvements in the optical cement joint between the fiber bundles and strip scintillators are required.

Data analysis is ongoing and efforts are underway to make calculations of the expected light output of the scintillator detector array for incident ions of varying *Z, A*, and energy. Two methods for the calculation of relative light output of plastic scintillator when ions of a particular energy pass through or are stopped in the scintillator will be compared for suitability in calibrating light output from the experimental setup. An empirical relationship such as the Birks formula [2], which relates light output to the stopping power directly, is a convenient method because stopping power tables for energetic ions passing through matter [3] are widely available and stopping power may also be caluclated directly by the Bethe-Bloch formula [5]. However, the Birks formula becomes a hindrance when the experiment involves many ion types, since the parameters L_0 and K will vary by ion type. For this situation, models with a specific Z dependence have been proposed. One such model (Energy Deposition by Secondary Electrons) relates light output dL/dx to the number of energy carries created due to energy loss of the ion in the scintillating material [6].

[1] X. Chen, Ph.D. Thesis, Texas A&M University, 2008.

[2] J. B. Birks, Phys. Rev. **86**, 569 (1952).

[3] J. F. Ziegler, J. P. Biersack, U. Littmark, *The Stopping and Range of Ions in Solids*, (Pergamon Press, New York, 1999).

[4] F. D. Becchetti, C. E. Thorn, M. J. Levine, Nucl. Instrum. Methods Phys. Res. **138**, 93 (1976).

[5] H. Bethe, Z. Phys. **76**, 293 (1932).

[6] K. Michaelian, Nucl. Instrum. Methods Phys. Res. **A356**, 297 (1995).

Comparative study of the GEANT4, EGSnrc and PENELOPE Monte Carlo codes for efficiency calculations of a plastic scintillator

V. V. Golovko, V. E. Iacob, J. C. Hardy, and D. Melconian

The precision required when measuring the *ft*-values of superallowed β decays as a test of the unitarity of the Cabibbo-Kobayashi-Maskawa mass-mixing matrix is a demanding 0.1%. One of the crucial requirements of a branching ratio measurement to this level of precision is a detailed understanding of the response function of our β detector, specifically to determine its efficiency as a function of energy. This response function must be simulated using Monte Carlo (MC) techniques due to the unavailability of sources of monoenergetic low-energy β particles. In order to judge the reliability of our simulated response functions, we have undertaken a comparative study of three MC codes: EGSnrc [1], GEANT4 [2] and PENELOPE [3]. All three codes claim to be able to describe $e^{\pm}$ interactions with matter from low energies (1 keV, 10 keV and 0.3 keV respectively) up to > 1 GeV, well above β-decay energies. The degree to which the three codes agree can be used to estimate the reliability of our simulated response functions and calculated β efficiency. In particular, EGSnrc and GEANT4 both use multiple scattering theories which rely on a judicious use of the step size for tracking the particles and are susceptible to spurious effects which may bias the results. PENELOPE on the other hand uses a mixed algorithm which is insensitive to the choice of step size, but which is significantly more CPU-time expensive.

The first comparison of the codes used the very simple geometry depicted in Fig. 1: a point-like source of positrons was set in the center of an infinitely long thin (76 mm) Mylar tape, positioned 4.92 mm in front of a 1 mm thick disk of BC408 scintillator with a diameter of 1.5 inches. Monoenergetic positrons were emitted isotropically with energies in the range of 200 keV to 20 MeV. The efficiency for

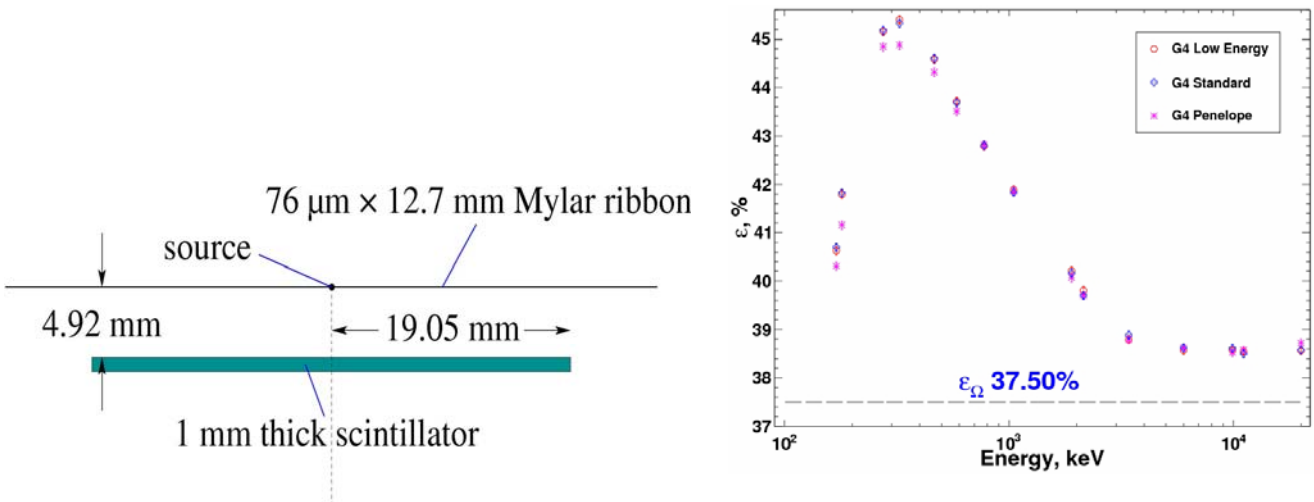

FIG. 1. Simplified geometry used in the MC simulations of the β-detector's efficiency (left) and results of a Geant4 simulations using the three different EM physics packages as compared to a purely geometrical calculation (right).

each incident energy was calculated as the ratio of the number of events where *any* energy was left in the scintillator to the total number generated. The results of GENT4 simulations using their "Low-energy", "Standard" and "Penelope" electromagnetic (EM) physics packages are shown on the right panel of Fig. 1. The geometrical efficiency was calculated as $\varepsilon = \frac{\Omega}{4\pi} = \frac{1}{2}\left(1 - \frac{D}{\sqrt{R^2 + D^2}}\right)$, where Ω is the solid angle defined by the cylindrical scintillator, *D* is the distance of the source from the front face of the scintillator, and *R* is the detector's radius. In our case, this leads to an efficiency of 37.5%. The deviation from the geometrical model is due to the effects of β scattering in the Mylar ribbon since results consistent with the geometrical efficiency were observed when the ribbon was not included in the geometry. Initially, this was a surprising effect since one might suppose that just as many positrons initially headed toward the scintillator get scattered away as those that get scattered into the direction of the scintillator. We found that the effect arises from positrons initially travelling along the plane of the Mylar ribbon; some of these events – which would not hit the scintillator if there was no Mylar foil – undergo scattering and are re-directed towards the scintillator resulting in an increased efficiency.

In Fig. 2, we show the comparison of the calculated efficiencies using GEANT4 to PENELOPE. Since EGSnrc gave results in complete agreement with PENELOPE, it is not included in this plot. One can see that the three different physics packages in GEANT4 agree with each other, but that there are

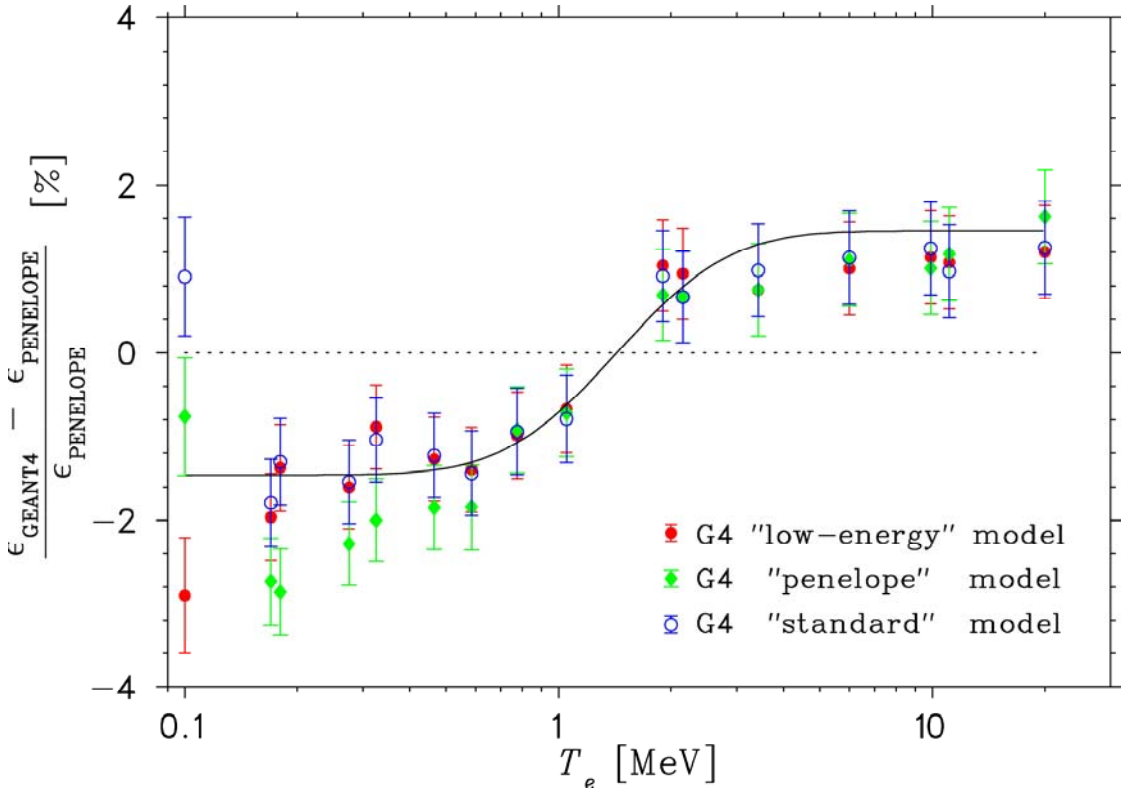

FIG. 2. The difference in scintillator efficiencies between PENELOPE and the various EM physics packages using Geant4. The EGSnrc code produced results in complete agreement with PENELOPE and so are not shown for clarity.

≈3% differences from the PENELOPE (and EGSnrc) predictions. The "Penelope" package of GEANT4, it should be pointed out, is *not* the same as PENELOPE itself because the algorithm used to describe multiple scattering remains the same regardless of which physics package is used in GEANT4. The different models used to describe multiple scattering gives rise to the small deviations observed in Fig. 2.

We have also performed simulations of the β decay of ^{207}Bi, ^{22}Na and ^{60}Co, and compared them to observed spectra where the absolute activity of the source was known to better than 1%. In all cases, agreement between the Geant4 and EGSnrc MC codes and the measured efficiency are in agreement. Simulations of these sources using PENELOPE are nearly completed, and preliminary results continue to indicate good agreement.

[1] NRCC Report PIRS701 and http://www.irs.inms.nrc.ca/inms/irs/EGSnrc/EGSnrc.html.
[2] S. Agostinelliae *et al.*, Nucl. Instrum. Methods Phys. Res. **A506**, 250 (2003).
[3] J. Sempau *et al.*, Nucl. Instrum. Methods Phys. Res. **B207**, 107 (2003).

Comparative analysis of the methods used in determination of half-life in a simple radioactive decay

V. Horvat and J. C. Hardy

Precise and accurate determination of a radioactive half-life requires specialized experimental techniques as well as careful statistical analysis of the results. This report focuses on the latter. The analysis described below was applied to a set of simulated data that resembled those obtained from our recent measurement of the ^{46}V half-life. The current world-average value for the half-life is $t_{1/2}$ = 422.50(11) ms [1]).

In the actual measurement [2], ^{46}V ions were produced in the ^{47}Ti(p,2n)^{46}V reaction by a ^{47}Ti beam from the Texas A&M K-500 cyclotron. The ejectiles passed through the MARS recoil spectrometer and, in repeated cycles, a separated beam of ^{46}V was implanted into a 76-μm-thick aluminized mylar tape for ~1s, after which the collected radioactive sample was moved in 180 ms to the center of a 4π proportional gas counter for the detection of beta particles. Signals produced by the betas were processed and then counted by a pair of multi-channel scalers over 500 consecutive time intervals (channels) for a total of 10 s. The resulting spectra typically contained about 5000 counts, with average background on the order of 0.01 per channel. In a given run, the whole process was repeated for about 800 cycles, i.e., until a total of approximately four million pulses were counted by each scaler. The number of runs exceeded 30 and the experimental conditions were deliberately altered from run to run in order to test for any systematic dependence on those conditions.

In the study reported here, simulated rather than real data were used in order to avoid dealing with the effects of dead-time corrections and to be able to determine the accuracy of the fitted results for half-life and background since, for simulated data, we know precisely what those properties are. The amount of simulated data produced and their quality was comparable to the data collected in a single actual run. Specifically, we generated 1000 cycles of 500 channels each with a total of 4,500,000 counts using the input background value of 0.01 per channel per cycle and a simple exponential decay with a half-life of exactly 422.5 ms. No dead-time effects were included.

Results from three different methods of analysis (methods 1, 2, and 3) are compared below. Each method was applied both on a cycle-by-cycle basis and to the sum of all data. The former approach will be referred to as the "cycle fit", while the latter will be referenced as the "sum fit". The equations used for both approaches are summarized in Tables 2 and 3 of Koslowsky *et al.* [3]. In method 1 of our analysis we use a simple fitting procedure aimed at minimizing χ^2 given by

$$\chi^2 = \sum_{i=1}^{N} W_i (Y_i - D_i)^2 , \qquad (1)$$

where D_i and Y_i are the experimentally determined and the theoretically expected number of events in channel i, and W_i is the statistical weight of the i-th term, which in the present application equals the reciprocal value of Y_i. N is the total number of channels.

Method 2 is similar to method 1, except that W_i is assumed to equal 1 for all i. This method is often referred to as unweighted regression and it is the default method of analysis in the most common general-purpose spreadsheet programs such as Microsoft's Excel™ and SPSS' SigmaPlot™.

Method 3, on the other hand, uses a maximum likelihood approach. It involves maximization of the probability that the measured spectrum is a representation of the fitting function. Since the data follow Poisson statistics, this probability, which in this application is known as the maximum likelihood estimator, is given by

$$L = \prod_{i=1}^{N} \frac{e^{-Y_i} Y_i^{D_i}}{D_i!} . \qquad (2)$$

As shown in Table I, all three methods reproduced the correct value for the half-life using a sum fit approach. Compared to the other two methods, method 3 was slightly more accurate. Regarding the background, method 2 underestimates the input value by many of its reported standard deviations, while method 1 overestimates the expected result by nearly two of its. Method 3 produced the most accurate result, well within its reported error bar of the input value. The background error for method 3 is the largest among the three methods, but only by a small margin. For illustration purposes, the sum spectrum of the simulated data is shown in Fig. 1 along with curves representing the fitted results from method 3.

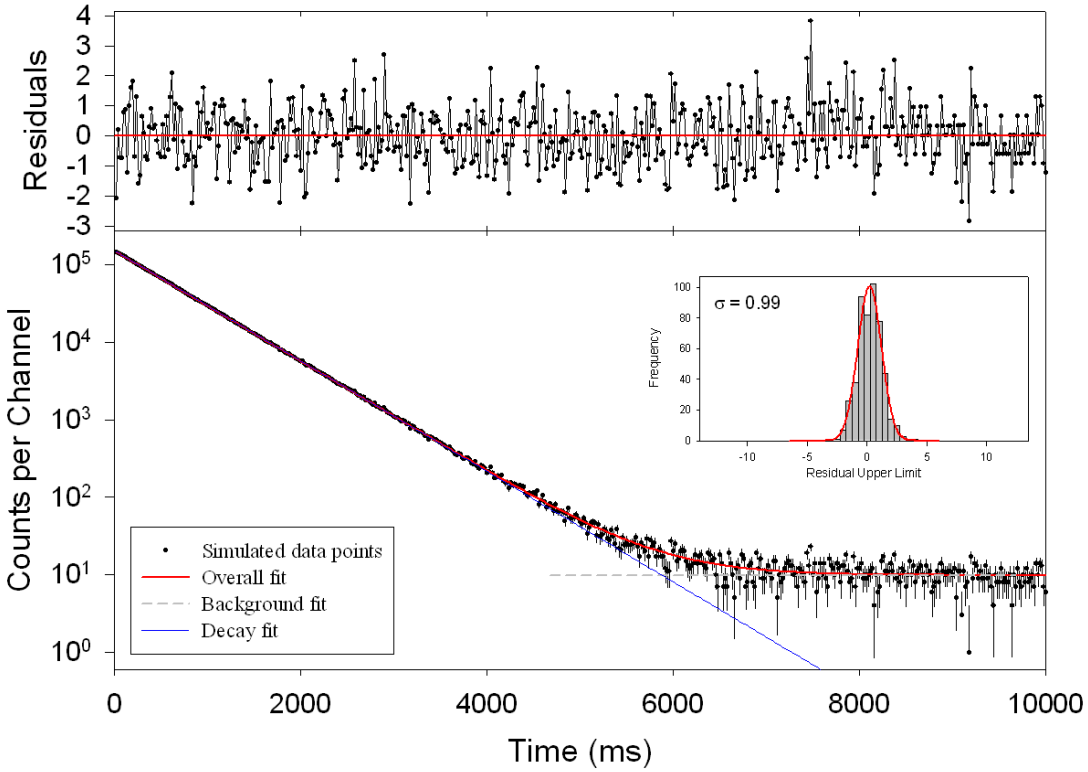

FIG. 1. Sum spectrum of the simulated data and the curves representing the fits with method 3 as described in the text.

Table I. Results of the sum-fit approach for the three methods described in the text applied to a set of simulated data with half-life 422.5s and a background of 10 counts per channel (in 1000 cycles).

Method	Half-life (ms)	Background per channel
1	422.41 ± 0.20	10.37 ± 0.20
2	422.68 ± 0.20	7.65 ± 0.15
3	422.42 ± 0.20	9.89 ± 0.22

Table II shows that in the cycle-fit approach method 1 produces completely erroneous results both for the background and the half-life. This can be traced to the fact that, in this method of fitting, the χ^2 [eq.(1)] can be reduced in two ways: either by a reduction in the absolute differences between the data points and their predicted values – the desired mechanism – or by a reduction in the statistical weights W_i (= 1 / Y_i), which tends to drive Y_i to higher, incorrect values. Of the other two methods, method 3 results in more accurate and more precise values of both the half-life and background compared to method 2.

Table II. Results of the cycle-fit approach for the three methods described in the text applied to a set of simulated data with half-life 422.5s and a background of 10 counts per channel (in 1000 cycles)

Method	Half-life (ms)	Background per channel
1	437.12 ± 0.25	124.7 ± 1.3
2	422.75 ± 0.37	7.8 ± 2.5
3	422.36 ± 0.19	9.95 ± 0.22

Since method 3 was found to be superior to the other two methods, it was also applied to a "global-fit" procedure [3], which is, in fact, a cycle-fit with a common value of the half-life that applies to all cycles. The resulting half-life value was 422.55(21) ms, which is accurate to about one part in 10,000, but the size of the error bar suggests that a result this good is just accidental. The error bar, apparently, was not reduced compared to that obtained in either the cycle fit or the sum fit. All three are effectively the same.

[1] J. C. Hardy and I. S. Towner, Phys. Rev. C **79**, 055502 (2009).

[2] H. I. Park, J. C. Hardy, V. E. Iacob, J. Goodwin, V Horvat, N. Nica, E. Simmons, L. Trache and R. E. Tribble, *Progress in Research*, Cyclotron Institute, Texas A&M University (2008-2009), p. XXX.
[3] W. T. Koslowsky, E. Hagberg, J. C. Hardy, G. Savard, H. Schmeing, K. S. Sharma, and X. J. Sun, Nucl. Instrum. Methods Phys. Res. **A401**, 289 (1997).

Upgrade of data-acquisition system for measuring β-decay half-lives

V. E. Iacob and J. C. Hardy

We require a precision of better than 0.1% in half-life measurements for the superallowed emitters we use to test the Standard Model *via* the unitarity of the Cabibbo-Kobayashi-Maskawa (CKM) matrix. This requires extreme care both in data acquisition and in the subsequent analysis. We have added a new feature to our data acquisition that allows us to record the time profile of the deposited activity for every cycle.

The β^+ emitters that we study are typically produced by a heavy-ion beam from the superconducting cyclotron impinging on a cryogenic hydrogen gas target kept at two atmospheres pressure. The ejectiles recoiling from the target pass through the MARS spectrometer, from which a pure beam of a single selected isotope is extracted into air, passed through a 0.3-mm-thick plastic scintillator as well as Al degraders, and eventually implanted in a 76-μm-thick mylar tape. We measure the half-life in a computer-controlled cyclic mode: First the radioactive sample is implanted in the tape (for up to about two half-lives); then the beam is turned off and the tape moved (in less than 0.2 s) so the activity is placed in the center of a proportional gas counter; finally the decay is multiscaled (for up to 20 parent half-lives). This cycle is repeated continuously until the desired statistics have been acquired.

One precision-limiting problem occurs in the decays of beta emitters which populate nuclei that are themselves radioactive with a similar half-life. This applies to the cases of ^{34}Ar [1] and ^{26}Si [2]. For such nuclei, the optimum precision for the parent half-life is achieved in a constrained fit of the combined parent and daughter decays, in which the total daughter activity is fixed relative to the activity of the parent. To determine this fixed ratio it is necessary to account for the decay of the parent – and consequent production of the daughter – which occurs during the sample-collection period, before the detection and multiscaling begins. The method used is described in more detail in [1]. A key requirement is that one must know the implantation history of the radioactive ions as well as the exact time it takes to transport the radioactive sample to the detector position.

While in a first approximation the intensity of the implantation beam can be considered constant in time, we have determined [1] that this is not exactly true. Because of local warming of the hydrogen-target gas on the beam path, and the associated lowering in gas density, we observe a drop in the radioactive beam intensity during approximately the first 0.1 s after the primary cyclotron beam is turned on and a partial recovery towards a quasi-constant value after another 0.1 s (see Fig. 8 in [1]). The magnitude of this fluctuation depends on the intensity of the cyclotron beam in the gas cell, which can change during an experiment from time to time.

Previously we have measured the beam time-profile in a separate experiment from the half-life measurement. However, to improve our control over this important parameter, we have added to our standard detection system (as described in [1]) the capability to measure the beam profile in each cycle. In the upgraded acquisition system we now record in each cycle three spectra: a beam profile and two time-decay spectra (associated to the two electronic chains processing the gas-counter signals). This is

done with a CMC206 universal logic module [3], programmed as a multiscaler module able to count three independent signals. Previously we only had two multiscaler channels available.

As with all precision measurements, consistency is a key factor. In our first test measurement, the new multichannel scaler CMC206 was included in our acquisition system in parallel with the "old" DDC-IS10A multiscalers (already verified in our previous measurements) and tested with standard ^{90}Sr sources (~1.0 and ~0.1 μCi). No discrepancies were identified. The same arrangement was then used in the study of ^{26}Si decay described elsewhere in this report [2]. Once again there were no discrepancies between the CMC and DDC multiscaler data. We now consider the new system to be fully commissioned and verified.

[1] V. E. Iacob, J. C. Hardy, J. F. Brinkley, C. A. Gagliardi, V. E. Mayes, N. Nica, M. Sanchez-Vega, G. Tabacaru, L. Trache, and R. E. Tribble, Phys. Rev. C **74**, 055502 (2006).

[2] V.E. Iacob *et al., Progress in Research,* Cyclotron Institute, Texas A&M University (2008-2009), p.I-XXXXXX "*^{26}Si half-life measurement"* in this progress report.XXXXX

[3] http://www.cmcamac.com/

JBN new cluster computing system

R. Wada, M. Huang, R. Burch, and K. Hagel

A new cluster computing system has been developed to be used primarily for theoretical simulations. The system consists of 16 1U rack mount PC's, mounted on one rack as shown in Fig. 1. Each PC has an Intel Core i7 920 CPU operated at 3.5GHz with 6GB memory. The CPU chips are cooled by water. This CPU has quadrant cores. Each core can be operated by Intel Hyper-Threading technology and the number of virtual cores can be eight (at the expense of a 30% slower process speed.) Therefore the system consists of 128 virtual CPU's. All jobs can be controlled by the Condor operating system in Scientific Linux SL 5.3. Each PC is booted through the network and no hard disk or optical driver is installed. Since the system is made for theoretical model simulations, such as those using the AMD transport model, no high data transfer rate job is supported at present.

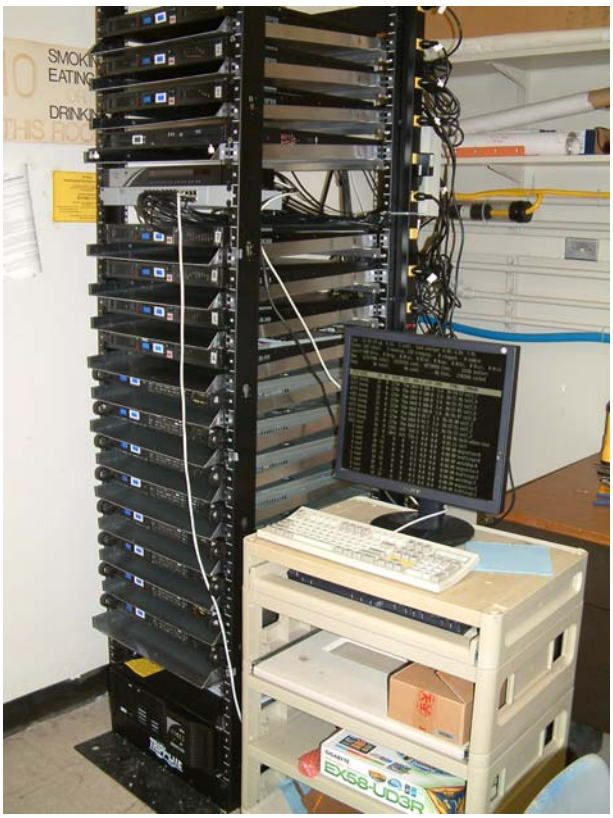

FIG. 1. A new cluster computing system

In order to evaluate the job process speed, an AMD-V job was submitted and the speed was compared to that of the existing newest PC of our group and that in the Riken Super Computer System. The job submitted was a simulation for central collisions for $^{64}Zn+^{58}Ni$ at 40A MeV. More than 100 events were generated in each case. The CPU process times required are shown in Table I.

Table I. Comparison for job process speed. The present Riken system was installed in 2003 and is scheduled to be up graded this summer. CPU times given are at full load, that is, for the new cluster, 8 jobs in each CPU.

	New cluster	JBN Group	Riken
CPU	Core i7 920 @ 3.5GHz	Xeon X5460 @ 3.1GHz	Xeon @ 2.66GHz
CPU time/event	1.5h	1.8h	4.2h

SECTION VI

PUBLICATIONS

PAPERS PUBLISHED
April 1, 2008 – March 31, 2009

Giant resonances in ^{116}Sn from 240 MeV ^{6}Li scattering, X. Chen, Y.-W. Lui, H.L. Clark, Y. Tokimoto, and D.H. Youngblood, Phys. Rev. C **79**, 024320 (2009).

Astrophysical S factor for the radiative capture ^{12}N(p,γ)^{13}O determined from the ^{14}N(^{12}N,^{13}O)^{13}C proton transfer reaction, A. Banu, T. Al-Abdullah, C. Fu, C.A. Gagliardi, R.E. Tribble, Y. Zhai, F. Carstoiu, V. Burjan, and V. Kroha, Phys Rev C **79**, 025805 (2009).

A new astrophysical S factor for the ^{15}N(p,γ)^{16}O reaction via the ANC method, A.M. Mukhamedzhanov, P. Bem, V. Burjan, C.A. Gagliardi, Z. Hons, M. La Cognata, V. Kroha, J. Mrazek, J. Novak, S. Piskor, R.G. Pizzone, A. Plunkett, S. Romano, E. Simeckova, C. Spitaleri, L. Trache, R.E. Tribble, F. Vesely, and J. Vincour, Phys. Rev. C **78**, 015804 (2008).

Performance evaluation of novel square-bordered position-sensitive silicon detectors with four-corner readout, A. Banu, Y. Li, M. McCleskey, M. Bullough, S. Walsh, C.A. Gagliardi, L. Trache, R.E. Tribble, and C. Wilburn, Nucl. Instrum. Methods Phys. Res. **A593**, 399 (2008).

First observation of a cluster states in the ^{14}O + ^{4}He interaction, Changbo Fu. V.Z. Golderg, G.V. Rogachev, G. Tabacaru, G.G. Chubarian, B. Skorodumov, M. McClesky, Y. Zhai, T. Al-Abdullah, L. Trache, and R.E. Tribble, Phys. Rev. C **77**, 064314 (2008).

Precise half-life measurement of the superallowed β^+ emitter ^{10}C, V.E. Iacob, J.C. Hardy, V. Golovko, J. Goodwin, N. Nica, H.I. Park, L. Trache, and R.E. Tribble, Phys. Rev. C **77**, 045501 (2008).

Correlated two-proton decay from ^{10}C, K. Mercurio, R.J. Charity, R. Shane, L.G. Sobotka, J.M. Elson, M. Famiano, A.H. Wousmaa, A. Banu, C. Fu, L. Trache, R.E. Tribble, and A.M. Mukhamedzhanov, Phys. Rev. C **78**, 032801 (2008).

Measurement of the 20 and 90 keV resonances in the ^{18}O(p,α)^{15}N reaction via THM, M. La Cognata, C. Spitaleri, A.M Mukhamedzhanov, B. Irgaziev, R.E. Tribble, A. Banu, S. Cherubini, A. Coc, V. Crucilla, V. Goldber, Mu. Gulino, G.G. Kiss, L. Lamia, J. Mrazek, R.G. Pizzone, S.M.R. Puglia, G.G. Rapisarda, S. Romano, M.L. Sergi, G. Tabacaru, L. Trache, W. Trzaska, and A. Tumino, Phys. Rev. Lett. **101**, 152501 (2008).

Q_{EC} values of the superallowed β emitters ^{50}Mn and ^{54}Co, T. Eronen, V.-V Elomaa, U. Hager, J. Hakala, J.C. Hardy, A. Jokinen, A. Kankainen, I.D. Moore, H. Pentilla, S. Rahaman, S. Rinta-Antila, J. Rissanen, A. Saastamoinen, T. Sonoda, C. Weber and J. Aysto**,** Phys. Rev. Lett. **100**, 132502 (2008).

Precise tests of the internal-conversion theory, J.C. Hardy, N. Nica, V.E. Iacob, C. Balonek and M.B. Trzhaskovskaya, Appl. Radiat. Isot. **66**, 701 (2008).

The use of GEANT4 for simulations of a plastic β-detector and its application to efficiency calibration, V.V. Golovko, V.E. Iacob and J.C. Hardy, Nucl. Instrum. Methods Phys. Res. **A594**, 266 (2008).

New calculations of the isospin-symmetry-breaking correction to superallowed Fermi beta decay, I.S. Towner and J.C. Hardy in *Rare Isotopes and Fundamental Symmetries*, Proceedings from the Institute for Nuclear Theory Vol. **16**, (World Scientific, Singapore, 2009) p. 51.

Superallowed nuclear beta decay: recent results and their ampact on V_{ud}, J.C. Hardy and I.S. Towner in *Rare Isotopes and Fundamental Symmetries*, Proceedings from the Institute for Nuclear Theory Vol. **16**, (World Scientific, Singapore, 2009) p. 41.

Probing the standard model with superallowed nuclear beta decay, J.C. Hardy and I.S. Towner in *Karlsruher Nuklidkarte: Commemoration of the 50th Anniversary*, edited by G. Pfennig, C. Normand, J. Magill and T. Fanghanel (Publications of the European Communities, Luxembourg, 2008) p. 116.

Superallowed beta decay: the role of nuclear structure in standard-model tests, J.C. Hardy and I.S. Towner**,** Acta Physica Polonica B **40**, 675 (2009).

Photodisintegration of 80Se: implications for the s-process branching at 79Se, A. Makinaga, H. Utsunomiya, S. GGoriely, T. Kaihori, S. Goko, H. Akimune, T.Yamagata, H. Toyokawa, T.Matsumoto, H. Harano, H. Harada, F. Kitatani, Y.K. Hara, S. Hohara, and Y.-W. Lui, Phys. Rev. C **79**, 025801 (2009).

M1 γ strength for Zicronium nuclei in the photoneutron channel, H. Utsunomiya, S. Goriely, T. Kono, T. Kaihori, A. Makinaga, S. Goko, H. Akimune, T. Yamagata, H. Toyokawa, T. Matsumoto, H. Harano, S. Hohara, Y.-W. Lui, S. Hilaire, S. Peru, and A.J. Koning, Phys. Rev. Lett. **100**, 162502 (2008).

T = 3/2 states in ^{13}C, B.B. Skorodumov, G.V. Rogachev, A. Aprahamian, V.Z. Goldberg, J.J. Kolata, S.Almaraz, H. Amro, E.D. Johnson, L.O. Lamm, M. Quinn, A. Teymurazyan, and A. Woehr Phys.Rev. C **78**, 044603 (2008).

Search for the Pygmy dipole resonance in ^{68}Ni at 600 MeV/nucleon, O. Wieland, A. Bracco, F. Camera, G. Benzoni, N. Blasi, S. Brambilla, F.C.L. Crespi, S. Leoni, B. Million, R. Nicolini, A. Maj, P. Bednarczyk, J. Grebosz, M. Kmiecik, W. Meczynski, J. Styczen, and T. Aumann, Phys. Rev. Lett. **102**, 092502 (2009).

Tensor interaction constraints from β decay recoil spin asymmetry of trapped atoms ,J.R.A. Pitcairn, D. Roberge, A. Gorelov, D. Ashery, O. Aviv, J.A. Behr, P.G. Bricault, M. Dombsky, J.D. Holt, K.P. Jackson, B. Lee, M.R. Pearson, A. Gaudin, B. Dej, C. Höhr, G. Gwinner, and D. Melconian, Phys. Rev. C **79**, 015501 (2009).

First measurement of the neutron asymmetry with ultracold neutrons, R.W. Pattie, Jr., J. Anaya, H.O. Back, J.G. Boissevain, T.J. Bowles, L.J. Broussard, R. Carr, D.J. Clark, S. Currie, S. Du, B.W. Filippone, P. Geltenbort, A. García, A. Hawari, K.P. Hickerson,5 R. Hill, M. Hino, S.A. Hoedl, G.E. Hogan, A.T. Holley, T.M. Ito, T. Kawai, K. Kirch, S. Kitagaki, S.K. Lamoreaux, C.-Y. Liu, J. Liu, M. Makela, R.R. Mammei, J.W. Martin, D. Melconian, N. Meier, M.P. Mendenhall, C.L. Morris, R. Mortensen, A. Pichlmaier, M.L. Pitt, B. Plaster, J.C. Ramsey, R. Rios, K. Sabourov, A.L. Sallaska, A. Saunders, R. Schmid, S. Seestrom, C. Servicky, S.K.L. Sjue, D. Smith, W.E. Sondheim, E. Tatar, W. Teasdale, C. Terai, B. Tipton, M. Utsuro, R.B. Vogelaar, B.W. Wehring, Y.P. Xu, A.R. Young, and J. Yuan, Phys. Rev. Letts. **102**, 012301 (2009).

Electron-capture branch of ^{100}Tc and tests of nuclear wave functions for double-β decays, S.K.L. Sjue, D. Melconian, A. García, I. Ahmad, A. Algora, J. Äystö, V.-V. Elomaa, T. Eronen, J. Hakala, S. Hoedl, A. Kankainen, T. Kessler, I.D. Moore, F. Naab, H. Penttilä, S. Rahaman, A. Saastamoinen, H.E. Swanson, C. Weber, S. Triambak, and K. Deryckx, Phys. Rev. C **78**, 064317 (2008).

***ft* value of the $0^+ \rightarrow 0^+$ β decay of ^{32}Ar: A measurement of isospin symmetry breaking in a superallowed decay**, M. Bhattacharya, D. Melconian, A. Komives, S. Triambak, A. García, E.G. Adelberger, B.A. Brown, M.W. Cooper, T. Glasmacher, V. Guimaraes, P.F. Mantica, A.M. Oros-Peusquens, J.I. Prisciandaro, M. Steiner, H.E. Swanson, S.L. Tabor, and M. Wiedeking, Phys. Rev. C **77**, 065503 (2008).

Neutron-rich rare isotope production in the Fermi energy domain and application to the Texas A&M radioactive beam upgrade, G.A. Souliotis, B. Stein, M. Veselsky, S. Galanopoulos, A.L. Keksis, Z. Kohley, D.V. Shetty, S.N. Soisson, S. Wuenschel, and S.J. Yennello. Nucl. Instrum. Methods Phys. Res. **B266**, 4692 (2008).

Effective nucleon mass and the nuclear caloric curve, D.V. Shetty, G.A. Souliotis, S. Galanopoulos, and S.J. Yennello, Phys. Rev. C **79**, 034603 (2009).

Nuclear Expansion and Symmetry Energy of Hot Nuclei, D.V. Shetty, G.A. Souliotis, S. Galanopoulos,Z. Kohley, S.N. Soisson, B.C. Stein, S. Wuenschel, and S.J. Yennello. J. Phys. G **36**, 075103 (2008).

How Stable are the Heaviest Nuclei, J.B. Natowitz, Physics **1**, 12 (2008).

Effect of medium dependent binding energies on inferring the temperatures and freeze-out density of disassembling hot nuclear matter from cluster yields, S. Shlomo, G. Röpke, J.B. Natowitz, L. Qin, K. Hagel, R. Wada, and A. Bonasera., Phys. Rev. C **79**, 034604 (2009).

The quantum nature of a nuclear phase transition, A. Bonasera, Z. Chen, R. Wada, K. Hagel, J.B. Natowitz, P. Sahu, L. Qin, S. Kowalski, T. Keutgen, T. Materna, and T. Nakagawa, Phys. Rev. Lett .**101** (2008) 122702.

Soft fragmentation of carbon monoxide by slow highly charged ions, E. Wells, T. Nishede, H. Tawara, R.L. Watson, K.D. Carnes, and I. Ben-Itzhak, Phys. Rev. A **77**, 064701 (2008).

Kα x-ray satellite and hypersatellite spectra of vanadium metal and oxides excited in heavy-ion collisions, R.L. Watson, V. Horvat, and Y. Peng, Phys. Rev. A **78**, 062702 (2008).

rp process and masses of N ≈ Z ≈ 34 nuclides, J. Savory, P. Schury, C. Bachelet, M. Block, G. Bollen, M. Facina, C.M. Folden III, C. Guénaut, E. Kwan, A.A. Kwiatkowski, D.J. Morrissey, G.K. Pang, A. Prinke, R. Ringle, H. Schatz, S. Schwarz, and C.S. Sumithrarachchi, Phys. Rev. Lett. **102**, 132501 (2009).

Measurement of the ^{208}Pb(^{52}Cr, n)^{259}Sg excitation function, C.M. Folden III, I. Dragojević, Ch.E. Düllmann, R. Eichler, M.A. Garcia, J.M. Gates, S. L. Nelson, R. Sudowe, K.E. Gregorich, D.C. Hoffman, and H. Nitsche, Phys. Rev. C **79**, 027602 (2009).

Charged particle transport and extraction studies in the NSCL gas cell for stopping radioactive fragments, M. Facina, C. Bachelet, M. Block, G. Bollen, D. Davies, C.M. Folden III, C. Guenaut, J. Huikari, E. Kwan, D.J. Morrissey, G.K. Pang, A. Prinke, R. Ringle, J. Savory, P. Schury, S. Schwarz, C. Sumithrarachchi, and T. Sun, Nucl. Instrum. Methods Phys. Res. **B266**, 4471 (2008).

Mass measurements of rare isotopes with the LEBIT facility at the NSCL, M. Block, C. Bachelet, G. Bollen, M. Facina, C.M. Folden III, C. Guénaut, A.A. Kwiatkowski, D.J. Morrissey, G.K. Pang, A. Prinke, R. Ringle, J. Savory, P. Schury, and S. Schwarz, Nucl. Instrum. Methods Phys. Res. **B266**, 4521 (2008).

Comparison of reactions for the production of ^{258,257}Db: ^{208}Pb(^{51}V,xn) and ^{209}Bi(^{50}Ti,xn), J.M. Gates, S.L. Nelson, K.E. Gregorich, I. Dragojević, Ch.E. Düllmann, P.A. Ellison, C.M. Folden III, M.A. Garcia, L. Stavsetra, R. Sudowe, D.C. Hoffman, and H. Nitsche, Phys. Rev. C **78**, 034604 (2008).

Comparison of complementary reactions for the production of ^{261,262}Bh, S.L. Nelson, C.M. Folden III, K.E. Gregorich, I. Dragojević, Ch.E. Düllmann, R. Eichler, M.A. Garcia, J.M. Gates, R. Sudowe, and H. Nitsche, Phys. Rev. C **78**, 024606 (2008).

Kα satellite and hypersatellite distributions of Ar excited in heavy-ion collisions, V. Horvat, R.L. Watson, and Y. Peng, Phys. Rev. A **79**, 012708 (2009).

Off-energy-shell p-p scattering at sub-Coulomb energies via the Trojan horse method, A. Tumino, C. Spitaleri , A.M. Mukhamedzhanov , G.G. Rapisarda, L. Campajola , S. Cherubini, S. Crucilla, Z. Elekes , Z. Fulop, M. Gulino , G. Gyurky, G. Kiss, M. La Cognata, L. Lamia, A. Ordine , R.G. Pizzone, S. Romano, M.L. Sergi , and E. Somorjai, Phys. Rev. C **78**, 064001 (2008).

Coulomb breakup problem, A.S. Kadyrov, I. Bray, A.M. Mukhamedzhanov, and A.T. Stelbovics, Phys. Rev. Lett., **101**, 230405 (2008).

Completeness of the Coulomb scattering wave functions, A.M. Mukhamedzhanov and M. Akin, Eur. Phys. J. A **37**, 185 (2008).

Benchmark on neutron capture extracted from (d,p) reactions, A.M. Mukhamedzhanov, F.M. Nunes and P. Mohr, Phys. Rev. C **77**, 051601(R) (2008).

Zero-point oscillations and nuclear charge radii, Tapas Sil and S. Shlomo, Physica Scripta **76**, 065202 (2008).

Mean-field approximation for finite nuclei and nuclear matter, S. Shlomo, Nucl. Phys. At. Energy **9**, #3 (25), 7 (2008).

Nucleon and Δ resonances in KΣ(1385) photoproduction from nucleons, Y. Oh, C.M. Ko, and K. Nakayama, Phys. Rev. C **77**, 045204 (2008).

Heavy ion collisions at LHC - last call for predictions, S.A. Abreu *et al.*, and C.M. Ko, J. Phys. G **35**, 05400 (2008).

Determining the density dependence of the nuclear symmetry energy using heavy ion collisions, L.W. Chen, C.M. Ko, B.A. Li, and G.C. Yong, Int. J. Mod. Phys. **17**, 1825 (2008).

Λ_c enhancement from the strongly coupled quark-gluon plasma, S.H. Lee, K. Ohnishi, S. Yasui, I.K. Yoo, and C.M. Ko, Phys. Rev. Lett. **100**, 222301 (2008).

Studying diquark structure of heavy baryons in relativistic heavy ion collisions, S. Yasui, S.H. Lee, K. Ohinishi, I.K. Yoo, and C.M. Ko, Mod. Phys. Lett. A **23**, 27 (2008).

Recent progress and new challenges in isospin physics with heavy-ion reactions, B.A. Li, L.W. Chen, and C.M. Ko, Phys. Rep. **464**, 113 (2008).

Ratios of heavy baryons to heavy mesons in relativistic nucleus-nucleus collisions, Y. Oh, C.M. Ko, S.H. Lee, and S. Yasui, Phys. Rev. C **79**, 044905 (2009).

Cross-sections and beam asymmetries for $K^+\Sigma^*$ - photoproduction from the deuteron at E_γ =1.5 – 2.4Gev, K. Hicks *et al.* (for LEPS Collaboration), Phys. Rev. Lett. **102**, 012501 (2009).

Electromagnetic probes at RHIC-II, G. David, R. Rapp, and Z. Xu, Phys. Rep. **462**, 176 (2008).

Nonperturbative heavy-quark diffusion in the quark-gluon plasma, H. van Hees, M. Mannarelli, V. Greco, and R. Rapp, Phys. Rev. Lett. **100**, 192301 (2008).

Heavy-ion collisions at the LHC – last call for predictions, S. Abreu *et al.*, J. Phys. G **35**, 054001 (2008).

Dilepton radiation at the CERN super proton synchrotron, H. van Hees and R. Rapp, Nucl. Phys. **A806**, 339 (2008).

Transverse momentum spectra of J/psi in heavy-ion collisions, X. Zhao and R. Rapp, Phys. Lett. B **664**, 253 (2008).

Heavy ion collisions at the LHC - last call for predictions, N. Armesto *et al.*, J. Phys. G **35**, 054001 (2008).

Photon bremsstrahlung and diffusive broadening of a hard jet, A. Majumder, R.J. Fries, and B. Muller, Phys. Rev. C **77**, 065209 (2008).

Quark and gluon degrees of freedom in high-energy heavy ion collisions, R.J. Fries, Nucl. Phys. **A805**, 242 (2008).

Probing nuclear matter with jet conversions, W. Liu and R.J. Fries, Phys. Rev. C **77**, 054902 (2008).

Heavy quark production from jet conversions in a quark-gluon plasma, W. Liu and R.J Fries, Phys. Rev. C **78**, 037902 (2008).

Decoherence and entropy production in relativistic nuclear collisions, Rainer J. Fries, Berndt Muller, and Andreas Schafer, Phys. Rev. C **79**, 034904 (2009).

Stress tensor and bulk viscosity in relativistic nuclear collisions, Rainer J. Fries, Berndt Muller, and Andreas Schafer, Phys. Rev. C **78**, 034913 (2008).

Coalescence models for hadron formation from quark gluon plasma, Rainer J. Fries, Vincenzo Greco and Paul Sorensen, Ann. Rev. Nucl. Part. Sci. **58**, 177 (2008).

Observation of two-source interference in the photoproduction reaction AuAu→AuAuρ^0, B.I. Abelev *et al*. (Star Collaboration), Phys. Rev. Lett. **102**, 112301 (2009).

Systematic measurements of identified particle spectra in *pp*, *d*+Au and Au+Au collisions at the STAR detector, B.I. Abelev *et al*. (STAR Collaboration), Phys. Rev. C **79**, 034909 (2009).

Beam-energy and system-size dependence of dynamical net charge fluctuations, B.I. Abelev *et al*. (Star Collaboration), Phys. Rev. C **79**, 024906 (2009).

System-size independence of directed flow at the Relativistic Heavy-Ion Collider, B.I. Abelev *et al*. (Star Collaboration), Phys. Rev. Lett. **101**, 252301 (2008).

A precision measurement of the muon decay parameter ρ and δ, R.P. McDonal, R. Bayes, J. Bueno, Yu.I Davydov, P. Depommier, W. Faszer, M.C. Fujiwara, C.A. Gagliardi, A. Gaponenko, D.R. Gill, A. Grossheim, P. Gumplinger, M.D. Hasinoff, R.S. Henderson, A. Hillairet, J. Hu, B. Jamieson, P. Kitching, D.D. Koetke, G.M. Marshall, E.L. Mathie, R.E. Mischke, J.R. Musser, M. Nozar, K. Olchanski, A. Olin, R. Openshaw, J.-M. Poutissou, R. Poutissou, M.A. Quraan, V. Selivanov, G. Sheffer, B. Shin, T.D.S. Stanislaus, R. Tacik, R.E. Tribble, Phys. Rev. D **78**, 032010 (2008).

Indications of conical emission of charged hadrons at RHIC, B.I. Abelev *et al*. (STAR Collaboration), Phys. Rev. Lett. **102**, 052302 (2009).

Spin alignment measurements of the K*^{0}(892) and ϕ(1020) vector meson in heavy ion collisions at $\sqrt{s_{NN}}$ = 200 GeV, B.I. Abelev *et al*. (STAR Collaboration), Phys. Rev. C **77**, 061902R (2008).

Forward neutral pion transverse single spin asymmetries in p+p collisions at $\sqrt{s_{NN}}$ = 200 GeV, B.I. Abelev *et al*. (STAR Collaboration), Phys. Rev. Lett. **101**, 222001 (2008).

Hadronic resonance production in d+Au collisions at 200 GeV at RHIC $\sqrt{s_{NN}}$ = 200 GeV, B.I. Abelev *et al*. (STAR Collaboration), Phys. Rev. C **78**, 044906 (2008).

Centrality dependence of charged hadron and strange hadron elliptic flow form $\sqrt{s_{NN}}$ = 200 GeV Au+Au collissions, B.I. Abelev *et al*. (STAR Collaboration), Phys. Rev. C **77**, 054901 (2008).

Longitudinal double-spin asymmetry for inclusive jet production in $\vec{p}+\vec{p}$ collisions at $\sqrt{s_{NN}}$ = 200 GeV, B.I. Abelev *et al*. (STAR Collaboration), Phys. Rev. Lett. **100**, 232003 (2008).

Enhanced strange baryon production Au+Au collisions compared to *p*+*p* at $\sqrt{s_{NN}}$ = 200 GeV, B.I. Abelev *et al*. (STAR Collaboration), Phys. Rev. C **77**, 044908 (2008).

Energy and system size dependence of phi meson production in Cu+Cu and Au+Au collisions, B.I. Abelev *et al.* (STAR Collaboration), Phys. Lett. B **673**, 183 (2009).

Charged hadron multiplicity fluctuations in Au+Au and Cu+Cu collisions from $\sqrt{(s_{NN})}$ = 22.5 to 200 GeV, A. Adare *et al.* (PHENIX Collaboration), Phys. Rev. C **78**, 044902 (2008).

Dilepton mass spectra in p+p collisions at $\sqrt{s}$ = 200 GeV and the contribution from open charm, A. Adare *et al.* (PHENIX Collaboration), Phys. Lett. B **670**, 313 (2009).

J/ψ production in $\sqrt{(s_{NN})}$ = 200 GeV Cu+Cu Collisions, A. Adare *et al*. (PHENIX Collaboration), Phys. Rev. Lett. **101**, 122301 (2008).

Quantitative constraints on the opacity of hot partonic matter from semi-inclusive single high transverse momentum pion suppression in Au+Au collisions at $\sqrt{(s_{NN})}$ = 200 GeV, A. Adare *et al*. (PHENIX Collaboration), Phys. Rev. C **77**, 064907 (2008).

Suppression pattern of neutral pions at high transverse momentum in Au + Au collisions at $\sqrt{(s_{NN})}$ = 200 GeV and constraints on medium transport coefficients, A. Adare *et al*. (PHENIX Collaboration), Phys. Rev. Lett. **101**, 232301 (2008).

Dihadron azimuthal correlations in Au+Au collisions at $\sqrt{(s_{NN})}$ = 200 GeV, A. Adare *et al*. (PHENIX Collaboration), Phys. Rev. C **78**, 014901 (2008).

Onset of π^0 Suppression Studied in Cu+Cu Collisions at $\sqrt{(s_{NN})}$ = 22.4, 62.4, and 200 GeV, A. Adare *et al*. (PHENIX Collaboration), Phys. Rev. Lett. **101**, 162301 (2008).

Particle-species dependent modification of jet-induced correlations in Au+Au collisions at $\sqrt{(s_{NN})}$ = 200 GeV, S. Afanasiev *et al.* (PHENIX Collaboration), Phys. Rev. Lett. **101**, 082301 (2008).

Source breakup dynamics in Au+Au Collisions at $\sqrt{(s_{NN})}$ = 200 GeV via three-dimensional two-pion source imaging, S. Afanasiev *et al.* (PHENIX Collaboration), Phys. Rev. Lett. **100**, 232301 (2008).

Single transverse spin asymmetries of identified charged hadrons in polarized p+p collisions at $\sqrt{s}$ = 62.4 GeV, I. Arsene, I.G. Bearden, D. Beavis, S. Bekele, C. Besliu, B. Budick, H. Bøggild, C. Chasman, H.H. Dalsgaard, R. Debbe, B. Fox, J.J. Gaardhøje, K. Hagel, A. Jipa, E.B. Johnson, R. Karabowicz, N. Katrynska, E.J. Kim, T.M. Larsen, J.H. Lee, G. Løvhøiden, Z. Majka, M. Murray, C. Nygaard, J.B. Natowitz, B.S. Nielsen, D. Pal, A. Qviler, C. Ristea, D. Röhrich, S.J. Sanders, P. Staszel, T.S. Tveter, F. Videbæk, H. Yang and R. Wada, Phys. Rev. Lett. **101**, 042001 (2008).

SECTION VII

APPENDIX

TALKS PRESENTED
April 1, 2008 – March 31, 2009

Nuclear Physics and (the Nuclear Science Advisory Committee's role in) Strategic Planning of the Isotope Program, **R.E. Tribble**, **Invited Talk**, Workshop on the Nation's Needs for Isotopes: Present and Future, Rockville, Maryland (August, 2008).

RIB Facilities: Present and Future, **R.E. Tribble**, **Invited Talk**, Exotic Nuclei and Atomic Masses, Ryn, Poland (September, 2008).

Report Latest Results on ρ and δ from Muon Decay, **R.E. Tribble**, **Invited Talk**, Institute for Nuclear Theory program on Standard Model tests in the LHC era, Seattle, Washington (October, 2008).

Extracting Reliable Spectroscopic Factors from Transfer Reactions: a case study $^{14}C(d,p)^{15}C$, **R.E. Tribble**, **Invited Talk**, Kernz08, Queenstown, New Zealand (December 2008).

NSAC update for NuPECC, **R.E. Tribble**, **Invited Talk**, NuPECC meeting, Glasgow, Scotland, (October 2008).

Nuclear Astrophysics: the need for Indirect Techniques and Nuclear Data, **R.E. Tribble**, **Invited Talk**, NNDC Symposium, Brookhaven National Laboratory, Upton, New York (November, 2008).

(Mostly) Nuclear Astrophysics, (a little) Stockpile Stewardship, and the TAMU Cyclotron Institute Upgrade Project, **R.E. Tribble**, Los Alamos National Lab., Los Alamos, New Mexico (July 2008).

Transverse Spin Physics in pp Collisions at RHIC, **C.A. Gagliardi**, **Invited Talk**, 25th Winter Workshop on Nuclear Dynamics, Big Sky, Montana (February 2009).

Spin Physics at RHIC, **C.A. Gagliardi**, Physics Department, University of Illinois at Chicago, Chicago, Illinois (October 2008).

Jet Production in Polarized pp Collisions at RHIC, **C.A. Gagliardi** (for the STAR Collaboration), **Invited Talk**, XVI International Workshop on Deep Inelastic Scattering (DIS2008), London, England, (April 2008).

Nuclear Physics for Astrophysics using Radioactive Beams: Indirect Methods, **L. Trache**, **Invited Talk**, 2nd Nuclear Physics and Atomic Energy Conference, Kyiv, Ukraine, (June 2008).

Breakup of Radioactive Nuclear Beams at Iintermediate Energies for Nuclear Astrophysics and Related Topics, **L. Trache, Invited Talk**, The Carpathian Workshops on Physics, Sinaia, Romania (June 2008).

β-delayed Proton-decay for Nuclear Astrophysics, **L. Trache**, NSCL workshop, NSCL, Michigan State University, East Lansing, Michigan (August 2008).

β-delayed p-decay of Proton-rich Nuclei ^{23}Al and ^{31}Cl and Explosive H-burning in Novae, **L. Trache**, 2008 APS Division of Nuclear Physics Annual Meeting, Oakland, California (October 2008).

Breakup of N=10 Proton-rich Nuclei at Intermediate Energies for Reaction Rates in Explosive H-burning in Novae, **A. Banu**, **Invited Talk**, The Carpathian Workshop on Physics, Nuclear Reactions with Exotic Nuclei for Astrophysics, Sinaia, Romania (June 2008).

Breakup of Proton-rich Nuclei ^{24}Si, ^{23}Al, ^{22}Mg, ^{21}Na at Intermediate Energies for Reaction Rates in Explosive H-burning in Novae, **A. Banu**, 10th Symposium on Nuclear Cosmos, Mackinac Island, Michigan (July 2008).

Nuclear Astrophysics at Texas A&M, **A. Banu**, **Invited Talk**, Workshop on Experiments with Reaccelerated Beams at NSCL, Michigan State University, East Lansing, Michigan (August 2008).

α-cluster Structure in Light N≠Z Nuclei, **V.Z. Goldberg**, International Conference on New Aspects of Heavy Ion Collisions Near the Coulomb Barrier (FUSION08), Chicago, Illinois (September 2008).

Resonance Reactions Induced by Radioactive Beams (Studies of Exotic Nuclei and Applications to Nuclear Astrophysics, **V.Z. Goldberg**, **Invited Talk**, 58th International Conference on Problems on Nuclear Spectroscopy and Nuclear Structure, Moscow, Russia (June 2008).

Unusual Decay Modes of Exotic Nuclei, **V.Z. Goldberg**, **Invited Talk**, International Conference on Nuclear Clusters and Excess Neutron Nuclei, St. Petersburg, Russia (June 2008).

New Renaissance of the Resonance Scattering (but with New Technique and New Ideas), **V.Z. Goldberg**, Department of Physics and Astronomy, University of Rochester, Rochester, New York (November 2008).

Possible Directions of Studies in Nuclear Structure and Nuclear Astrophysics at the Cyclotron of the Gumilyev Eurasian Universit, **V.Z. Goldberg**, Lecture Course on Nuclear Physics and Astrophysics, Astana, Kazakhstan (June 2008).

Constraints on ΔG through Longitudinal Double Spin Asymmetry Measurements of Inclusive Jet Production in Polarized p+p Collisions at 200 GeV, **M. Sarsour** (for the STAR Collaboration), 18th International Symposium on Spin Physics (SPIN 2008), Charlottesville, Virginia (October 2008).

Longitudinal Double Spin Asymmetry for Inclusive Jet Production in Polarized p+p Collisions at 200 GeV, **M. Sarsour** Physics Department, Brookhaven National Laboratory, Upton, New York (July 2008).

π^0 Transverse Single-Spin Asymmetries (A_N) at η = 4.1 in p+p Collisions at $\sqrt{s}$ = 200 GeV, **J. Drachenberg** (for the STAR Collaboration), 18th International Symposium on Spin Physics (SPIN 2008), Charlottesville, Virginia (October 2008).

Precision Measurements for Weak Interaction Studies and Symmetry Tests, **J.C. Hardy, Invited Talk**, Mass Olympics - Workshop at the European Center for Theoretical Studies in Nuclear Physics and Related Areas (ECT*), Trento, Italy (May 2008).

Superallowed Beta Decay: The Role of Nuclear Structure in Standard Model Tests, **J.C. Hardy, Invited Talk**, Zakopane Conference on Nuclear Physics, Zakopane, Poland (September 2008).

Superallowed $0^+ \rightarrow 0^+$ Beta Decay and CKM Unitarity: A New Overview and Improved Precision, **J.C. Hardy, Invited Talk**, The Fifth International Conference on Exotic Nuclei and Atomic Masses (ENAM08), Ryn, Poland (September 2008).

Superallowed $0^+ \rightarrow 0^+$ Beta Decay and CKM Unitarity: The Contribution from Nuclei with A > 56, **J.C. Hardy, Invited Talk** Workshop on Scaling the Heights of the N=Z Line above ^{56}Ni at the European Center for Theoretical Studies in Nuclear Physics and Related Areas (ECT*), Trento, Italy (September 2008).

Superallowed Nuclear Beta Decay: A Window on the Weak Interaction – Precision Meets Pandemonium, **J.C. Hardy, Invited Talk**, Popular Scientific Symposium on Journey Towards and Beyond the Drip Lines, dedicated to Bjorn Jonson on the occasion of his retirement as professor of Physics at Chalmers University, Gothenburg, Sweden (October2008).

Testing CVC and CKM-Unitarity with Superallowed Nuclear Beta Decay: An Updated Survey and Analysis, **J.C. Hardy, Invited Talk**, Workshop on Low Energy Precision Electroweak Physics in the LHC Era, Institute for Nuclear Theory, University of Washington, Seattle, Washington (November 2008).

Superallowed $0^+ \rightarrow 0^+$ Beta Decay and CKM Unitarity: A New Overview and Improved Precision, **J.C. Hardy,** University of Jyvaskyla, Jyvaskyla, Finland (March 2009).

Overview of Precision Internal Conversion Measurements as Tests of Internal conversion Theory, **N.Nica, Invited Talk**, 2nd Workshop for Radioactive Data Evaluators: Training sessions of the Decay Data Evaluation Project (DDEP-2008), Bucharest, Romania (May 2008).

Monte Carlo Studies of β-Detector Efficicency with GEANT4 for Precise β^+-Branching-Ratio Experiments, **V.V. Golovko**, V.E. Iacob, and J.C. Hardy, 2008 APS Meeting, St. Louis, Missouri (April 2008).

Improved β Decay Branching Ratios, **V.E. Iacob**, J.C. Hardy and V.V. Golovko, 2008 APS Meeting, St. Louis, Missouri (April 2008).

Precise Half Life Measurement of ^{26}Si, **V.E. Iacob,** V. Golovko, J. Goodwin, J.C. Hardy, N. Nica, H.I. Park, L. Trache and R.E. Tribble, 2008 APS Division of Nuclear Physics Annual Meeting, Oakland, California (October 2008).

The Latest Precision ICC Measurement from TEXAS A&M, **N. Nica,** US Nuclear Data Program (USNDP) Meeting, Brookhaven National Laboratory, Upton, New York (November 2008).

How Idiosyncratic is the Weak Force? **J.C. Hardy**, Lecture to REU Students, Cyclotron Institute, Texas A&M University, College Station, Texas (July 2008).

Overview of Precision Internal Conversion Measurements as Tests of Internal Conversion Theroy, **N. Nica,** National Institute of Physics and Nuclear Engineering, Bucharest, Romania (May 2008).

The ft Values of β-decaying Nuclei: How Can Nuclear Physics Continue to Reduce the Uncertainty in the Value of V_{ud}?, **D. Melconian, Invited Talk**, 5th Internationall Conference on Exotic Nuclei and Atomic Masses, Ryn, Poland (September, 2008).

β decay Correlation Studies Using Very Cold, Highly Polarized Sources, **D. Melconian, Invited Talk**, XXXII Symposium on Nuclear Physics, Cocoyoc, Mexico (Jan 2009).

Symmetries in Nature: A Glimpse into the Beauty and Art of Science, **D. Melconian, Invited Talk**, Saturday Morning Physics at Texas A&M University, College Station, Texas (February 2009).

Hard Probes at RHIC, **Saskia Mioduszewski**, **Invited Talk**, The Winter Workshop on Nuclear Dynamics, South Padre Island, Texas (April 2008).

Photon-Hadron Correlations at RHIC, **Saskia Mioduszewski**, **Invited talk**, Electromagnetic Probes Workshop of the RHIC/AGS Users' Meeting, Upton, New York (May 2008).

Present Experimental Status: High-p_T and Initial State, **Saskia Mioduszewski**, **Invited Talk**, International Conference on Hard and Electromagnetic Probes of High-Energy Nuclear Collisions, Illa a La Toxa, Spain (June 2008).

High-p_T Probes, **Saskia Mioduszewski**, **Invited Talk**, Tamura Symposium, Austin, Texas (November 2008).

Direct Gamma - Charged Hadron Azimuthal Correlations, **Ahmed Hamed,** (for the STAR Collaboration), **Invited Talk,** International Conference on Hard and Electromagnetic Probes of High-Energy Nuclear Collisions, Illa a La Toxa, Spain (June 2008).

Direct Photon - Charged Hadron Azimuthal Correlation Measurements, **Ahmed Hamed** (for the STAR Collaboration), 34th International Conference on High Energy Physics, Philadelphia, Pennsylvania (August 2008).

One More Ingredient for Energy Loss Quantification, **Ahmed Hamed,** Hot Quarks Workshop (Workshop for Young Scientists on the Physics of Ultrarelativistic Nucleus-Nucleus Collisions), Estes Park, Colorado (August 2008).

Direct Gamma-Charged Hadron Azimuthal Correlation Measurement from STAR, **Ahmed Hamed,** The Quark Matter Conference, Knoxville, Tennessee (March 2009).

γ + Jet Analysis in $\sqrt{(s_{NN})}$ = 200 GeV Au + Au Collisions with STAR, **Martin Codrington**, **Invited Talk**, (as a result of winning the poster competition), Gordon Research Conference on Nuclear Chemistry, New London, New Hampshire (June 2008).

Probing Very Low Density Nuclear Matter in Heavy Ion Collisions, **J.B. Natowitz**, **Invited Talk**, American Chemical Society National Meeting, New Orleans, Louisiana (April 2008).

Nuclear Collisions and the Nuclear Equation of State, **J.B. Natowitz**, **Invited Talk**, American Chemical Society National Meeting, Philadelphia, Pennsylvania (August 2008).

Low Density Clustering in Near-Fermi-Energy Collisions, **J.B. Natowitz**, **Invited Talk**, Flerov Laboratory, Dubna, Russia (May 2008).

Clusterization and Symmetry energies in Low Density Nuclear Matter, **J.B. Natowitz**, **Invited Talk**, Gordon Research Conference on Nuclear Chemistry, New London, New Hampshire (June 2008).

Probing Quantum Phase Changes in Nuclear Reactions, **J.B. Natowitz**, **Invited Talk**, 2008 APS Division of Nuclear Physics Annual Meeting, Oakland, California (October 2008).

Rapidity Densities of Produced Hadrons in p + p collisions, **K. Hagel**, 2008 APS Division of Nuclear Physics Annual Meeting, Oakland, California (October 2008).

Particle Production in p + p Reactions at $s^{1/2}$*=200 GeV,* **K. Hagel**, Hot QCD 2008, Cuernavaca, Mexico, (May 2008).

Nuclear Equation of State: What can we learn about Neutron Stars from Atomic Nuclei? **S.J. Yennello**, **Invited Talk**, 2008 APS Division of Nuclear Physics Annual Meeting, Oakland, California (October 2008).

What We Can Learn about the Symmetry Energy of the Nuclear Equation of State from Heavy-Ion Collisions? **S.J. Yennello**, **Invited Talk**, 235th ACS National Meeting, New Orleans, Louisiana (April 2008).

Probing the Nuclear Equation of State with Peripheral Collisions at Fermi Energies, **S.J. Yennello**, **Invited Talk**, Gordon Research Conference in Nuclear Chemistry, New London, New Hampshire (June 2008).

Nuclear Reactions: Exploring phase Transitions in Excited Nuclear Material, **S.J. Yennello**, University of Oklahoma, Norman, Oklahoma (December 2008).

Isospin Observables near the Fermi Energy, **S.J. Yennello**, **Invited Talk**, Workshop on Nuclear Symmetry Energy at Medium Energies, Catania, Italy (May 2008).

Probing the Nuclear Equation of State with Peripheral Collisions at Fermi Energies, **G.A. Souliotis**, 17th Symposium of the Hellenic Nuclear Physics Society, Univ. of Ioannina, Ioannina, Greece (May 2008).

Semiclassical Calculations of Peripheral Heavy-Ion Collisions at Fermi Energies and the Nuclear Equation of State, **G.A. Souliotis,** D.V. Shetty, S. Galanopoulos, and S.J. Yennello, 2008 APS Division of Nuclear Physics Annual Meeting, Oakland, California (October 2008).

Isoscaling Studies of Reconstructed Quasi-Projectiles in ^{24}*Mg,* ^{40}*Ca+*^{112,124}*Sn Reactions at 32 MeV/u,* **S. Galanopoulos,** G.A. Souliotis, A.L. Keksis, M. Veselsky, M. Jandel, D.V. Shetty, Z. Kohley, S. Soisson, B. Stein, S. Wuenschel, and S.J. Yennello, 2008 APS Meeting, St. Louis, Missouri (April 2008).

Change in T_{lim} *as a Function of N/Z,* **S. Wuenschel**, S. Galanopoulos, K. Hagel, Z. Kohley, L.W. May, J.B. Natowitz, D.V. Shetty, S.N. Soisson, G.A. Souliotis, B.C. Stein, R. Wada, and S.J. Yennello, Gordon Research Conference in Nuclear Chemistry, New London, New Hampshire (June 2008).

Fragment Emission and Production in Peripheral Collisions in the Intermediate Energy Regime, **S.N. Soisson,** B. Stein, G. Souliotis, D. Shetty, A. Keksis, S. Wuenschel, and S.J. Yennello, 2008 APS Division of Nuclear Physics Annual Meeting, Oakland, California (October 2008).

N/Z Equilibration in Peripheral Reactions on the FAUST Array, **B.C. Stein,** S.N. Soisson, G.A. Souliotis, D.V. Shetty, S. Galanopoulos, A.L. Keksis, S. Wuenschel, Z. Kohley, L. May, and S.J. Yennello, 2008 APS Division of Nuclear Physics Annual Meeting, Oakland, California (October 2008).

Isotopic Width Distributions and Symmetry Energy, **S. Wuenschel**, S. Galanopoulos, K. Hagel, Z. Kohley, D.V. Shetty, S.N. Soisson, G.A. Souliotis, B.C. Stein, and S.J. Yennello, 2008 APS Division of Nuclear Physics Annual Meeting, Oakland, California (October 2008).

Differences in the Transverse Flow of ^{3}*H and* ^{3}*He Fragments,* **Z. Kohley,** E. Bell, D.V. Shetty, G.A. Souliotis, S. Soisson, B. Stein, L. May, S.J. Yennello, and NIMROD Collaboration, 2008 APS Meeting, St. Louis, Missouri (April 2008).

Microscopic Calculations of Dynamics and N/Z Equilibration in Peripheral Collisions Below the Fermi Energy, **G.A. Souliotis,** D.V. Shetty, S. Galanopoulos, and S.J. Yennello, 2008 APS Meeting, St. Louis, Missouri (April 2008).

A Dual Axis Dual Lateral Position Sensitive Charged Particle Detector, **S.N. Soisson,** B.C. Stein, L. May *et al.* 2008 APS Meeting, St. Louis, Missouri (April 2008).

K and L X-ray Transitions in Multiply Ionized Atoms Produced in Heavy Ion Collisions, **V. Horvat**, R.L. Watson, and Y. Peng, The 12th International Conference on the Application of Accelerators in Research and Industry, Fort Worth, Texas (August 2008).

Equation of State of Symmetric and Asymmetric Nuclear Matter, **S. Shlomo**, **Invited Talk**, Department of Physics, Rostock University, Rostock, Germany (May 2008).

Mean-Field Approximation for Finite Nuclei and Nuclear Matter, **S. Shlomo**, **Invited Talk**, Department of Physics, Ben-Gurion University, Beer-Sheva, Israel (May 2008).

The Equation of Symmetric and Asymmetric Nuclear Matter, **S. Shlomo**, **Invited Talk**, Department of Physics and Astronomy, Tel-Aviv University, Tel-Aviv, Israel (May 2008).

Mean-Field Approximation for Finite Nuclei and Nuclear Matter, **S. Shlomo**, **Invited Talk**, The 2nd International Conference on Current Problems in Nuclear Physics and Atomic Energy (NPAE-Kyiv200), Kiev, Ukraine (June 2008).

The Nature of the Low Energy Isovector Dipole Excitation in Neutron-Rich Nuclei, **S. Shlomo**, **Invited Talk**, Hokudai-TORIJIN-JUSTIPEN-EFES Workshop on Perspectives in Resonances and Continua on Nuclei, Onuma Park, Japan (July 2008).

A Modern Nuclear Energy Density Functional, **S. Shlomo**, **Invited Talk**, JUSTIPEN-EFES-Kokudai-UNIDEF meeting, Onuma Park, Japan (July 2008).

Neutron Skin and Giant Resonances, **S. Shlomo**, **Invited Talk**, PREX Workshop, Jefferson Lab., Newport, News, Virginia (August 2008).

Modern Energy Density Functional for Properties of Nuclei and Nuclear Matter, **S. Shlomo**, **Invited Talk**, Department of Physics, University of Arizona, Tucson, Arizona (September 2008).

Giant Resonances and Nuclear Matter Equation of State, **S. Shlomo**, **Invited Talk**, Department of Physics, University of Arizona, Tucson, Arizona (September 2008).

Modern Energy Density Functional for Properties of Nuclei and Nuclear Matter, **S. Shlomo**, **Invited Talk**, SARAF Workshop, Male-Hahamisha, Israel (October 2008).

Modern Energy Density Functional for Properties of Nuclei and Nuclear Matter, **S. Shlomo**, **Invited Talk**, Symposium (Honoring Hans A. Weidenmueller) on Penetrating Physics by Random Matrices, UNAM, Cuernavaca, Mexico (March 2009).

Mini-Black Holes and Nucleons, Scattering and Absorption, **A.M. Mukhamedzhanov**, **Invited Talk**, Catania National Lab., Catania, Italy (June 2008).

Indirect Techniques in Nuclear Astrophysics, **A.M. Mukhamedzhanov**, **Invited Talk**, Nucleus 2008, Moscow, Russia (June 2008).

Benchmark on Neutron Capture Extracted from (d,p) Reactions, **A.M. Mukhamedzhanov**, **Invited Talk**, Lowrence Livermoor National Laboratory, Livermoor, California (October 2008).

Mini-Black Holes and Nucleons, Scattering and Absorption, **A.M. Mukhamedzhanov**, **Invited Talk**, Lowrence Livermoor National Laboratory, Livermoor, California (October 2008).

Trojan Horse as Indirect Technique in Nuclear Astrophysics, **A.M. Mukhamedzhanov**, **Invited Talk**, Nuclear Theory Workshop (INT 09-40W) on Solar Fusion Cross Sections for the pp Chain and CNO Cycle, University of Washington, Seattle, Washington (January 2009).

Trojan Horse as Indirect Technique in Nuclear Astrophysics, **A.M. Mukhamedzhanov**, **Invited Talk**, National Superconducting Cyclotron Laboratory, Michigan State University, East Lansing, Michigan (January 2009).

Mini-Black Holes and Nucleons, Scattering and Absorption, **A.M. Mukhamedzhanov**, **Invited Talk**, National Superconducting Cyclotron Laboratory, Michigan State University, East Lansing, Michigan (January 2009).

Predictions for Heavy Ion Collisions at LHC, **C.M. Ko**, **Invited Talk**, International Workshop on Heavy Ion Physics at LHC, Wuhan, China (May 2008).

Recent Progress and New Challenges in Isospin Physics with Heavy-Ion Reactions, **C.M. Ko**, **Invited Talk**, International Conference on Nuclear Physics and Astrophysics: From Stable Beams to Exotic Nuclei, Cappadocia, Turkey (June 2008).

Relativistic Heavy Ion Collisions and Hot Dense Matter, **C.M. Ko**, **Invited Talk**, Summer School on Nuclear Collective Dynamics IV, Istanbul, Turkey (June 2008).

Exotic Particle Production in Relativistic Heavy Ion Collisions, **C.M. Ko**, **Invited Talk**, The International Workshop on QCD Phase Transition and Heavy Ion Collisions, Hefei, China (July 2008).

Charm as a Probe of sQGP, **C.M. Ko**, **Invited Talk**, Symposium in Honor of the Scientific Career of John M. Alexander, American Chemical Society Meeting, Philadelphia, Pennsylvania (August 2008).

Charm as a Probe of QGP, **C.M. Ko**, **Invited Talk**, 8th International Workshop on Relativistic Aspects of Nuclear Physics, Rio de Janeiro, Brazil (November 2008).

Charm as a Probe of QGP, **C.M. Ko**, **Invited Talk**, International Workshop on Heavy Quark Physics in Nucleus-Nucleus Collisions, Los Angeles, California (January 2009).

Transport Models for Heavy Ion Collisions: From Below Coulomb Barrier to Ultrarelativistic Energies, **C.M. Ko**, **Invited Talk**, International Symposium on Penetrating Physics by Random Matrices, Cuernavaca, Mexico (March 2009).

Probing Dense Nuclear Matter by Heavy Ion Collisions, **C.M. Ko**, **Invited Talk**, International Workshop on High-Order Actions and Their Applications in Many-Body, Few-Body, and Classical Problems, Barcelona, Spain (March 2009).

Heavy Flavor in the sQGP, **R. Rapp**, **Invited Talk**, 24th Winter Workshop on Nuclear Dynamics, South Padre Island, Texas (April 2008).

Quarkonia, Heavy Quarks and sQGP, **R. Rapp**, **Invited Talk**, International RIKEN-BNL Research Center Workshop on Understanding QGP through Spectral Function and Euclidean Correlators, Brookhaven National Laboratory, Upton, New York (April 2008).

Electromagnetic Probes in Heavy-Ion Collisions – Theory, **R. Rapp**, **Invited Lecture Series**, European Center for Theoretical Research in Nuclear Physics and Related Areas (ECT*), Doctoral Training Programme 2008 on Nuclear Matter under Extreme Conditions, Trento, Italy (April 2008).

T-Matrix Approach to Heavy Quarks in the Quark-Gluon Plasma, **H. van Hees**, 3rd International Conference on Hard and Electromagnetic Probes in High-Energy Nuclear Collisions (Hard Probes 2008), Illa da Toxa, Galicia, Spain (June 2008).

Nonperturbative Heavy-Quark Transport at RHIC, **R. Rapp**, **Invited Talk**, 417th WE-Heraeus Seminar on Characterization of the QGP with Heavy Quarks, Physikzentrum Bad Honnef, Bad Honnef, Germany (June 2008).

Charm(onium) Transport and Quark Coalescence in the QGP, **R. Rapp**, **Invited Talk**, PHENIX Collaboration Meeting, University of Illinois at Urbana-Champaign, Urbana, Illinois (July 2008).

Chiral Symmetry, Hadrons in Medium and Dileptons in Heavy-Ion Collisions, **R. Rapp**, **Invited Lectures**, 20th Indian Summer School of Physics and 4th HADES Summer School, Rez/Prague, Czech Republic (August 2008).

Heavy Flavor Hadronization, **R. Rapp**, **Invited Talk**, International Workshop on the Statistical Model of Hadron Formation and the Nature of the QCD Hadronization Process, ECT* Trento, Italy (September 2008).

Theory and Phenomenology of Heavy Flavor at RHIC, **R. Rapp**, **Invited Plenary Talk**, International Conference on Strangeness in Quark Matter, Tsinghua University, Beijing, China (October 2008).

Covariant and Selfconsistent Vertex Corrections for Pions and Isobars in Nuclear Matter, **F. Riek**, McGill University, Montreal, Quebec, Canada (November 2008).

Theoretical Aspects of Heavy Quarkonia in Heavy-Ion Collisions, **R. Rapp**, **Invited Talk**, Tamura Symposium, University of Texas, Austin, Texas (November 2008).

Charmonium as Probe of Quark-Gluon Plasma, **X. Zhao**, Shanghai Jiao Tong University, Shanghai, China (December 2008).

Thermal Kinetic Approach to Charmonium Production in Heavy-Ion Collisions, **X. Zhao**, Tsinghua University, Beijing, China (December 2008).

Thermal Kinetic Approach to Charmonium Production in Heavy-Ion Collisions, **X. Zhao**, University of Science and Technology, Hefei, China (December 2008).

Thermal Kinetic Approach to Charmonium Production in Heavy-Ion Collisions, **X. Zhao**, Central China Normal University, Wuhan, China (December 2008).

Quarkonia in Medium and in Heavy-Ion Collisions, **R. Rapp**, Brookhaven National Laboratory, Upton, New York (February 2009).

Medium Effects on Vector-Meson Production in Nuclei, **F. Riek**, Argonne National Laboratory, Chicago, Illinois (February 2009).

Recombination of Quarks in Nuclear Collisions, **R.J. Fries**, **Invited Talk**, ACS National Meeting, New Orleans, Louisiana (April 2008).

Bulk Viscosity in Nuclear Collisions, **R.J. Fries**, RIKEN Workshop on Hydrodynamics in Heavy Ion Collisions and QCD Equation of State, Brookhaven National Laboratory, Upton New York (April 2008).

Probing Nuclear Matter with Jet Chemistry, **R.J. Fries**, 3rd International Conference on Hard and Electromagnetic Probes in High-Energy Nuclear Collisions (Hard Probes 2008), Illa da Toxa, Galicia, Spain (June 2008).

Heavy Ions: Selected Topics, **R.J. Fries**, **Invited Talk**, STAR Collaboration Meeting, University of Cailifornia at Davis, Davis, California (June 2008).

Effective Probes of QCD Matter: A Summary, **R.J. Fries**, **Invited Summary Talk**, Workshop on Effective Probes of QCD Matter, Duke University, Durham North Carolina (June 2008).

Flavor as a QGP Probe at High P_T, **R.J. Fries**, **Invited Talk**, PHENIX Collaboration Meeting, University of Illinois, Urbana-Champaign, Illinois (July 2008).

Stress Tensor, Bulk Viscosity, Entropy Production, **R.J. Fries**, **Invited Talk**, YITP Workshop on Entropy Production before QGP, Yukawa Institute, Kyoto, Japan (August 2008).

Strangeness and other Flavors as QGP Probes at High P_T, **R.J. Fries**, Hot Quarks 2008, Estes Park, Colorado (August 2008).

Recombination of Quarks and Statistical Model, **R.J. Fries**, **Invited Talk**, International Workshop on the Statistical Model of Hadron Formation and the Nature of the QCD hadronization Process, ECT* Trento, Italy (September 2008).

Direct Photons in Heavy Ion Collisions, **R.J. Fries**, **Invited Talk**, Tamura Symposium, University of Texas, Austin, Texas (November 2008).

High Momentum Probes of QCD Matter, **R.J. Fries**, **Invited Talk**, 4th Workshop on High-P_T Physics at LHC, Prague, Czech Republic (February 2009).

RESEARCH PERSONNEL AND ENGINEERING STAFF

April 1, 2008 - March 31, 2009

Faculty and Research Group Leaders

Charles M. Folden III, Assist. Prof. of Nuclear Chemistry – From 10/1/08
Rainer Fries, Assist. Professor of Physics
Carl A. Gagliardi, Professor of Physics
John C. Hardy, Professor of Physics
Che Ming Ko, Professor of Physics
Dan Melconian, Assist. Professor of Physics
Saskia Mioduszewski, Assist. Prof. of Physics
J. B. Natowitz, Professor of Chemistry, Bright Chair
Ralf Rapp Associate Professor of Physics
Shalom Shlomo, Senior Scientist
Robert E. Tribble, Professor of Physics, Director
Rand L. Watson, Professor of Chemistry
Sherry J. Yennello, Professor of Chemistry
Dave H. Youngblood, Professor of Physics
Akram M. Zhanov, Senior Scientist

Research Staff

Henry Clark, Accelerator Physicist (50%)
Grigor Chubaryan, Research Scientist
John C. Hagel, Research Scientist (50%)
Vladimir Horvat, Research Scientist (50%)
Victor Iacob, Associate Research Scientist
Yiu-Wing Lui, Research Scientist
Ninel Nica, Assist. Research Scientist
George Souliotis, Associate Research Scientist
Livius Trache, Research Scientist
Ryoichi Wada, Research Scientist

Visiting Scientists

Aldo Bonasara – From 6/9/08 To 10/15/08
Youssef El Masri _ From 7/1/08 To 8/31/08
Vladilen Goldberg
Ajay Kumar – From 7/31/08 To 11/30/08
Ian Towner – From 6/19/08 To 8/31/08

Accelerator Physics and Radiation Line Staff

Juha Arje, Research Scientist – To 7/23/08
Joseph Brinkley, Research Associate
Henry Clark, Accelerator Physicist (50%)
Vladimir Horvat, Research Scientist (50%)
Bruce Hyman, Research Associate
George Kim, Accelerator Physicist
Don May, Accelerator Physicist
Gabriel Tabacaru, Accelerator Physicist

Computer Systems Staff

Robert Burch, Jr., Systems Analyst/Sr. Microcomputer/LAN Administrator
John C. Hagel, Research Scientist (50%)

Engineering Staff

Greg Derrig, Senior Mechanical Engineer
Robert Olsen, Senior Mechanical Engineer

Postdoctoral Research Associates

Adriana Banu
Xinfeng Chen – From 5/12/08 To 7/21/08
Zhiqiang Chen – To 7/2/08
Rory Clarke
Pibero Djawotho – From 9/30/08
Stratos Galanopoulous – To 9/10/08
Victor Golovko – To 8/12/08
Ahmed Hamed
Seweryn Kowalski – From 8/19/08 To 10/21/08
Krishichayan
Wei Liu – To 6/30/08
Yong S. Oh
Felix Riek – From 7/1/08
Ricardo Rodriguez – From 8/4/08
Brian Roeder – From 7/22/08
Murad G. Sarsour – To 7/31/08
Dinesh Shetty – To 8/7/08
Hendrik van Hees
Au Kim Vuong – To 5/31/08
Jun Xu – From 10/13/08

STUDENTS

April 1, 2008 - March 31, 2009

Graduate Students

Marisa Alfonso – From 11/1/08
Richard Behling – From 10/31/08
Jonathan Button
Matthew Cervantes
Xinfeng Chen – To 5/12/08
Martin Codrington
James Drachenberg
David Carson Fuls
John Goodwin
Liaoyuan Huo
Zach Kohley
Feng Li – From 6/1/08 To 8/31/08
Matthew McCleskey
Hyo-In Park
Lijun Qin – To 8/1/08
Ellen Simmons
Sarah Soisson
Alexandria Spiridon
Brian Stein
Sara Wuenschel
Xingbo Zhao

Undergraduates and Student Technicians

Hannah Childress – To 8/22/08
Alfredo J. Echeverria
Jennifer Erchinger – From 5/27/08 To 9/1/08
Katie Huseman – To 9/4/08
Jennifer Jeffress – From 5/27/08 To 6/30/08
Toby Martin
Thomas Merket
Ashley Noack
Kara Peek – To 1/22/09
Robert Polis
Wade Ben Smith
Amanda Spaw – From 1/23/09

ORGANIZATIONAL CHART - CYCLOTRON INSTITUTE

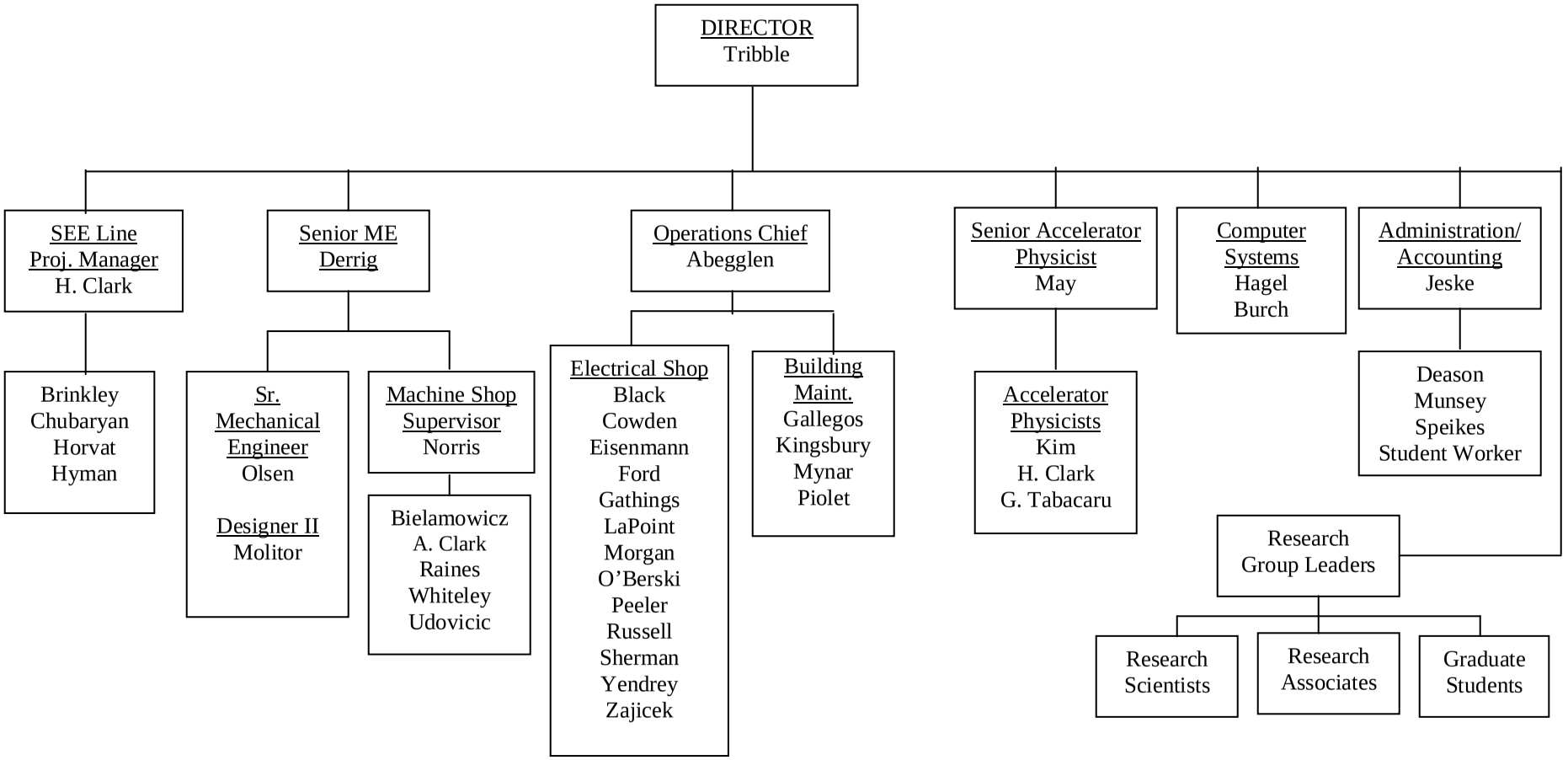

STUDENTS WHO RECEIVED GRADUATE DEGREES
FROM THESIS WORK CONDUCTED
AT
THE CYCLOTRON INSTITUTE

April 1, 2008 – March 31, 2009

Name	Year	Thesis Title	Advisor	Present Position
Xinfeng Chen	2008	*Giant Resonance Study by ^{6}Li Scattering*	D. H. Youngblood	Post Doc., Department of Chemistry, University of Washington, St. Louis, Missouri
Lijun Qin	2008	*Low Density Nuclear Matter in Heavy Ion Collisions*	J. B. Natowitz	Hewlett-Packard Co., Houston, Texas

INSTITUTE COLLOQUIA AND SEMINARS
April 1, 2008-March 31, 2009

2008

April 4	Dr. Pasi Huovinen, Deparment of Physics, Purdue University, West Lafayette, Indiana	*From Perfect Liquid to Viscous Fluid: Hydrodynamics at RHIC*
April 8	Dr. Alejandro Sonzogni, National Nuclear Data Center, Brookhaven National Laboratory, Upton, New York	*Data and Tools Available at the National Nuclear Data Center*
April 15	Dr. J. A. Gladysz, Department of Chemistry, Texas A&M University, College Station, Texas	*Novel New Approaches to (Catalyst) Recovery, Remediation, and Rapid Reaction Sequences Involving Fluorous Phases*
April 16	Professor G. Viesti, INFN and Dapartimento di Fisica, Universita di Padova, Podova, Italy	*The EURITRACK Project: Status of a Tagged Neutron Inspection System for Cargo Containers*
April 24	Professor Claudio Spitaleri, University of Catania and INFN Laboratori Nazionali del Sud, Catania, Italy	*The Trojan Horse Method in Nuclear Astrophysics: Recent Applications*
April 25	Dr. Yongseok Oh, Cyclotron Institute, Texas A&M University, College Station, Texas	*Photoproduction of Strangeness: $K^*\Lambda/K^*\Sigma$ Production and $K\Sigma^*(1385)$Production*
May 8	Dr. Kris Hagel, Cyclotron Institute, Texas A&M University, College Station, Texas	*Particle Production in p + p Reactions at $\sqrt{S_{NN}}$ = 200 GeV*
June 10	Dr. Swapan Kumar Basu, Variable Energy Cyclotron Centre, Kolkata, India,	*What's Going On at the Cyclotron Centre, Kolkata*
June17	Dr. Dongwon Lee, Lawrence Berkeley National Laboratory, Berkeley, California	*Study of Proton-Rich Nuclei Using Radioactive and Stable Ion Beams at the Lawrence Berkeley National Laboratory*
July 8	Professor Y. El Masri, Institute of Nuclear Physics – Catholic University of Louvain-la-Neuve, Belgium	*Proton Induced Fission on Actinide Nuclei at Energies 26.5 and 62.9 MeV*

August 5	Professor Y. El Masri, Institute of Nuclear Physics – Catholic University of Louvain-la-Neuve, Belgium	*Elemental Analysis by Nuclear Techniques (PIXE, RBS and ERDA) in Materials of Cultural Heritage and Other Scientific and Industrial Applications Carried Out at the LLN, VdG and the Louvre Museum Tandem Facilities*
August 12	Professor Zbigniew Majka, Facility for Antiproton and Ions Research, Darmstadt, Germany and Jagiellonian University, Krakow, Poland	*FAIR Project – Status and Research Program*
August 15	Professor J. J. Das, Inter University Accelerator Centre, New Delhi, India	*Possible Upgrade of IUAC Tandem-Linac Facility for Neutron Rich RIBS*
August 15	Dr. Su Houng Lee, Yonsei Univeristy, Seoul, Korea	*Diquark, Exotics and Heavy Ion Collisions*
August 25	Professor Y. El Masri, Institute of Nuclear Physics – Catholic University of Louvain-la-Neuve, Belgium	*Microscopic Studies of Light Charged Particle and Neutron Production in ^{nat}Si Using Proton and Alpha Beams of Energies between 20 and 65 MeV*
September 2	Professor Aurel Bulgac, University of Washington, Seattle, Washington	*The Incredible Many Facets of the Unitary Fermi Gas*
September 26	Mr. Xingbo Zhao, Cyclotron Institute, Texas A&M University, College Station, Texas	*Charmonium Production in Heavy-Ion Collisions*
October 3	Dr. V. Z. Goldberg, Cyclotron Institute, Texas A&M University, College Station, Texas	*α–Cluster Structure in Light N≠Z Nuclei*
October 7	Dr. Raj K. Gupta, Physics Department, Panjab University, Chandigarh, India	*Clusters in Nuclei*
October 13	Dr. Ken-ichiro Yoneda, RIKEN NISHINA Center for accelerator-Based Science, Wako, Japan	*Current Status of the Radioactive Isotopes Beam Factory (RIBF) and SAMURAI Project at RIKEN*
October 14	Dr. Timothy Hallman, Brookhaven National Laboratory, Upton, New York	*Characterizing the New State of Strongly Interacting Quark-Gluon Matter Discovered at RHIC*
October 16	Professor W. H. Dickhoff, Department of Physics, Washington University, St. Louis, Missouri	*Data-Driven Path to the Dripline – How Correlations Change as a Function of Nucleon Asymmetry*

October 31	Dr. Felix Riek, Cyclotron Institute, Texas A&M University, College Station, Texas	*Covariant and Self Consistent Vertex Corrections for Pions and Isobars in Nuclear Matter*
November 6	Professor L. G. Sobotka, , Department of Chemistry, Washington University, St. Louis, Missouri	*Studies of a) Correlations, b) Continuum Structure and c) the Caloric Curve of God's Quantum Dots*
November 24	Dr. Sandeep S. Ghugre, UGC-DAE Consortium for Scientific Research, Kolkata, India	*Spectroscopy of Nearly Spherical Nuclei Using the Indian National Gamma Array (INGA)*
November 25	Dr. Hideki Hamagaki, Center for Nuclear Study (CNS), University of Tokyo, Tokyo, Japan	*Electro-Magnetic Measurements at RHIC PHENIX*
December 2	Professor James P. Vary, Department of Physics and Astronomy, Iowa State University, Ames, Iowa	*Today's Atomic Nucleus – Bridge from Quarks to the Cosmos*
December 5	Professor Bao-An Li, Department of Physics, Texas A&M University at Commerce, Commerce, Texas	*Constraining the EOS of Neutron-Rich Nuclear Matter and Properties of Neutron Stars with Central Heavy-Ion Collisions*

2009

January 27	Dr. Cheuk-Yin Wong, Oak Ridge National Laboratory, Oak Ridge, Tennessee	*The Momentum Kick Model Description of the Ridge and Jet Quenching*
January 30	Mr. Steffen A. Bass, Department of Physics, Duke University, Durham, North Carolina	*What Do We Know about the Shear-Viscosity of QCD Matter?*
February 17	Mr. Timothy Daniels, Department of Physics and Astronomy, University of North Carolina, Chapel Hill, North Carolina	*Spin-Correlation Coefficients and Phase-Shift Analysis for $p+^3He$ Elastic Scattering*
February 24	Professor O. Zeynalova, JINR-Joint Institute for Nuclear Research, Dubna, Moscow, Russia	*DSP Algorithms for Fission Fragment and Prompt Fission Neutron Spectroscopy*
February 26	Dr. Victor Golovko, Department of Physics, Queen's University, Kingston, Ontario, Canada	*The Use of Geant4 for Simulation of the DEAP1 Detector*
March 3	Dr. Hendrik van Hees, Justus-Liebig Universität, Giessen, Germany	*Heavy Quarks in the Quark-Gluon Plasma*

March 10	Ms. Jill Berryman, NSCL, Michigan State University, East Lansing, Michigan	*Magnetics Dipole Moment of the Short-lived Radioisotope ^{55}Ni Measured by β-NMR Spectroscopy*
March 13	Dr. Hendrik van Hees, Justus-Liebig Universität, Giessen, Germany	*Dileptons in Heavy-Ion Collisions*
March 17	Professor Jerimy C. Polf, M. D. Anderson Cancer Center, University of Texas, Hoston, Texas	*Proton Radiotherapy at M. D. Anderson Cancer Center: Clinical Practice and Current Research*
March 24	Dr. Lixin Chen, Cyclotron Institute, Texas A&M University, College Station, Texas	*Mass Measurement of Stored and Cooled Exotic Nuclei with Schottky Mass Spectrometry*
March 31	Dr. R. Gianluca Pizzone, Dipartimento di Metodologie Fisiche e Chimiche, Universita di Catania and Laboratori Nazionali del Sud, Catania, Italy	*Trojan Horse Method as an Indirect Technique for Nuclear Astrophysics*